SOFT ROBOTIC FABRIC AND CLOTHING FOR ADAPTIVE PERSONAL THERMAL MANAGEMENT

ZHANG XIAOHUI

PhD

The Hong Kong Polytechnic University

2024

The Hong Kong Polytechnic University

School of Fashion and Textiles

Soft Robotic Fabric and Clothing for Adaptive Personal Thermal Management

Zhang Xiaohui

A thesis submitted in partial fulfilment of the requirements

for the degree of Doctor of Philosophy

April 2024

CERTIFICATE OF ORIGINALITY

I hereby declare that this thesis is my own work and that, to the best of my knowledge and belief, it reproduces no material previously published or written, nor material that has been accepted for the award of any other degree or diploma, except where due acknowledgement has been made in the text.

__________________ (Signed)

ZHANG Xiaohui (Name of Student)

Abstract

Recently, personal thermal management technology has been garnering substantial interest in the fashion and textile field, primarily due to the significance of thermal comfort for human beings. As a fundamental and indispensable requirement, it ensures the optimal performance of the human body. Failure to maintain thermal comfort can cause serious health issues and may even prove fatal in extreme conditions. In general, humans possess a remarkable ability to maintain their core body temperature within a narrow range of around 37 °C. Hence, textile and clothing play a pivotal role in managing body thermal comfort. However, most clothing exhibits only static thermal properties, which may not adequately accommodate complex and unpredictable weather conditions. Thus, this study aims to investigate the thermal behavior of textile and develop fabric and clothing that can adapt to variations in environmental conditions, such as temperature and radiation. Specifically, this study would integrate soft robotic elements with traditional textiles to create smart textiles with dynamic thermal properties, thereby establishing a new paradigm in adaptive personal thermal management.

The study explores the innovative application of soft robotics incorporated with textiles to achieve personal thermal regulation. These soft robotic elements have the unique ability to alter the properties of textile, specifically the geometric shape. Such changes in thickness and coverage area can significantly influence the thermal conductivity, thermal convection, or thermal radiation through fabric. This can be particularly beneficial for people experiencing thermal discomfort in different

environmental conditions, as the soft robots have the ability to regulate their shape, thereby achieving optimal thermal comfort. These soft robotic elements are highly reversible, which allows for reversible alterations to the shape of the wearable robots. Moreover, soft robotic textiles can be equipped with sensors or responsive materials, which can enable them to automatically adapt to changes in the external environment. Such adaptive thermal management systems are realized through a combination of fabric substrates, soft robotics, and either passive or active control systems, offering a groundbreaking approach to maintaining thermal comfort across diverse conditions.

In the first part of the study, we introduced an innovative passive soft robotic fabric engineered for adaptive thermal protection. This fabric leverages the unique capabilities of soft actuators, which incorporate a low boiling point fluid to enable significant volume changes during phase transitions. As ambient temperatures rise, the fluid evaporates, causing the soft actuators to expand. This expansion separates the fabric layers, creating an insulating air gap that effectively minimizes heat transfer from the environment to the skin. Conversely, under normal conditions, the fluid remains in its liquid state, allowing the actuators to contract and the fabric layers to come into contact, thereby reducing thermal resistance. The results of the study demonstrate that the use of a low boiling point fluid within soft robotic elements can dynamically adjust the fabric's thickness, providing reversible thermal insulation. This adaptability ensures personal thermal comfort across diverse environmental conditions, highlighting the transformative potential of soft robotics in advancing thermal management capabilities in textiles.

In the second part of the research, we developed dynamic soft robotic clothing specifically designed for adjustable thermal resistance in cold weather conditions. These garments feature soft actuators that mimic the structure of the human skeleton, providing a snug and comfortable fit that ensures both warmth and flexibility. Utilizing pneumatic technology, the actuators employ air as an insulating material, delivering lightweight yet highly efficient thermal performance. A key innovation in this design is the active control system, which allows the clothing to respond swiftly and safely to changes in temperature. Experimental results confirm that the fabric's thickness can be dynamically adjusted to suit various ambient temperatures. The deformation capabilities of the soft robotic elements enable the fabric's geometry to adapt, maintaining body comfort even with a temperature change of up to 5°C. This highlights the significant potential of soft robotics in enhancing the adaptability and comfort of thermal clothing.

In the third part of the study, we developed a breathable three-dimensional (3D) knitted fabric that leverages the principles of soft robotics to enhance thermal management. This fabric's intricate 3D structure is achieved through the inherent physical forces of the yarn within the loops, forming a complex sculptural shape through an entirely automated process. The fabric can seamlessly transition between 3D and 2D states, allowing for adjustments in thickness and consequently altering thermal resistance. Additionally, the coated sections of the fabric are designed to stretch and conform to the body's contours during these transitions, enhancing coverage and comfort. The surface coatings also play a critical role in reflecting solar radiation, thereby facilitating radiative cooling. An active control system is integrated into this design, enabling precise control over the deformation of the soft actuators attached to the fabric, thus facilitating the transition between 3D and 2D states. Experimental results demonstrate that when the fabric is stretched from a 3D to a 2D configuration, there is a notable reduction in thermal resistance alongside an effective radiative cooling effect. This underscores the potential of soft actuators in transforming traditional textiles into smart fabrics capable of dynamic thermal regulation and enhanced adaptability to environmental conditions.

In conclusion, this research systematically and scientifically developed three innovative soft robotic fabrics designed to provide adaptive personal thermal management. These fabrics, integrated with advanced soft robotics technology, offer dynamic adaptability to varying environmental conditions, ensuring consistent thermal comfort. The evaluation of their thermal properties, supported by a rigorous evaluation system and human trials, demonstrated their effectiveness in real-world scenarios. The integration of soft robotics allows these textiles to dynamically alter their structure and thermal properties, showcasing features such as reversible deformation and lightweight insulation through pneumatic actuators. The fabrics can transition between three-dimensional and two-dimensional states, optimizing thermal resistance and enabling effective radiative cooling through specialized surface coatings. Active control systems further enhance functionality by ensuring quick and responsive adjustments to temperature changes. While the proposed textiles exhibit promising adaptive capabilities, they also present certain limitations that need addressing. Nonetheless, this study not only paves the way for the adoption of robotic technology within the textile and clothing industry but also offers a preliminary exploration that supplements existing research. It provides valuable insights for refining and evolving intelligent textiles. As artificial intelligence (AI) technology becomes increasingly prevalent, its integration with these smart fabrics could further enhance their intelligence and adaptability, marking a significant advancement in the field of personal thermal management.

List of publications

Journal Papers:

[1] **Zhang, X**., Chao, X., Lou, L., Fan, J., Chen, Q., Li, B., ... & Shou, D. (2021). Personal thermal management by thermally conductive composites: A review. Composites Communications, 23, 100595.

[2] **Zhang, X.,** Wang, Z., Huang, G., Chao, X., Ye, L., Fan, J., Shou, D. (2024). Soft Robotic Textiles for Adaptive Personal Thermal Management. Adv. Sci. 2024, 2309605.

To submit:

[1] **Zhang, X**., Shou, D. Soft pneumatic actuator-driven textiles for controllable body warming.

[2] **Zhang, X**., Shou, D. Breathable, dual-mode 3D knitted fabric for body warming and radiative cooling.

Acknowledgements

I would be happy to express my big thanks to the following people for their support and encouragement throughout my entire PhD study. Firstly, I would like to express my sincere appreciation and gratitude to my chief supervisor, Dr Dahua Shou and co-supervisor, Prof. Jintu Fan, in School of Fashion and Textiles, The Hong Kong Polytechnic University. Dr Shou has given me invaluable guidance, support, and advice to my research. And his extensive knowledge and insights also play an important role in shaping my work. Besides, I would like to express my thanks to the technicians in the Laboratories of MN, QT and W core for their technical supports.

Then, I would like to thank all my colleagues, Mr Xu, Dr Liu, Dr Li, Dr Feng, Dr Liang, Dr Zhu. Dr Du, Mr Kuang, Miss Wan, who have given valuable advice and support to help me improve my research. Special thanks to my colleagues, Mr Gu, Dr Chao, Dr Huang, Dr Wang and Dr Mo, for their assistance to my research. In addition, I would like to thank my friends, Dr Wei, Dr Li, Dr Liu, Miss Kan and Mr Liu for their encouragement throughout my PhD periods.

Finally, I would like to thank my family for their unwavering support and encouragement during my study and give me power to overcome difficulties.

Table of contents

List of Figures

List of Tables

Chapter 1 Introduction

1.1 Research background

Comfort management is an essential and fundamental requirement for human beings, ensuring the proper work of the body. Comfort is difficult to define because it is complex, varying between individuals and changing all the time, which is deeply affected by the temperature and humidity of the external environment and individual physiological and psychological statuses [1]. Thermal comfort is considered the most essential part of body comfort. It is defined as being “that condition of mind that expresses satisfaction with the thermal environment” [2]. Lack of thermal comfort can lead to reduced work productivity and health-related problems because it is associated with humans' ability to maintain core temperature. Humans have a remarkable capacity to manage their core body temperature at around 37 °C within a quite narrow range [3]. At this temperature, the human body can work at its optimum. To keep the core temperature, it is vital to balance heat generation and heat loss. When people are exposed to a relatively low temperature, the core body temperature drops and a variety of body responses, such as vasoconstriction, shivering, and stopping sweating, are activated to hold the body heat and generate more heat to keep it warm. In contrast, people require increased heat dissipation to cool the body when they stay in a hot environment or engage in activities that causes excessive sweating. In those conditions, perspiration and sweat evaporation become an effective way to improve the cooling effect. Figure 1-1 shows the exchange of heat and moisture between bodies and the environment [4]. However, the human body's ability to regulate its core temperature is quite limited.

The surface temperature of naked body skin varies rapidly in harsh environments, such as intense sunlight, heavy rain, and cold wind, leading to discomfort, heat or cold stroke, and even death. A variation in ± 7 °C could cause death. Therefore, maintaining the body's heat balance is important to maintain core body temperature under stable conditions. Thus, fabrics and clothing are developed to protect the human body under such extreme conditions, where the human body cannot maintain thermal comfort through auto-thermal regulation.

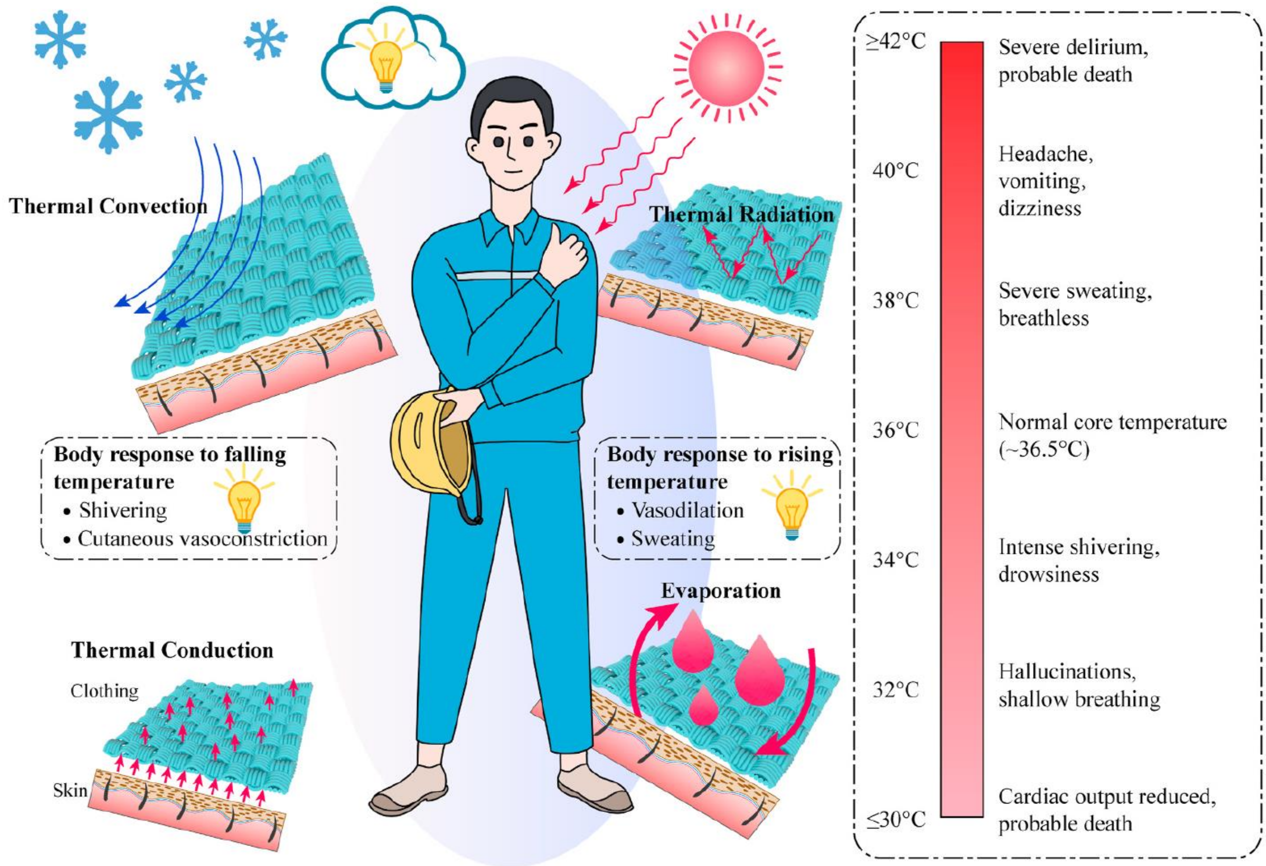

Figure 1-1 Mechanism of heat transfer in human-clothing-environments and the potential adverse physiological reactions to a variation in core temperature [4].

Textile and clothing play an important part in managing body thermal comfort. Clothing can be seemed as the second skin of human body, permitting people to survive and work in extreme conditions and aiding in regulating heat and moisture exchange between bodies and ambient conditions in the body-clothing-environment system [5, 6]. When the environmental temperature is higher than body temperature, heat mainly transfer from environment to bodies, increasing body temperature and resulting in discomfort. Clothing applied in this condition should block heat input and dissipate body heat and sweat to avoid overheating. When the environmental temperature is lower than body temperature, human body may lose heat to the atmosphere. Thus, clothing need to reduce heat release by maintaining the balance of heat generation and loss to establish a feeling of thermal comfort. Besides clothes, with the rapid development of technology, devices like air conditioning and infrared heater have also been widely equipped to buildings to help regulate body thermal comfort. People rely on those energy--intensive systems to achieve thermo--physiological comfort [7]. When people stay in the indoor condition, the using of air conditioning (HAVC) systems can regulate thermal comfort with high efficiency by cooling or heating the entire room. However, the HAVC systems consume a lot of electricity. The building operation accounts for 30% of global energy consumption [8]. Most of those energy is used to keep thermal comfort in buildings [9]. A considerable amount of energy has been wasted for empty space temperature control [10, 11]. Moreover, due to the climate changes and rapid growth of population, the percentage of heat regulation may grow to 80% by the end of year 2050 [8]. Predominantly using of HVAC system also has negative environmental sequences, resulting in ozone depletion and global greenhouse [12]. 20% of global greenhouse gas emission was generated by HAVC systems [8].

Due to the increasing awareness about environmental problems and global energy crisis, energy--free and ecofriendly free alternatives to regulate thermal comfort are urgently required to replace existing systems [13]. To keep thermal comfort of human body in a 2 °C expanded set--point range can save 20% of HVAC energy [14]. On the other hand, as mentioned above, clothing has the large potential for regulating body temperature. Therefore, thermal regulated textiles, the closest to human body, can manage the microclimate near the skin flexibly, which has been an emerging and promising solution to maintain thermal comfort without large--area heating or cooling. In comparison of novel building materials to achieve building thermal management, textiles-based management, controlling the skin temperature of individuals, are much more energy--efficient and cost efficient as clothing only regulate microclimate in body—clothing-environment system.

Notably, actual daily life is more complex when considering the temperature difference between outdoor and indoor scenario. In modern society, people often find themselves staying or working in various environments that aim to maintain thermal comfort, such as air-conditioned rooms, cold storage, thermostatic chambers, and ice rinks [15]. People may step from a cold environment to hot one in summer days, from a warm one to a cold one in winter or suffer from unpredictable environmental changes in some special conditions, resulting in suddenly change of surroundings. In such conditions, human body may be difficult to adapt in such short time [15]. Large temperature difference between human body and ambience can cause severe discomfort and even illness such as cold and hypothermia. Under such conditions, a smart textile that can maintain thermal comfort should be designed to adapt to the temperature variations. Those smart clothing can keep a constant temperature and humidity in the microclimate created by the body-clothing system. There are also a number of outdoor jobs under heat waves in summer, cold snap in winter or some other extreme environment such as fire, mines and foundries without contact with hot or cold objects. It is impossible to install air-conditioning systems in those workplaces. The sudden environmental changes may also occur in circumstances. Smart clothing to sense and react to the atmospheric conditions is necessary. Particularly, in such cases, clothes are the only approach to keep body temperature for people [10].

In recent years, various kinds of intelligent clothing with unique thermal and moisture resistance to adapt to ambient conditions have been developed with the development of semiconductor industry. They focused on the mechanism of heat exchange between human body and environment, which can be divided into four modes, i.e., conduction, convection, radiation and evaporation. The process of heat transfer from the human body to the environment is facilitated by the contact of the human body with clothing, wherein heat is transported through the fibers and air within fabric layers between the body and the environment *via* thermal conduction. [11]. Heat conduction often occurs on two contacted objects with different temperature and the heat transfers from the object with high temperature to the one with low temperature [16]. The temperature difference decides the heat flow speed between the two surfaces. By introducing highly or less conductive materials, the thermal conductive performances of the whole fabric system can be managed. Convective ventilation may occur if the body move or there is airflow around body [14]. Human body can also gain heat from other hot objects, which may not contact with them. Sun, electronic heater, and fire can release heat to cold objects by thermal radiation [12]. The human body can also sweat due to excessive activities to dissipate body heat [15]. In general, the aforementioned four heat transfer mechanisms occur in one system simultaneously: if the skin temperature is lower than or comparable with that of the surroundings, the human body gains external heat by conduction, convection, and radiation and gets rid of excessive heat by sweat evaporation for heat balance; if the skin temperature is much higher than that of the surroundings, the loss of body heat through conduction, convection, and radiation is hindered by clothing insulation. From calm states to intensive sports and working activities, the personal regulation of heat transfer becomes more challenging, with considerably varied degrees of metabolic heat generated [5].

In summary, heat and cold stress not only influence personal health but also curtail work productivity of people, restraining the growth of global economy. Human beings face severe sustainability-related challenges in recent years. Therefore, new strategies and solutions to improve human body thermal comfort control under both indoor and outdoor environment is critical and promising. Personal thermal management (PTM) technology, which focus on controlling temperature of human body instead of the entire building interior space, can facilitate thermal comfort of humans efficiently. It has received increasing attention from researchers and manufacturers all around the world to manage heat and moisture transfer between human body and ambient environment as it can lessen the global energy crisis and environmental concerns. Traditional fabric and clothing have successfully designed to keep body comfort. We wear thin clothes in summer to keep cool while thick clothes in winter to keep warm. However, the traditional fabric, like cotton T-shirt in summer, may be unable to resist strong solar irradiation. And in winter, multilayered fabrics are used to block heat dissipation from human body, which are bulky and less breathable. Traditional fabric and clothing have fixed thermal resistance, thermal comfort may not be maintained in extremely hot or cold conditions [4] and varied with ambient temperature changes. Failure to maintain thermal comfort of human body may lead to heat or cold stress, resulting in severe medical emergencies and even fatalities. What's more, when the external temperature changes, we must put on or off to maintain thermal comfort. If our clothing can regulate the thermal resistance to adapt to temperature variations, we would not need to increase or decrease clothes very often. Functional fabric and clothing based on adaptive personal thermal management is eagerly demanded. Those clothing have been developed to reversibly change the shapes of the textile system by stimuli from body or environment, adapting to the conditions to keep thermal comfort. On the other hand, such smart clothing has also been an important part of functional clothing and fashion industry. Due to the rapid development of society, culture and economy in recent years, the design of smart wearable devices has grown rapidly. Smart clothing, referring to the new class of wearable textile design system integrating with interactive technologies, has become a hot topic among scientists and manufacturers. Smart textiles market has been broadly labelled based on the end use, which focus on wear comfort, health and functionality. Notably, the thermoregulation is the utmost priority for bringing comfortability to the wearer.

Soft robotics have been developed rapidly [17]. Comparing with traditional "hard" robotics, soft robotics are flexible, compliant and lightweight devices, and safe for human operators with simple fabrication methods. They can achieve large deformation, high motion complexities and various functions in a relatively simple way. Recently, textiles are applied in robotics field for wearable robots and devices as the textiles exhibit soft and flexible nature, hierarchical structure and anisotropic properties. The robotic clothing tends to be more flexible and softer with lightweight, which can improve the safety, hand-feel and wear comfort of wearers. The porous structure of textiles also allows excellent heat and moisture transmission of the textile-robots system. Researchers have developed textile-based wearable robots for grasping, locomotion assistance, dressings with shape changing, haptics, communication and thermoregulation [18], as shown in Figure 1-2. The robotic clothing can assist in personal thermal regulation by altering the properties of the textiles dynamically, especially the geometric shape. The variations of porosity, thickness and coverage area on yarn and garment level can change the clothing breathability [19], thermal conductivity and radiative properties, controlling the heat and moisture transfer between human body and external environment. Generally, the deformation of the soft robotics is recoverable, indicating the reversible shape changing of the textile-based wearable robots, thus, the thermoregulation properties are also reversible. By integrating sensors or responsive materials, the robotic garments adapting to the changes of the external stimulus to maintain thermal comfort of bodies is achievable.

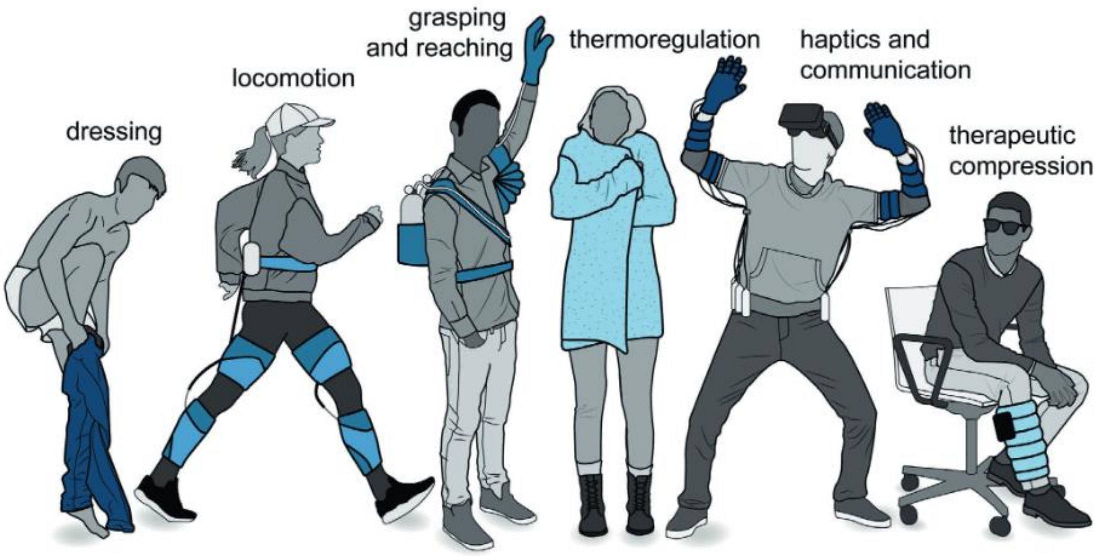

Figure 1-2 Common use of the textile-based robots [18]. The application includes dressing, locomotion, grasping, thermoregulation, communication and therapeutic compression.

1.2 Research objectives

Due to the demands of human thermal comfort, global energy consumption and the desire for fashion design, innovative solutions are needed to solve these problems. Therefore, cheap and sustainable personal thermal wear is still urgently needed to avoid health hazards, address environmental concerns and significantly reduce energy consumption by cooling and heating buildings. Robotics are flexible, compliant and lightweight devices that can be safe for human operators. They can achieve large deformation, high motion complexity and various functions in a relatively simple way. Notably, the development of soft wearable robots allows to wear robots like clothes or integrate robots with clothes with functionalities [20]. Textiles fabricated by weaving, knitting, and nonwoven methods have gained increasing interest in soft robotics due to their soft and flexible nature, hierarchical structure, and anisotropic properties [21]. In this study, a systematic study would be conducted to develop innovative soft robotic fabric and clothing for adaptive personal thermal management. The objectives include:

(1) To design and construct thermally adaptive fabric and clothing system integrated with soft robotic actuators that can respond to changes of human thermo-physiology and environmental conditions.

(2) To integrate soft robotic elements to fabric and clothing by different means, in order to efficiently vary the significant geometrical structures of the fabric (viz., thickness, porosity, pore size, air gap, etc.) to achieve controllable thermal comfort properties.

(3) To explore the underlying mechanisms of heat and moisture transportation within soft robotic fabric system under different temperature and humidity.

(4) To evaluate the performance by evaluating the thermal and moisture resistance of the fabric and clothing system under different thermal climates and validate the proposed theoretical models by experimental results.

1.3 Outline

Chapter 1: General introduction of the study is given in this chapter, including the background, research aim and the outline.

Chapter 2: Literature reviewing the development of materials, structures and devices applied in personal thermal management are discussed. Soft robotics and actuators for adaptive personal thermal management are highlighted.

Chapter 3: The methodology part introduces the techniques, strategies and evaluation methods adopted to achieve the stated research aim, including the raw materials, fabrication methods and evaluation systems used for preparation and analysis of soft robotic fabric and clothing for adaptive thermal management.

Chapter 4: Soft robotic textiles for passive thermally adaptive insulation.

Chapter 5: Soft pneumatic actuator-driven textiles for controllable body warming.

Chapter 6: Pneumatic actuator-driven breathable 3D knitted fabric for thermal insulation and radiative cooling.

Chapter 7: Conclusions and future perspectives.

Chapter 2 Literature review

2.1 Human-clothing-environment heat transfer mechanism

The critical requirement for human survival is the body's heat balance, which is fundamentally divided into two components: internal-corporeal and external heat transfer. Intra-corporeal heat transfer is the process of heat being exchanged between different layers of skin and through blood circulation, while external heat transfer occurs due to radiation and convection [22]. External heat transfer refers to the heat transfer between the human body and the ambient environment in which they reside, which would be discussed in this study. Heat transfer forms include heat conduction, convection, radiation and evaporation, as described in Figure 1-1. Thermal conduction occurs in two adjectives, affected by the temperature difference and the thermal conductivity of the materials. Heat convection is associated with air flow. Strong air flow leads to high heat convection because the speed of air flow affects the movement of air inside fabric and clothing. Radiation is another effective heat transfer method [23-25], which can be controlled by managing the emissivity or reflectivity of materials [10]. Multilayer photonic structures and metamaterials integrated with fabric and clothing have successfully promoted radiative cooling and imparted air-water permeability simultaneously. Evaporation also contributes to human body heat and moisture transfer, especially in body cooling [26, 27]. Sweat evaporation can take heat and moisture away from the skin surface to the environment to enhance the cooling effect. Unidirectional liquid transport fabric allows one-way liquid transport from the body skin to the outside of the fabric, reducing sweat accumulation on the skin and increasing evaporation rate to enhance cooling effect [28].

The heat transportation between human body and ambient environment can be described by Eq.(2-1) [22]. All variables are presented in per unit skin area, [W/m^2].

$$q_{st} = q_m - (q_{cond} + q_{conv} + q_r + q_{e,s} + q_{res} + q_{wk}) \tag{2-1}$$

Where q_{st} indicates the energy stored by the body; q_m indicates the metabolic rate of the body; q_{cond} represents heat flux on the skin surface induced by conduction; q_{conv} is heat flux on the skin surface induced by convection; qr is heat flux on the skin surface induced by thermal radiation; $q_{e,s}$ is vaporization heat dissipation rate on the skin surface; q_{res} is vaporization heat dissipation rate by respiration; q_{wk} is heat dissipation rate by external work of human body [22].

In fact, heat transfer through fabric involves a complex multi-mode process, encompassing not only conduction heat transfer through solid yarn and the air space between yarns and fabrics, but also natural convection between yarn spaces, radiation through yarns and gaps between yarns, and moisture evaporation from yarns. The contribution of these modes is influenced by ambient temperature. In the following part, advanced textiles with regulated thermal properties, including thermal conduction, convection, evaporation and radiation, are discussed and summarized.

2.2 Advanced textiles with regulated thermal properties

In the past decades, functional fabric and clothing and advanced materials have been an emerging and popular research topic to manage physiological comfort, especially thermal comfort of human body [29]. According to the mechanism of heat transfer modes mentioned above, an enormous amount of research effort has been made to design and fabricate textiles with regulated thermal properties. This section reviews advanced textiles fabricated with different approaches developed in recent years.

2.2.1 Textiles with regulated thermal conductive property

As the human body contacts textiles, heat conduction is the dominant mode of heat transfer at the interface of human skin and the inner layer of fabric and clothing. More importantly, heat conduction is the only route of heat transport inside the fabric, which is worth investigating for effective personal thermal management [14]. Thermal conductivity is used to evaluate the effectiveness of heat transfer between adjacent objects. In colder environments, the importance of maintaining a suitable body temperature becomes paramount for humans. As such, the incorporation of low thermal conductivity composite materials and structures into fabric and clothing designs proves beneficial in minimizing heat loss. Conversely, in hot climates, it is necessary to enhance the loss of heat from the human body to avoid heat stress. This can be achieved by using highly conductive components.

Heat removal is an important issue for people staying in a hot environment or engaging in strenuous exercise. Materials with high thermal conductivity are in high demand for the preparation of cooling textiles. Carbon nanomaterials are widely used as thermally conductive coatings because they have higher thermal conductivity. Graphene, a single layer of carbon atoms arranged in a hexagonal pattern, exhibits exceptional tensile strength and superior thermal conductivity, reaching up to ~5000 W/(m·K) at room temperature. Fibers made of large graphene sheets were inserted with small graphene sheets in a highly ordered manner, enhancing thermal conductivity to 1290 W/(m·K) [30, 31].The thermal conductivity of single-wall carbon nanotubes (SWCNTs) and multi-wall carbon nanotube (MWCNT) have been measured as 3500 W/(m·K) and 3000 W/(m·K) respectively [32]. MWCNT and graphene particles coated on cotton fabric could significantly enhancing the thermal conductivity by 132% and 842%, while the air permeability was also reduced by 64% and 73%, respectively [33]. A newly designed E-textile fabric was created by nano-soldering of CNTs into nonwoven fabrics (NWF) and then depositing reduced graphene oxide (rGO) on top [34]. The rGO/CNTs/NWF achieved the thermal conductivity of 2.90 W/(m·K), much greater than the 0.03 W/(m·K) of a NWF with continuous structures of CNTs/rGO. Even after the rGO/CNTs/NWF was stirring in water at rate of 700 rpm, the effective thermal conductivity only reduced slightly to 1.96 W/(m · K), which showed promising durability and washability. However, the lengthy and costly fabrication process of graphene fibers still limits the large-scale production. Meanwhile, coated fibers and fabrics were often stiff and less skin friendly.

Boron nitride (BN) is also highly conductive due to diamond-like molecular structure, which has a high in-plane thermal conductivity up to 300-600 W/(m·K) [33, 35]. The aligned BN nanosheets, which were uniformly dispersed in poly (vinyl alcohol) (PVA) matrix, were fabricated into highly conductive fibers using a scalable 3D printing method, shown in Figure 2-1 [36]. BN nanosheets were scientifically engineered to exhibit an exceptional cooling effect by providing uniform and aligned packing, demonstrating superior cooling efficiency that is 55% higher than conventional cotton fibers.

However, it is crucial to note that the cooling effect is more pronounced in colder environments, where the demand for cooling performance was not as pressing. Synthetic polymers, such as Gel-spun, that contain ultra-oriented fibers made of ultrahigh molecular weight polyethylene (UHMWPE), could also exhibit superior cooling efficiency due to their ability to retain water vapor, thereby allowing for effective heat dispersion. They have been developed with exceptionally high thermal conductivity for the thermal management community [37]. The gel spinning method could enhance the polymer thermal conductivity, subsequently leading to the production of individual microfibers, yarns, and fabrics. Furthermore, the effective in-plane thermal conductivity of the woven fabric with the value of ~10 W/(m·K) was 2–3 orders of magnitude higher than that of traditional textiles.

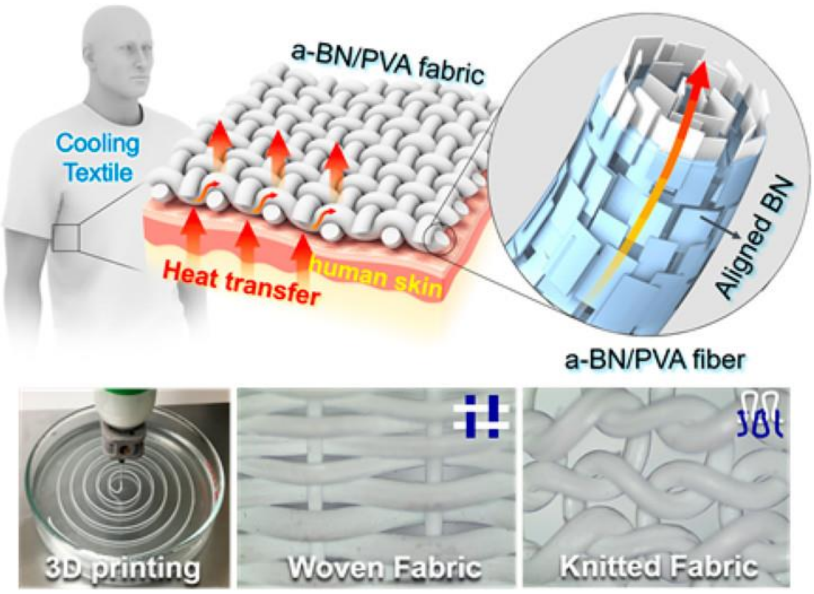

Figure 2-1 Schematic illustration of a novel thermal regulation textile created by a-BN/PVA fiber and the photo images showing the fabrication process, plain woven and knitted fabric [36].

Materials with low thermal conductivity are the perfect candidates to fabricate fabric and clothing for body warming and thermal insulation. Natural fibers, such as cotton, down and wool, have been widely used as the first choice for fabricating thermally insulated fabrics and clothing because of their intrinsic low thermal conductivity due to trapped air within or around fibers. The thermal conductivity of wool fibers varied within the range 0.036–0.067 W/(m·K) [38], the thermal conductivity of cotton fibers ranged from 0.026 to 0.065 W/(m·K) [33]. Compared to cotton and wool fibers, down fibers are more hydrophobic and less hydroscopic, with higher thermal insulation even in a humid environment [39]. The thermal conductivity of air is much lower than that of fibrous polymers and composites, indicating the more significant contribution of conductive fibers to the heat transfer process, while more pronounced impact of immobilized air occurs in fabrics on thermal insulation. However, natural fibers are sensitive to humidity and moisture, resulting in large variations of thermal conductivity. The effective thermal conductivity of completely wet cotton fibers ranged between 0.65 W/(m·K) and 0.70 W/(m·K), a range comparable with that of liquid water itself [40].

Besides natural fibers, synthetic and artificial fibers with reduced thermal conductivities were developed for various applications. The thermal conductivity of those fibers was determined by their molecular, morphological and geometrical characteristics, as well as the post-processing method. Inorganic fibers including ceramics, glass, and basalt possess high chemical stability and high flame resistance properties that are promising for applications in extreme thermal environments. Cai et al. investigated those nonwoven fabrics made by basalt fibers had exhibited the best thermal protective performance compared with fabrics made by Nomex (polyisoph-thaloyl meta phenylene diamine), PPS (polyphenylene sulfide), P84 (polyimide) when exposed to environments of intense heat, and the insulating temperature reached up to 200 °C [41]. Nevertheless, such inorganic fibers were generally brittle and stiff, and due to their low tolerance of handling and poor flexibility, they were widely used in functional textiles that require reliable thermal insulation more urgently than wear comfort [42].

As inorganic materials lack compatibility, more organic materials were investigated to be applied in personal thermal management. The organic synthetic fibers made from polyimide (PI), polyphenylene sulfide (PPS) and polyaramid have stable molecular chains and low moisture absorbance, providing excellent heat resistance in the application of thermal protection [16]. Compared with inorganic materials, organic materials were more flexible and lightweight, which have been commercially and extensively used for personal thermal protective wears. However, the stiffness and poor absorption of moisture still affected their wear comfort.

One easy and efficient way to achieve low thermal conductivity is to trap air into fibers or fabrics to increase thermal resistance. Hollow and porous fibers [43] with special geometric structures tended to minimize the weight of fabric and trap more dry air in the hollows, showing exceptionally high heat resistance in cold weather. Particularly, porous fibers with high porosity could weaken the air circulation and limits convection heat transfer, providing excellent thermal insulation properties under wide ranges of working temperature. Inspired by natural organism, a “freeze-spinning” approach has been employed by Cui et al. to realize hair-like hollow and hierarchical fibers, which mimicked polar bear hairs [44]. As shown in Figure 2-2, up to 87% porosity could be achieved and the axially aligned porous structure within the fiber has better modify the mechanical strength without compromising breathability and wearability. Textiles woven by the biomimetic fibers with 30 μm pores and 0.4 mm thickness demonstrated the best thermal insulation in 1-layer textile. The temperature difference between the textile surface and the stage reached 7.9 °C and 8.2 °C when the stage temperature was biased from room temperature to −20 °C or 80 °C. High porosity not only brought low thermal conductivity but also blocked air flow within individual micropores, weakening thermal convection simultaneously. However, the complex fabrication methods and high cost limit its commercialization.

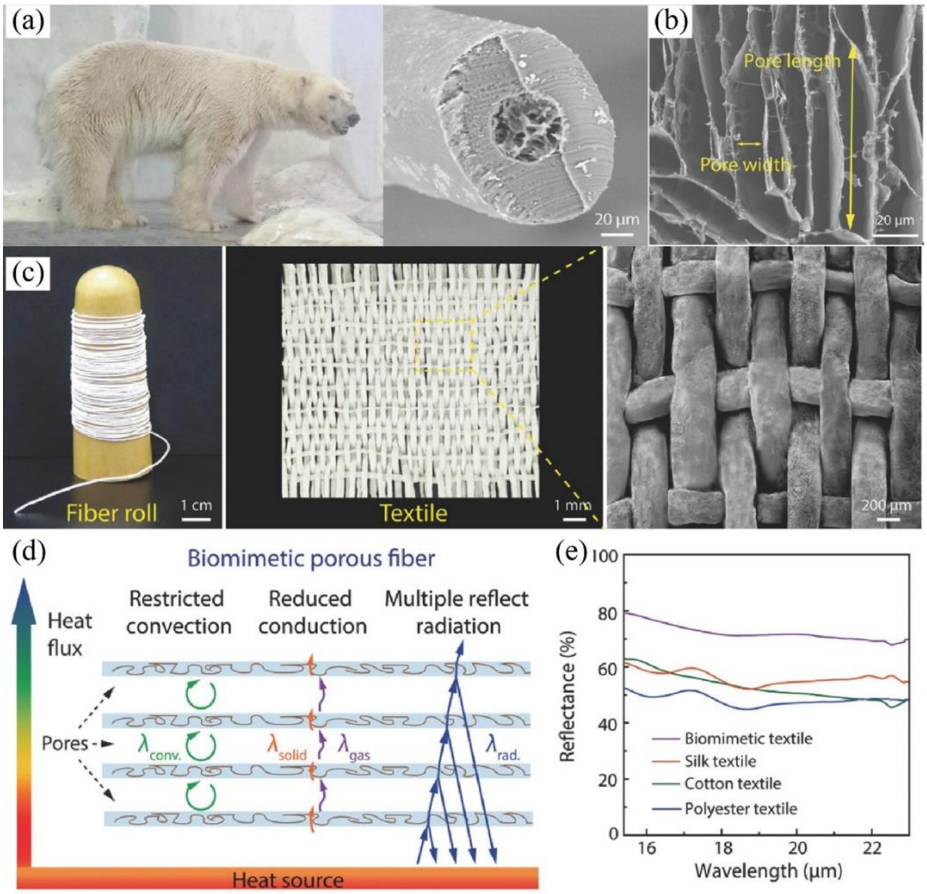

Figure 2-2 Biomimetic porous fiber inspired by polar bear hair [44]. (a) Photo image of a polar bear. (b) SEM images showing aligned shell of a polar bear hair. (c) The optical image showing the fiber collected in a roll, woven fabric fabricated by the fiber. (d) Schematic illustration of thermal conductivity. (e) Reflectance of the proposed and existing textiles.

Shaped fibers with unique cross section were also recognized as good thermal insulator. Compared with fabric made by round fibers, fabric made by those shaped fibers can trap more air between fibers, showing lower thermal conductivity. A post-processing surface coating technique could also be applied to change the effective thermal conductivity of fibers and fabrics, without loss of their softness and flexibility. Coating materials with low thermal conductivity included aluminum oxide ($Al2O_3$), zirconium oxide (ZrO_2) and fumed silica (SiO_2), which have been used to reduce the thermal conductivity of cotton fibers by 19.1–44.5% [49]. However, the durability of those coated fabric during washing and wearing, poor fastness and release of particles were still challenged. Aerogel was synthetic, highly nano-porous, lightweight and excellent insulative materials, which had lower thermal conductivity and lower density than air [50]. Aerogel, which has a low thermal conductivity, was often used in high-temperature environments to resist incoming heat flux and prevent heat loss from the human body in cold conditions. It was often mixed with microfibers using construction modes such as fiber-aerogel networks, fibers in aerogel, and aerogel in fibers. Silica-based aerogel was an ideal thermal insulator with highly porous nature, whose makeup was up to 99% air [51]. The thermal conductivity was 0.005–0.1W/(m·K), density was 0.003–0.5 g/cm^3 and the porosity was 80–99.8% [52]. Silica contributed to poor heat conduction, while the pores in silica aerogel with micro-meter or nano-meter size blocked air circulation. A highly thermal insulative aerogel-doped poly (vinyl chloride)-coated fabric composites were designed by Jabbari et al. by coating silica aerogel on woven polyester fabric, reducing weight and enhancing thermal insulation properties by ~26% (from 0.205 to

0.152 W/(m·K) [53]. However, the rigidity, fragility, high cost are still limitations. Silica-based aerogel was hydrophobic. The irreversible collapse of pores may increase density ang then lead to poor air permeability. Yang et al. [54] fabricated porous cellulose acetate/polyacrylic acid (CA/PAA) wrapped SF aerogel fibers with high porosity (86%) and high tensile strength (2.6 ± 0.4 MPa). The thermal conductivity of CA/PAA-wrapped SF aerogel fibers was measured as 0.031 W/(m·K), exhibiting good thermal insulation under both hot and cold environments. Meanwhile, the multiscale porous structure of the fibers restricted air movement in the hollow fiber shell, which reduced the thermal convection significantly. The application of silk fibroin aerogel also prevented infrared radiation. Inspired by the microstructures of the hair of polar bears, carbon tube aerogel (CTA) composed of hollow carbon tube fibers was fabricated, which showed the merits of polar bear hair. The lowest thermal conductivity of the CTA was only 0.023 W/(m·K), lower than the thermal conductivity of dry air. However, the fabrication process is still complex and relatively inefficient.

Table 2-1 displays the thermal conductivity, features and applications of materials used for personal thermal management. In order to regulate the thermal conductivity of textiles, research have developed functional fibers, fabric and post-processing methods, which have gain impressive results for body warming and cooling. However, the complex fabrication methods, high cost, stiffness and limited durability still need to be solved by the future work.

Table 2-1 Thermal conductivity of the materials applied for personal thermal management [4].

Materials	Features	Applications	Thermal conductivity

			(W/(m·K))
Wool fiber	Hollow structure	Sweater, blanket	0.036 - 0.067 [38]
Down fiber	Sub-branches with certain crotches	Down jacket, duvet	— [39]
Cotton fibers	Empty cavities	Garments, Quilt	0.026 - 0.065 [33]
Palm fibers	Gap between single fiber, hollow structure	Ropes, Rain capes and mattresses	0.0555
Peat fibers	High hairiness and wide fiber size distribution	Garments	0.055 - 0.085 [45]
Ceramics fiber	High chemical stability	Astronaut suits and firefighter apparel in extreme thermal environments	0.03
Glass fiber			0.05
Asbestos fiber			0.198 - 0.244
Polyimide	Highly stable molecular chains	Functional textiles and clothing	0.025
Polyphenylene sulfide			0.027
Polyaramid			0.244 - 0.337
Graphene	Outstanding thermal conductivity	Passive cooling and heating textiles	Up to 5000 [46]
PVA/BN	3D printing	Cooling textiles	— [36]
Profiled fiber	Special geometric structures	Warming garments	—
Biomimetic fibers	Aligned shell hollow core	Thermal insulation garments	— [44]
Porous Silk Firoin-	High porosity,	High-performance	— [47]

Based Aerogel Fibers	continuous, strong	thermal insulation materials	
Aluminum oxide (Al_2O_3), zirconium oxide (ZrO_2) and fumed silica (SiO_2)	Low thermal conductivity	Passive thermally insulated textiles	— [48]
UHMW-PE fiber	Gel-spun, Ultra-oriented fibers	Cooling garments	Up to 25 [37]

2.2.2 Textiles with regulated thermal convective property

Thermal convection of textiles refers to natural convection. The traditional strategy to enhance or weaken air convection is to adjust the structure of fabrics by changing the arrangement of fibers and yarns to create different pore size and space. Larger pores and high porosity may result in quick release of heat from skin surface to environment. Chimney effect is the movement of air into and out of a chimney-like channel due to air buoyancy, shown in Figure 2-3a. Air buoyancy occurs when there is a difference in inside-to-outside air density due to temperature and moisture differences. The difference of air density leads to pressure difference, providing force for the chimney effect. Warm air inside moves out the channel to the ambience. The cool air enters into the channel, heated by the hot surface inside and then moves out. The circulation process, better known as the chimney effect, harnesses the continuous air flow within the vertical channel to enhance the heat transfer coefficient, thereby intensifying the overall convective heat transport [49]. In very loose clothing, chimney effect may occur as the gap between fabric layers or fabric and human body can provide a channel for air motion.

As shown in Figure 2-3b, human skin can be seemed like a hot surface, heated the air in the gap. The ventilation of the trapped air removes heat through openings on clothing, such as collars, cuffs and hem [56]. Therefore, zippers, buttons and pockets can be assembled when designing clothing to control chimney effect. The steeper the thermal gradient and the higher the chimney's position, the stronger the buoyancy force and chimney effect would be. Actually, the natural convection is weak, which is often integrated with other thermal transfer mode or enhanced by introducing force convection.

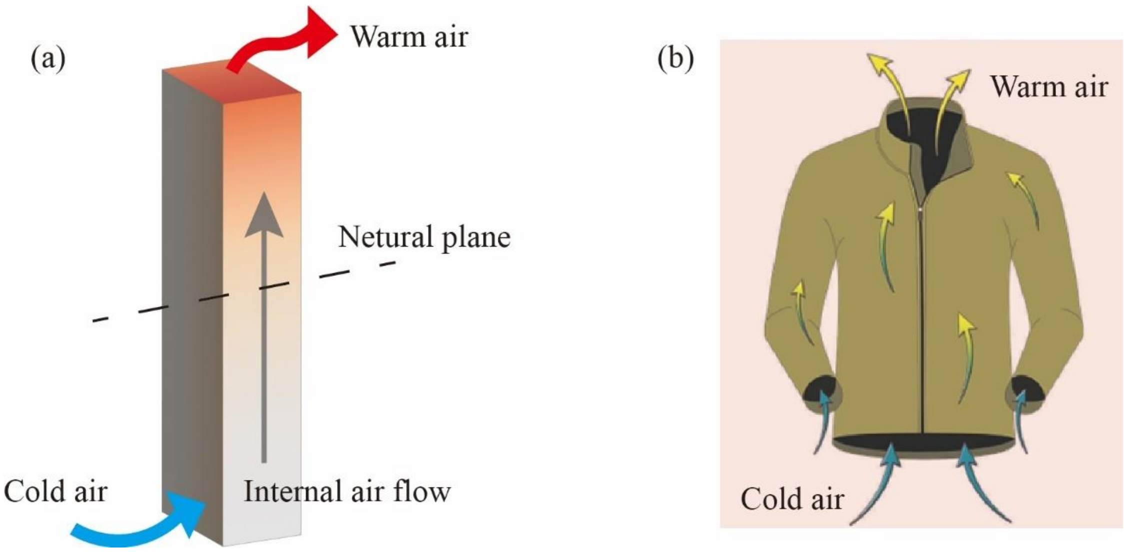

Figure 2-3 Chimney effect. (a) Mechanism of the chimney effect. (b) Clothing with chimney effect. [50]. The colder air can enter the clothing system from the openings of the garment and warmer air inside could be squeezed out from other openings.

2.2.3 Textiles with regulated thermal radiative property

When people are exposed to direct sunlight, fabric and clothing made from materials are heated by the sunlight and pores in fabrics allow sunlight to pass through. People may feel hot and discomfort under intense solar radiation. Materials to reduce the penetration of solar light to skin and reflect them can achieve demanded cooling effect. Therefore, radiative property-engineered fabric and clothing can passively manage radiative heat transport for human body cooling and warming without energy consumption. Depending on the ambient conditions, the clothing can reflect solar irradiation (0.3−2.5 μm) back to environment in sunny condition or allow infrared (IR) radiation (8-14 μm) emitting from human body in cold condition. Human body can emit IR light to lose heat at a peak emission of 9.5 μm into deep space by utilizing the atmospheric window. Therefore, blocking IR emission can be applied to reduce heat loss from body and keep warm in cold conditions.

According to Kirchhoff's law, the relationship of IR transmittance, reflectance and absorptance can be described by the equation below.

$$\textit{Transmittance} + \textit{Reflectance} + \textit{Absorptance}=1 \tag{2-2}$$

Clothing can be seemed like a black body. It can absorb radiation in all frequencies of infrared, which means that the absorption of IR is equal to the emission. Therefore, managing the solar reflectance and the IR emissivity of clothing are the efficient way to develop radiative cooling and warming fabric and clothing. The clothing should be able to emit thermal radiation of human body or reflect solar irradiation as much as possible to achieve maximum cooling effect in hot environment. The emissivity of fabric and clothing should be near one or they should be highly transparent to infrared wavelength. The reflectance of fabric and clothing should be near one to reduce solar absorption. In the contrary, the reflectivity of the fabric and clothing to infrared light should be near one to achieve heating in cold condition. Notably, the fabric and clothing of human should be opaque to visible light for both cooling and heating purpose [51].

Radiative cooling textiles can be used in hot environment for cooling effect, which are designed based on two principles. First, the fabric and clothing should allow transmission of IR light from human body to enhance heat loss. On the other hand, the fabric should reflect solar irradiation back to the out atmosphere to block heat input. In contrast, warming fabric and clothing are required to reflect IR back to human body to reduce heat loss. Combining materials with different emissivity of IR radiation and solar light reflectance, especially visible light (400-700 nm) and near-infrared light (700–2500 nm), can be useful way to develop radiative cooling/warming textiles for personal thermal management [52].

It has been found that polyethylene (PE) was transparent to infrared radiation and opaque to visible light, which was a favorable material for radiative cooling and warming [53, 54]. Researchers from Stanford University proposed one kind of nonporous polyethylene textile for human body radiative cooling in 2016 [55]. Compare with normal PE, nonporous PE had interconnected pores that were 50-1000 nm in diameter, which were comparable to the wavelength of visible light. They can scatter solar light, making the PE film is opaque to human eyes, which was essential for clothes. In order to improve the wearability performances, such as air permeability, water wicking and mechanical strength, post processing was added. The simulated skin temperature reduced 2.7 °C and 2.0 °C when covered with nanoPE and processed PE, respectively, compared with those covered with cotton. After one year, their group demonstrated a nanoporous metallized polyethylene textile for personal heating, which had achieved a high IR reflectivity of 98.5% on IR-transparent nanoPE (96.0%) [56].

Nanoporous Ag film was coated on nanoPE *via* electroless plating method firstly. Then, the nano-Ag/PE was laminated onto cotton fabric to form a three-layer structure (cotton/Ag/PE). The nano porous Ag film was an IR reflective layer with the pore size smaller than IR wavelength but larger than diameter of water molecular. Remarkably, the nanoPE served as outer substrate not only provided protection for the metal coating but also retained lower IR emissivity of the underlaying layer. Then, a dual-mode textile for both human body cooling and warming were designed to realize those two opposite functions within one textile [57]. It had a bilayer emitter embedded inside an infrared-transparent nanoPE layer, exhibiting asymmetric thicknesses on each side. The bilayer emitter could control the emissivity while the nanoPE could ensure the free radiation of IR from human body to ambience. For cooling mode, the high-emissivity layer faced to the environment to increase emission. The thickness of nanoPE layer near the skin was small to enhance heat conduction from human body to the emitter efficiently. While for the warming mode, the textile needed to be flipped. The low-emissivity layer faced out to decrease emission. Meanwhile, the emitter-to-skin distance increased to block heat conduction from human body. The artificial skin temperature could maintain within 32 °C to 36 °C even if the environmental temperature varied between 16 °C and 25 °C. However, the temperature of skin covered by conventional fabric would follow the trend of environment temperature changes. In 2018, they [58] reported uniform and continuous nanoPE microfibers fabricated by melt extrusion method, achieving large-scale production. Nanopores were embedded in the fiber to scatter visible light without comprising mid-IR transparency. NanoPE fabrics produced by industrial machine using the microfibers could lower the skin temperature by 2.3 °C, saving more than 20% energy needed for indoor cooling. Then in 2019, a new strategy was proposed to realize facile coloration of IR-transparency PE textiles by utilizing inorganic nanoparticles as a coloring component [59]. The colored fabric showed high IR-transparence of 80% and cooling effect with 1.6-1.8 °C temperature reduction, as well as intense visible color and better washing stability.

Table 2-2 Application of polyethylene (PE) for personal thermal management.

Materials	Features	Thermal mode	Effect
Nonporous PE textile [55]	—	Radiative cooling	Temperature reduced 2.7 °C
Nanoporous metallized PE textile [56]	Breathable	Radiative heating	High IR reflectivity of 98.5%
A bilayer emitter [57]	Dual mode	Radiative cooling and heating	Temperature could maintain within 32 °C to 36 °C
Continuous nanoPE microfibers [58]	Large-scale production	Radiative cooling	Lower the skin temperature by 2.3 °C
IR-transparency PE textiles [59]	Colorful	Radiative cooling	1.6-1.8 °C temperature reduction

From nanoPE film to fabric produced by nanoPE microfibers and then the coloration of PE fabric, researchers moved closer to fabricate energy-efficient and cost-effective PE textiles for radiative cooling and warming. However, those PE fabrics were not suitable for outdoor cooling as they could not reflect solar light. The radiative cooling systems can transfer heat to space through thermal radiation due to the large temperature difference between the Earth and the outer space. The infrared thermal radiation can be emitted from the Earth's surface to the cold space through the atmospheric window without additional energy consumption [13]. Therefore, radiative cooling textiles were designed to achieve strong solar reflectance in solar spectrum (0.3-2.5 μm), which could avoid solar heating, and high thermal emittance in atmospheric window (8-13 μm) to lose heat to space in outdoor conditions.

A fabric with enhanced IR radiation and reduced solar energy absorption simultaneously is desired. Song et al. designed a bilayer structure for summer clothes [60]. PA6 electrospinning fibers (PANFs) were deposited on the nanoporous PE membrane (PENM). The PENM outside had pores with sizes of 100−1000 nm, allowing for IR transmission and moisture transporting, and blocking water passing through. PANF inside were 100 nm in diameter with beads (230 nm), reflecting visible light efficiently. The heat loss power of the designed fabric was approximately 14.13 W/m^2 higher than cotton fabric, indicating good cooling capability. In 2020, Song proposed a novel fabric with tri-layered structure, containing PA, PVDF and PE, for both outdoor and indoor personal thermal management, which could reflect up to 90% of sunlight and reduce body temperature by 4.5–6.5 °C under direct solar light [61].

In order to improve the mid-infrared (MIR) emissivity, Zeng et al.[62] designed a hierarchical-morphology meta fabric for passive daytime cooling, containing a titanium oxide-polylactic acid TiO_2-PLA) composite woven textile laminated with a thin polytetrafluoroethylene (PTFE) layer. The meta fibers fabricated by melt spinning method exhibited super tensile strength, flexible and strong enough for machine sewing and weaving/knitting. This fabric had a solar reflectance of 92.4% within the 0.3 to 2.5 mm spectral region, and a peak average emissivity of 94.5% within the AASW. The high emissivity between 4 to 25 μm indicated its potential application in personal thermal management. Results from human subject test showed that the temperature of body part covered by meta fabric was 4.8°C lower than that covered by cotton fabric. Although the metal fabric has successfully demonstrated efficient radiative cooling performance, necessary air permeability and pretty wear comfort, the drawback still existed as sweat absorption and transport were not considered when people sweated in hot weather. Another paper reported a passive cooling fabric by introducing evaporation cooling to achieve synergistic effect, which break through the traditional single passive cooling mode [63]. Porous poly (vinylidene fluoride-co-hexafluoropropylene) ($P(VdF-HFP)_{HP}$) coated on the upper side of the fabric exhibited higher solar reflectivity (90%) and higher IR emissivity (83%). While hygroscopic salts, $CaCl_2$, were loaded on the inner side of the fabric to capture water vapor and evaporate in the daytime to dissipate heat. The temperature could reduce 10.8 °C under direct sunlight in outdoor environment.

Table 2-3 has summarized the materials for radiative cooling. Bilayer structure, tri-layered structure and hierarchical structure are all have been investigated, which have demonstrated higher reflectance and excellent cooling performance when compared with traditional textiles. However, most of the experimental results were obtained from hotplate or simulated skin, which may not mirror the actual cooling effects of human body as it is a complex system. In addition, the air permeability and washability are still challenging for those coating fabric. The mechanism of those materials can be found in Figure 2-4.

Table 2-3 Materials for radiative cooling.

Materials	Features	Effect
PANF-PENM fabric	A bilayer structure; Moisture transporting	Heat loss power 14.13 W/m^2 higher than cotton fabric [60]
PA, PVDF and PE	Tri-layered structure	Higher solar reflectivity (90%); 4.5–6.5 °C temperature reduction [61]
TiO_2-PLA, PTFE	Hierarchical morphology Weaving/knitting	Reflectance of 92.4% in the solar radiation region; 4.8 °C temperature reduction [62]
P(VdF-HFP)	Synergistic effect of passive cooling and evaporation cooling	Higher solar reflectivity (90%); 10.8 °C temperature reduction [63]

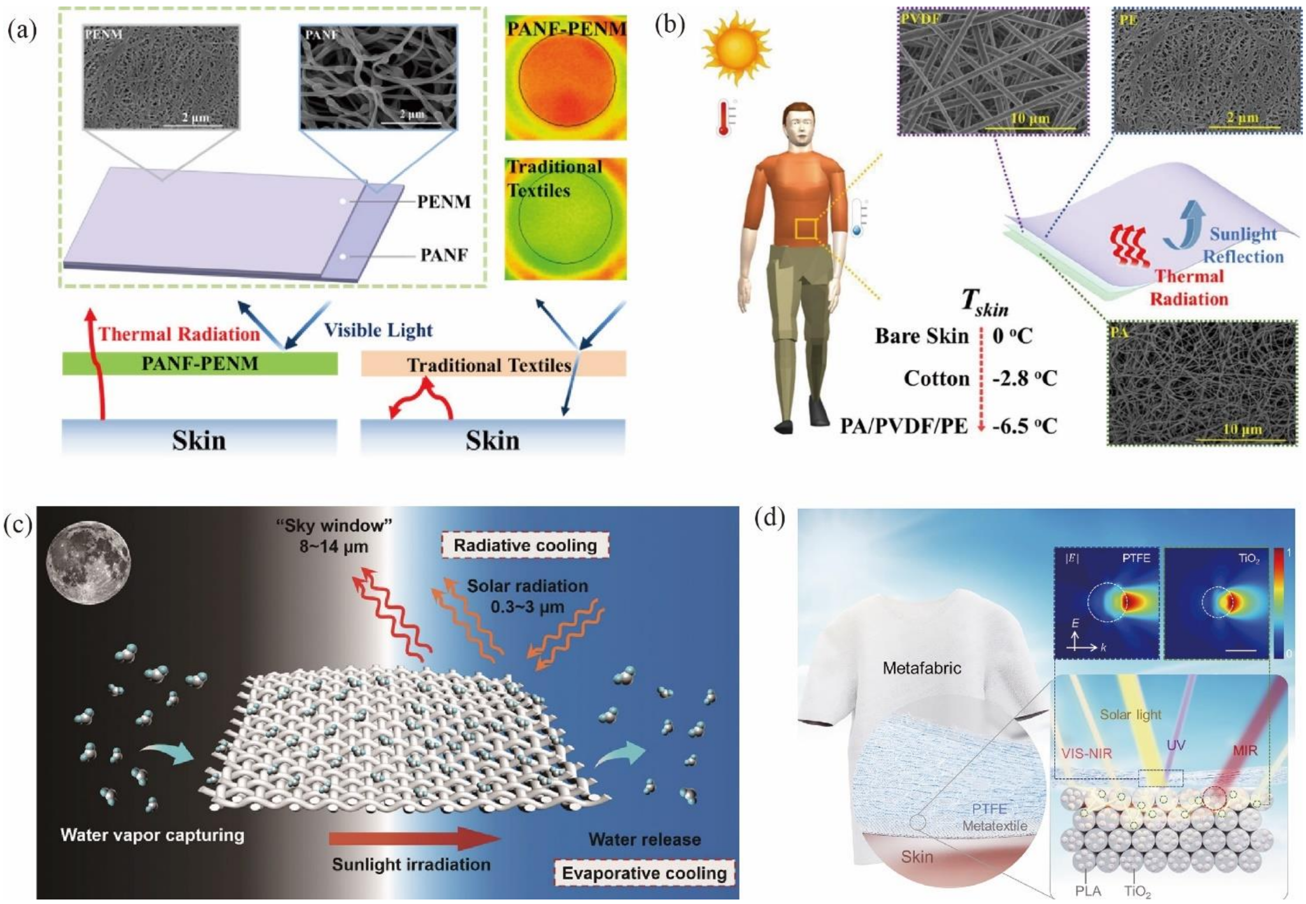

Figure 2-4 Structural design and working mechanism of the materials for radiative cooling. (a) PANF-PENM fabric [60]. (b) Tri-layered fabric [61]. (c) A composite flexible fabric with the synergistic effect [63]. (d) Schematic of the metafabric [62].

2.2.4 Textiles with regulated evaporative property

To avoid overheating, human body can lose heat by sweating and evaporation of sweat. If the sweat on the skin cannot be removed timely, human body still feel discomfort. Textiles with regulated evaporation properties to enhance sweat wicking and evaporation can be an efficient way to maintain body temperature. Naturally, water or sweat absorbed by fabric and clothing can evaporate driven by human body temperature. Traditional hydrophilic materials, like cotton, can absorb sweat but retain it, leading to wet sticky sensations and even excessively cold sensations. While hydrophobic fabrics made by polyester can repel water from outer and inner surface to block sweat transport from skin [51]. As excessive sweat on the skin may cause undesirable adhesion from wetted textiles and cold sensations. Recently, double-layer hydrophobic/hydrophilic fabrics [64], cotton fabrics printed with fluorocarbon-based hydrophobic finishes [65] and biomimetic fibrous Murray membrane [66] were designed, aiming to improve the sweat transfer through fabrics. However, those fabric may have reduced thermal insulation performance when they were wet, resulting in cold sensation and even hypothermia, which was quite normal for people with excessive sweat. Therefore, functional fabric exhibiting highly efficient sweat transport and little undesirable excessive cold is urgently required.

Intensive efforts have been done to utilize the asymmetric wettability of fabric for directional liquid transport to control human body thermal and moisture, which was defined as Janus technologies. Directional liquid transport was a common phenomenon in nature. Spider silk, cactus spines and shorebirds which can achieve directional liquid transport have inspired the design of Janus fabric. For those fabric, the inner layer was hydrophobic while the outer layer was hydrophilic. Sweat passed through the internal layer and arrived on the external layer and then evaporated to keep thermal comfort, minimizing the undesirable effect on wet adhesion and heat when the sweat removed. Dai et al. proposed a hydrophobic/super hydrophilic Janus polyester/nitrocellulose (PE/NC) textile with asymmetric hydrophilic conical micropores for directional liquid transport by a simple laser perforation method [67]. The PE/NC textile could pump the sweat from the hydrophobic layer to the super hydrophilic layer through asymmetric hydrophilic conical micropores from large to small (LTS) openings, which avoided sweat sticky and maintain body temperature. In addition, plasma polymerization [68] and deposition [69] were also widely used to fabricate Janus fabric for unidirectional liquid transport.

Furthermore, smart elements integrated with Janus fabric have been advanced means to effectively regulate thermal and moisture of human body. Inspired by the Janus wettability of lotus leaf, a Janus silk e-textiles were designed for wet-thermal comfort and highly efficient biofluid monitoring [70]. Silk materials were modified as a fabric substrate and sensing electrode to monitor sweat. The work integrated thermal and moisture comfort with sensing technology, presenting a new type of smart textiles for personal thermal management.

Cooling through evaporation has been proved to be efficient heat loss mode, which has attracted increasing attention as means of simple, cost-effective and green strategy to cool human body without external energy consumption. The heat taken away by evaporation could improve cooling effect. Li and co-workers [71] have prepared a single-sided superabsorbent cooling woven fabric by altering the arrangement of weft and warp yarns inside the fabric without any chemical treatment. The fabric showed a water absorbency of 370% and a water retention time of 90 min. The skin temperature test under outdoor environment showed that the temperature of skin covered by the cooling fabric decreased more than 5 °C and the cooling duration was much longer than other fabric. Integrated cooling (i-Cool) textile was developed by Peng et al from Stanford University for personal thermal and perspiration management. Thermal conductive matrix and sweat transport channel were integrated in one fabric system to work synergistically [72]. When people sweat, nylon 6 nanofibers absorbed water and wicked it from the skin surface to the outer surface by the sweat transport channel. The sweat spread on the outer surface to large area for fast evaporation. Meanwhile, body heat was transferred to the evaporation area, assisting fast evaporation. The results demonstrated 3 °C cooling effect could be realized.

Textiles with regulated evaporation properties have attracted widespread attention as they can manage thermal comfort of human body without energy consumption. However, those textiles adopted passive liquid transport technology, showing insufficient capability of sweat and lower cooling effect. More novel and smart textiles integrating with health care monitoring are still needed.

2.2.5 Responsive textiles for personal thermal management

Stimuli-responsive materials can alter their pattern, color and geometric structure autonomously or programmable upon small external signals [73]. In recent years, responsive textiles for personal thermal management have developed rapidly as it can interact with human body and ambient conditions by responding to variations of temperature, moisture, light, PH etc., which may lead to variations of the inner morphology of textiles, including pore switch, change of thickness or fiber structure and color. Those textiles demonstrate an adaptive response to diverse conditions, which are more energy efficient.

Phase change materials (PCM) were generally applied in the field of personal thermal management due to the stored latent heat, which could regulate temperature by absorbing and releasing heat during phase change process [74]. When the PCM absorbs heat and the temperature reached its melting point, it would transfer from solid to liquid state. And during the phase change process, the temperature of the materials maintained steady at the melting point until all became liquid. If the temperature reached the crystallization point, the material would release heat and change to liquid state. Researchers have successfully used to manage thermal comfort of human body by packing them into small bags and then putting into pockets of clothing or encapsulating into fibers or particles [75] and then coating on or fabricated in conventional clothing. PCM could respond to temperature changes between ambient environment and human bodies to achieve a comfortable thermal state. However, the large weight, short working duration and liquid leakage existing still limit its applications in various conditions [76]. Furthermore, the PCM treated fabric may have high water resistance and lower flexibility.

Another temperature sensitive materials are shape memory alloy (SMA). It can respond to the stimuli and change from the permanent shape to the temporary shape. The temporary shape was trained by mechanical deformation, which was time-consuming. In normal conditions, SMA keep permanent shape and when it is triggered by an external stimulus. Samples have been incorporated into a multi-layered protective fabric assembly to modify the thickness of the air gap for temperature-sensitive thermal insulation [77]. Nitinol-based SMA springs exhibited a bidirectional shape-memory effect in hot conditions, adjusting the microclimate structure and regulating the internal temperature. When these springs separated clothing layers, a continuously created air gap dramatically reduced the thermal conductivity as the air layer thickness and fraction increased, as demonstrated in Figure 2-5. The thermal conductivity ranged from 0.0116 W/(m·°C) to 0.0515 W/(m·°C) as the temperature increased from 150 °C to 400 °C. However, for some nitinol SMAs, the original shape could not be recovered unless an external load was imposed, indicating the limitations of cycled thermoregulation.

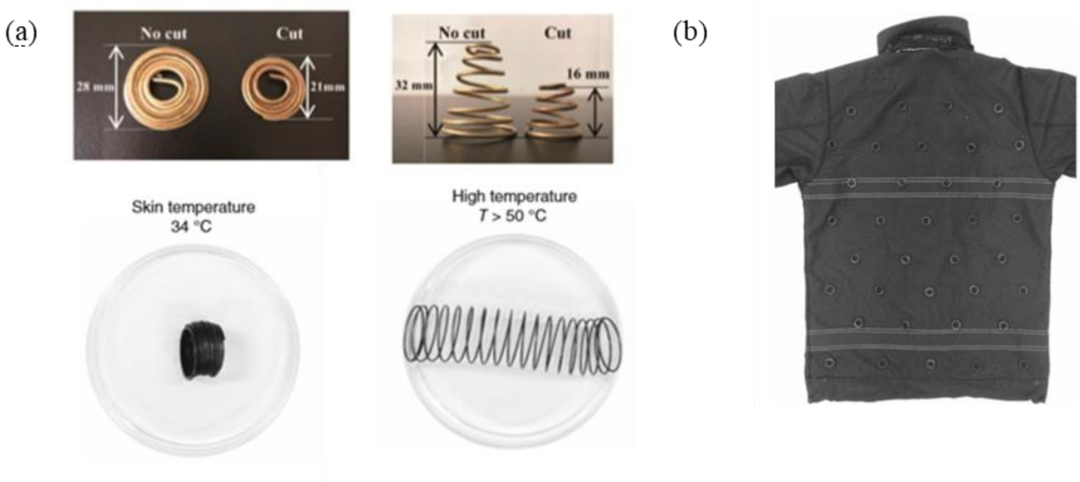

Figure 2-5 SMA springs applied for firefighter's turnout gear [77]. (a) Spring made by shape memory alloy. Under the normal temperature (i.e., 34 °C), the spring stay compressed state with small length/ height. If the temperature exceeds its transition temperature (i.e., 50 °C), the spring is stretched with large length/ height. (b) Back side of the clothing with SMA spring.

Wang et al. [15] reported a Janus textile, which was temperature-responsive, with reversible one-way water transportation and adaptive thermal management by coating two types of responsive polymers with different critical solution temperature (CST) on opposite sides of cotton fabric. Under high temperature conditions, liquid could be transported from the size with lower CST to the other side with upper CST and evaporated quickly. Upon exposure to an air-conditioned room or cold working conditions, the polymer liquid remained trapped on the inside of the fabric to maintain warmth. The expansion and contraction of the polymers and crosslinked polymer networks formed a reversible wettability gradient on both sides of the fabric, thus creating a capillary force gradient for the transportation of the liquid, and pore size changes to inhibit thermal convection. These two mechanisms worked in tandem to create adaptive thermal and moisture management, enhancing water evaporation by 50% and reducing temperature by 1.2-2.3 °C in hot conditions, and increasing 3.3 °C in cold conditions compared to pure cotton fabric.

Researchers from Shanghai Tech University developed a thermochromic silks (TCS) by introducing thermochromic ink coating on silk fiber [78]. When the heat source approached to the TCS fabric, the fabric color would change rapidly. The results showed that the reflectance of aq-Bl-28 TCS fibers increased more than 10% after heating, indicating its potential in temperature management and real-time dynamic textile displays. The tensile strength and toughness of TCSs were 443.1 MPa and 56.0 MJ m^{-3}, respectively, proving the possibility to be processed by industrial textile techniques. As each color had its own specific response temperature, the color showed different response rate, which could be applied in various scenarios. For example, in summer, the surrounding temperature was high enough to switch the TCS fabric to light color. The light-colored clothing received lower degree of heat radiation under sunlight, and then people worn such clothes would have a rather cool feeling. In contrast, the clothing was dark in cold conditions, absorbing more heat to keep warm. As the color changing was activated by temperature variations and work under solar irradiation, it would not make a difference if it was worn inside, covering by other clothes.

Compared with temperature sensitive materials, moisture or humidity sensitive materials are more effective as it can be activated by human sweat. Reversible humidity sensitive clothing to regulate personal thermal comfort was reported by Zhong's group by using a thermo-moisture responsive Nafion sheet from DuPont (Figure 2-6a-b) [79]. The first design mimicked the pores on skin surface. When people sweated, the inner side of the sheet absorbed liquid and swelled, creating a differential expansion between inner and outer layer which caused the pre-cut flaps bend upward and opened to generate pores. The humidity level and the temperature inside the fabric could be reduced. If the sweat stopped, the pores could close automatically. The second design inserted the bending sheet between fabric layers to achieve tunable thickness of fabric. If the humidity increased, the bending sheets would become flat, reducing of air gap between fabric layers to reduce thermal insulation. The insulation layer could recover when the humidity level reduced. Kim's group proposed human-skin-inspired adaptive textiles, which could respond to human sweat and create pores due to the bending of a moisture-driven actuator adhered on conventional fabric [80]. The mechanism of this smart textile was similar to the work above, demonstrated in Figure 2-6c. Nevertheless, this human-skin-inspired adaptive textiles required less responsive materials and the integration with conventional also improved its wear comfort. Researchers also developed the biohybrid films from genetically tractable microbial cells, which was moisture responsive. The film could reversibly change its shape rapidly when the surrounding humidity varied. A sandwich-structured biohybrid film for making sweat-responsive wearables is illustrated in Figure 2-6d [19]. The flaps could open when the wearer sweated, effectively removing the sweat on the skin and reducing the surface temperature. However, the shape changing of such moisture sensitive materials highly depended on the humidity level, resulting in nonuniform deformation of the clothing system. Meanwhile, the applied conditions of the sheet may be limited as the force was too small to open pores or created air gap if compressed by other fabric and clothing. The pre-cut flaps may affect the appearance.

Researchers in University of Maryland developed an IR-adaptive textile to manage personal thermal comfort directly [81]. A thin layer of carbon nanotubes was coated on triacetate-cellulose bimorph fibers to fabricate smart yarn with a bundle of metal fibers. When temperature and humidity increased, the yarn collapses and the meta-elements on neighboring fibers became closer, inducing resonant electromagnetic coupling. Then, the emissivity of the textile matched the body radiation to enhance heat dissipation. When cold or dry, the yarn became loose, reducing heat exchange. The state change of the yarn also accompanied with the increase and decrease of the pore size, showing in Figure 2-6e, indicating the synergistical work of adaptive gating of radiation with convection and evaporation. The infrared radiation could be regulated more than 35% when the skin temperature changed.

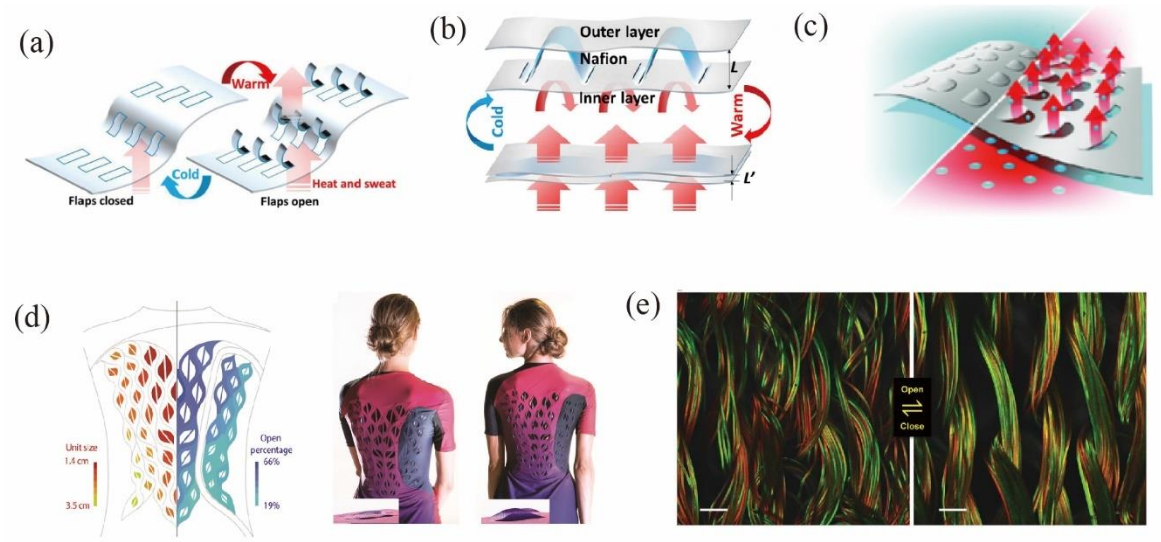

Figure 2-6 Illustration of the reversible deformation induced by moisture or humidity gradient. (a) Schematic of the Nafion sheet with openable flaps [79]. (b) Schematic of the Nafion sheet with reversible structure [79]. (c) Mechanism of the materials with openable flaps [80]. (d) Design of a garment prototype based on heat sweat maps [19]. (e) Fabric made by bimorph metafibers on open and close state [81].

Table 2-4 has summarized the typical responsive materials applied for personal thermal management, which also introduced the features, applications and some drawbacks. Textiles based on temperature sensitive materials, like PCM and SMA, humidity sensitive materials and infrared sensitive materials have been successfully developed in the past years, demonstrating significant heating and cooling effect on regulating temperature of humans. The limitation of responsive textiles is that they respond to external stimuli, which means that only when body or environment temperature and humidity changes, the fabric system works. In addition, the deformation degree is highly dependent on the stimulus. They would not make a difference if they were not in the proper positions.

For example, the light responsive materials would not work if they were covered by other fabric since they were unable to absorb light. The limited duration time is still a challenge for PCM and SMA. Sometimes, the responsive materials cannot reach comfortable microclimate in a short time due to the slower responsive speed.

Table 2-4 Responsive materials for personal thermal management.

Materials	Features	Applications	Drawbacks
Phase change materials [74]	Temperature responsive; phase changing	Cooling textiles	Heavy; Limited working time
Shape memory alloy [77]	Temperature responsive; strong deformation force	Textiles for thermal protection	Time-consuming training process;
Responsive polymers [15]	Temperature responsive; flexible	Textiles for one-way water transportation	—
Thermochromic silks [78]	Temperature responsive; color changing, thermal radiation	Sports clothing	Only for outer clothing
Nafion sheet [79]	Humidity sensitive; fast	Sports clothing	Weak deformation

	response speed		force
Biohybrid films [80]	Moisture responsive; skin friendly	Sports clothing	Weak deformation force
Bimorph fibers [81]	Moisture responsive; skin friendly; large-scale production	Sports clothing	Limited working range

2.2.6 Active cooling/heating textiles

The textiles mentioned above are all passive cooling/warming fabric and clothing as no other external energy is required, which is more energy efficient. However, the efficiency of the work and the occasions used may be limited. In this section, active heating/cooling textiles for personal thermal management with additional power input have been developed. Thermoregulation effects become more pronounced under varying thermal environments and activities specific to individuals.

In cold conditions, people may need extra heat for survival as bodies cannot provide sufficient energy due to the large amount of heat loss. Warming fabric and clothing with heating elements have come into an integrity and maturity chain of the textile industry. Based on Joule heating mechanism, by integrating electrically conductive materials, such as carbon-based materials, conductive polymers and metallic materials, fabric and clothing could generate constant heat to warm human body. Current clothing has successfully achieved uniform heat distribution to avoid excessive warming and cooling.

Compared with active heating, active cooling is far more challenging as many cooling devices are stiff and cannot integrate with garment properly. Implanting ventilation units into clothing to improve thermal exchange and accelerate sweat evaporation was efficient, which included fans (Figure 2-7a), and air-conditioned clothing and device designed by Sony (Figure 2-7b). Zhao et al has investigated the enhanced cooling performance of garments with ventilation fans and openings. They found that the manikin tests showed the ventilation units placed where had strong sweat could provide a more significant cooling effect [82]. During the human subject tests, the local skin temperatures at the chest and the scapula were observed to decrease significantly, while no significant change was observed in the mean skin temperature and core temperature of the whole body [83]. Sony's Reon Pocket could be used to manage the body temperature, which was operated by a smartphone. Peltier effect was applied by the devices to heat or cool human body. Liquid cooling garment (LCG) was the most common and simplest active cooling device, displaying in Figure 2-7c. The liquid circulation inside the tubes powered by a pump possessed advantages of superior cooling efficiency, dependability, and adjustable capacity. This mechanism efficiently removed heat at a rapid pace. At a flow rate of 224.5 mL/min, under a 45 ℃ ambient temperature, a maximum duration time of 3.36 hours has been successfully achieved [84]. Nevertheless, the cooling effect round the body may be not uniform. Heavy weight, bulky structure and great power consumption still exist.

Figure 2-7 Active cooling clothes. (a) Clothing with fans. Working of fans can enhance air flow inside the clothing, accelerating sweat evaporation for body cooling. (b) Cooling clothes designed by Sony. Smartphone-sized device called the Reon Pocket that operates like a mobile air conditioner for body cooling. (c) Liquid cooling garment. The tubes integrated with clothing are obvious.

Thermoelectric devices (TEDs) have gained increasing attention for personal cooling applications since they were solid state, containing small factors, and the cooling power was adjustable. Hong et al. [85] developed a highly flexible and wearable TEDs that could reduce the skin temperature more than 10 °C, and improve the coefficient of performance up to 1.5 and achieve long term operation (>8h). The TEDs could be seamlessly incorporated into garments with extended cooling and heating capabilities by integrating high-aspect-ratio TE pillars with double elastomer layers and air gap thermal insulation to attain minimal thermal conductance within the TEDs while still maintaining flexibility. The superior COP and localized cooling attributes highlighted its impressive energy-saving potential for personal thermal management applications. Figure 2-8 shows the wearable TED and the mechanism.

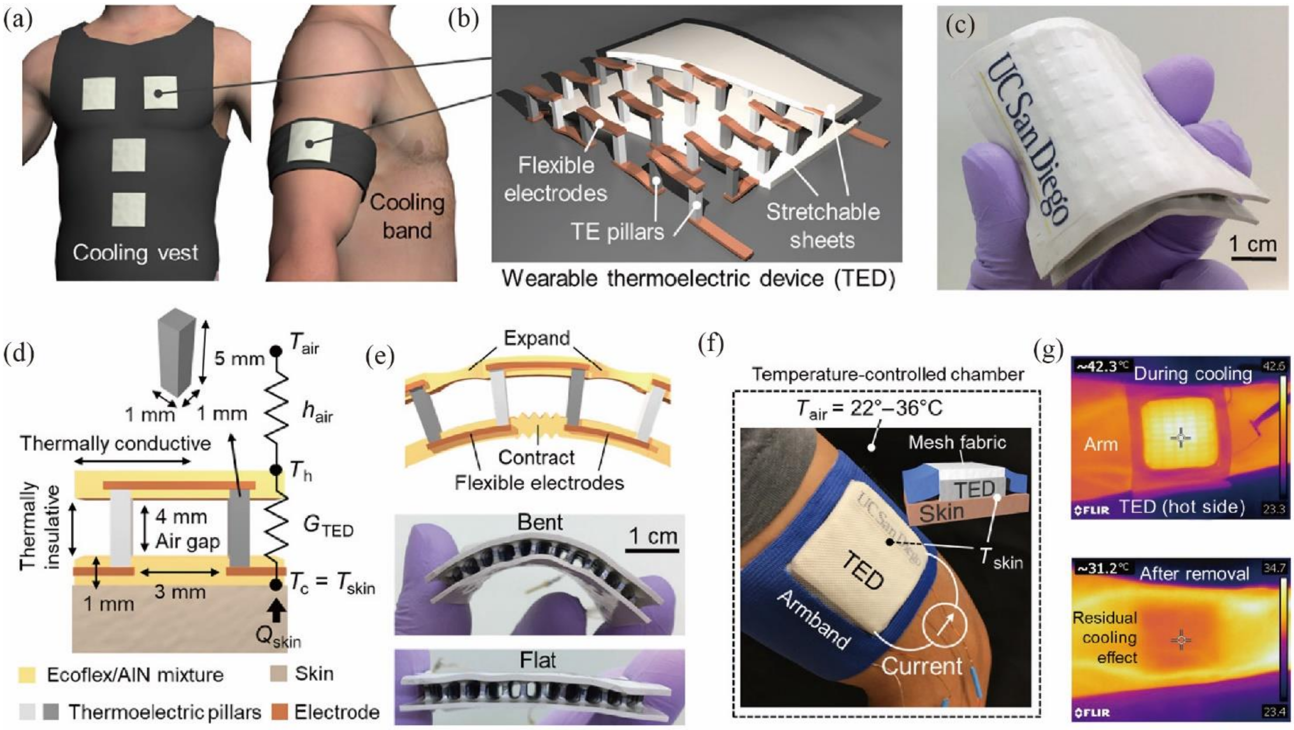

Figure 2-8 Wearable TED [85]. (a-d) Schematic illustration of garments with TEDs and the internal structures. (e) Schematic diagram showing the flexibility. (f) Image of the TED in human arm. (g) Thermal images when human skin was covered by TED and when TED was removed.

Joule heating was the most common, efficient and simplest approach for warming clothes. For those warming fabric, large amount of energy often consumed as they would stop generate heat without power input. Compared with warming effect, cooling effect was more challenging. Garments with ventilation fans often followed by openings, which resulted in aesthetic problems and the degradation of mechanical properties. All those systems required a power source, which was normally battery. Therefore, they may not work for a long time due to the energy density and the maximum discharge current.

2.3 Textile technology with soft robotics

Soft robotics (Figure 2-9) are a quick developing field in recent years. Collaborative efforts have been done to combine soft robotics with textiles (Figure 2-10) to design soft wearable robots [18, 86, 87]. For example, soft robotics embedded into fabric and clothing could assist body movement, including walking, running and sit-to-stand motions [18]. A soft robotic compression garment was designed to apply pressure and warmth on the shoulders rhythmically, which successfully improved the meditation experience and helping individuals with focused attention [88].

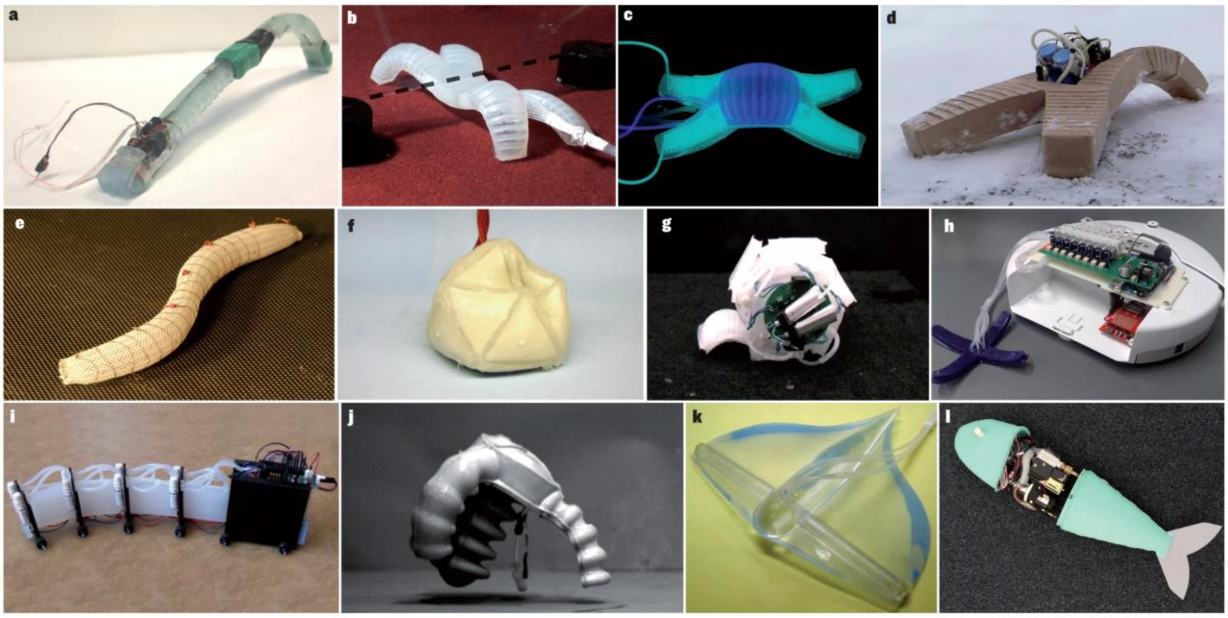

Figure 2-9 Demonstration of soft robotics systems inspired by various biological systems [89].

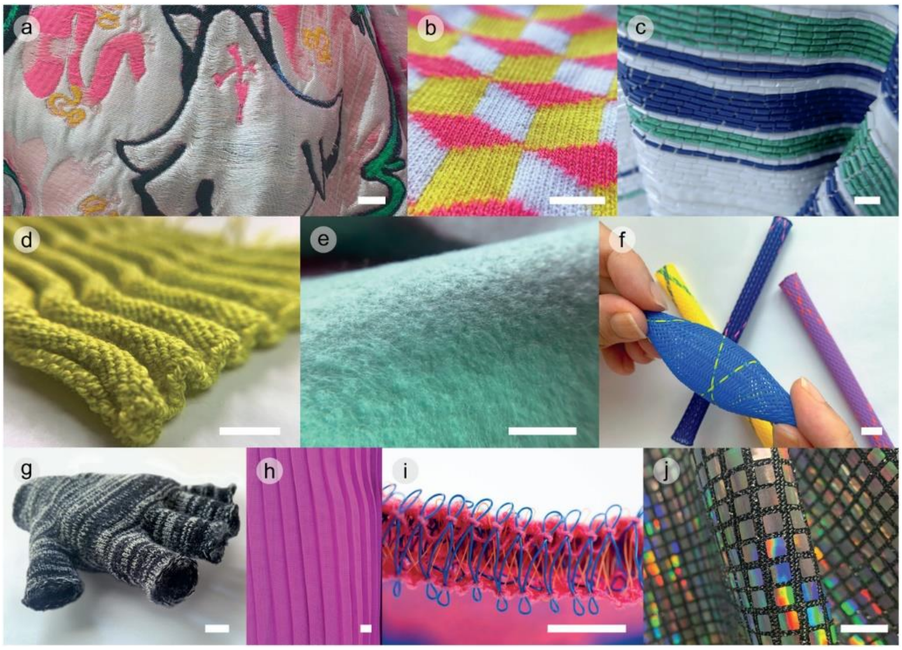

Figure 2-10 Demonstration of textiles made by different materials and fabrication methods [18].

Cui et al. proposed the soft robotic fabric (SRF) for personal thermoregulation [90, 91]. The SRF had an air-driven system inspired by soft pneumatic robotics. Flexible silicone (Ecoflex TM 00-30) was selected to fabricate inflatable soft actuators for low viscosity. The thermal insulation of fabric could be modified by controlling the volume of trapped air to change fabric thickness. The results showed that the thickness of SRF could increase more than 12 times after inflation, creating large air gap between fabric layers or fabric and human body to block heat loss from body skin. The adjustable thickness means adjustable thermal insulation, showing the potential of SRF for dynamic thermal management. Meanwhile, the fabric could lift an object 270 times heavier than its own weight, indicating that the fabric had superior strength to undertake external pressure and maintain air space and thermal insulation. The use of silicone rubber still resulted in large weight, weak air permeability, fragility and inadequate wearability performance that limited the practical application to PTM.

However, it exhibited the potential of soft robotics integration with fabric and clothing to be applied in personal thermoregulation. Figure 2-11 illustrates the design of the soft robotic fabric.

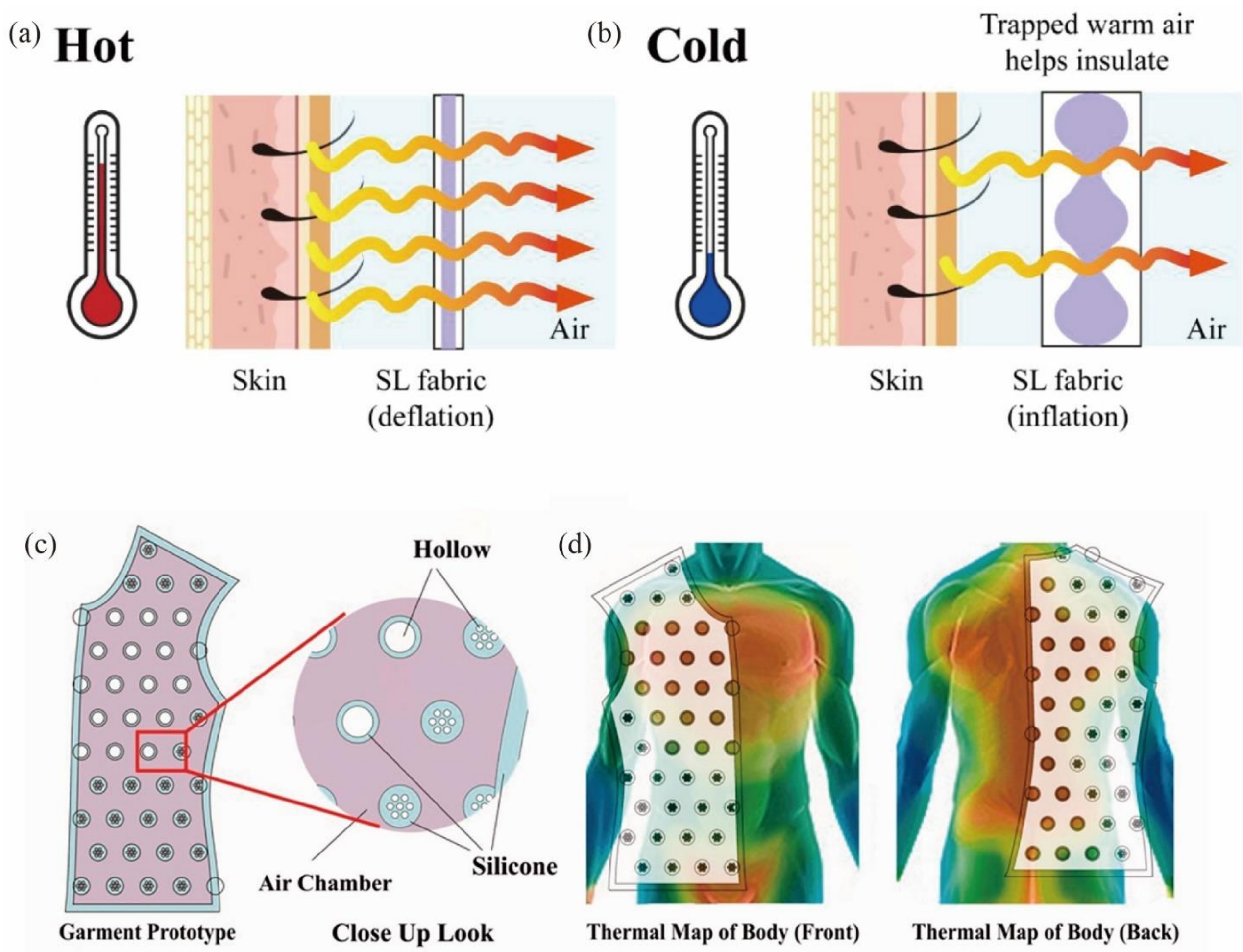

Figure 2-11 Soft robotic fabric [90]. (a) SL fabric in deflated state to increase thermal transfer from skin to hot environments. (b) SL fabric in inflated state to reduce thermal transfer from skin to the cold environment by trapping stable air as insulation material. (c) Design of clothing prototypes according to human thermal map. (d) Front and back view of clothing prototypes.

2.4 Summary

The contents above introduce design principles of textiles for PTM and summarize outstanding works in recent years. Many works have been done to design functional fibers, which can be sewn, woven or knitted by commercial machine, fabrics and other devices. In order to improve thermal regulation, fabric system may have more than one heat transfer mode. Synergistical effect of different mechanism were more popular for enhanced thermal properties. Smart textiles, including responsive materials and active heating/cooling textiles, have gained intense attention in recent years. Combining the advantages of passive textiles and active cooling/heating textiles could provide an avenue in the design of an efficient fabric and clothing for PTM. The studies on soft robotic and textiles also provide a new pathway in developing fabric and clothing for adaptive personal thermal management.

2.5 Research gaps

Through the continuous efforts of researchers, significant progress has been made in the fields of fibers/yarns, garment fabrication, and advanced materials and structures for adaptive personal thermal management. These novel fabric and clothing can help cool the human body's temperature by both insensible perspiration and sweating, warm the body by providing thermal insulation, and protect against strong solar ultraviolet radiation. Smart clothing, which can sense changes in the environment or body and respond accordingly, is also fabricated. Some methods have successfully achieved personal thermal management under different conditions. Nevertheless, challenges related to poor air permeability and bulky nature limiting body movements have not yet been addressed, impeding practical use and industrialization of current fabric and clothing.

Several key issues including inefficient ability to adapt with the dynamically varied human thermo-physiology and environmental conditions [92], inadequate working range of the temperature and humidity and heavy cost of materials and fabrication methods still exist. In order to achieve adaptive thermal management, researchers have tried to explore materials and structures that can respond to temperature and humidity variations directly, which are classified as passive due to their operation modes. For example, shape memory allays combining with firefighters' suit can change the thickness of the fabric systems to affect thermal insulation properties [77]. Specifically, introducing insulation is a representative passive heating technology, which has low cost and simple implementation. However, the reliability, mechanical properties and durability still limit their practical applications. Active heating/cooling designs are actuated by external power, including thermoelectric devices [85], fans and air conditioning systems [93]. Among them, flexible thermoelectric devices, excellent alternative to cooling textiles, are soft and easy to integrate into apparel, which can drop skin temperature efficiently. However, a large amount of energy is consumed due to continuous work of the devices. Moreover, those additional active control devices not only increase the cost and weight of the fabric system but also are followed by complicated installation process. Hence, only few research focusing on active control of thermal comfort have been proposed for adaptive personal thermal management. The recently developed materials and fabrics including the nanomaterials are often expensive, limiting the large-scale production and commercialization. Chemical treatments are widely used in the fabrication process, which are sometimes toxic to human body and often less environmental-friendly. The research gaps were summarized. The limitations and potential risks of existing technologies were evaluated, including their inability to adapt to variable climates and unpredictable environmental impacts, as well as the risks associated with scalability, energy efficiency, and accessibility. Research is therefore needed to develop a fabric and clothing system that combines the advantages of passive platforms with the dynamic adaptation of active control.

Chapter 3 Methodology

3.1 Introduction

Following the literature review and theoretical framework discussed in previous chapters, this chapter describes the research methodology of this study, explaining the techniques, strategies and evaluation methods employed to achieve the stated research objective. According to the thermal management mechanism, the study was carried out from three aspects, which include: (i) increasing or decreasing the thermal resistance of the fabric and clothing system to influence heat transfer by conduction; (ii) enhancing or weakening the air flow of the body-clothing-environment system to change the thermal convection; (iii) varying the emissivity or reflectance of fabrics and clothing to control thermal radiation. Thermal properties can be regulated by more than one principle to achieve enhanced functions. Based on the research goal, soft robotic fabrics and clothing for adaptive personal thermal management could be fabricated in our research. Soft robotic fabric and clothing are generally flexible material assemblies consisting of soft robotic elements or actuators, control units, and substrate fabric. Control units are added to fabrics to determine deformation and actuation, programmably changing significant structural parameters to achieve personal thermal management. Commercial fabrics and self-designed fabrics are both selected as substrate fabrics, which may be decided by the final use of clothing. The research flowchart is shown in Figure 3-1.

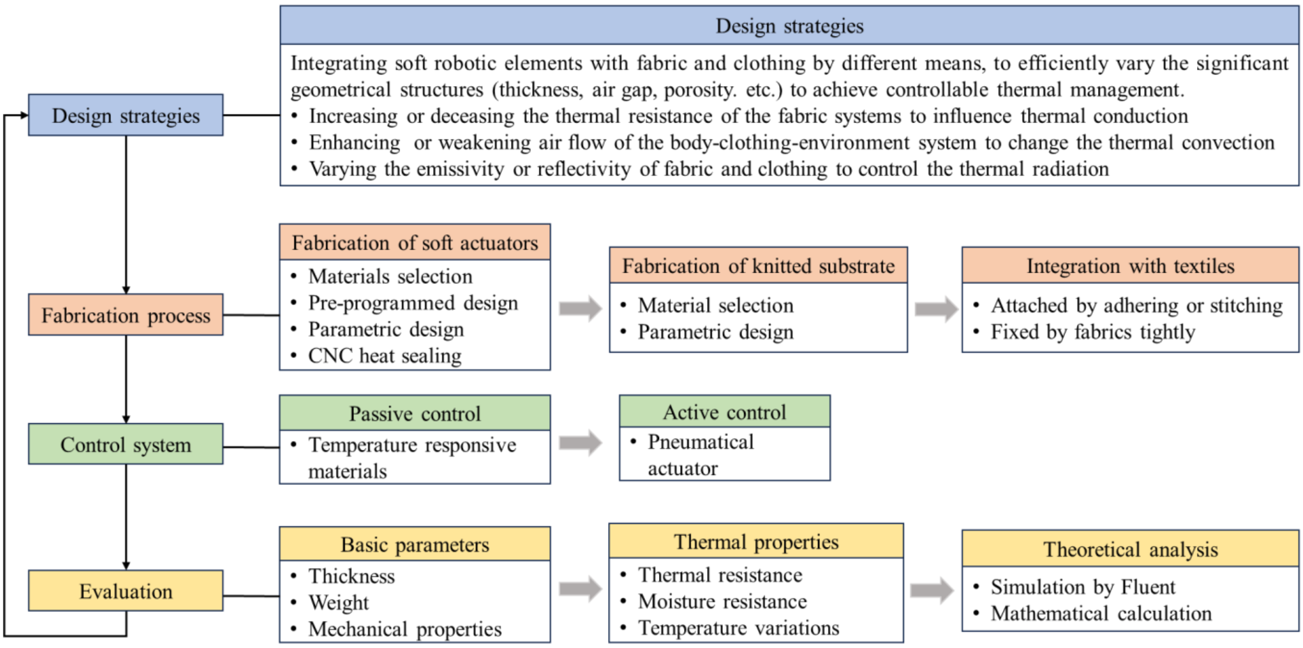

Figure 3-1 Research flowchart for this study. Design strategies are fundamental to fabric and clothing design. The fabrication process includes the fabrication of actuators and knitted substrates, as well as the integration of actuators and other fabrics. The control system refers to both passive and active control of the proposed fabric and clothing.

Design strategies are fundamental to fabric and clothing design. The fabrication process includes the fabrication of actuators and knitted substrates, as well as the integration of actuators and other fabrics. The control system refers to both passive and active control of the proposed fabric. Based on the research flowchart shown in Figure 3-1, the following studies were conducted based on the design strategies mentioned above. Soft robotic elements are integrated with fabrics and clothing in different ways to achieve controllable thermal management. The geometrical structure of fabrics and clothing, such as thickness, air gap, and porosity, can be changed by the deformation of soft robotic elements, which can lead to variations in thermal properties. The following studies focus on the dynamic thermal management of air gap, fabric thickness, or radiative properties through the control of soft robotic actuators. In the fabrication process of the proposed fabric and clothing, consideration should be given to the comfort and feasibility of wearing. On the other hand, the difficulties of fabrication methods, durability and aesthetics also need to be considered for rapid fabrication, large-scale production and commercialization in the future. When designing soft robotic actuators, the structure of the actuators should be optimized to obtain optimal thermal and wear comfort. Material selection must take into account basic parameters, thermal properties and durability.

3.2 Generation of the concept

As summarized in Chapter 2 (Literature Review), still air, which is a natural resource that can be infinitely utilized, is an excellent thermal insulator. The advantages are lightweight, almost no cost, and green and pollution-free. On the other hand, it is well known that the thermal insulation properties of fabric and clothing can be determined by the still air stored inside the clothing because air is the best thermal insulator in nature. Traditional clothing made of cotton, wool, and down fiber all have excellent thermal insulation due to the still air entrapped by the fibers. In the natural world, many creatures exhibit the remarkable ability to alter their physical state to acclimate to temperature shifts. The dove has a dense plumage that facilitates heat dissipation in warm environments (Figure 3-2a). When ambient temperature drops, fluffy feathers can retain more stagnant air near the body, minimizing heat loss (Figure 3-2b). Drawing from the adaptive behaviors observed in doves under diverse environmental conditions, we have developed clothing that incorporates thermally adaptive insulation technology. This technology enables the reversible alteration of the textile air gap between fabric layers, thereby dynamically adjusting the fabric thickness to regulate heat transfer between the environment and the human body.

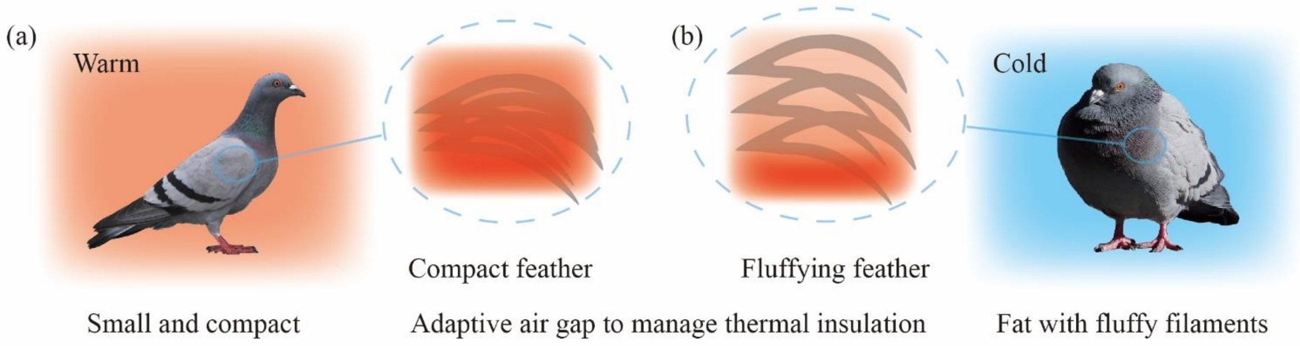

Figure 3-2 Bioinspired design of thermal insulation. (a) Dove with compact feather under warm conditions (left). Compact feather allowing more heat transfer (right). (b) Dove with fluffy feather under cool conditions (right). Fluffying feather blocking heat transfer (left).

In addition, as summarized in the literature review, much research has been done to manage thermal radiative properties. Among them, materials inspired by squid skin have successfully achieved dynamic thermal radiation by controlling the surface microstructure to adjust infrared reflectance [94-96]. From the foregoing, it can be concluded that the management of thermal radiation depends on the properties of the surface. Inspired by this theory, we designed a dual-mode textile that can exhibit reversible thermal radiative properties, which can transmit between the lower reflectance layer and the higher reflectance layer. In the warming mode, the fabric surface has a lower solar reflectance, while in the cooling mode, the fabric surface exhibits a higher solar reflectance to achieve radiative cooling.

In this thesis, three innovative fabrics and clothing designs are proposed, each tailored to manage thermal insulation and radiation properties effectively. The first textile is engineered for individuals working in extremely hot environments, such as fire scenes or high-temperature workshops, to protect against heat stress. The second fabric is optimized for cold conditions, aiming to reduce heat loss and adapt to fluctuating temperatures, thereby maintaining thermal comfort in dynamic environments. The final fabric is designed for summer days, providing adaptability to rapidly changing weather conditions, from sunny to rainy or stormy, ensuring comfort throughout the day.

The fabrics and clothing discussed in Chapter 4 are innovative soft robotic textiles designed for passive thermal adaptation in hot environments. These textiles incorporate soft robotic elements capable of transitioning between deflated and inflated states, thereby creating adjustable air gaps between fabric layers. The thickness of these air gaps, which are critical for thermal insulation, can be precisely managed through the manipulation of the soft robotic elements. Given that still air serves as an excellent thermal insulator, the dynamic control of air gap thickness allows for effective thermal management. In this system, soft robotic elements function as an intermediate layer within the garment, encapsulated by a flame-retardant outer shell fabric. This configuration not only forms stable air gaps but also minimizes airflow within the fabric system, enhancing insulation. The use of a low boiling point fluid within the actuators allows them to respond autonomously to temperature fluctuations, passively controlling their deformation. This integration of soft robotics within textile engineering highlights a novel approach to optimizing thermal insulation and protection in high-temperature conditions.

The fabrics and clothing detailed in Chapter 5 are advanced textiles driven by soft pneumatic actuators, developed for precise thermal regulation and body warming in cold conditions. This fabric system mirrors the structural design of the textiles discussed in Chapter 4, utilizing pneumatic actuators to dynamically adjust the air gap in response to changing environmental conditions. This capability enables the fabric to effectively adapt its thermal insulation properties. The selected cover fabric is both breathable and waterproof, offering robust protection from wind, rain, and storms while maintaining wearer comfort. Unlike the passive control mechanism employed in the previous chapter, the active control facilitated by the pneumatic actuators provides enhanced safety and intelligence. This integration of soft robotics into textile applications exemplifies a cutting-edge approach to achieving adaptive thermal management, thereby optimizing protection and comfort in varying cold environments.

The textiles explored in Chapters 4 and 5 focus on creating an air gap through the deformation of soft robotic elements, serving as the intermediary layer within the fabric system. While many fabrics naturally form air gaps, particularly in three-dimensional (3D) structures, Chapter 6 advances this concept by proposing a breathable 3D knitted fabric enhanced with soft robotics. This fabric is designed for optimized thermal insulation and radiative cooling. In this chapter, we introduce a 3D knitted fabric that incorporates pneumatic actuators, leveraging the deformation capabilities of soft robotic elements. The integration allows the fabric to dynamically transition between 3D and 2D states.

This transformation not only alters the fabric's thickness but also modulates its reflective properties. By embedding soft robotics within the 3D knitted structure, the fabric achieves superior adaptability in managing both thermal insulation and radiative properties, representing a significant innovation in textile engineering for environmental responsiveness.

3.3 Models and design rationales

3.3.1 Design principle of fabric thermal insulation

The thermal insulation properties of materials are determined by thermal conductivity or thermal resistance. Thermal conduction refers to the transfer of internal energy from a high temperature region to a low temperature region, usually through the movement of electrons or lattice vibrations within a material and microscopic collisions of particles between two adjacent materials [97], shown in Figure 3-3a-b. The mechanisms behind thermal conduction, including electronic transport and phonon transport, are strongly influenced by the lattice structures and chemical components involved [98], shown in Figure 3-3c. Maintaining the core temperature of the human body within a narrow range requires the selection of appropriate clothing. This garment plays a crucial role in heat dissipation, acting as a medium through which heat flows from the body's skin to the surroundings, and provides thermal insulation in extremely cold or hot conditions. Fourier's Law, an important scientific principle, states that the rate of heat transfer through a medium is proportional to the negative gradient in the temperature, viz.,

$$Q = -\lambda A \cdot \frac{\partial T}{\partial x} \tag{3-1}$$

where Q is the heat flux, λ is the thermal conductivity coefficient the system, and ∂T/∂x is the temperature gradient. In the steady state, heat transfer is mainly characterized by effective thermal conductivity, which can be controllably by introducing highly conductive composite fillers or creating highly porous structures filled with thermally insulative phase such as encapsulated still air.

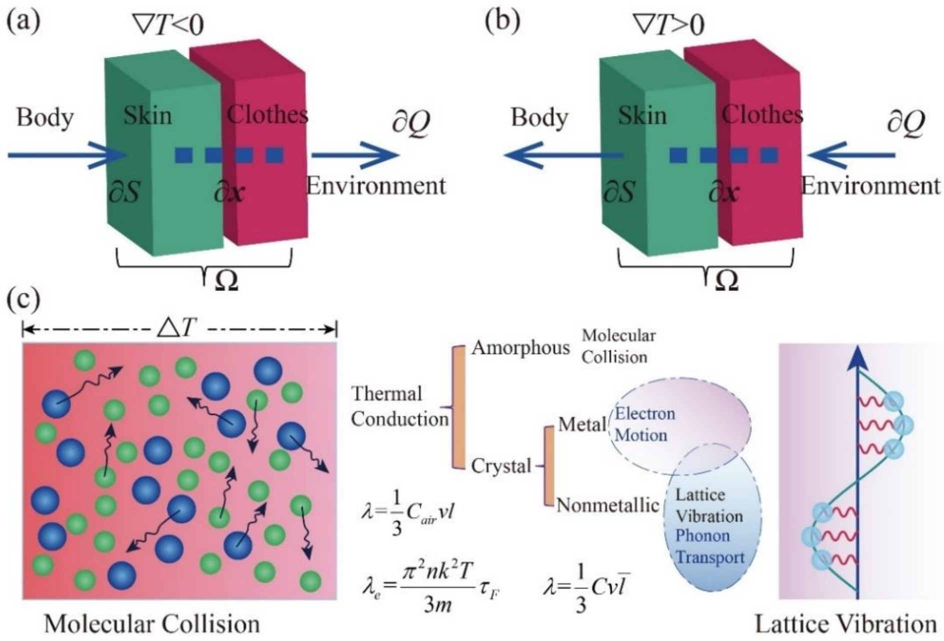

Figure 3-3 Schematic of thermal conduction. (a) Thermal resistance models of heat transfer from body to environment. (b) Thermal resistance models of heat transfer from environment to body and (c) Two main modes of thermal conductivity including lattice vibration and electron motion [4].

In fact, thermal conduction within the system of the human body and clothing is often an unsteady heat transfer process. For any material point $\boldsymbol{x}$ within the system domain Ω, the heat conduction equation deriving from the first law of thermodynamics (also called the conservation of energy) should be satisfied:

$$\rho(\boldsymbol{x})\cdot C(\boldsymbol{x})\cdot \boldsymbol{T}'(x)+div(\boldsymbol{q}(\boldsymbol{x}))-Q(\boldsymbol{x})=0,\ x\in\Omega \tag{3-2}$$

where $\boldsymbol{\rho}(\boldsymbol{x})$ and $C(\boldsymbol{x})$ are the density and the specific heat respectively of the material point and $T(\boldsymbol{x})$ and $q(\boldsymbol{x})$ are the local temperature and heat flux respectively. On the basis of the Fourier's law, the heat flux $q(\boldsymbol{x})$ is given as:

$$q(\boldsymbol{x})=-\lambda(\boldsymbol{x})\cdot\nabla T(\boldsymbol{x}) \tag{3-3}$$

where λ is the thermal conductivity of the material points $\boldsymbol{x}$. The process of heat transfer from skin through clothing to the environment (or the opposite path) can be equivalent to a series model of heat resistances. Moreover, heat always transfers along the decreasing direction of the temperature gradient and the total energy of the system in the model is given as:

$$Q=\frac{|T_S-T_{clo}|}{\delta/S\lambda}=\frac{\nabla T}{R_\lambda},\ \text{where } R_\lambda=\frac{\delta}{S\lambda} \tag{3-4}$$

where R_λ is the thermal resistance of the system, which depends on the thermal conductivity of materials and the cross-sectional area of structures. It can be found from Eq. (3-4) that the thermal resistance of a system increases with the decrease of the effective sectional area and thermal conductivity. For a combined system including both skin and clothing, the thermal conductivity of the skin is generally intrinsic without dependence on external effects. Therefore, the effective thermal conductivity properties of a microclimate system can mainly be tailored by adjusting the spatial microstructures and materials of the fabrics and clothing.

3.3.2 Design principle of fabric thermal convection

The human body exchanges heat with its surrounding air or forced wind through convective heat transfer, which is mainly determined by the air permeability of clothing and the external flow velocity of air. Warmer bodies can cause the air around them to become warmer, and this heated air rises, generating a natural convection boundary layer. Notably, if the air is stationary, it is considered natural convection. Conversely, if the air is in motion, it is classified as forced convection. Usually, convection is exclusively associated with fluids. The Newton's law stipulates that the rate of convective heat loss is directly proportional to the temperature difference between the body and its surroundings, under the influence of either natural or forced convection [99].

$$Q = hA\Delta T \tag{3-5}$$

where Q is the convective heat flow rate, h is the convective heat transfer coefficient, A is the surface area of the object, and ΔT is the temperature difference. Natural convection occurs due to the density gradient of a fluid caused by the temperature difference, without any external sources such as fan, pump, or air conditioner. Forced convection is generated with the heat ventilated by airflow driven by an external pumping device, wind, or body movement.

3.3.3 Design principle of fabric passive radiative cooling

Radiant heat dissipation by the human body is an important part of personal thermal management. Passive radiative cooling also a hot topic as surface of Earth can cool themselves by radiating to the outer space through the atmospheric window (8-13 μm). Mid-IR (MIR) thermal radiation with a peak of 9.5 μm, which is emitted by human body, is in the range of 8-13 μm. Thus, passive radiative cooling has been an efficient approach to achieve personal thermal management. Radiation is the process by which the body gains heat from hot surroundings, or rejects heat toward a cold environment, based on the transfer of electromagnetic radiation with the thermal motion of particles in matter. The degree of particle motion that leads to dipole oscillation or charge-acceleration for conversion from thermal to electromagnetic radiation is characterized by temperature. Thus, the heat transfer of radiation is highly sensitive to temperature. The Stefan-Boltzmann law states that the total radiant heat power is proportional to the fourth power of the absolute temperature of the emitting surface [100].

$$Q = \varepsilon a|T|^4 \tag{3-6}$$

where |T| represents the absolute temperature of the body, ε is the emissivity of the body, and a is the Stefan–Boltzmann constant. In the field of radiative thermoregulation, the potential for heating or cooling is promising. This is possible through various heat transfer controls which can be achieved by adjusting the emissivity and reflectivity of the chosen material.

This section provides an in-depth analysis of PRC models and calculations, which are fundamental building blocks for accurate assessment of cooling magnitudes of various types of cooling systems, including radiative cooling systems [101]. The net cooling power (P_{net}) associated with radiative cooling, a primary focus of this section, is calculated based on several key factors, including the outgoing radiative power generated by the cooling structure (P_{rad}), the amount of atmospheric radiation (P_{atm}) incident on the structure, solar irradiance (P_{sun}) incident on the structure, and non-radiative heat ($P_{nonradiative}$) absorbed by the structure when considering the surrounding effects. The heat balance of the radiative cooler can be described in Eq. (3-7) to Eq. (3-13) and the schematic is shown in Figure 3-4.

$$P_{net} = P_{rad} - P_{atm} - P_{sun} - P_{nonradiative} \quad (3\text{-}7)$$

Where, $$P_{rad} = 2\pi \int_0^{\frac{\pi}{2}} \sin\theta \cos\theta \int_0^{\infty} I_B(T_S, \lambda)\varepsilon(\lambda, \theta)\, d\theta d\lambda \quad (3\text{-}8)$$

$$P_{atm} = 2\pi \int_0^{\frac{\pi}{2}} \sin\theta \cos\theta \int_0^{\infty} I_B(T_{amb}, \lambda)\varepsilon(\lambda, \theta)\varepsilon_{atm}(\lambda, \theta)\, d\theta d\lambda \quad (3\text{-}9)$$

$$I_B(T, \lambda) = \frac{2hc^2}{\lambda^5 (e^{\frac{hc}{\lambda kT}} - 1)} \quad (3\text{-}10)$$

$$\varepsilon_{atm}(\lambda, \theta) = 1 - t(\lambda)^{\frac{1}{cos\theta}} \quad (3\text{-}11)$$

$$P_{sun} = 2\pi \int_0^{\infty} I_{sun}(\lambda)\varepsilon(\lambda, \theta_{sun})\, d\lambda \quad (3\text{-}12)$$

$$P_{nonradiative} = h_c(T_{amb} - T_s) \quad (3\text{-}13)$$

Where T_S is the surface temperature of the material. T_{amb} is the ambient temperature, ε_{atm} represents the spectral and angular atmospheric emittance. The spectral and angular emissivity of a radiative cooler, ε(λ, θ), is a key factor that determines the amount of heat dissipated from the device. Additionally, the atmospheric transmittance, t(λ), and the atmospheric emissivity, ε_{atm}(λ, θ), are functions of wavelength and zenith (θ) and account for the absorption of radiation by the atmosphere. The combined convection and conduction heat transfer coefficient, h_c, also influences the rate of heat loss from the cooler.

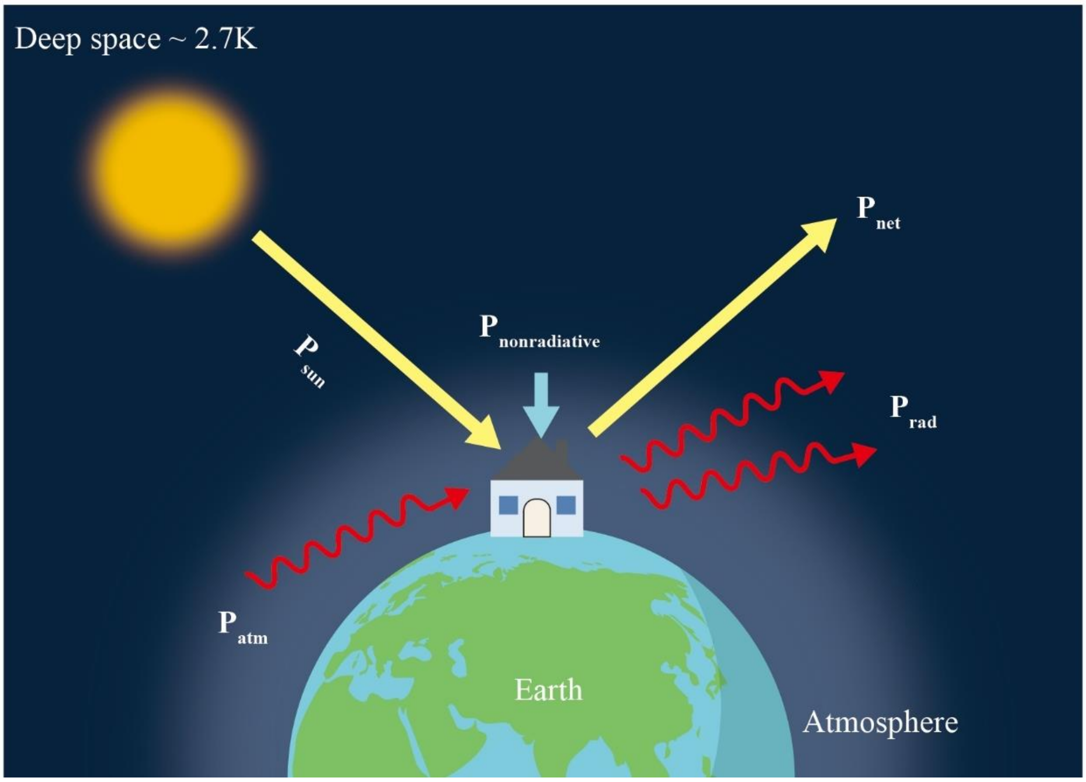

Figure 3-4 Schematic of energy flows into and through a radiative structure.

According to the energy balance theory above, net cooling power is the comprehensive manifestation of the four factors. In order to achieve passive cooling properties, P_{atm}, P_{sun} and $P_{nonradiative}$ should be minimized. Specifically, the surface of the materials must be designed to have strong emission at the wavelength range between 8 and 13 μm, which corresponds to a region of the electromagnetic spectrum where the atmosphere is transparent. In addition, the coating must exhibit high reflectivity at visible and near-infrared (Vis-NIR) wavelengths, which are typically utilized for astronomical observations.

3.4 Research methods

3.4.1 Fabrication of soft robotic elements

The proposed textile fabrication process should be viewed from two perspectives, clothing system and the control system. The fabric and clothing system is the core component of the proposed textiles. This fabric can be constructed using commercial machines, which operate as a dependent system that manipulates thermal properties by adjusting the geometric structure. In addition, traditional garments can be transformed to achieve preferred properties by integrating newly designed components. As illustrated in Figure 3-1, the fabric fabrication process encompasses three distinct stages: fabricating soft robotic actuators, fabricating the knitted substrate, and integrating the actuators and the substrate. The actuators are manufactured using airtight fabric to construct pneumatic elements. The heat-sealing technique is applied to seal the airtight fabric into actuators with the desired shape. Furthermore, weft knitting technology is employed to prepare the substrate for actuators. The final step is to amalgamate the actuators with the substrate to ensure the resilience and stability of the entire fabric system. In conclusion, the proposed fabrication process aims to develop textiles that can control thermal properties and integrate new functionalities through novel fabrication techniques.

Soft robotic elements can be made of soft and flexible materials, such as coated fabric, silicone tubing, and elastomer, which determines the deformation method, intensity, and angle of the fabric. The raw materials of the components are environmentally friendly and durable, especially with extreme wear comfort. Three steps are generally included: (i) The shape deformation of soft actuators is designed firstly and accurately by precise calculation to achieve programmable actuation. (ii) Materials and fabrication methods are selected according to their properties and end-use. (iii) Post-processing would be carried out by combining with or treating other materials to functionalize the performance of soft robotic actuators.

3.4.2 Fabrication of knitted substrate

Since the soft robotic elements can be separated units or a complete unit, fixing these elements can be a challenge due to slippage. To fix these elements, knitted substrates are proposed and designed in these studies to ensure a stable fabric and clothing system. Generally, knitted substrates have three functions: i) Fix soft robotic elements to ensure a stable clothing system. ii) Behave like a substrate for changing shape. iii) Provide stretchability for dimensional variations due to deformation of soft robotic components. The knitted thermal substrates involved in these studies could be fabricated using a computerized flat knitting machine. The CMS 822 ki multi-gauge is ready for anything: it can implement varieties of multi-piece knitting highly flexibly and productively. Weft knitted fabric is very elastic, stretchable and comfortable to wear. It does not struggle easily and is very cost-effective.

3.4.3 Integration of soft robotic elements and knitted substrate

The most important step is to integrate soft robotic elements into fabric and clothing, which are often applied depending on the end applications and materials used. For the textiles discussed in Chapter 4 and 5, the soft robotic elements are inserted into the knitted substrate channels and then covered by the outer shell fabric based on the end use. For the textile proposed in Chapter 6, the soft robotic elements are stitched together with the 3D knitted fabric to achieve desired deformation.

3.4.4 Design of control system

The key to the control mechanism is dynamic management. Internal characteristics, such as pressure, volume, and stress, of soft robotic elements determine the extent of deformation, affecting the transport of heat and moisture through fabrics. As the internal characteristics change, the geometric structure of the fabric changes, resulting in varying pore size, thickness and radiative properties. According to the requirements of fabric and clothing on appearance, comfort, weight, durability and washability, the control-mechanical device would be designed to have both maximum thermoregulation efficiency and excellent wearable properties. The wearer of the device and the soft robotic elements would have no visible difference from conventional attires and would not be affected in terms of color or texture choices. The control system may be active or passive. The active control system consists of a pump, a sensing & control unit and a power unit. The entire system would be powered by small portable rechargeable batteries. They apply electrical energy to change the internal pressure or volume of the soft robotic elements, by air inflation & deflation of the pump or evaporation-condensation process of the responsive materials. The sensing & control unit can respond to changes in heat and humidity and act adaptively. In addition, the passive control system containing responsive materials, such as phase change materials, which can provide sufficient force for deformation of the fabric system without external energy consumption, was also applied.

3.5 Evaluation methods

3.5.1 Experimental methods

Proposed and designed fabric and clothing must undergo a comprehensive assessment to assess whether the applications meet the objectives. The results collected can be used to modify and improve the design immediately. The evaluation of the proposed fabric and clothing involves basic properties, thermal properties, and theoretical analysis. Basic properties refer to thickness, weight and mechanical properties. The thickness of the fabric can determine the thermal resistance of the fabric, the most important factor for the proposed fabric. The weight of the fabric is also an essential parameter as the large weight of the clothing may affect the wear comfort. Mechanical properties would also be assessed to ensure the durability of the fabric.

The evolution of thermal properties is the main test in this study as all fabrics and clothing proposed are designed for thermal management. The thermal comfort properties of the proposed soft robotic garment were evaluated by subject and object testing. We would initially test the fabric using the sweating hotplate (YG(B)) 606G thermal and moisture resistance tester (Wenzhou Darong Textile Instrument Co., Ltd, ASTM F1868, 2009), measuring the thermal and moisture resistance at different degrees of deformation of soft robotic elements (e.g., varying thickness and porosity, changing pore sizes, and opening/closing pores).

The sweating guarded hotplate can be used to test the thermal and moisture resistance of textiles, which can simulate heat transfer between human skin and the environment through fabric and clothing.

Thermal behavior is determined by dry thermal insulation and the transfer of moisture through fabric and clothing. Thermal and moisture resistance are generally used to characterize the thermal properties of textiles. Thermal resistance (Rct) is defined as the ratio of the temperature difference between two faces of an object to the amount of heat flowing through the object vertically per unit of time. The dry heat flow can be transported by conduction, convection and radiation. Higher thermal resistance means lower heat transfer. Moisture resistance (Ret) is defined as the ratio of the difference in water vapor pressure on both sides of the sample to the evaporation heat flow passing vertically per unit of time. The evaporation heat flow can be carried out by diffusion of moisture or ventilation. If the moisture resistance is higher, it may be difficult to transfer moisture through the sample. The value of thermal and moisture resistance is often the main criterion for deciding whether fabric or clothing can be used in a thermally demanding environment.

$$Rct = \frac{(T_s - T_a) \cdot A}{Q} \tag{3-14}$$

$$Ret = \frac{(P_s - P_a) \cdot A}{Q} \tag{3-15}$$

Where: Rct—the thermal resistance, m^2 K W^{-1}; T_s—the mean surface temperature of the hotplate, K; T_a—the mean ambient temperature, K; A—the total surface of the hotplate, m^2; Q—the total heating power supplied for the hot plate, W. Ret—the moisture resistance, m^2 Pa W^{-1}; P_s—the mean moisture pressure of the hotplate, Pa; P_a—the mean ambient moisture pressure, Pa; Q—the total evaporation power supplied for the hot plate, W.

The sweating hotplate, which mimics the heat and moisture transfer mechanisms of human skin, was used to measure thermal and moisture resistance according to ASTM F1868. When determining thermal resistance, no water can be used, and the heat flux and temperature difference will be monitored. The thermal resistance of soft robotic fabric with a fixed area (2,500 cm^2) at different levels of air gap will be assessed by inflation or deflation. The temperature difference across the fabric (i.e., skin temperature = 35 ºC and environmental temperature = 20 ºC) will be fixed, while the different heating power consumptions will be recorded to determine the corresponding thermal resistance. To measure the moisture resistance, the environmental and skin temperatures will be the same but the humidity difference (i.e., skin humidity = 100% and environmental humidity = 40% at environmental temperature = 35 ºC) will be fixed. Different moisture resistances will be determined under different degrees of air gaps by inflation and deflation. The thermal and moisture resistance of similar commercial products such as Nudown vest and down jackets will be tested for benchmark comparison following the same test standard.

Temperature sensors were used to reflect the variations of temperature directly. In these studies, temperature data logging meters with USB interface (Anbai, AT4208) were used. This handheld multi-channel temperature meter adopts a high-performance ARM microprocessor that can collect multi-channel temperature data simultaneously and respond quickly. The accuracy can reach 0.2 °C ± 2 digits. And the working range of this device is -200 °C ~ 1300 °C, thus it can be used in extreme conditions with high reliability, meeting the requirements of our testes. All thermal IR images were obtained by an infrared camera (Fluke Ti400). Subjective evaluation of thermal comfort by thermal human manikin or human trials was also conducted. The heating manikin, which mimics the heat dissipation of human skin, would be used to measure skin temperature under different thermal conditions. And a climate chamber allows temperature variation from 5 ºC to 30 ºC is used to realize temperature variations. The thermal manikin is covered by a liquid circulation system, with the skin temperature varying by a controllable input of heat power. Human trials were also conducted to collect the wearer's real-time skin temperature when ambient temperature changes.

3.5.2 Numerical studies

To understand the complex heat transfer through fabric and clothing, numerical modeling of heat transfer would be applied. The application of numerical models can be useful to identify and characterize important parameters that affect thermal properties. Simultaneously, modeling results can also help optimize clothing design. Heat transfer from the skin side to the ambient environment can be simplified as heat transfer from the skin and through the fabric and air gap between fabrics. Therefore, this thesis developed a 2D numerical model using Fluent software to investigate heat transfer phenomena within the air gap between clothing, which involves fluid flow and coupled heat transfer by means of heat conduction and convection. Air motion and heat transport within the gap can be controlled by mass conservation equation, momentum conservation equation, and energy conservation equation [102].

Mass conservation equation:

$$\frac{\partial \rho}{\partial t} + \frac{\partial}{\partial x}(\rho u) + \frac{\partial}{\partial x}(\rho v) = 0 \tag{3-16}$$

Momentum conservation equations:

$$\frac{\partial(\rho u)}{\partial t}+\frac{\partial}{\partial x}(\rho uu)+\frac{\partial}{\partial x}(\rho vu)=\frac{\partial P}{\partial x}+\frac{\partial}{\partial x}\left(\mu\frac{\partial u}{\partial x}\right)+\frac{\partial}{\partial y}\left(\mu\frac{\partial u}{\partial y}\right) \quad (3\text{-}17)$$

$$\frac{\partial(\rho v)}{\partial t}+\frac{\partial}{\partial x}(\rho uv)+\frac{\partial}{\partial x}(\rho vv)=\frac{\partial P}{\partial y}+\frac{\partial}{\partial x}\left(\mu\frac{\partial v}{\partial x}\right)+\frac{\partial}{\partial y}\left(\mu\frac{\partial v}{\partial y}\right)+F_y \quad (3\text{-}18)$$

Energy conservation equation:

$$\frac{\partial(\rho h)}{\partial t}+\frac{\partial}{\partial x}(\rho uh)+\frac{\partial}{\partial x}(\rho vh)=\frac{\partial P}{\partial y}+\frac{\partial}{\partial x}\left(k\frac{\partial T}{\partial x}\right)+\frac{\partial}{\partial y}\left(k\frac{\partial T}{\partial y}\right)+Q_R \quad (3\text{-}19)$$

Where ρ represents the air density; u and v represent sir velocities in x and y directions, respectively; P represents the pressure; μ represents the air viscosity; F_y represents the buoyancy force induced by the air density variation; h represents enthalpy; k represents the thermal conductivity; T is temperature; Q_R is the heat transfer by thermal radiation.

On the other hand, the finite difference time domain (FDTD) method is chosen to investigate transient thermal analysis, especially radiation, which is widely used because it is simple and computationally efficient. FDTD technique is a numerical method that samples the electrical and magnetic components of the electromagnetic field across both spatial and temporal dimensions. This method effectively transforms Maxwell's rotation equations, which incorporate time-dependent variables, into a set of distinct equations. This approach permits the numerical solution of the electromagnetic field in space, propagating sequentially along the time axis. The mathematical formulation of the FDTD method is presented below [103, 104]. The Maxwell equation can be described as

$$\nabla\times E=\frac{\partial B}{\partial t}-M \quad (3\text{-}20)$$

$$\nabla \times H = J + \frac{\partial D}{\partial t} \tag{3-21}$$

$$\nabla \cdot D = \rho \tag{3-22}$$

$$\nabla \cdot B = 0 \tag{3-23}$$

Where $M = \sigma_m H$, $J = \sigma_e E$. σ_m and σ_e represent the permeability and electrical conductivity respectively, corresponding to the magnetic loss and electrical loss of the medium respectively.

3.6 Summary

As previously discussed, the development of fabric and clothing follows a specific flowchart outlined in Figure 3-1. This process begins with the strategic design of fabric and clothing, involving comprehensive studies of consumer needs and market trends, which in turn inform the choice of materials, patterns, and colors to create aesthetically pleasing and comfortable clothing. This process then continues with the creation of clothing systems, which involves the development of soft robotic elements and knitted substrates. Furthermore, the integration of these elements into the final clothing system is crucial to achieving the desired functionality and performance. These soft robotic elements may be controlled using passive control methods that rely on stimulus sensitive materials or active control methods that require the use of electric fields. The research methodology used in this study was a blend of theoretical calculations that allowed the researchers to predict the behavior of textile-based systems and experimental validation that was conducted to verify these predictions, thereby providing a strong basis for the development of new soft robotics systems. Three types of textiles were designed and fabricated, taking into account heat transfer modes such as heat conduction, convection, and radiation, which are all important factors that affect the performance of clothing. Additionally, factors that may influence these parameters, such as the properties of the materials used, patterns of textile structures, and environmental conditions, were examined to ensure that the final prototypes were optimized for maximum performance and durability. Finally, fabric and clothing prototypes were created to demonstrate the feasibility of the design strategy, which provided a visual representation of the proposed solution and allowed for preliminary testing of the functionality of soft robotics systems.

Chapter 4 Soft robotic textile for passive thermally adaptive insulation

4.1 Introduction

Nowadays, heat hazards are common dangers for those staying in high-temperature conditions, especially firefighters, the first responders to unpredictable fires. Failure to prevent intense heat can lead to severe skin injuries and even fatality. It is reported by the U.S. Fire Administration (USFA) that there were an estimated 15,200 injuries and 3655 deaths, including 86 firefighters during firefighting operations [105]. In indoor conditions, body thermal comfort can be maintained by using air conditioning to heat or cool the building's space, while on the outside, the only approach to managing body temperature is clothing. [10]. Therefore, it is highly desirable to develop effective thermal protective fabric to regulate body temperature against excessive heat stress [106].

Traditional thermal protective clothing (TPC) is generally made of multilayered fabric with a thick thermal liner [107, 108], resulting in large weights and poor air permeability. Moreover, the thermal conductivity of the fabric system is fixed, yet they may be unable to respond quickly and efficiently to sudden temperature changes. Several studies have been conducted to develop smart fabric and clothing that can automatically adapt to ambient temperature using temperature sensitive materials. Preliminary studies incorporating aerogel [109-112] and phase change materials (PCM) [74, 113] with traditional fabric have successfully improved thermal protective properties and achieved dynamic management of the thermal properties. Smart thermally adaptive fabric has adopted passive thermoregulating mechanisms, allowing simpler fabrication methods and enhanced energy efficiency but also limiting body movements and resulting in sweat accumulation. Challenges related to short duration and high moisture resistance [114] of such designs have not been resolved. Current methods of removing barriers are to incorporate shape memory alloys (SMAs) [77], varying the geometrical structures of the fabric to a large air gap space, which is substantially effective as still air has much lower thermal conductivity than fibrous polymers and composites [4, 115]. However, SMAs may exhibit a one-way shape memory effect, which cannot return to desirable shape at certain temperatures [79]. Consequently, developing a fabric system that can respond reversibly to sudden temperature changes is imperative.

4.2 Design strategy and working mechanism

Taken together, the ideal TPC should be thermally responsive, which can keep different shapes in various thermal states to maintain thermal comfort without sacrificing flexibility and water transmission. The presence of an air gap between fabric layers can also improve thermal protection properties as its thermal conductivity is lower than textiles. Here, we propose a soft robotic textile (SRT) for thermally adaptive insulation incorporating low boiling point fluid that is packaged as intelligent thermal actuators (STA), engineering fabric thickness by directly controlling the air space between fabric layers to regulate thermal insulation properties. Thermally driven actuators have been extensively explored in robotics due to their easy fabrication methods and compact implementation.

The low boiling point fluid has an extreme volume change as it moves from liquid to vapor, leading to actuators inflation [116, 117] and then separating fabric layers to create an air gap to block heat transfer. In addition, knitted fabric with channels was applied as the thermal liner and the package of smart thermal actuators showed excellent thermal insulation and stability. This fabric demonstrates its reversible adaption to temperature changes, high efficiency, and simple fabrication. Generally, increasing the thickness of the air gap can lead to better thermal insulation of clothing as thermal conductivity could be enhanced. Nevertheless, the insulation performance of the air gap may be weakened because natural convection heat transfer may occur as the thickness of the air gap increases.

Figure 4-1 illustrates a SRT that can passively adjust its thickness for adaptive thermal insulation in different temperature environments, using a smart thermal actuator (STA) based on a low boiling point fluid. This unique thermally protective textile is designed to maintain thermal comfort under temperate conditions by employing a thin fabric with low thermal resistance. In contrast, it can increase the air gap between fabric layers, which boosts thermal resistance and blocks heat during exposure to higher temperatures. Conventional thermal protective textiles have a static structure with a fixed thermal resistance. Consequently, firefighters must wear such clothing before entering a fire scene, which can hinder both heat and moisture transfer from the skin to the surrounding air. This can cause discomfort due to overheating, especially in summer. When entering a high-temperature environment such as a fire scene, the bulk and weight of traditional protective clothing can restrict movement and potentially reduce work efficiency. The design of the SRT shown in Figures 4-1a and 4-1b addresses this issue. When outside the fire scene, the SRT maintains a lightweight and highly thermally conductive state due to its thin, compact fabric structure. However, when a firefighter enters the fire scene and the ambient temperature rises, STA activates, causing an increase in fabric thickness and thermal resistance. If the firefighter exits the hot conditions, the lower temperature triggers the STA to return to its original state, resulting in a reversible deformation of the SRT. Therefore, the SRT can become thin with low thermal resistance at regular temperatures to ensure comfort, yet automatically adapt to protect the wearer from heat by widening the air gap for improved thermal resistance. It then turns thin as the temperature drops, allowing one piece of clothing to be suitable for a wide range of temperatures.

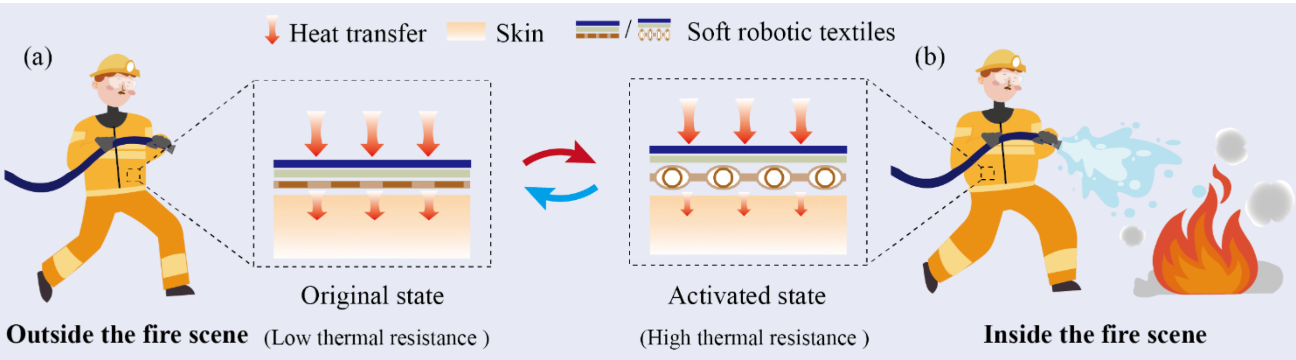

Figure 4-1 Design concept of thermally adaptive soft robotic textiles. (a) Under normal conditions, the SRT's slim profile and reduced thermal resistance facilitate the transfer of heat and moisture away from the skin. (b) Upon exposure to a fire environment, the SRT activates to provide enhanced thermal protection maintaining lightness and breathability. Specifically, outside fire events, SRT layers deflate for low thermal resistance; when activated in a fire scenario, the layers separate, creating an insulating air gap that impedes heat transfer.

Figure 4-2 illustrates an SRT that can passively adjust its thickness for adaptive thermal management. Figure 4-2a provides the structure of the SRT. The SRT contains a flame-retardant outer shell, a breathable waterproof moisture barrier, a porous knitted thermal liner (Figure 4-2b) and thickness-changeable STAs (Figure 4-2c). The knitted thermal liner includes channels to package and fix STAs and clasps to connect the channels. The low boiling point fluid is injected into the STA, whose boiling point is 61 °C, enabling it to undergo reversible phase changes from liquid to vapor in response to temperature fluctuations. STA can achieve reversible phase change between liquid and vapor under temperature variations. In summary, temperature variation can reversibly alter the textile air gap between fabric layers and then dynamically change fabric thickness to control heat transfer between the environment and the human body.

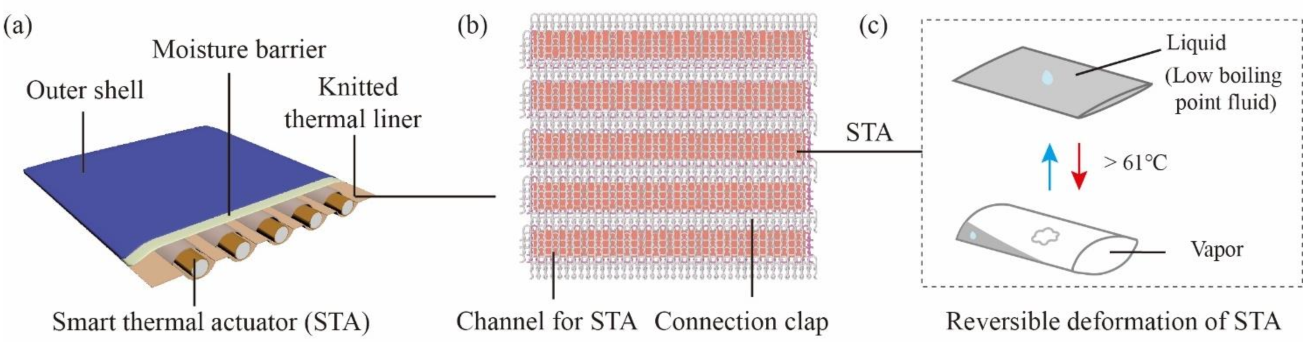

Figure 4-2 Components of the SRT. (a) Schematic of the SRT which contains flame-retardant outer shell, breathable moisture barrier, knitted thermal liner and smart thermal actuator (STA). (b) Structure of the knitted thermal liner with STAs inside. (c) Reversible deformation of STA. The phase change process of the low boiling point fluid inside the STA with large volume variation. Under normal temperature, the low boiling point fluid is liquid. When the temperature increases, the fluid starts to

evaporate and change into vapor. When the temperature decreases, the fluid starts to condense and recover to the liquid state.

4.3 Materials and fabrication

4.3.1 Materials

1) Heat sealed fabric

We would apply thermoplastic polyurethane (TPU) coated nylon fabrics to fabricate the STA purchased from Alibaba. Nylon fabric with one side coated with commercially available thermoplastic polyurethane (TPU) was selected as the heat-sealed fabric for its liquid and vapor impermeability. TPU fabric is an environmentally friendly inflatable material that is commonly used in the production of lightweight inflatable boats. Nylon fabric provides remarkable tear and tensile strength. TPU is a thermoplastic elastomer that can be melted and processed, with exceptional tensile strength and durability. The TPU coating provides both water resistance and airtightness, effectively preventing liquid penetration and air transmission. Nylon fabrics are durable and flexible as the substrate and films are impermeable for creating hollow soft robotic skeletons for inflation. In particular, the TPU films can also be used as adhesives for sealing the robotic units when heated and pressurized at 200 ºC. TPU-coated fabrics can maintain their flexibility while being durable and waterproof. They are also soft, safe, abrasion-resistant, and tear-resistant, and have excellent bending and tensile strength, large elongation breaks, and low-temperature resistance. They can be used to make survival suits, outdoor wear, and other safety wear, indicating the durability and feasibility of the present embodiment. TPU-coated nylon fabric specifications are illustrated in Table 4-1, provided by the manufacturer.

Table 4-1 Specification of the TPU coated nylon fabric.

Basic fabric	100% nylon oxford fabric
Yarn	420 D
Structure	Plain woven
Pattern	TPU coated on one side
Weight	480 ± 20 g/m^2
Thickness	0.45 ± 0.02 mm

2) Low boiling point fluid

Low boiling point fluid refers to fluids with a lower boiling point, which have been exploited by actuators. Ethanol, Novec™ 7000, and Novec™ 7100 are all low boiling point fluids. In previous research, pouch motors have been designed by incorporating low boiling point fluid with a polyethylene bag. A small amount of fluid heat sealed inside can lead to large deformation in shape when the fluid evaporates due to heat application. The low-boiling point fluid used in this study is Novec™ 7100 (3M) engineered fluid with 61 °C as its boiling point, which is non-explosive, non-flammable, non-conductive and low toxicity. The fluid has a low global warming potential (GWP) and zero ozone depletion potential, determining its excellent environmental, health and safety profile. Thus, Novec™ 7100 is suitable to be applied in designing human clothes.

3) Cotton yarn

The yarn used to knit the 3D fabric is cotton, purchased from Alibaba. Cotton yarn is often used to make clothes and clothing because it is soft and breathable. The cotton yarn used here is 21s/2. The cotton yarn has good hygroscopicity. It can absorb moisture from the surrounding environment under normal conditions. Thus, it is skin-friendly, making people feel soft and comfortable. In addition, the moisture in the fabric made of cotton can evaporate when the humidity around it increases and the temperature is higher, maintaining the water balance to keep people more comfortable. Cotton fiber has extremely low thermal conductivity, which is a poor conductor of heat. Thus, textiles made of pure cotton fiber exhibit good thermal insulation. Under 110 ℃ of temperature, cotton fabric can only evaporate moisture, thus not causing any damage to the fiber, thus improving the washability and wearability of cotton fabrics. Cotton fiber has a strong resistance to alkali, so it would not be damaged in alkaline solution, which is beneficial for post-consumption pollution washing, disinfection and impurity removal. Pure cotton fabric has undergone extensive testing and practice and has no irritation or side effects when in contact with the skin, which makes it beneficial and harmless to the human body for long-term wear, with excellent hygienic properties.

4) Other fabric included

Wicking fabric is woven fabric with 100% cotton. The outer shell is 100% Nomex (327 g/m^2). The traditional moisture barrier is 100% meta-aramid/PTFE film (89 g/m^2). The breathable moisture barrier is polyester fabric (92 g/m^2). The traditional thermal liner is 100% cotton/Cotton fabric (263 g/m^2). The knitted thermal liner is knitted fabric with 100% cotton (752.9 g/m^2).

4.3.2 Fabrication of STA

Figure 4-3a presents the TPU fabric, and Figure 4-3b depicts the heat-sealing machine for heat sealing. Figure 4-3c describes the manufacturing process. 1) Two layers of TPU material were layered with wicking fabric sandwiched in between. 2) The integrated fabric system was sealed using thermal bonding technology with a heat sealer to create multiple long strips of bags. The width of the sealed area was determined by the dimensions of the heat sealer heater. 3) The low boiling point fluid was injected into the non-sealed area, also known as the air chamber, and absorbed by the wicking fabric. 4) The TPU was quickly sealed in a vacuum to prevent liquid loss by the heat sealer. 5) The STAs that were constructed were cut to match the sealed shape. The air chamber is a sealed-off space designed to facilitate the conversion of the low boiling point fluid between liquid and vapor.

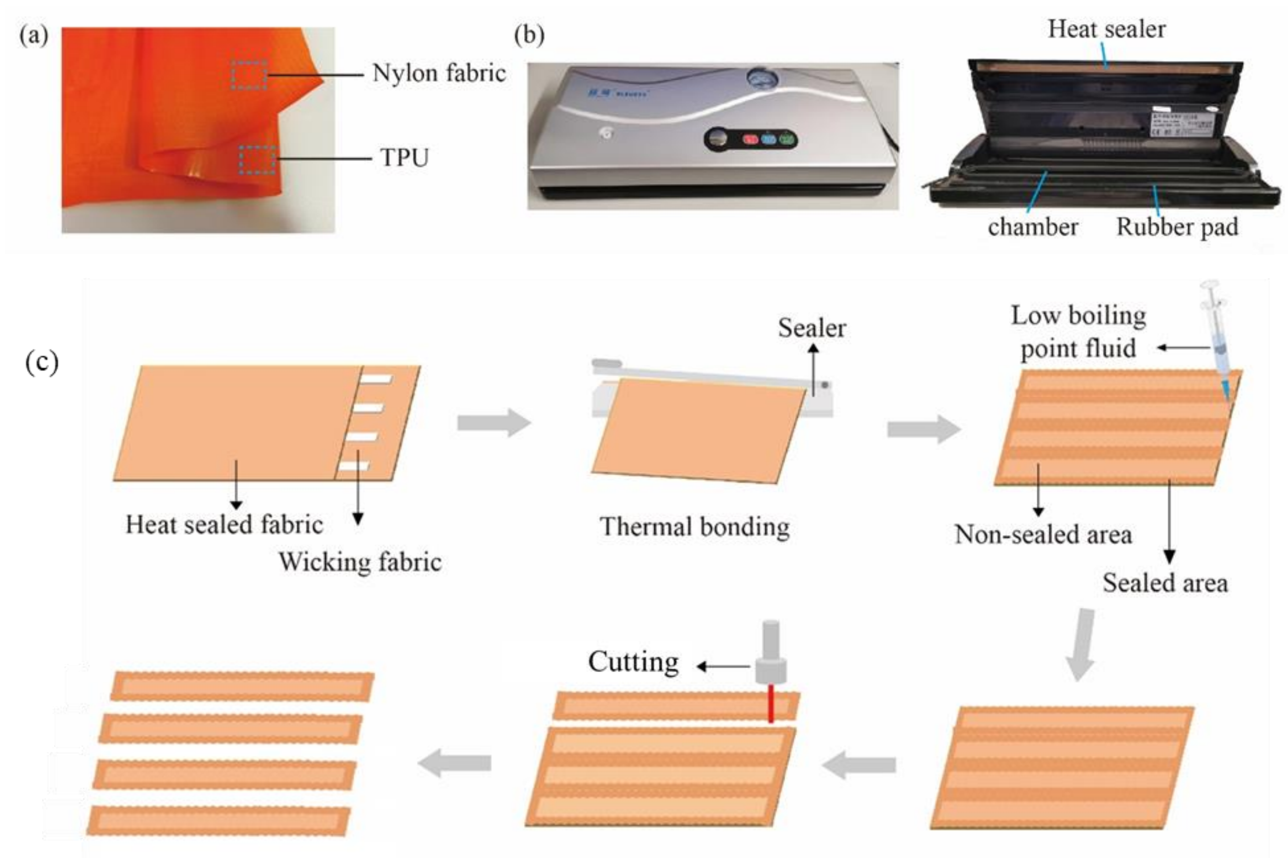

Figure 4-3 Fabrication of STAs. (a) TPU fabric with one side coated by TPU. (b) Heating sealer. The heating sealer has an air chamber to achieve vacuum packing of STA. (c) Fabrication process of STAs. Thermal bonding technology is applied to seal the edges of the heat-sealed fabric, avoiding liquid or vapor leakage. The surface with TPU coating was sealed together by thermal bonding technology using heat sealer, which may allow for larger-scale industrial manufacture.

The STA has been sealed like a rectangular bag with 5 mm as the width of the sealed edge. The non-sealed area, also known as the air chamber, is rectangular with wicking fabric inside, which can be inflated due to the large volume of vapor generated when the fluid evaporates. As shown in Figure 4-4a, the STA has three layers of cotton fabric sticked between the heat-sealed fabric layers as wicking fabric. Wicking fabric can absorb and maintain liquid, ensuring a uniform distribution of low boiling point fluid at the same time. Figure 4-4b displays a photograph of the STA in a deflated and inflated state. The deflated STA is flat. When fully inflated, the surface becomes elevated, and the height of the STA also increases.

Figure 4-4 Demonstration of the STA. (a) Shape and size of STA. (b) Images of the STA in fully deflated state and fully inflated state.

4.3.3 Fabrication of knitted thermal liner

The highly porous knitted fabric with periodic plain and rib stitches is used to fix STAs. The front and rear bars can knit plain stitches separately and form disconnected fabric layers, which would provide sufficient space for inflation and deflation of STAs. The rib stitches knitted by two bars together can connect the plain stitch. The rib areas would effectively reduce air convection when STAs are inflated, while maintaining high breathability. Figure 4-5 shows the design of the knitted thermal liner with STA channels and connection clasp fabricated by a flat knitting machine. Figure 4-5a is the knitting notation for the knitted thermal liner. The channel part is knitted with a single jersey. The needles are knitted on the front and rear needle beds, forming two separate layers. The connection part is fabricated by the rib stitch to connect the single jersey. As shown in Figure 4-5b, the grey part is the channel for STAs while the white part is the connection clasp. The channel width and connection clasp can be adjusted by changing the knitting course numbers to match STAs with different parameters.

The channel has two layers for wrapping the STA and the connection clasp connects the channels. Figure 4-5c is the rear side of the knitted thermal liner.

Figure 4-5 Design and fabrication of the knitted thermal liner. (a) Knitting notation for the thermal liner. (b-c) Images of the knitted thermal liner with connection clasp and channel for STA.

4.3.4 Integration of the fabric and STAs

After fabrication of the STAs and the knitted thermal liner, these components would be integrated together to form a fabric system. Figure 4-6a demonstrated that when the STA is fully deflated, the knitted thermal liner with STA inside was flat with minimum thickness. If the STA was fully inflated, the inflated STA would separate the channels and the connection clasp would rise to the middle of the entire structure with the maximum thickness, as shown in Figure 4-6b. Thus, the air gap was created and separated by the connection clasp. Images of the knitted thermal liner with STAs inside the channel in a fully deflated and inflated state are illustrated in Figure 4-6c and d, respectively. The outer shell fabric and the moisture barrier are shown in Figure 4-6e and f, respectively. Figure 4-6g displays the structure of the entire fabric and clothing system with the thermal liner as the inner layer. Integrating these materials involves three steps. The first step is to sew the outer shell fabric, the moisture barrier and the knitted thermal liner together along the channel direction. Then, the STAs are inserted into the channels one by one. The width of the channel is larger than that of STAs, which means it is easy to insert them. The last step is to sew the channel of the knitted fabric to ensure that the STAs would not slip out of the channels.

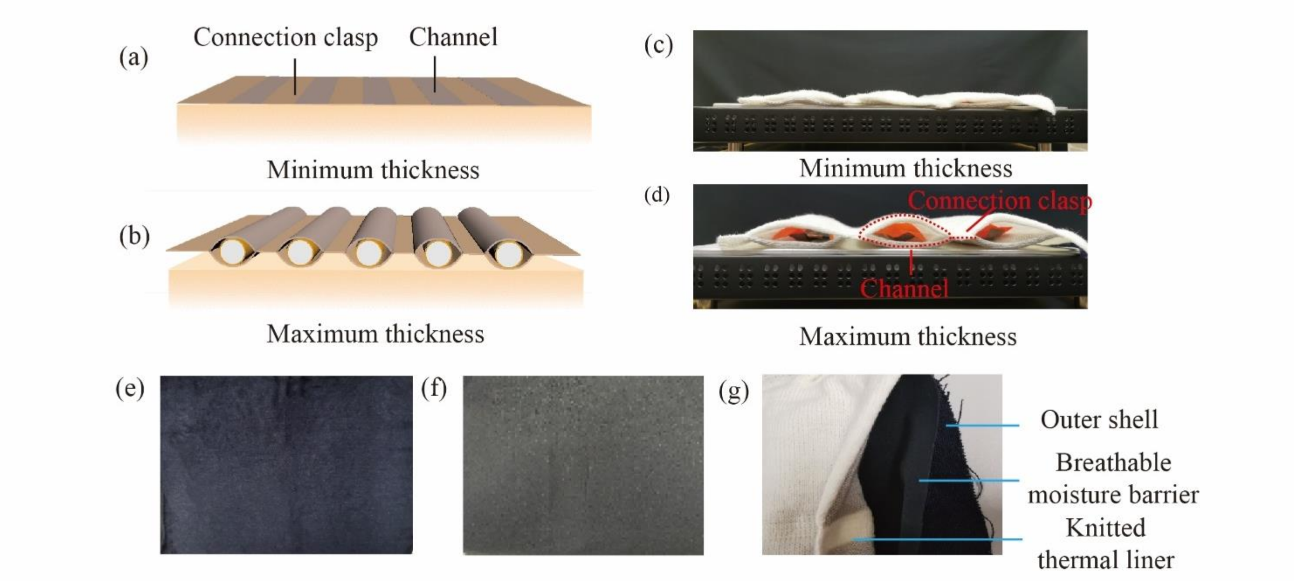

Figure 4-6 Integration of the proposed clothing. (a) Schematic diagram of STA in knitted thermal liner when fully deflated with minimum thickness. (b) Schematic diagram STA in knitted thermal liner when fully inflated with maximum thickness. (c-d) Images of the STA in knitted thermal liner when fully deflated and inflated. (e) Outer shell fabric. (f) Moisture barrier. (g) Structure of the proposed fabric.

4.4 Characterization of the STA

4.4.1 Mechanism of the actuators

Figure 4-7a demonstrated the deformation mechanism of the STA. The low boiling point fluid can absorb heat from the ambient environment and evaporate to produce vapor, leading to STA inflation. If the ambient temperature decreases, vapor releases heat and condenses into liquid. After fabrication, the STAs were placed on a hot plate at room temperature to observe its deformation. This process would be repeated multiple times to verify the reversible performance of STAs. Figure 4-7b shows the relationship between hot plate temperature and STA thickness. The width used is 30 mm and the maximum thickness of the STA is 19.1 mm. The cross section of the STA during the deformation process is shown in Figure 4-7c. At room temperature, the STA is flat and thin in a liquid state. When the temperature increases, the STA evaporates due to continuous heat absorption and maintains a mixed liquid-vapor state, and then a fully vaporized state with maximum thickness. STA thickness varies with the low boiling point fluid phase. The maximum thickness of the STA is determined by the original width of the STA air chamber.

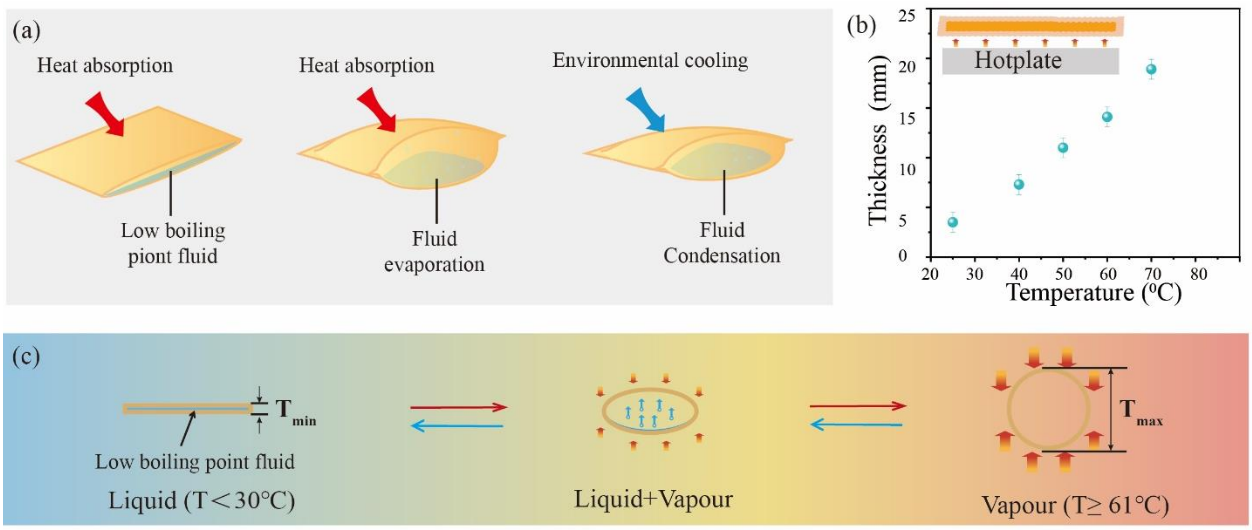

Figure 4-7 Characterization of the STA. (a) Reversible deformation of the STA between liquid and vapor. The low boiling point fluid is liquid under the normal temperature. When the environmental temperature increases, the fluid would absorb heat and start evaporating. While when the temperature decreases, the environmental cooling can lead to vapor condensation. (b) Relationship between

temperature and thickness when the STA is set on a hotplate. (c) Cross-section of the SAT during the deformation process. At room temperature, the fluid is liquid, and the STA is fully deflated and keeps flat state. When the temperature increases, the fluid evaporates due to continuous heat absorption and keep a liquid-vapor mixed state as the environmental cooling effect is strong. When the temperature exceeds the boiling point fluid, the STA is fully inflated with vapor inside whose cross-section can be seemed like a circle. And at this state, the STA exhibit the maximum thickness, which is approximately equal to the diameter of the circle.

A leak test was carried out to verify the strength of the sealed area to prevent any possible leakage of vapor and liquid. A small STA was immersed in hot water (temperature >80 °C) to heat the boiling point and to observe bubble formation. As shown in Figure 4-8a, when the STA is immersed in hot water, it absorbs heat and the fluid evaporates and generates a large amount of vapor, causing the liquid level in the beaker to rise. And a vertical view showed that the STA in hot water was fully inflated without bubbles, indicating there was no vapor leak. In addition, another test was performed to obtain the maximum pressure the STA can withstand, as shown in Figure 4-8b. The results showed that STA can withstand a pressure of 1.96 MPa.

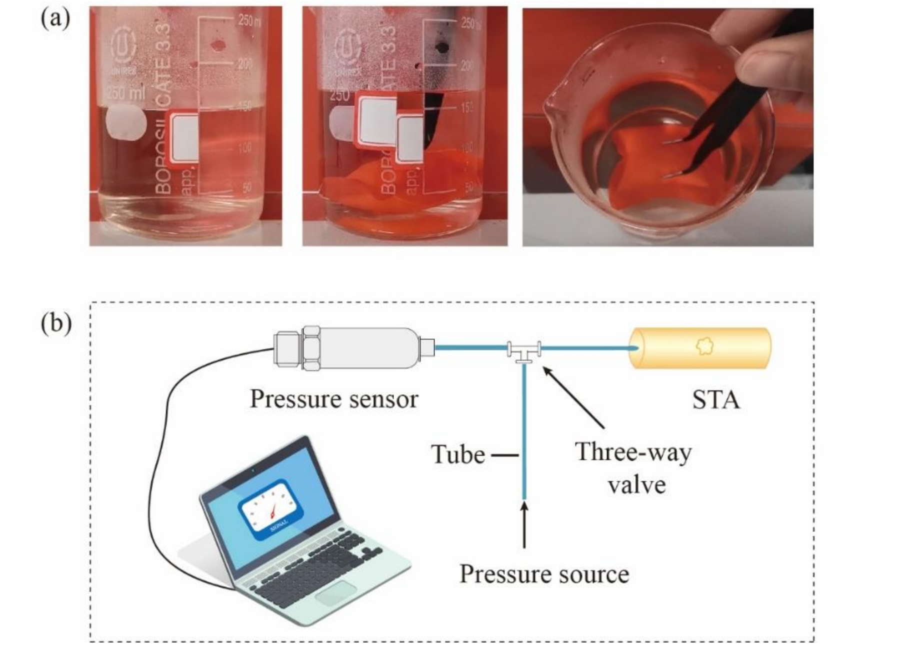

Figure 4-8 Testing of the leakage and bonding strength of the STA. (a) Leakage test of STA. From left to right: hot water, STA immersed in hot water and vertical view of the setup. (b) Setup to test the maximum pressure that the STA can undertake.

The wicking fabric applied is shown in Figure 4-9a, which is made of cotton with a woven structure. In order to test the wicking performance of the cotton fabric, a transparent bag with a low boiling point fluid (5 mL) was first prepared, shown in Figure 4-9b. When the fabric is inserted into the bag, Figure 4-9c-d showed that the liquid in the bag was reduced to a small amount after adding cotton fabric because most of the liquid was absorbed by the wicking fabric.

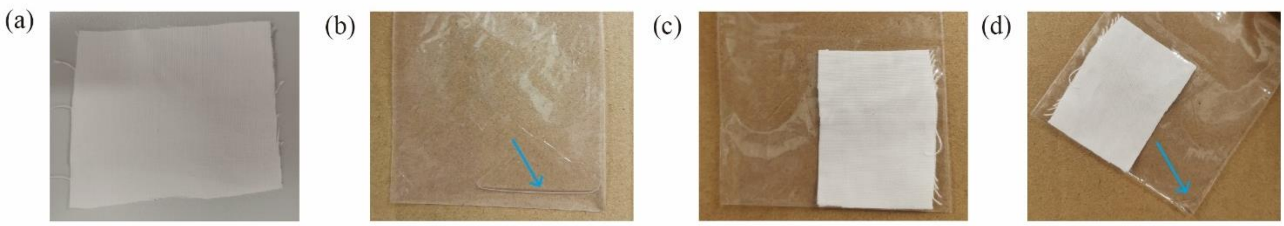

Figure 4-9 Wicking performance of the wicking fabric. (a) Photo image of wicking fabric made by

cotton. (b) Low boiling point in a transparent bag. (c-d) Demonstration of wicking performance. The cotton fabric can absorb the liquid. Upon tilting the bag, the remaining liquid is significantly reduced.

4.4.2 Theoretical model of the actuators

According to the liner actuation modes proposed by Koya Narumi for Pouch Motors [118-120], According to the liner actuation modes proposed by Koya Narumi for Pouch Motors [116-118], the STA is in a thin sheet shape with no pressure as shown in Figure 4-10a. In order to facilitate the analysis of STA deformation, the following parameters are used for the air chamber, regardless of the sealed edges. When there is a passive pressure (P) inside the STA, the geometry is an airfoil shape with cylindrical surfaces on the top and bottom layers due to the extension of the top and bottom surfaces, and contraction of the two edges and rotation of the points, as shown in Figure 4-10b. Figure 4-10c shows the parameters of the activated STA, the cross section of which can be assumed to be an ellipse, and the front view of the ellipse is shown in Figure 4-10d. The minor axis of the ellipse (H) can be seemed as the height of the STA.

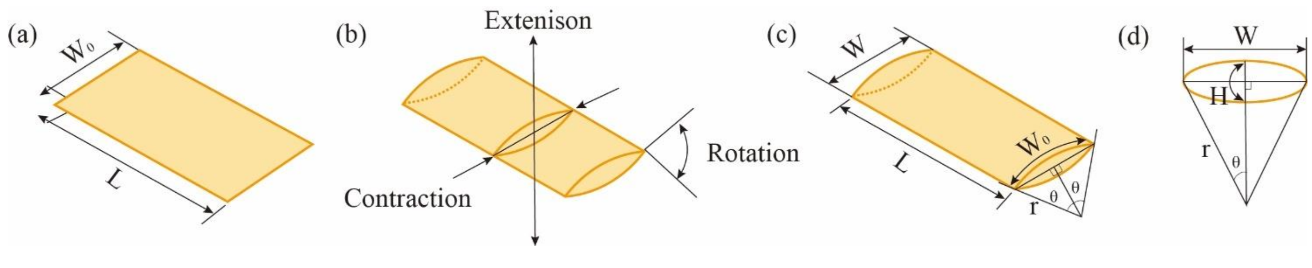

Figure 4-10 Deformation model for STA. (a) STA in a thin sheet. (b) Dimension change of the STA. (c) Model of the single STA in activated state. (d) Front view of the cross section of STA.

When the temperature rises, the liquid evaporates, increasing the internal pressure and STA volume (V). At the same time, the width (W), height (H) and radius of curvature (r) of the cylindrical surfaces are also changed. It is assumed that the TPU fabric is inextensible with zero bending stiffness, and the STA length (L) is constant during the deformation process. W_0 is the original width of the STA when fully deflated, it is the central angle of the circular segment, and W is the width of the STA cross section.

The width of the STA has already been analyzed theoretically as

$$W(\theta) = W_0 \frac{sin\theta}{\theta} \tag{4-1}$$

The height of the STA can be derived as

$$H(\theta) = \frac{W_0(1-cos\theta)}{\theta} \tag{4-2}$$

The volume of the STA can be derived as

$$V(\theta) = \frac{{W_0}^2 L}{2}\left(\frac{\theta-\cos\theta\sin\theta}{\theta^2}\right) \tag{4-3}$$

The theoretical minimum contraction ratio of the STA occurs when the STA is thin without liquid evaporation. The height of the STA is equal to the thickness of fabric layers. While the maximum contraction ratio of the STA can be achieved when θ is $\frac{\pi}{2}$. And the cross section of the STA can be assumed to be a circle. Under this condition, the maximum height of a single can be derived before fabrication according to the original width (W_0) as the circumference is twice the original width.

Based on the analysis of the working principle, the height of the air gap of the proposed garment is determined by the STA size. The air gap between the fabric layers can provide additional thermal protection for the wearer. Air is a good thermal insulator compared to other fabric materials. Based on previous literature, thermal insulation can be enhanced when the height of the air gap increases as the conduction heat transfer through the air gap decreases [121-123]. However, thermal insulation can be reduced when the height of the air gap exceeds a certain value, which is also called critical air gap. Beyond the critical air gap value, the air gap height may be sufficient to establish natural convection, leading to faster heat transfer and subsequently weakening thermal insulation properties. Total heat transfer increases or decreases depending on the relative magnitude of decrease in conduction and increase in convective heat transfer. Therefore, the height of the air gap needs to be designed to obtain desirable thermal insulation properties.

Based on previous studies, the critical air gap could be in the range of 9-12 mm, even depending on the moisture content of the fabrics. Fabric with this air gap can provide the best thermal protection against heat and flame [122]. According to Eq. (4-2), if the selected air gap height is 12 mm, the total air gap thickness of the proposed clothing should be 24 mm, which means that the original STA width is 37.68 mm. While the selected air gap height is 9 mm, the total air gap thickness of the designed garment is 18 mm. This indicates that the original width of the STA is 28.26 mm. Thus, the original width of the STA designed for soft robotic textile could be in the range of 28.26-37.68 mm.

After the above analysis, the STA's air chamber measured 30 mm × 300 mm in size. The original width of the STA was 30 mm, which was able to achieve a maximum height of 19.1 mm, as shown in Figure 4-11a. The relationship between the original width in the fully deflated state and the maximum thickness of the STA was also shown in Figure 4-11c. The width of the wicking fabric used was 28 mm and its length was 300 mm, as shown in Figure 4-11b. Overall, the smaller width of the wicking fabric ensured that it could be easily inserted into the STA's air chamber.

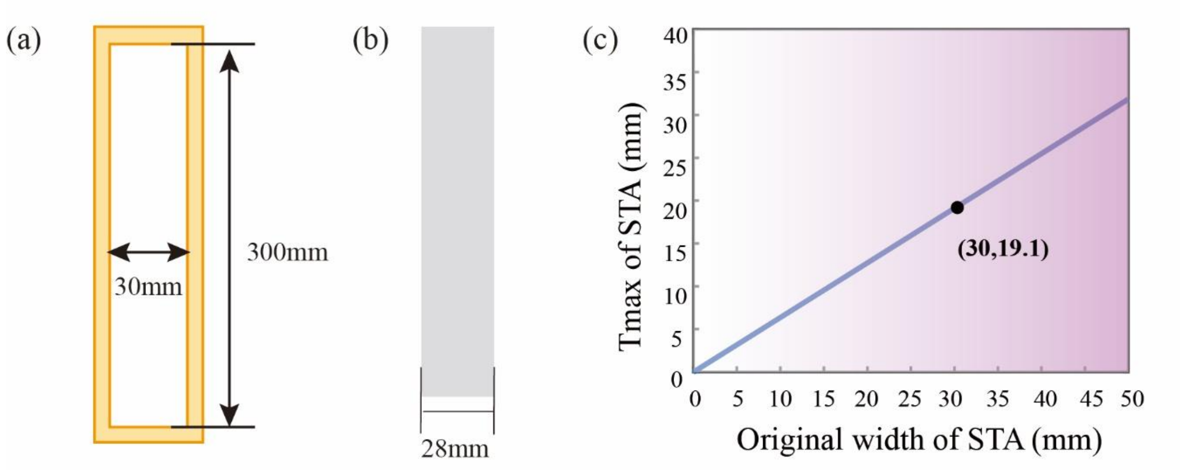

Figure 4-11 Size of STA components. (a) Size of the STA. (b) Size of the wicking fabric. (c) Relationship between the original width in fully deflated state and the maximum height of the STA in fully inflated state.

4.4.3 Internal pressure of STAs and their characterization

According to the product information from 3M, the variation of vapor pressure with temperature for 3M Novec^{TM} 7100 Engineered Fluid can be calculated using the following formula:

$$\ln P = 22.415 - 3641.9[1/(t + 273)] \quad (4\text{-}4)$$

P = Vapor Pressure in Pascals

t = Temperature in °C

According to the relationship showed in Figure 4-12, the boiling point of the fluid is 61 °C, the corresponding pressure is near 105 Pa, equal to one atmosphere. Based on the pressure test results, the sealed area can withstand a pressure of 1.96 MPa at a corresponding temperature of 185.5 °C. This indicates that the maximum operating temperature for the smart thermal actuators is 185.5 °C. If the temperature within the actuators exceeds 185.5 °C, these devices could potentially explode, leading to the release of vapors. According to the operating temperature, 1 mL of low boiling point fluid was injected into STA. If the volume is less than 1 mL, the STA may not be fully inflated when the temperature approaches its boiling point. If the volume exceeds 1 mL, the STA may explode at the maximum operating temperature due to excessive internal pressure.

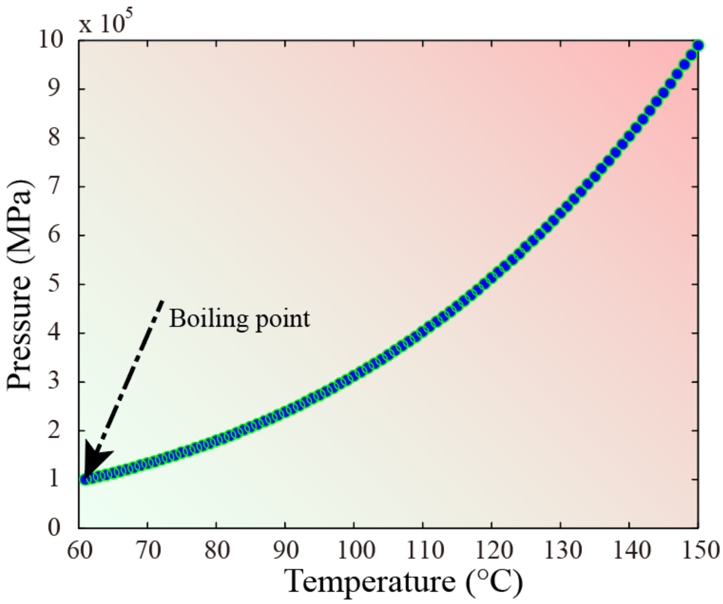

Figure 4-12 Relationship between temperature and the pressure of Novec^{TM} 7100.

4.4.4 Amount of the low boiling point fluid and the volume of STA

As mentioned above, the STA can be inflated because a large amount of vapor is released when the liquid evaporates. Therefore, the volume of liquid injected into STA is significant. The STA may not fully inflate due to the small amount of liquid. If the liquid is too much, the weight and cost of the STA would increase. On the other hand, the large volume of liquid also leads to a large amount of vapor, which may bring higher internal pressure, exceeding the maximum STA pressure. Thus, the minimum volume of liquid V_l [m^3] required should be calculated.

Assuming that the maximum theoretical volume of the STA filled with vapor is V [m^3]. The maximum amount of vapor in a single STA is n_v [mol]. According to the state equation PV = nRT,

$$n_v = \frac{P}{RT}V \tag{4-5}$$

The mass of the liquid m [kg] can be derived as

$$m = Mn_v \times 10^{-3} \tag{4-6}$$

Where M [g/mol] is the molar mass of the liquid. The density of the liquid is ρ [kg/m^3], thus

$$\begin{aligned} V_l &= \frac{m}{\rho} \\ &= \frac{Mn_V \times 10^{-3}}{\rho} \\ &= \frac{M}{\rho}\frac{P}{RT}V \times 10^{-3} \end{aligned} \tag{4-7}$$

According to Eq.(S-3), the maximum volume of STA appears when θ is $\frac{\pi}{2}$. Therefore,

$$\begin{aligned} V_l &= \frac{M}{\rho}\frac{P}{RT}V\left(\frac{\pi}{2}\right) \times 10^{-3} \\ &= \frac{M}{\rho}\frac{P}{RT}\frac{{W_0}^2L}{\pi} \times 10^{-3} \end{aligned} \tag{4-8}$$

According to the product information from 3M, M=250, ρ=1520. For STA, W_0=0.03 m, L= 0.3 m. The boiling point of the liquid is 61 °C. Thus, the temperature should be at least 334 K to drive the actuator, and the pressure should be 99807.64 Pa at this temperature. R is 8.31 J/(mol·K). Based on the above parameters, it can be inferred that the minimum volume of liquid required for the proposed STA used is calculated as 0.51 mL. In order to guarantee the total inflation of the STA, the volume of liquid injected into this paper is 1 mL.

4.4.5 Mechanical properties of STA

To test the mechanical properties of STA, breaking and bonding strength tests were carried out under the standard, *D5035 Textile Breaking Strength/Elongation Strip Method*, by universal machine, Instron 4411. The distance between the clamps is set as 75mm. The breaking elongation was 27.16 mm, and the breaking load was 385.77 N. The bonding strength of the sealed area of STA was 312 N, which is approximately 81% of the breaking strength of TPU fabric. The fabrics before and after the tests were illustrated in Figure 4-13.

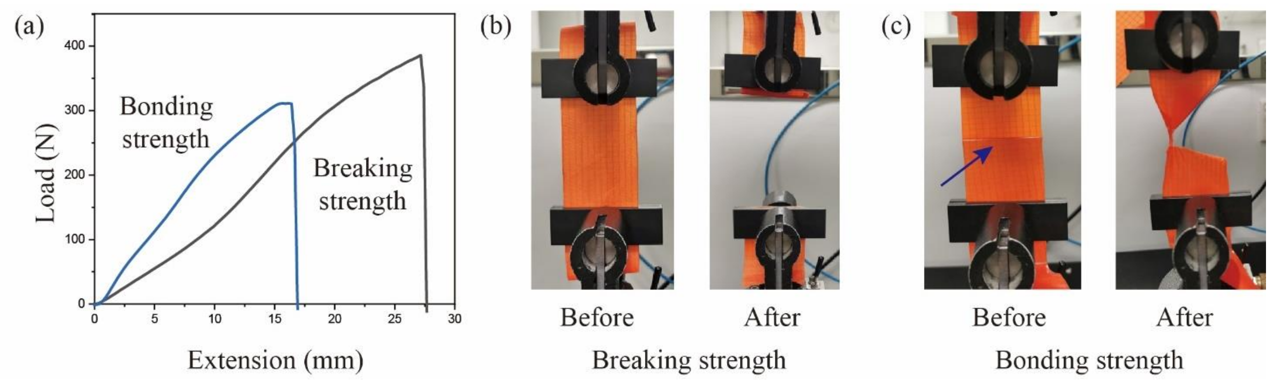

Figure 4-13 Breaking and bonding strength test. (a) Breaking and bonding strength test results. (b) TPU fabric before and after breaking strength test. (c) Sealed TPU fabric before and after bonding strength test.

4.4.6 Durability of STA

To assess the durability of STA, we conducted washing tests under the modified standard: *ISO 6330:2021*. For the washing tests, we fabricated two small STAs and washed them repeatedly, monitoring weight fluctuations as a key determinant of durability. As illustrated in the table below, alterations in sample weights were minimal, suggesting that this change may be negligible.

Table 4-2 Weight of the samples during washing test.

Washing time		0	1	2	3	4	5
Weight (g)	1#	1.9769	1.9874	1.9909	1.9914	1.9905	1.9851
	2#	1.8229	1.8316	1.8325	1.8321	1.8302	1.8189

4.5 Theoretical analysis of the proposed clothing

To fully comprehend the thermal protection performance of clothing, it is critical to accurately measure and quantify the dimensions of the air gaps present within the fabric. According to previous research, the air gap between fabric layers can effectively improve thermal insulation properties as the thermal conductivity of air is lower than conventional fibers applied in thermal protective clothing. However, the insulation effect of the air gap may be weakened by natural convection occurring when the air gap size is large enough. In order to reduce the influence caused by natural convection, a knitted thermal liner with channels was developed to wrap the actuators. As most of the previous literature has analyzed air gap widths ranging from 6.4 mm to 19.1 mm, this study discusses clothing with different air gap widths of 6.4 mm, 12.7 mm, 19.1mm and 25.4 mm by numerical modeling programmed with ANSYS-FLUENT. The height of the fabric was considered uniform.

The simulation setup is illustrated in Figure 4-14. In this study, a 2D air gap was used to investigate dry heat transfer between clothing layers. In order to simplify the simulation cases, all fabrics included in these cases were considered uniform materials with static thermal properties. The red line represents the heat source, which is set to a constant temperature, and the blue line represents the outer layer, which is set to a non-windy state. Heat could only dissipate heat through heat conduction and convection. The gas environment was constructed to act as an ideal incompressible gas, replicating the natural convection phenomena that can occur within the air gap [102]. And the outer layer of fabric only dissipates heat to the environment through thermal convection. The temperature of the condition is set as 25 °C. The heat transfer of the outer fabric and the ambient environment can be considered as natural convection, with a heat flux of 5 W/m^2. Skin and fabric layers can be seemed as non-penetrating in the model, which is assumed as the fabric is set under non-windy conditions. A single unit was selected to study heat transfer phenomena, whose two ends are periodic. For clothing on the body, the air gap between the skin and the environment may be vertical. However, for most tests to investigate the thermal properties of clothing, the air gap is horizontal. In this study, both horizontal and vertical air gaps were studied. Figure 4-14a illustrates the arrangement for the horizontal direction, while Figure 4-14b shows the arrangement for the vertical direction. Figure 4-14c shows the schematic of the simulation configuration.

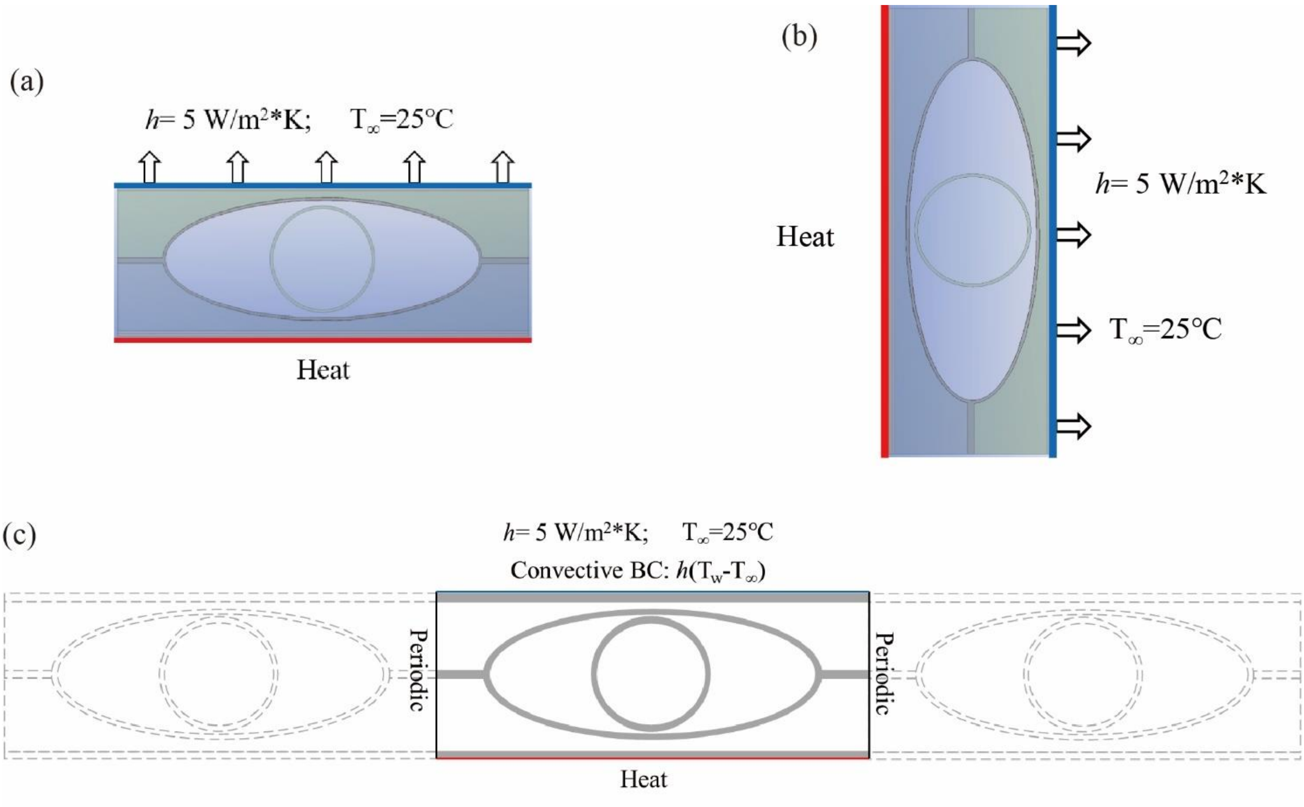

Figure 4-14 Simulation setup. (a) Setup for horizontal direction. (b) Setup for vertical direction. (c) Schematic for simulation configuration.

Figure 4-15a shows the results of the clothing with knitted thermal liner having different air gaps in the horizontal direction. When the original channel width was 60 mm, the clothing with a 19.1 mm air gap shows a lower temperature than the 6.4 mm and 12.7 mm due to the larger air gap. However, when the air gap width was 25.4 mm, the temperature was much higher. As mentioned above, the possible reason is that the larger air gap leads to stronger thermal convection, enhancing heat transfer. Then, in order to discuss the relationship between the channel width of the knitted thermal liner and heat transfer, two other types of widths were selected. When the original channel width is 35 mm, it can wrap the actuator tightly. The original channel width of 87 mm, which is the maximum length in the unit, indicates that there is no connection clasp between channels. As shown in Figure 4-15b, the maximum and proposed channel length illustrate a much lower temperature. This could be explained by the simulated velocity variations between the air gaps in Figure 4-15d-e. When the actuators are tightly wrapped, the air gap of the connecting portion is larger, resulting in stronger heat convection, as shown in Figure 4-15b. While the maximum and proposed channel length showed weaker thermal convection, shown separately in Figure 4-15e-f. In fact, when the width of the channel is much larger than the actuator, the supporting force provided by the inflated actuator may not be sufficient to separate the edge of the channel. The ideal structure mentioned in Figure 4-15e may not exist. Consequently, it was not adopted. Additionally, a case with the actuator on the knitted thermal liner was also calculated. Figure 4-15c showed that the actuators wrapped by the knitted thermal liner had a lower temperature, indicating the efficiency of the proposed structure. Figure 4-15g showed the velocity variations when the STAs were placed on the thermal liner. Compared to STAs wrapped by channels, the velocity was much stronger, leading to rapid heat transfer. Based on the simulation results, it can be concluded that the proposed structure of the SRT has a higher thermal insulation performance.

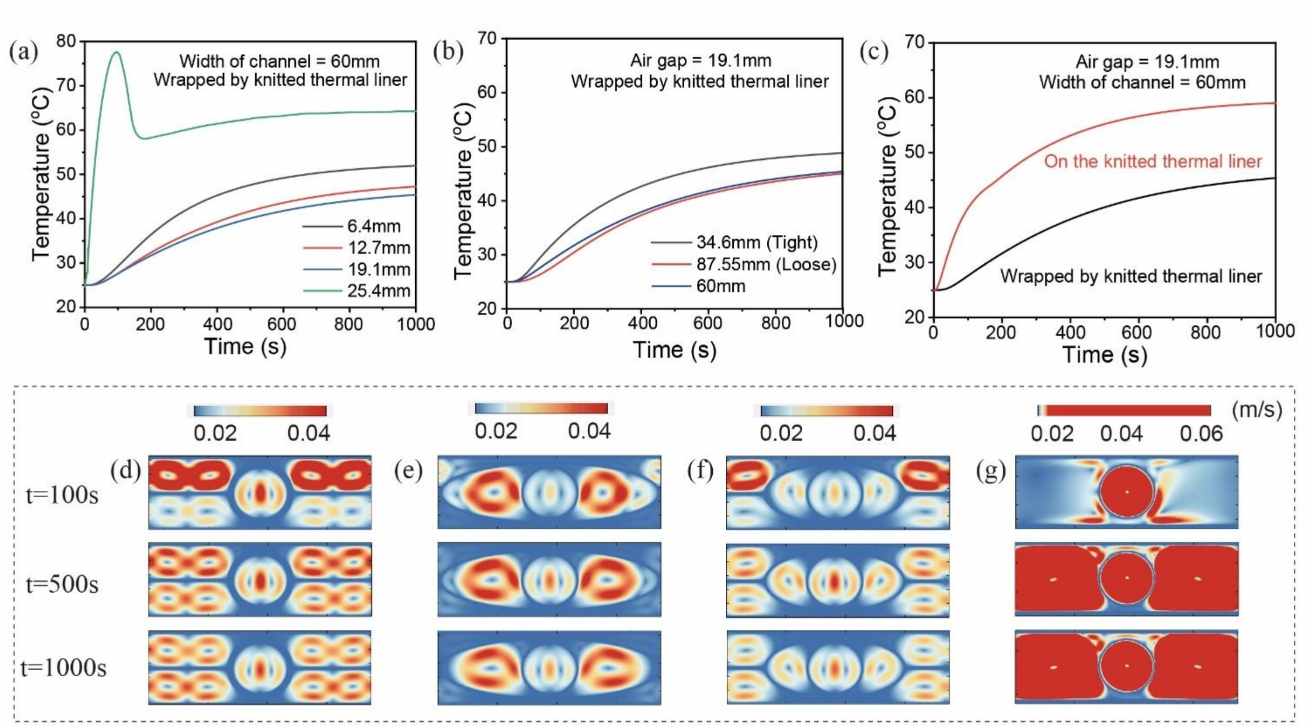

Figure 4-15 Simulated results of clothing with different air gap. (a) Relationship between exposure time and temperature of the SRT with different air gap. (b) Relationship between exposure time and temperature of the SRT with width of channels. (c) Relationship between exposure time and temperature of the textiles with different STAs position. (d) Simulated velocity variations at 100 s, 500 s and 1000 s when the channels wrap the actuators tightly. (e) Simulated velocity variations at 100s, 500 s and 1000 s when the channels reach the maximum length. (f) Simulated velocity variations at 100 s, 500 s and 1000 s under the proposed length. (g) Simulated velocity variations at 100 s, 500 s and 1000 s when the STAs are put on the thermal liner.

In most tests, the air gap of the clothing is placed horizontally. Whereas the orientation of the air gap in fabric systems may be vertical, horizontal and inclined. Therefore, the model with air gap in vertical orientation was also concerned. The simulated results are shown in Figure 4-16. The orientation of the air gap in clothing influences convective heat transfer directly through the air gap due to buoyancy, which occurs when there is a temperature difference in fluid. Therefore, both horizontal and vertical air gaps were simulated. Figure 4-16a shows the horizontal air gap, while Figure 4-16b shows the vertical air gap. As shown in Figure 4-16c, the fabric with actuators wrapped by knitted thermal liner showed a lower temperature. And they had smaller temperature differences even when the orientation of the air gap was different.

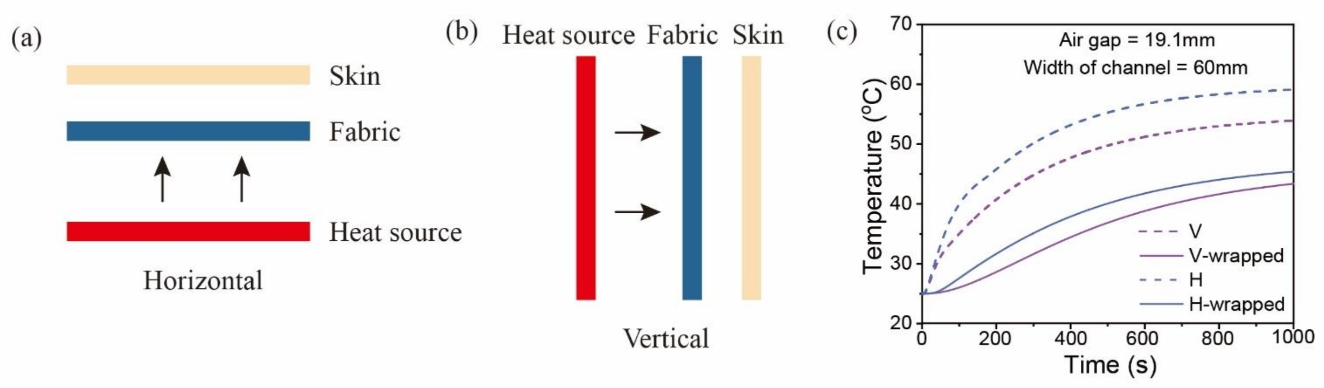

Figure 4-16 Simulated results of air gap direction on thermal properties. (a) Setting up the experiment horizontally. (b) The vertical orientation of the experiment. (c) Comparison of results when STAs and textiles were set in different directions. V and H mean that the STAs were placed on the knitted thermal liner and the SRT in vertical and horizontal directions separately. V-wrapped and H-wrapped means that the STAs were wrapped by the knitted thermal liner and the SRT in vertical and horizontal directions respectively.

4.6 Results and discussion

4.6.1 Thermostability of the proposed textile

Furthermore, to examine the thermostability of the materials used in the proposed textile, we performed a thermogravimetry (TG) test. The outer shell is the layer that comes into direct contact with fire and heat. Its function is to resist external fire or heat without damaging the overall protective function of the suit, that is, fire prevention and thermal insulation. The TG test results, illustrated in Figure 4-17, reveal that the outer shell's weight begins to decrease at 250 ℃. Meanwhile, the weights of the TPU fabric, knitted thermal liner, and moisture barrier begin to reduce at 325 ℃, 372 ℃, and 335 ℃ respectively - all above 250 ℃. These findings suggest that these materials possess greater thermostability than the outer shell. Therefore, the materials utilized exhibit strong resilience to high ground fire temperatures. Vertical burning test were varied out. The results showed that the damaged length was less than 1cm and the afterflame time is less than 2s, indicating excellent flame retardancy.

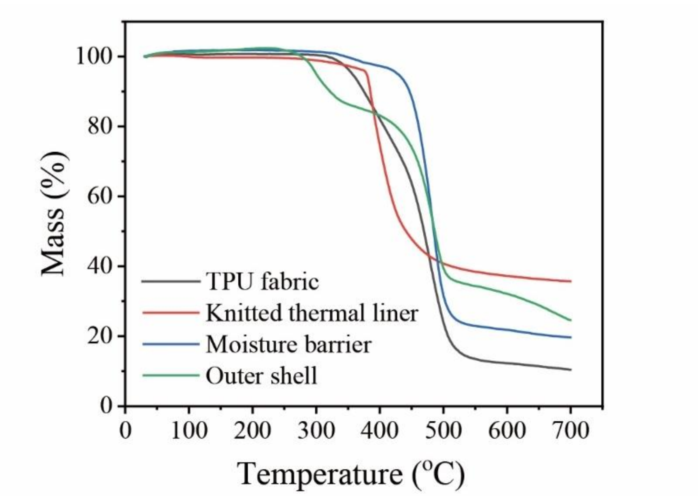

Figure 4-17 TG results of the fabrics used for the proposed textile.

4.6.2 Deformation of the SRT and its properties

As the traditional moisture barrier is impermeable, a breathable moisture barrier was selected to improve thermal comfort performance. The thermal and moisture resistance of the conventional and proposed moisture barrier was measured, as illustrated in Figure 4-18a. Compared to the traditional moisture barrier, the breathable moisture barrier has comparable thermal resistance and significantly lower moisture resistance. As the traditional moisture barrier had considerable large moisture resistance (Ret), more than 350 $m^2 \cdot Pa/W$, which was almost 50 times the Ret of the breathable moisture barrier (7.481 $m^2 \cdot Pa/W$), indicating the necessity of using breathable moisture barrier. Figure 4-18b displayed the cross section of the SRT in a fully deflated and fully inflated state. The application of the knitted thermal liner can fix the STAs to avoid slippage. And the air gap between STAs can be divided into small parts to weaken thermal convection due to the existence of the connection clasp. The initial state of the SRT was flat with a smaller thickness. While fully inflated, the thickness increased, as shown in Figure 4-18c. Finally, a complete garment, intentionally designed to observe the deformation of the garment during actual use. Radiant heat was directed to the front and back of a manikin outfitted in our garment, emulating real-world conditions of a user actively involved in a fire scene (Figure 4-18d) by two radiant heat exposure equipment. By comparing the various states of the garment, we were able to clearly distinguish between the initial state of the garment and its activated state. Changes in thickness can be distinctly seen in Figure 4-18e and 4-18f, respectively.

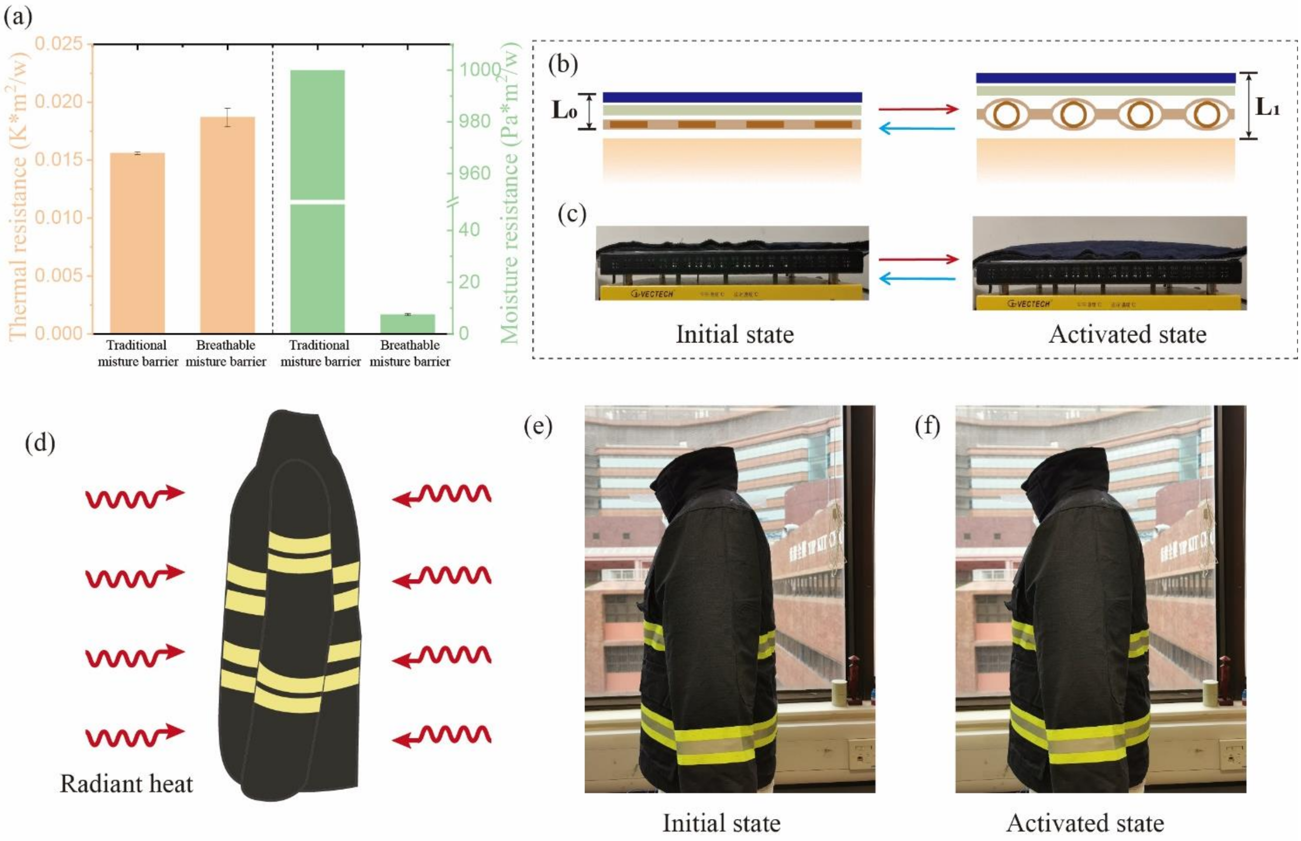

Figure 4-18 Thermal properties of the moisture barrier and the deformation of the SRT. (a) Thermal and moisture resistance of the traditional and the breathable moisture barrier. (b) Cross-section view of the soft robotic clothing under fully deflated state and fully inflated state. (c) Images of the SRT in initial state and fully activated state. (d) Schematic illustration of clothing exposed to radiant heat. (e) Image of the proposed clothing in initial state. (f) Image of the proposed clothing in activated state.

4.6.3 Evaluation of the thermal properties under exposure of radiant heat source

After assembling the fabric system, thermal protection and thermal comfort were evaluated. The performance of our proposed soft robotic textile was characterized by radiant heat exposure testing and hot surface contact testing. The temperature of the fire environment is generally 100-300 °C, and the heat flux is round 1-10 kW/m^2 [124]. Considering the properties of the selected thermal protective fabric, the temperature of the outer layer for the radiant heat exposure testing and hot surface contact testing is 117 °C and 120 °C separately. The radiation exposure test setup was shown in Figure 4-19a. Experimental results were demonstrated in Figure 4-19b. Traditional textile (TT) exhibited a higher internal layer temperature during the test procedure when compared to SRT. In response to radiant heat exposure, the low boiling point fluid absorbs heat, gradually turning to vapor, thus enhancing the thickness of the SRT. The thermal resistance of the SRT gradually increased at the beginning and reached a stable value upon complete transfer from liquid to vapor. Thus, TT exhibited a faster rate of internal temperature growth than SRT, indicating a lag in heat retention. As human skin temperature around 44 °C has been identified to be the pain threshold. When the surface temperature of the skin exceeds 44 °C, the skin may get burned. While if the temperature approaches 56 °C, the skin may receive second degree burn, which may be irreversible. The time between starting to feel pain and receiving a second degree burn is called the pain alarm time, which should be as long as possible to allow the wearer to escape dangerous conditions. [124]. Thus, time to reach 44 °C (t_{44}) and 56 °C (t_{56}) and the final temperature of the inner layer (T_{fa}) were collected and demonstrated in Figure 4-19c. The application of SRT effectively extended the time of the inner layer to reach 44 °C and 56 °C, especially the time to reach 56 °C. And the T_{fa} also dropped 22.8%, from 65.9 °C to 50.9 °C. Especially, t_{56} could not be reached by SRT, also proved by the T_{fa} which was below 56 °C. The temperature and velocity distribution of the SRT were simulated, illustrated in Figure 4-19d. The results showed that the use of knitted thermal liner could separate the air gap into smaller parts, weakening the thermal convection.

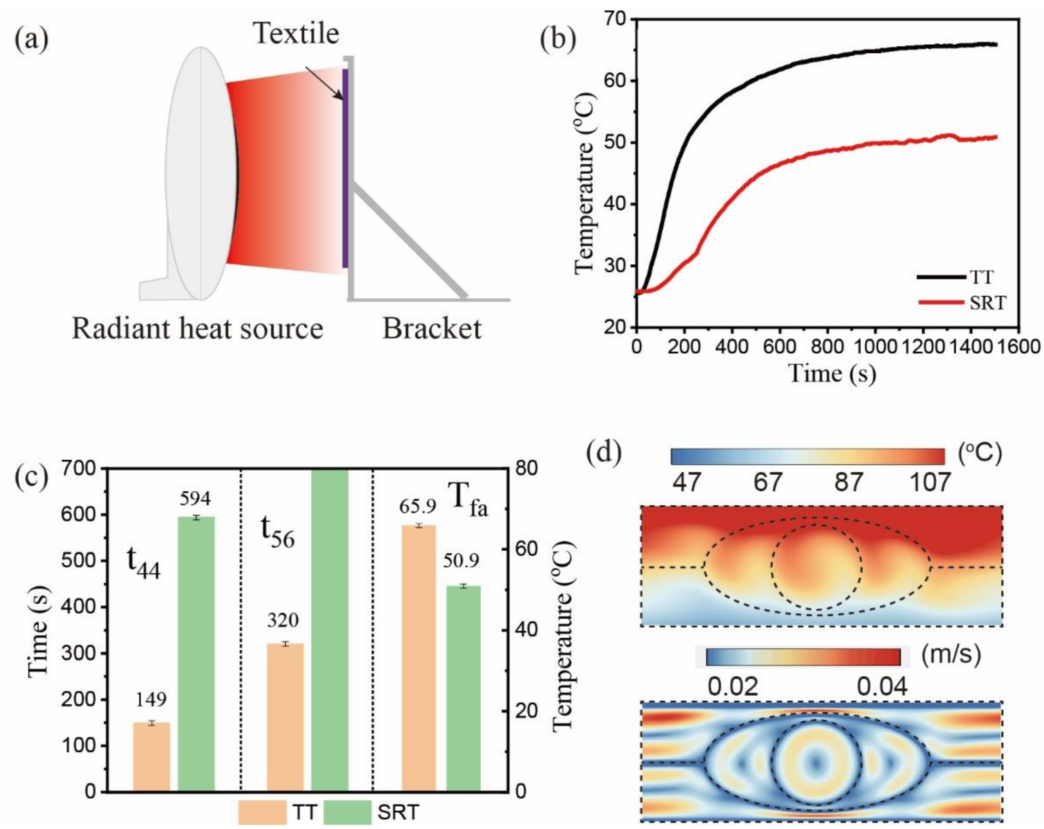

Figure 4-19 Experimental results of SRT under radiant heat source. (a) Setup for heat exposure test. (b) Temperature variations in the inner layer of TT and SRT when exposed to radiant heat. (c) Time to reach 44 ℃ and 56 ℃ and the final temperature when exposed to radiant heat. (When t_{56} = 700s, it means the temperature did not reach 56 ℃ throughout the process.) (d) Simulated results of temperature and velocity distribution of SRT when exposed to radiant heat.

4.6.4 Evaluation of the thermal properties under hot surface contact test

Next, we obtained results from hot surface contact tests [125] by put fabric on a high-temperature hotplate (120 ℃) with outer layer contacting with heat source. Heat transferred from the hot plate to the fabric from the outer layer to the inner layer, actuating STAs inside the fabric to inflate and changing the distance between the inner layer and the hot plate surface. The setup was shown in Figure

4-20a. And as shown in Figure 4-20b, the temperature-contacting time curve indicated that the SRT had lower inner layer temperature (more than 10 °C) than the TT. As shown in Figure 4-20c, the time difference value of t_{44} tended to be quite small, indicating the STAs were not actuated yet or the deformation of STAs was very small when the temperature reached 44°C. However, the time difference value of t56 was remarkable because the actuators had been fully actuated. T_{fa} also dropped 24.5% from 66.1 °C to 49.9 °C. As shown in Figure 4-20d, temperature and velocity distributions of SRT were also simulated. It is obvious that the existence of the knitted thermal liner, especially the connection clasp can divide the air gap into smaller parts, reduce the natural convection, indicating the efficiency of the knitted thermal liner.

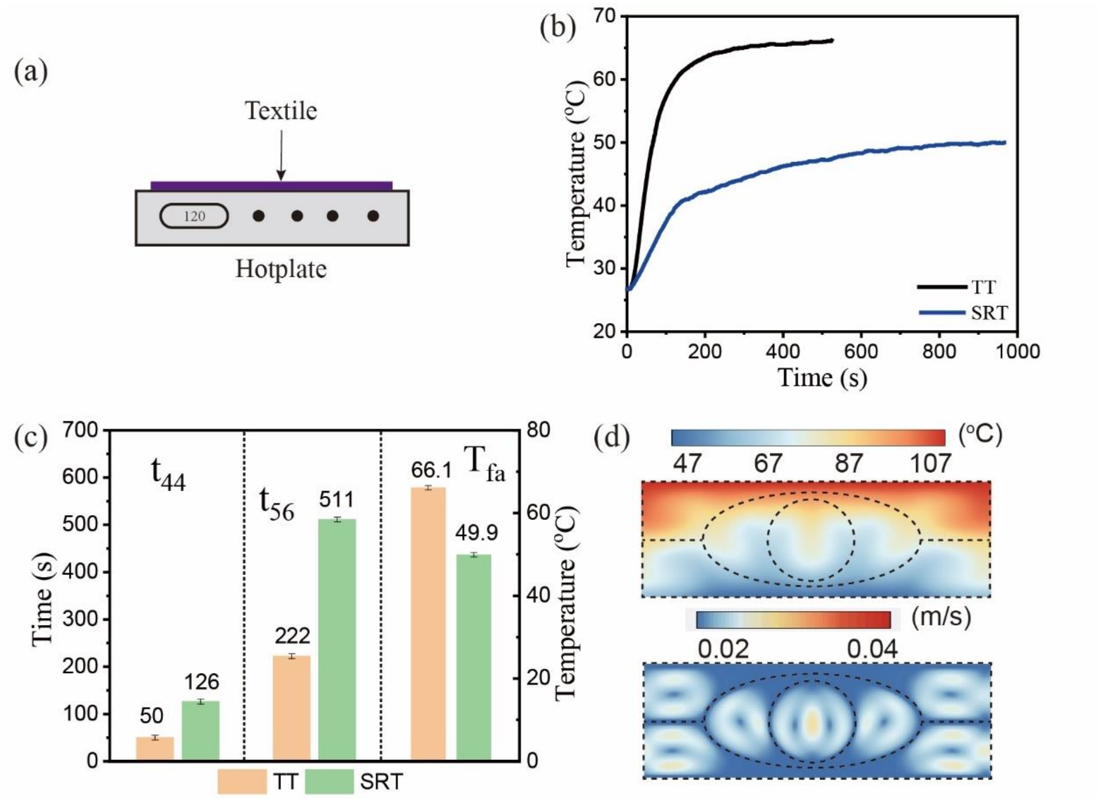

Figure 4-20 Experimental results of SRT under hot surface contact. (a) Setup for hot surface contact test. (b) Temperature variations in the inner layer of TT and SRT when contacting with hot surface. (c)

Time to reach 44 ℃ and 56 ℃ and the final temperature when contacting with hot surface. (d) Simulated results of temperature and velocity distribution of SRT when contacting with hot surface.

4.6.5 Evaluation of the thermal properties by sweating guarded hotplate

Then, thermal comfort tests, including thermal resistance and moisture resistance tests, were conducted to evaluate the thermal insulation of fabrics and the transfer of moisture from the human body to the ambient environment. Figure 4-21a displays the structure of the sweating hotplate for thermal comfort evaluation. As shown in Figure 4-21b, compared to TT, SRT exhibited lower thermal resistance in the deflated state, but higher thermal resistance in the inflated state. The difference in moisture resistance, shown in Figure 4-21c, between the deflated state and the inflated state was no more than 20 $Pa \cdot m^2/W$ and the maximum moisture resistance was less than 70 $Pa \cdot m^2/W$, confirming the feasibility of the knitted thermal liner. The thickness of the textiles was illustrated in Figure 4-21d. SRT had a smaller thickness in deflated state, and a lager thickness in inflated state than TT.

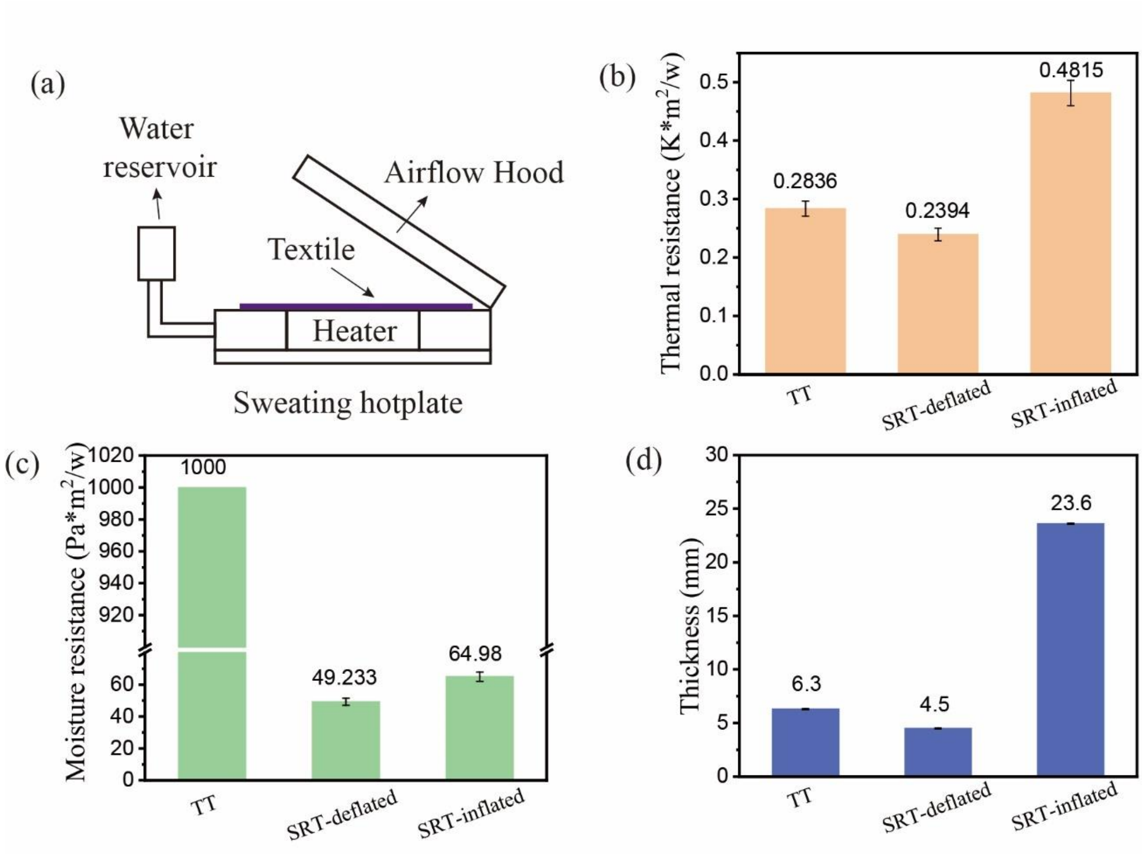

Figure 4-21 Experimental results of SRT from sweating guarded hotplate. (a) Setup for thermal and moisture resistance. (b) Thermal resistance of TT, deflated SRT and inflated SRT. (c) Moisture resistance of TT, deflated SRT and inflated SRT. (d) Thickness of TT, deflated SRT and inflated SRT.

4.7 Summary

In general, we have proposed soft robotic textiles for thermally adaptive insulation that exhibit excellent performance for thermal protection. The unique and generalizable mechanism depends on the reversible phase change of the low boiling point fluid under different temperature conditions, and particularly enhanced by the use of knitted fabric as the thermal liner. Liquid-vapor conversion behaves like thermal switches that can adapt to changes in the ambient environment, so wearers do not need to add or reduce clothing. Normally, the fabric system is activated by the passive heating system from ambient heat without extra energy sources. Particularly, active heating systems can replace passive heating systems where ambient temperature is absent or limited. Our materials are all low-cost commercial products, and easily fabricated by scalable and facile processes, indicating their large-scale production. Overall, our soft robotic textile for thermally adaptive insulation exhibits excellent performance to help people survive in a demanding environment.

Chapter 5 Soft pneumatic actuator-driven textile for controllable body warming

5.1 Introduction

Warming textiles play an important role in clothing development projects, which are essential for people to work or live in cold environments where people may not survive without additional clothing for thermal insulation. Based on the introduction and literature in Chapter 1 & 2, the distribution of heat and moisture significantly influenced human survival in cold environments. When the ambient temperature is lower than the human body temperature, body heat is released to the environment. Clothing plays a crucial role in regulating the heat loss of the human body and ensuring that the body maintains a stable temperature. Warming clothing aims to prevent excessive heat loss to maintain the body's heat balance. Notably, we may need clothes to protect ourselves from rapidly changing circumstances. For example, when people walk into a cold outdoor environment from a warm house, the ambient temperature drops the moment people step out the door. Normally, people need to add thick clothing to avoid excessive heat loss, resulting in temperature variations. Even outside, the temperature undergoes significant daily fluctuations, which may change suddenly due to unpredictable rain, wind, or hail. Clothes may not provide enough insulation for the body. Notably, people climbing mountains may feel colder in the process as the temperature decreases 1 °C when the attitude rises 100 m. For those climbers, wearing thick clothes can effectively blocking heat loss. However, thick clothing often has a heavy weight, which not only carries a heavy load, limits body movements, but also affects air permeability. Clothing, regulating the heat loss of the human body, is critically needed to maintain body temperature. The climber may sweat a lot due to the high/medium-intensity continuous exercise in the process. Poor moisture permeability can cause sweat to accumulate near the skin. Therefore, smart clothing that can adapt to temperature variations with fairly moisture transfer properties is required.

Traditional cold protective materials, including cotton and down jacket, have constant thermal resistance values, indicating limited thermal capacity. These materials can trap air around them to create an air layer to increase their thermal insulation properties, which rely on the excellent thermal conductivity of air. Air is a well-known thermal insulation material that is lightweight and cost-effective. Creating an air gap between fabric and clothing layers to reduce heat loss from the human body to the outside environment has been a major method. Air gap provides a microclimate buffer to limit heat and moisture transfer through fabrics [126]. Therefore, the use of air gaps within fabric layers to manage the thermal properties of the human body has become an important method. As mentioned in Chapter 2, researchers have tried to trap air between fabric layers to protect the human body in cold conditions. Commercial clothing also uses air gaps to enhance thermal insulation to avoid cold stress. NuDown has successfully designed a vest and jacket using air as thermal insulation material. The Nudown garment (Figure 5-1a) allows wearers to adjust and control the ideal temperature for themselves by a pump regardless of environmental conditions. They use air, the infinite natural resource, as insulation materials, which are one of the most efficient and heat-retaining substances.

Skyscrape's insulating fabrics (Figure 5-1b) are another garment whose thermal insulation material is air. This garment is temperature-responsive without other wires, sensors, or pumps. The fabric can function as a thermometer, increasing fabric thickness in cold conditions and reducing it in warm conditions, which depends on the expansion and contraction of yarns in the fabric.

Figure 5-1 Commercial jackets utilizing still air for thermal insulation. (a) Nudown jacket. (b) Skyscrape's insulating fabrics and the deformation principle.

As air is an infinitely available natural resource in nature, these garments are much more cost-effective and energy efficient. However, the disadvantages are also obvious. For the soft robotic fabric mentioned in Chapter 2, the application of silicone not only results in heavy weight but also poor wear comfort. Durability is also a major challenge as it is liable to break, which can lead to air leakage. While the Nudown jacket is impermeable, the moisture transferred outside is blocked. Skyscrape's clothing has been designed with light weight and air permeability in mind to improve wear comfort. However, the force that the fabric can provide is still small, which may affect the deformation of the garment when it is covered by other fabric. Based on the review of current garments with tunable thermal insulation properties, we proposed a soft robotic fabric and garment, using still air as thermal insulation materials, for wearers to adapt to different thermal conditions, which are lightweight, flexible and breathable.

5.2 Design strategy and working mechanism

The proposed soft robotic clothing comprises a soft robotic-clothing system and a control system. The soft robotic-clothing system can be worn personally like normal clothing, which can alter the thickness of the air gap between fabric layers to change thermal resistance and allow moisture to transfer from the human body to ambient conditions such that sweat may not accumulate on the skin. The soft robotic-clothing system relates to a control system. In particular, the control system is configured to monitor temperature changes, provide feedback to the control center, respond to signals, and activate working units to increase or decrease the air volume of the soft robotic-clothing system. The soft robotic-fabric system comprises soft robotic units. These units may be fabricated from soft and deformable materials, such as airtight fabric, silicone, and tubes. The units can be attached, stitched, or wrapped by other fabrics. They may have one or more air chambers to allow fluid movement, such as air and liquid. The soft robotic unit can store gas inside to manage the unit's shape through expansion or bending. The volume of gas inside could determine the thickness of the soft robotic units that are precisely controlled by the control system. Soft robotic units include hollow parts. The void portion between the branches of the soft robotic units allows moisture to transfer from the human body to the ambient environment, achieving lower moisture resistance. The soft robotic fabric system further comprises a knitted interlining. Knitted interlining can be fabricated by commercial weft knitting machines that can be produced on a large scale. It has channel portions and connection portions. The channels have two separate layers according to the shape of the soft robotic units to wrap and fasten them. The connecting portion is a one-layer fabric that connects these channels. In particular, the connection portion can be positioned between the middle of the knitted interlining when the soft robotic units are activated, weakening the air convection inside the air gap. The channel size is 1-2cm larger than the soft robotic units so that the soft robotic units can be easily inserted into the channels. The knitted substrate is made of soft, skin-friendly cotton yarn, and the soft robotic fabric system includes a shell fabric. The shell fabric is waterproof and breathable, blocking liquids and chemicals from the outside and allowing heat and moisture to transfer from the human body to the environment. The control system comprises a working unit, a data collection unit, a processing center, and a power supply. The working unit is a peristaltic pump that can compress the flexible tube inside to force air to move through the tube. The reversible rotation of the pump depending on the direction of the applied current can determine the direction of air movement to move into or out of the soft robotic units. One end of the peristaltic pump has a longer silicone tube to connect to the soft robotic units. The control system comprises a data collection unit. A temperature sensor is installed in the outer layer of the soft robotic fabric system to monitor temperature variations and transmit data to the processing center. The control system further comprises a processing center. The processing center is an Arduino micro controller that can receive, process and output signals to control the working unit programmly and accurately. The control system further comprises a power supply to support the operation of the entire control system.

5.2.1 Mechanism of the soft robotic clothing

According to the introduction of clothing for body warming, a soft robotic fabric and clothing would be designed by trapping still air between fabric layers. As the thickness of the air gap has a significant impact on the thermal resistance value of clothing, the proposed soft robotic fabric and clothing aims to adjust the air gap size to achieve multi-level thermal insulation, which can adapt to environmental temperature changes based on managing thermal conductivity by controlling the height of the air gap between fabric layers. The air gap size of several gears can be established by adjusting the air volume inside the actuator.

The entire garment system includes a soft robotic clothing with soft pneumatic actuators and a control section to detect, collect and manage signals. As shown in Figure 5-2, when the ambient temperature is suitable for the body, the soft pneumatic actuator is fully deflated while the entire garment is quite thin (left). Under this condition, the fabric layers of the garment contact each other with higher thermal conductivity. The heat and moisture from skin side can transfer through clothing to outside. If the temperature decreases, the signal will be collected, transmitted and reflected to the working pump to inflate the soft pneumatic actuator. And then the clothing is a bigger size. The "size" of the clothing would be determined by the air volume inside, depending on the time of inflation. If the temperature rises again, the air volume will be reduced to reduce the size of the garment. The deformation of the soft pneumatic actuator is reversible, indicating the tunable thermal resistance of the soft robotic fabric and clothing. The smallest size of the garment appears when the actuator is fully delayed, and the largest size occurs when the actuator is fully inflated.

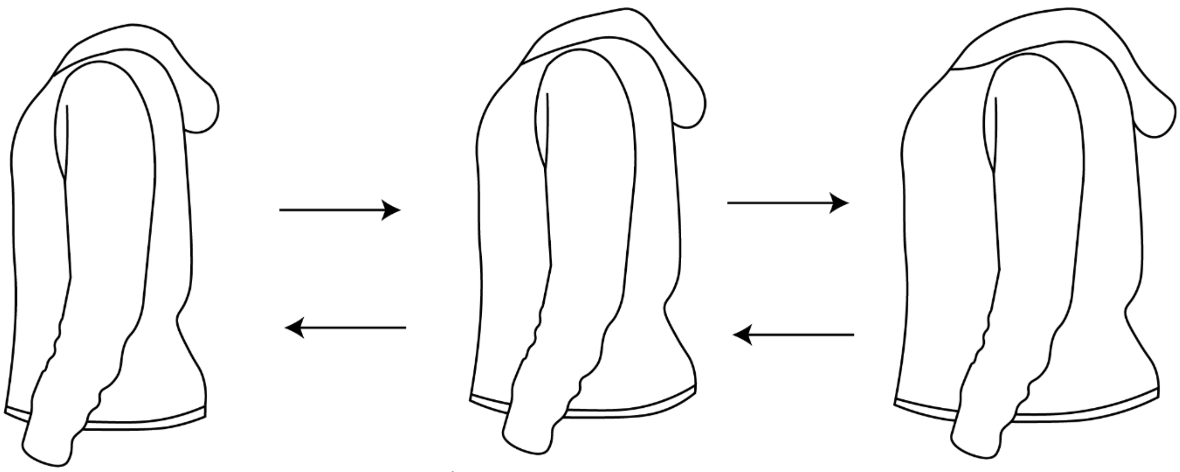

Figure 5-2 Reversible deformation of the soft robotic clothing. Fully deflated state means that there is no air inside and the clothing has the minimum thickness. Fully inflated state means the clothing has the maximum thickness.

When the pneumatic actuator between fabric layers is inflated, the expanded actuators push the outer shell away from the skin side and create an air gap between them to enhance thermal insulation. If the air volume inside the actuator decreases, the clothing looks thin with reduced thermal insulation. The reversible deformation of the pneumatic actuator can lead to thickness variations throughout the whole clothing system, controlling the thermal insulation properties. Figure 5-3 shows the cross section of the pneumatic actuators during the deformation process. When wearers remain in a condition at a suitable temperature, the clothing is completely deflated with fabric layers contacting each other. The thermal resistance of the entire fabric system is lower, allowing large amounts of heat transfer from the body to the ambience. When the ambient temperature decreases, the system can detect changes in the ambient temperature. The pump works to inflate actuators to increase the air gap between fabric layers, enhancing thermal resistance and blocking heat loss from the human body. If the temperature rises again, the actuators would be deflated to reduce the air volume and then weaken the thermal insulation. This deformation process is reversible, which is controlled according to the temperature. The entire garment is designed with a skeleton-like structure for better compatibility with the human body, reinforcing flexibility and breathability. We have made personalized, fully adjustable warmth a game-changing reality.

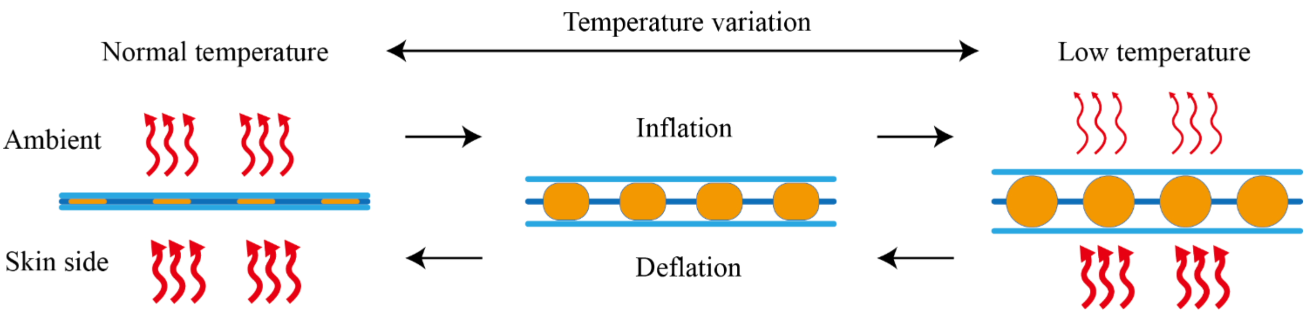

Figure 5-3 Deformation of the cross section of the pneumatic actuators. Under normal temperature, the thickness of the fabric is small with lower thermal resistance, allowing more heat transfer to the ambient environment. Under low temperature, the thickness of the fabric is large with higher thermal resistance, blocking heat transfer to the ambient environment.

5.2.2 Inspiration of the soft robotic actuator

In order to ensure that the soft robotic actuator can fit the human body after inflation, a pneumatic skeleton-like structure was proposed, which is also called soft robotic skeleton. Figure 5-4a shows the human skeleton and Figure 5-4b is a soft robotic skeleton-like structure. As the inflatable structure needs to revolve around the body, the soft robotic skeleton, which mimics the shape of the human skeleton, can fit the human body well. The vertical part of the structure is the main airway connecting the entire inflatable structure, based on the shape of the curvature of the human spine. The horizontal strip structure may look like ribs.

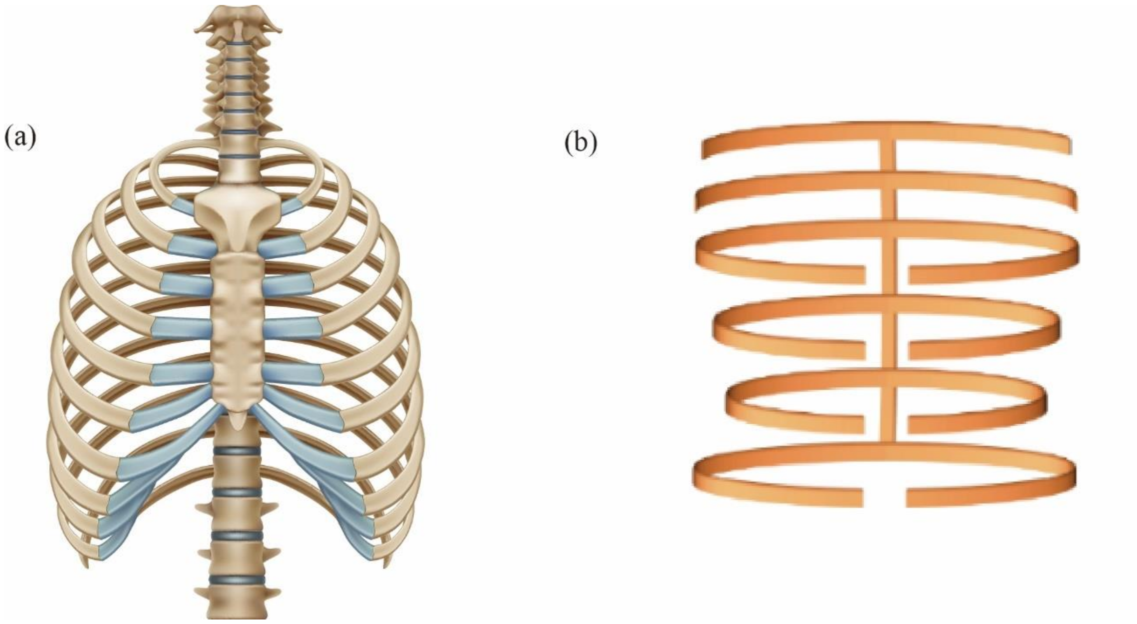

Figure 5-4 Inspiration of the soft robotic skeleton. (a) Human skeleton. (b) Skeleton-like soft robotic structure.

5.2.3 Design of the knitted substrate

As the inflated soft robotic skeleton is an air bag, it may not fit well with the human body. A knitted substrate is applied in this study to achieve three functions. Firstly, the knitted fabric has channels for soft robotic skeletons to fix the actuator and avoid slippage. Secondly, the knitted substrate is soft and flexible, which can be fabricated as clothing. Thus, the skeleton inside the channels can be constrained by the channel. Under the constraints of knitted fabric, the soft robotic skeleton can fit the human body well even in an inflated state. The outer layer of the channels can provide a slight restraint force, which can reduce the slight movement of the skeleton between the clothing and the human body, thus better preserving the still air. Finally, the knitted substrate has connection clasps between channels, which can be used to divide the air gap into smaller parts to reduce thermal convection. The schematic diagram of the knitted substrate is illustrated in Figure 5-5. The dark blue part represents the channels for the soft robotic skeleton and the light blue part represents the connection clasps. The size of the knitted substrate, involving channel space and connection clasps, is designed according to the size of the soft robotic skeleton to ensure that the soft robotic skeleton can be fixed well.

Figure 5-5 Schematic diagram of the knitted substrate, including the front panel (left) and back panel (right). The dark blue part is the channels for soft robotic skeleton and the light blue part is the connection clasps.

5.3 Materials and fabrication

5.3.1 Materials

Materials used in this study include TPU fabric for soft robotics, cotton yarn for knitted substrates, and a revised commercial jacket as the outer shell for outdoor coats. The TPU fabric and cotton yarn are the same as described in Chapter 4. Commercial cotton yarns are used to fabricate the knitted interlining, which acts as the substrate to fasten the soft robotic skeletons. The specification of cotton yarn is 21s/2. The outer shell fabric was purchased from Taobao.

5.3.2 Fabrication of soft robotic skeleton

A modified Computerized Numerical Control (CNC) machine is used to fabricate soft robotic units, which can achieve precise control, modular design and large-scale production. A silicone pad with a thickness of 8 mm is placed on the machine working plate. An electric soldering iron is integrated with the machine as a heater. The heater can provide stress and heat (i.e., 200 °C) to TPU fabric and move programmly to seal them together to desirable pattern. Figure 5-6 shows the images of the CNC machine. The width of the heater is 3mm, which is the width of the sealing edges. And the working speed of the heater is 5 cm/min to ensure enough time for sealing. Notably, compression force from the heater was applied on the TPU fabric to ensure enough sealing force.

The schematic design process is shown in Figure 5-7a. A skeleton pattern is created by the heater with 3mm-sealed edges. Then, cuts are made to remove the other parts to obtain the skeleton structure. The bottom of the soft robotic skeleton is open for insertion with a tube by a charging connector. Figure 5-7b shows the charging connector and the method of integration with TPU fabric. The dashed line shows the air flow channel.

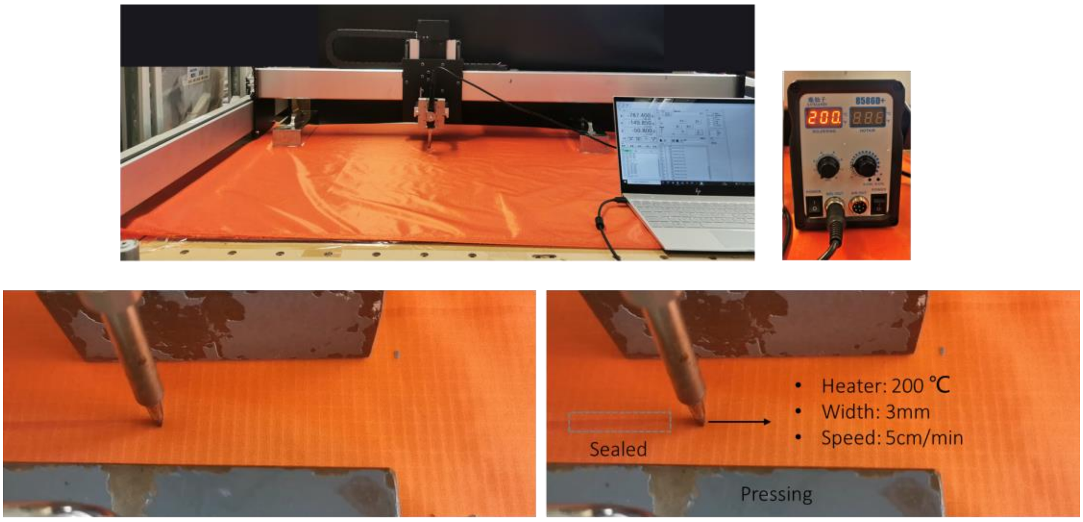

Figure 5-6 Images of the CNC machine, including a heater with temperature of 200 °C, a computer to control the movement of the heater and two heavy press iron to fix the TPU fabric.

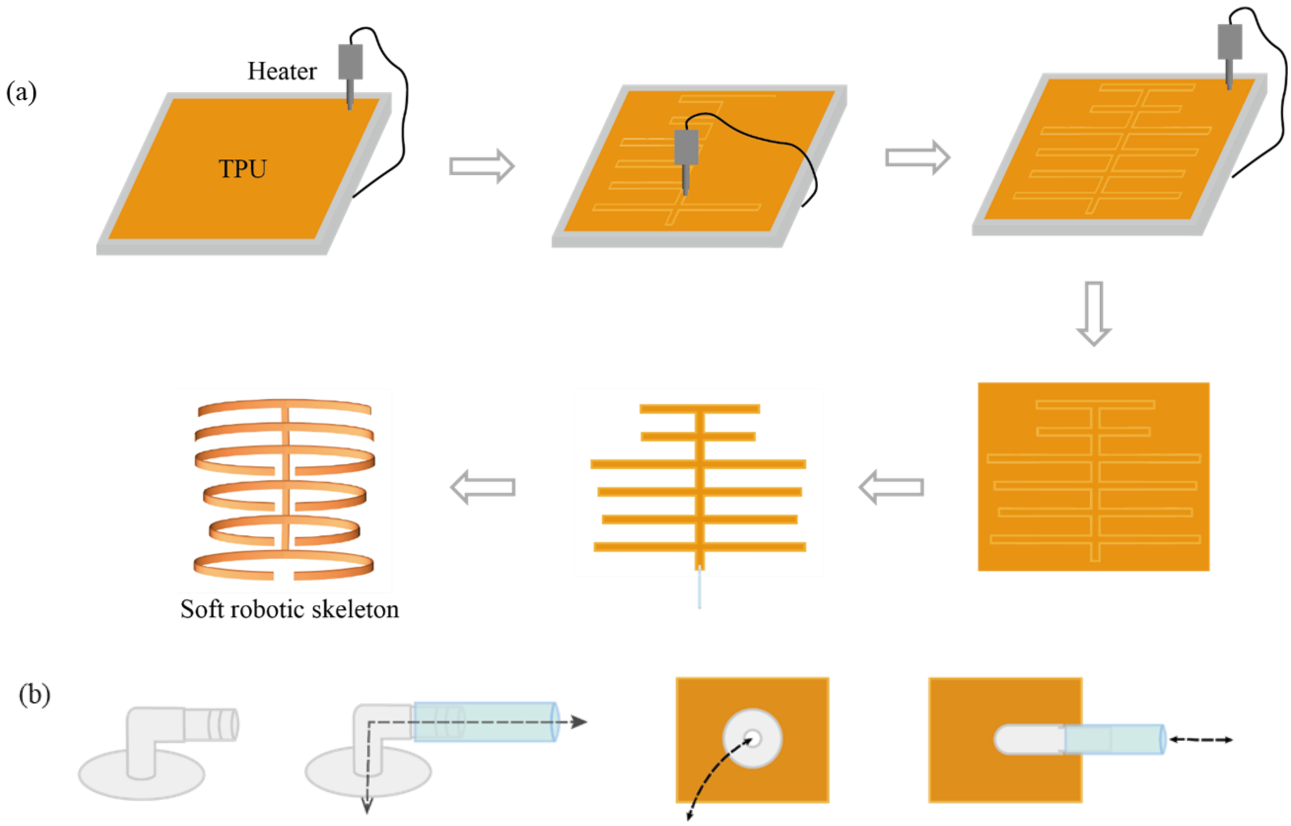

Figure 5-7 Fabrication of the soft robotic units. (a) Fabrication process, including sealing and cutting. (b) Charging connector and its integration with TPU fabric.

A prototype of soft robotic clothing was developed, manufactured and tested. A detailed description of the soft robotic units used in clothing prototypes is shown in Figure 5-8. The length of the soft robotic units is designed according to the girth of the human torso that was used for subsequent experiments so that it can be next to the skin worn. And the length of each branch can be adjusted according to the actual girth of the wearers. Thus, the deformation may be more obvious.

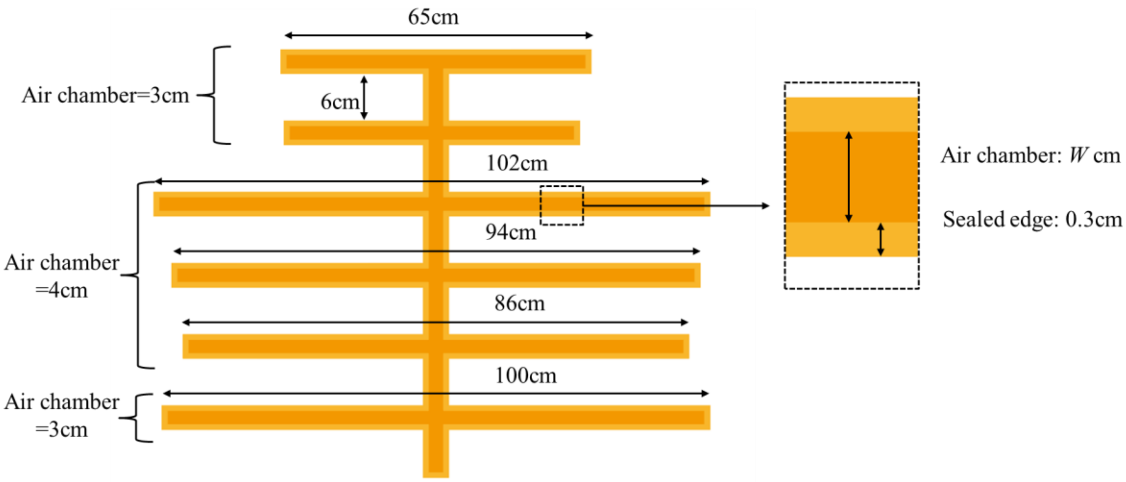

Figure 5-8 Dimension description of the soft robotic units. The branches have the chamber width of 3cm. The length of the branches is designed according to the human torso that would be used in the following experiments.

5.3.3 Fabrication of fabric substrate for the soft robotic skeleton

Double-layer knitted fabrics are fabricated using a computerized flat knitting machine (CMS 822 ki multi). Figure 5-9 shows the structural design of the knitted interlining. The light green part is designed for the air chamber of the soft robotic skeleton, which has two layers. And the dark green is the connection part, which is a one-layer fabric to connect the two-layer part.

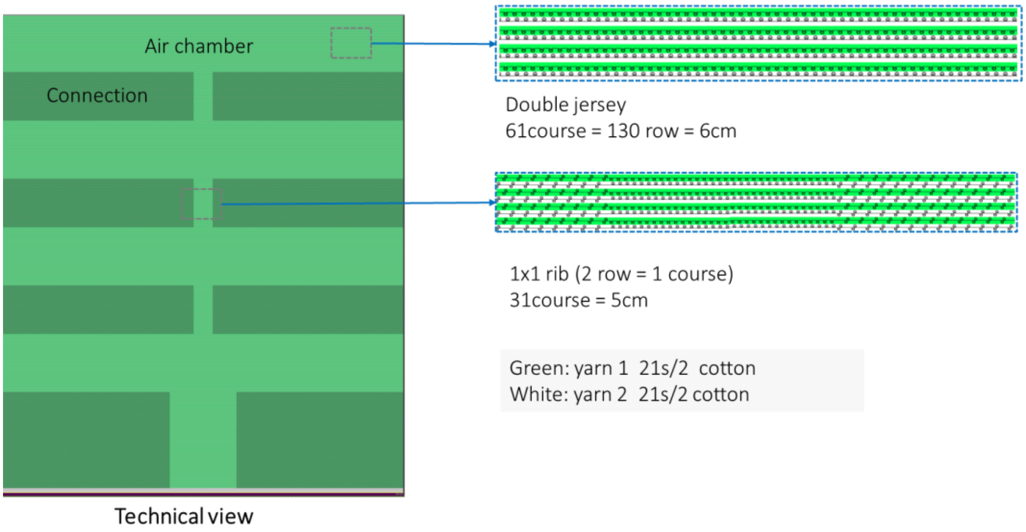

Figure 5-9 Structure design of the knitted substrate. The air chamber is knitted by double jersey with two separated layers to provide channels for soft robotic skeleton. The connection part is knitted by 1x1 rib by half gauge technology, where two rows form one course.

For further human trials, the knitted substrate for both men and women were fabricated. Figure 5-10 and 5-11 show the knitted interlining of the men's and women's versions. The white parts are the channels for soft robotic skeleton and the grey parts are the connection. It is obvious that there is a vertical channel on the back side of the knitted interlining, which is designed for the vertical chamber of the soft robotic skeleton. The interlining is slightly tight, aiming to ensure that the air gap generated due to the deformation of the soft robotic skeleton, avoiding effect by the existing air gap between fabric layers.

Figure 5-10 Knitted substrate for men's version. The front side of the of the garment (left 1). The back side of the garment (left 2). The front side of the man wearing knitted substrate (right 2). The back side of the man wearing knitted substrate (right 1).

Figure 5-11 Knitted substrate for women's version. The front side of the of the garment (left 1). The back side of the garment (left 2). The front side of the woman wearing knitted substrate (right 2). The back side of the woman wearing knitted substrate (right 1).

The parameters of the knitted substrates were illustrated in Table 5-1, where the weight, shoulder width, cloth width and cloth length are all demonstrated. As the knitted fabric shows excellent stretchability, the knitted substrates designed can be applied to people whose body size can have a small range.

Table 5-1 Parameters of the knitted substrates.

	Weight (g)	Shoulder width (cm)	Cloth width (cm)	Cloth length (cm)
Men	332.15	53.0	49.5	69.0
Women	248.57	39.5	38.0	66.0

5.3.4 Integration of the fabric and the soft robotics

The pattern of the knitted fabric was designed according to the shape of the skeleton, whose channel width was twice that of the skeleton, allowing an easy insertion process. After fabrication of the knitted substrate, the soft robotic skeleton is manually inserted into the channels. Then, the outer shell was fabricated to achieve tight covering of the knitted fabric, ensuring uniformity of the air gap. Finally, a tube was applied to connect the soft robotic skeleton to the pump. The weight of the soft robotic clothing and the components are listed in Table 5-2, including a men's and a women's version.

Table 5-2 Weight of the soft robotic clothing.

Component	Weight (g)
Soft robotic units	109.90 (men) /100.50 (women)
Knitted interlining	332.15 (men) / 248.57 (women)
Outer shell fabric	330.00
Charging connector + Tube	6.70
Total	778.75 (men) / 685.77 (women)

5.3.5 Design of the control system

The soft robotic units deform into a clothing skeleton, resulting in optimal thermal performance under different thermal conditions. The control device is used to regulate the thermal insulation of soft robotic clothing by changing the amount of air or the air pressure of soft robotic skeletons through inflation and deflation. The control device consists of a temperature sensor, a pressure sensor, a peristaltic pump, a tiny single board microcontroller, and a small rechargeable battery. The control device applies electrical energy to drive the peristaltic pump, regulating the amount of air in the soft robotic units by inflation and deflation. In response to the temperature signal detected by the sensor in the control device, the peristaltic pump operates for inflation or deflation, automatically regulating the structure and thickness of the clothing system as well as its heat and moisture transport properties. The entire system would be powered by a small rechargeable battery. A high-quality rechargeable battery is selected, which has a service life of more than 2 years. The battery can also be replaceable.

Figure 5-12 is a flowchart of the control system. When the system starts, it starts first. Then the temperature sensors work to collect the real-time temperature and send it to the center. If the temperature meets the preset function, no power is provided, and the pump maintains the stop state. If the temperature is higher than the preset value, a backward voltage is provided, and the pump works to deflate the actuator. Otherwise, the forward voltage is provided, and the pump works to inflate the actuator.

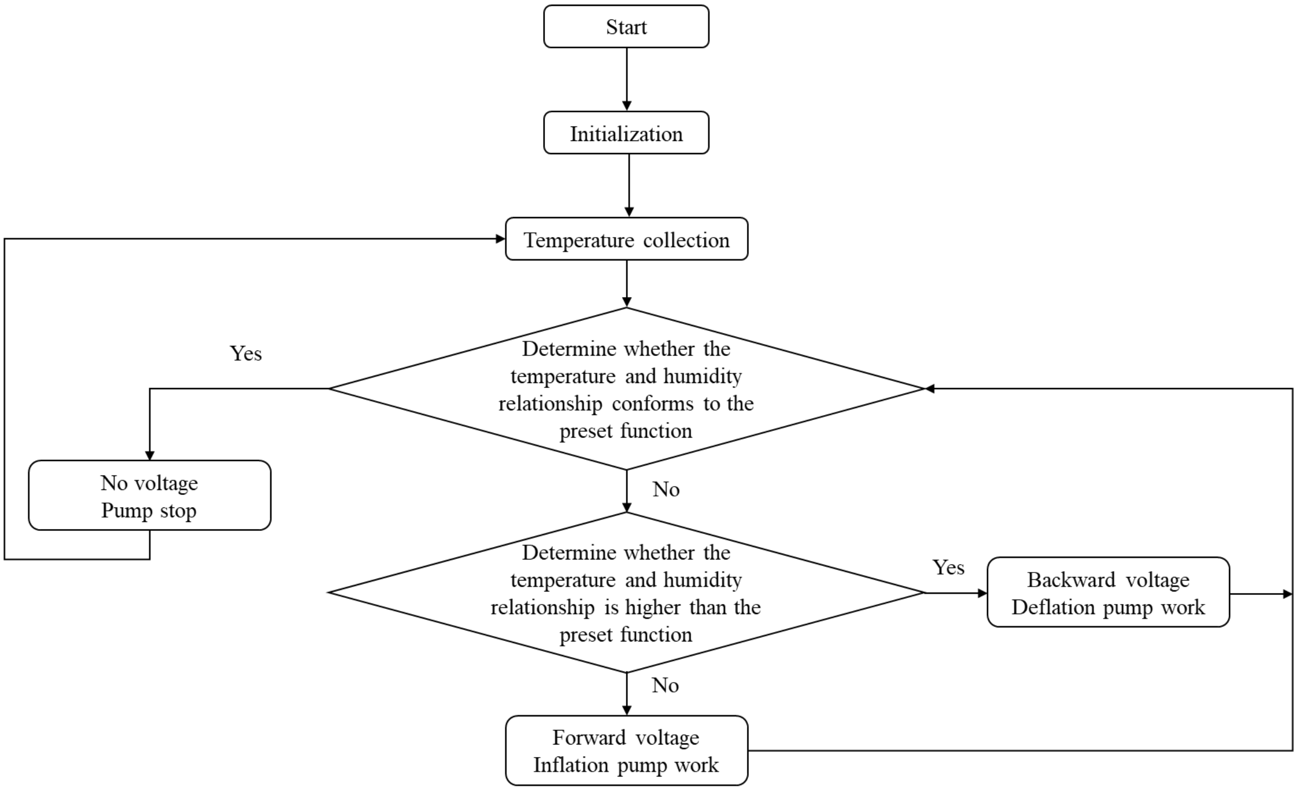

Figure 5-12 Flowchart of the control system.

The target temperature range would be divided into several levels, corresponding to different amounts of air inside the soft robotic units. The thickness of the air gap can be pre-determined based on numerical simulation to achieve optimal thermal properties. Air can be controlled programmatically by the time of inflation and deflation. In addition, we also explore the regulation of thermal resistance by controlling the internal air pressure, which can vary according to different temperature levels. The pump works very quietly, and the time is right to gradually adapt the thermal insulation to different thermal conditions. In order to maintain high safety, high-quality charging batteries or power banks, especially those that can be placed in consumers' pockets, are applied to the control device. Figure 5-13a shows a flowchart of the control device. The power supply can provide power to the system to ensure the normal operation of the device. The pressure sensor can detect the real-time pressure value, and then adjust the volume of the gas inside. The temperature sensor can detect changes in the temperature of the external environment and provide feedback to the control part. Figure 5-13b shows the entire control system. The pump is self-designed, and a brief introduction is shown in Appendix-A. And the image of the board is shown in Figure 5-13d. Figure 5-13c shows the Arduino image, which contains the locations of the main units, which are 4.8 cm*4.2 cm*2 cm in size and 22.659 g.

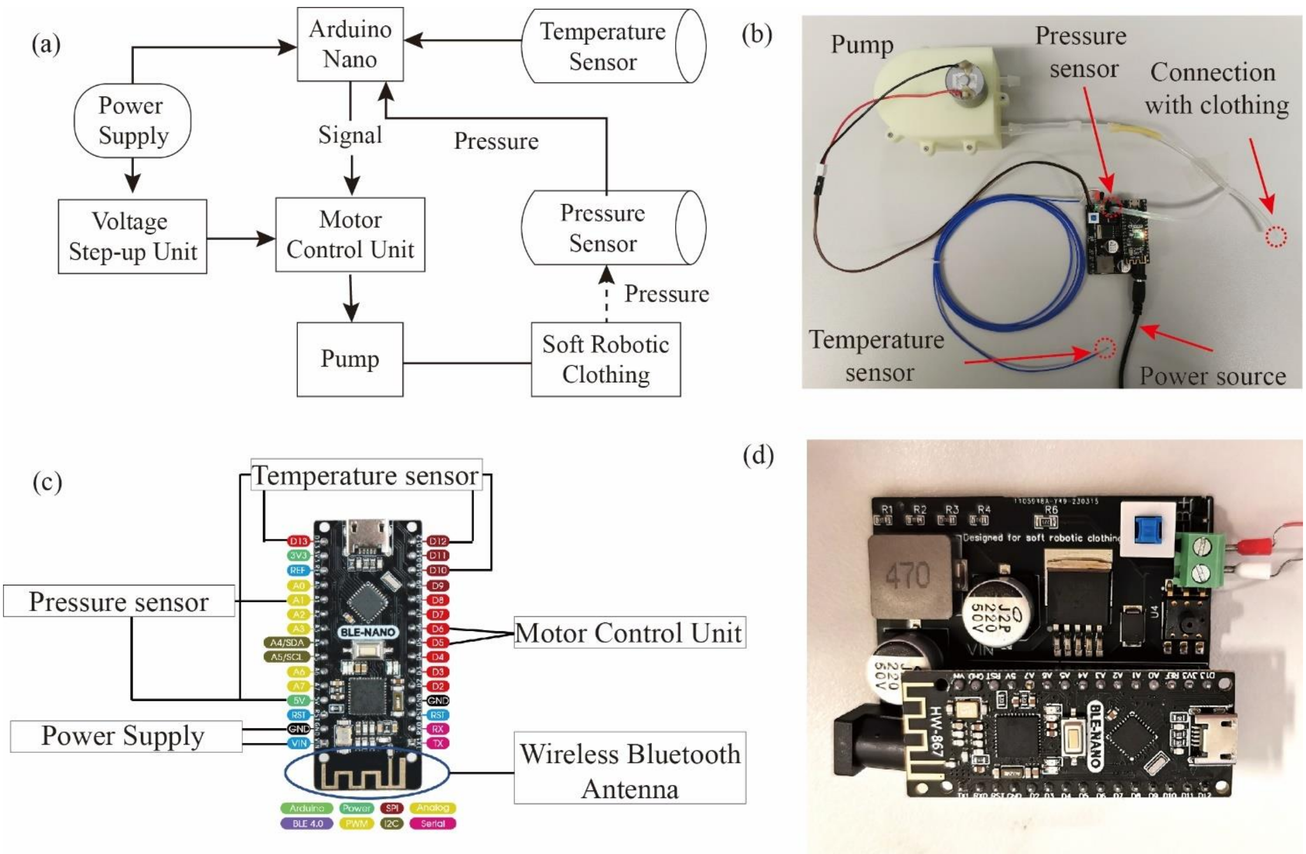

Figure 5-13 Design of the control device. (a) Flowchart of the control device. (b) Control device. (c) Image of the Arduino board. (d) Image of the overall specification.

Several levels can be divided according to temperature variations and pressure inside the actuator to adapt to different conditions. When the control system starts working, it can first detect the ambient temperature and give feedback to the center. Preset temperature values are set as the transition temperature to activate the soft robotic skeleton. At the same time, air pressure is also detected and collected, which is related to the temperature level. Code is essential for controlling the system. For a clear explanation of the control system, one example is provided in Figure 5-14. When the control system is powered on, the program starts first. In this section, five levels are divided. 20 ℃ [0], 16 ℃ [1], 12 ℃ [2] and 8 ℃ [3] are selected as reference and the corresponding air pressure is selected as 18-22%, 38-42%, 58-62%, 78-82% and 100% respectively. When the actuator is fully inflated, the pressure is set at 100%. And the pressure is 0% when the actuator is fully deflated. As shown in Figure 5-14, when the temperature is larger than 16 ℃ [1], and smaller than 20 ℃ [0], the air pressure should maintain between 38-42%. If the air pressure is less than 38%, a forward voltage is given to inflate the actuator, increasing the air mount inside to ensure suitable thermal properties. If the air pressure is 38-42%, no voltage is given. Otherwise, if the air pressure is higher than 42%, the backward voltage is given to deflate the actuator, reducing the amount of air inside. The control system code is shown in Appendix-B.

```
else if((t <= fTempCtr[0]) && (t > fTempCtr[1]))
{    {  if(pres < 38)
  {
   digitalWrite(digitalOutPin1, HIGH);
   digitalWrite(digitalOutPin2, LOW);
  } else if(38 <=pres <42)
  {
   digitalWrite(digitalOutPin1, LOW);
   digitalWrite(digitalOutPin2, LOW);
  }
   else {
   digitalWrite(digitalOutPin1, LOW);
   digitalWrite(digitalOutPin2, HIGH);
   }
  Serial.print("Level 2 ");
  Serial.print(pres);
  Serial.print("% ");
  Serial.print(t);
  Serial.println("C");
  delay(2000);
}
```

Figure 5-14 Image of the code for the control system.

5.4 Characterization of soft robotic units

5.4.1 Theoretical model of the soft robotic units

Actually, the deformation of the soft robotic units mentioned in this study is the same as that discussed in Chapter 4. The ideal cross section of the soft robotic skeleton during inflation process is shown in Figure 5-15. The height of the actuator is decided by the volume of air inside. When the actuator is fully inflated, the cross section tends to be a circle.

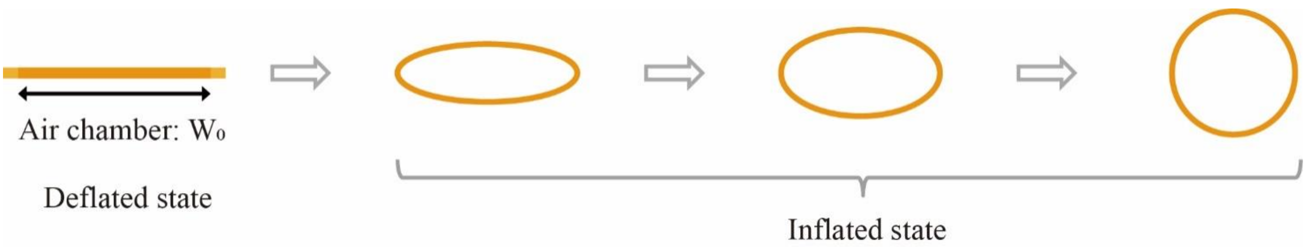

Figure 5-15 Cross section deformation process of the soft robotic skeleton from fully deflated state to fully inflated state.

The Eq. (4-1), (4-2) and (4-3) may also be used in this part to design deformation of the soft robotic skeleton. The maximum shrinkage ratio of the actuator can be obtained when θ is $\frac{\pi}{2}$. And the cross section of the actuator can be assumed to be a circle. Under this condition, the maximum height of a single can be derived before fabrication according to the original width (W_0) as the circumference is twice the original width. According to the equations, the relationship between the angle and the real-time width of the actuator is shown in Figure 5-16a. The original widths selected are 10 mm, 20 mm, 30 mm and 40 mm. It is obvious that the real-time width reduces as the angle increases and reaches the minimum when angle is π/2. Figure 5-16b shows the relationship between the angle and the real-time height of the actuator. As the angle increases, the air volume inside also increases, inflating the actuator and leading to an increase in height. The height reaches the maximum value when the angle is π/2, which is equal to the minimum width of the actuator at that time, assuming that the final cross-sectional shape of the actuator is a circle. Figure 5-16c demonstrates the relationship between the angle and the real-time volume of the actuator.

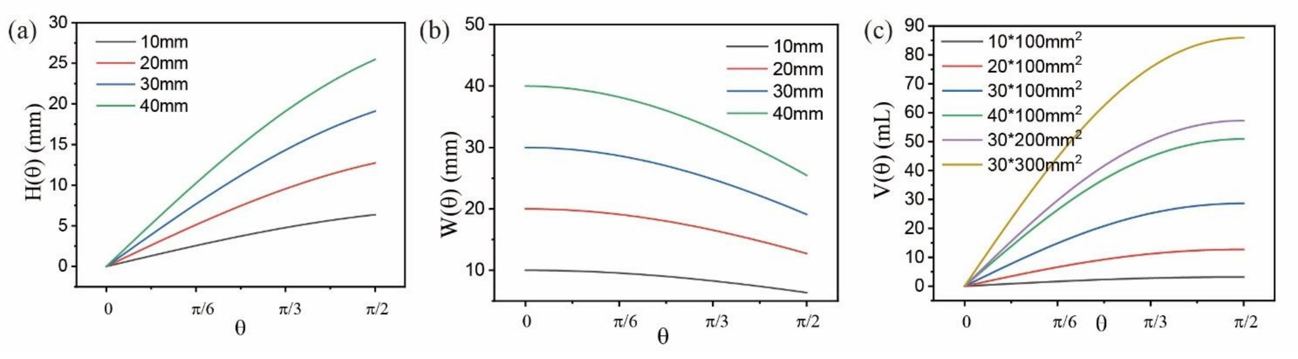

Figure 5-16 Relationship between the angle and the real-time width, height and volume of the actuator. The range of the angle is 0 to $\pi/2$. For 10*100 mm^2, 10 means the original width of the actuator and 100 is the total length of the actuator.

In summary, the air gap height of the fabric system can be pre-calculated according to the designed model, which is determined by the height of the actuator. And the actuator volume under different states can also be calculated, which can provide reference for the inflation time and pump flow.

5.4.2 Optimization of the air gap of the proposed fabric

Heat transfer in the air gap includes thermal conduction, convection and radiation under dry heat exposure. The still air has an excellent thermal insulator due to its low thermal conductivity. According to previous literature, the air gap entrapped with the clothing layers has a great influence on body heat dissipation. Creating an air gap to adjust the thermal performance of clothing has been an effective and sustainable method as the air is clear and renewable. However, when the temperature difference between the air layers is large enough, natural convection may be generated due to the difference in air density. The amount of Ra numbers is used to determine whether natural convection in the air gap occurs. The value of Ra number could be obtained by [127],

$$R_a = \frac{g\beta(T_f - T_s)L_{air}^3}{\alpha v} \quad (5\text{-}1)$$

Where g represents the gravity acceleration, g/m; β represents thermal expansion coefficient of the air, K^{-1}; T_f represents the surface temperature of the fabric, K; T_s represents the surface temperature of the skin, K; L_{air} is the thickness of air gap, m; α represents the thermal diffusivity of air, m^2/s; v represents the kinematic viscosity of air, m^2/s.

When R_a is greater than the critical value, the buoyant force can overcome the fluid resistance and initiate natural convection. To reduce heat loss caused by natural convection, the size of the air gap must be calculated before design. As mentioned in the evaluation method, the thermal insulation of the proposed fabrics would be investigated by the sweating hotplate. Under the standards, the temperature of the hotplate and the ambient environment are 35 °C and 20 °C, respectively. Thus, T_f is 20 °C and T_s is 35 °C. The temperature of air under such conditions can be the average of T_f and T_s, which is 27.5 °C (300.5 K). g is 9.81 m/s; β is 1/300.5 K^{-1}; α is 2.234×10^{-5} m^2/s; v is 1.581×10^{-5} m^2/s. For the air gap in horizontal direction, when the air gap is filled with air without other materials and R_a is 1708, L_{air} is 10.7 mm according to Eq. (3-1), which means that the height of the designed air gap should be less than 10.7 mm under this condition to reduce heat dissipation leading to natural convection. For the vertical air gap, the critical value of R_a is 1000. Under such conditions, the critical height of the air gap is 9 mm.

Based on the above analysis, if the height of the air gap is greater than the critical value, natural convection can be enhanced, affecting the thermal insulation of fabric and clothing. On the other hand, the smaller air gap in clothing may not provide sufficient protection for the human body. Therefore, we propose knitted fabric in these studies to divide the large air gap into small parts to avoid strong natural convection.

5.4.3 Optimization of the moisture resistance of the proposed fabric

As mentioned above, the TPU fabric is completely airtight. The body covered by TPU fabric may not change moisture in the ambient environment, which also means that the fabric is not breathable. Thus, the void portion of the soft robotic elements is required to ensure moisture transfer and then reduce the moisture resistance of the clothing system. In order to find the optimum moisture resistance, the relationship between moisture resistance and void ration of TPU fabric used was also investigated. Firstly, two layers of fabric were sealed together to simulate the fully deflated state of soft robotic elements covered by shell fabric. The sample size is 25 cm * 25 cm. When the void ratio is 0%, the sweating hotplate is fully covered by TPU fabric, as shown in Figure 5-17a-b. TPU fabric with a void ratio of 4% and 8% were also illustrated. The void portion is an independent square in the center of the samples. The designed pattern is called pattern a. The results of the relationship between void ratio and the moisture resistance were shown in Figure 5-17e. When the void ratio is 0%, the moisture resistance is more than 1000 $m^2 \cdot Pa/W$, indicating that the fabric is not breathable. When the void ratio increases, the moisture resistance is effectively reduced. Increase of the void area can effectively reduce moisture resistance. According to the results, the soft robotic units designed should have a larger void ratio to ensure smaller moisture resistance to achieve thermal comfort. However, the large void area also means reduced thermal resistance and insufficient support force for the shell fabric. In order to solve the problem of insufficient support force, the void portion was divided into several parts. Another shape of the void portion was designed, which is shown in Figure 5-17c-d. The voids are parallel to each other and divided by soft units (left), which is called pattern b. To enhance the support force, separate soft robotic units are connected (right), which is called pattern c.

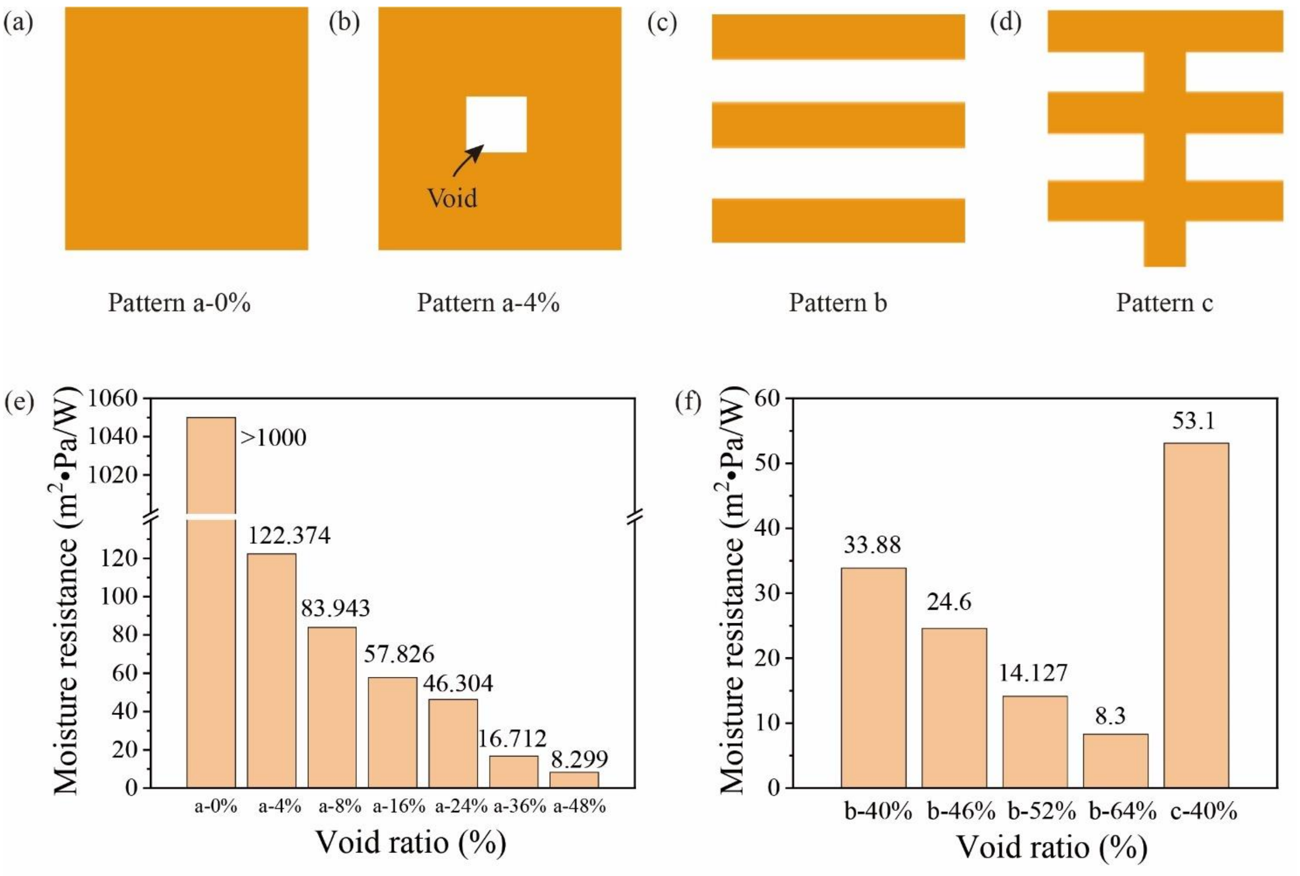

Figure 5-17 Moisture resistance of the two-layer TPU fabric with void part. (a-b) Pattern-a. (c) Pattern-b. (d) Pattern-c. (e) Moisture resistance of pattern-a. (f) Moisture resistance of pattern-b and pattern-c.

The moisture resistance of these two patterns was illustrated in Figure 5-17f. When the void ratio of pattern b increased, the moisture resistance was also reduced. Compared to pattern a-48%, pattern b-40% has higher moisture resistance, indicating that the continuous and independent void portion exhibits smaller moisture resistance. The possible reason may be that when the void part is continuous, the convection there is stronger than those separated parts, which can enhance moisture escape from the skin side. While for pattern c-40%, its moisture resistance is 53.1 $m^2 \cdot Pa/W$, which is larger than that of pattern b-40%. This results also prove that more small pieces of void part may lead to increased moisture resistance.

In summary, when designing the pattern of soft robotic units, moisture resistance and support force must be considered. Based on the above results, in order to maintain the higher breathability and sufficient support force, a skeleton-like structure of a soft robotic unit was more suitable for clothing. The soft robotic skeleton not only provides desirable thermal comfort, but also fits well with the human body curve to ensure wear comfort.

5.4.4 Amount of air required by the soft robotic skeleton

The amount of air required by the soft robotic skeleton can be calculated by the volume equation. The length of the soft robotic skeleton is the total length of the main vertical chamber and all branches. And then, the inflation time can be obtained according to the volume and the flow of pump. The volume of the soft robotic skeleton designed in this study in fully inflated state is 2199.3 cm^3, which means that the required air is 2199.3 mL. The flow rate of the pump used is 650 mL/min. Thus, the total inflation time of the soft robotic skeleton is about 204 s.

5.5 Theoretical analysis of the proposed clothing

In this numerical study, the 2D air gap model was adopted to investigate heat transfer between clothing layers. The simulation setup is illustrated in Figure 5-18, which is similar to the model set in Chapter 4. To simplify the simulation cases, all fabrics included in those cases were considered as uniform materials with static thermal properties. The red line represents the skin side, which is set as to a constant temperature, 35 °C. And the blue line represents the outer layer, which is set in a non-windy condition. Heat could only dissipate heat through heat conduction and convection. The gas environment was constructed to behave as an ideal incompressible gas, replicating the natural convection phenomena that can occur within the air gap. And the outer layer of fabric only dissipates heat to the environment through thermal convection. The temperature of the condition is set as 20 °C. The heat transfer of the outer layer fabric and the ambient environment can be considered as natural convection, with a heat flux of 5 W/m^2. The skin and fabric layers can be seemed as non-penetrating in the model, which is assumed as the fabric is set under non-windy conditions. A single unit was selected to study heat transfer phenomena, whose two ends is periodic. For clothing on the body, the air gap between the skin and the environment may be vertical. However, for most tests to investigate the thermal properties of clothing, the air gap is horizontal. In this study, both horizontal and vertical air gaps were studied. Figure 5-18a illustrates the arrangement for the horizontal direction, while Figure 5-18b shows the arrangement for the vertical direction. Figure 5-18c shows a schematic for the simulation configuration.

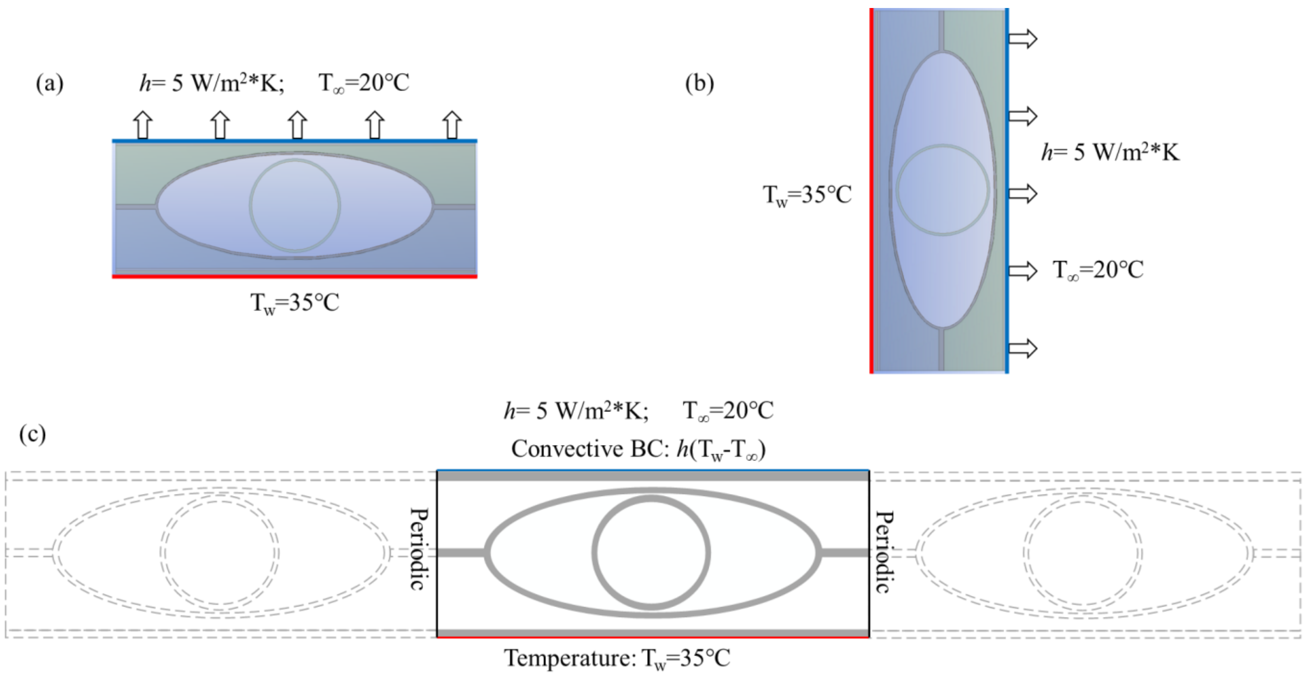

Figure 5-18 Simulation setup. (a) Setup for horizontal direction. (b) Setup for vertical direction. (c) Schematic for simulation configuration.

Based on the analysis of the above air gap optimization, the critical air gap values for horizontal and vertical direction are 10.7 mm and 9 mm, respectively. Thus, the total air gap discussed in this section is 19.1 mm and 25.4 mm. The model without and with connection clasp were both investigated to prove the effect of the connection part on heat transfer, especially thermal convection. Figure 5-19a-b shows the model without and with a connection clasp when the air gap is 19.1 mm, respectively. As shown in the temperature distribution images, it is clear that the model with the connection clasp has a lower upper surface temperature. The temperature is uniform, which may be explained by velocity images, where the air velocity is higher, leading to more heat transfer. Figure 5-20a-b shows the model without and with a connection clasp when the air gap is 25.4 mm, respectively. The distribution of temperature and air velocity also proves that the application of knitted fabric with connection clasp can increase thermal resistance and reduce heat transfer from the heat surface to the bottom.

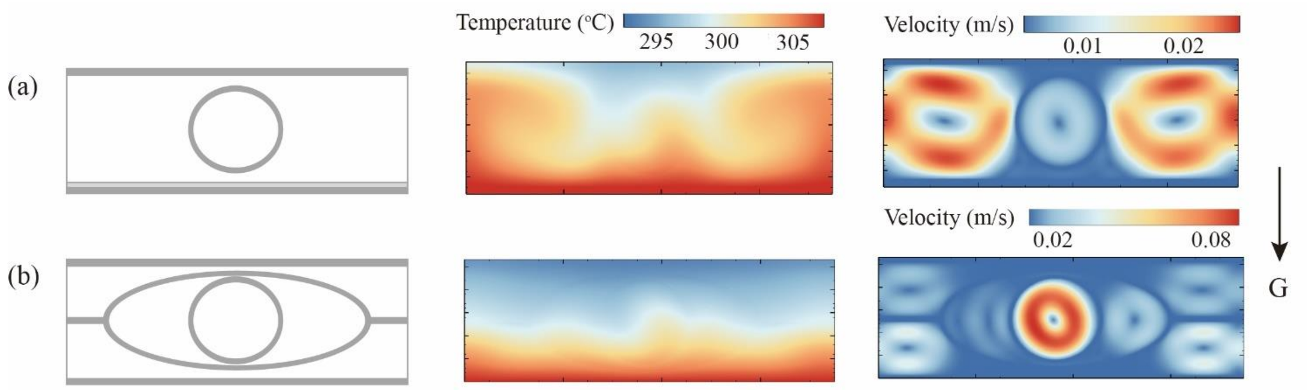

Figure 5-19 Simulated results of the temperature and velocity when the air gap is 19.1 mm, which is set horizontally. (a) Model without connection clasp. (b) Model with connection clasp. The upper surface temperature of the model without connection clasp showed higher temperature then the one with connection clasp. The air velocity within the air gap was higher than the one with connection clasp.

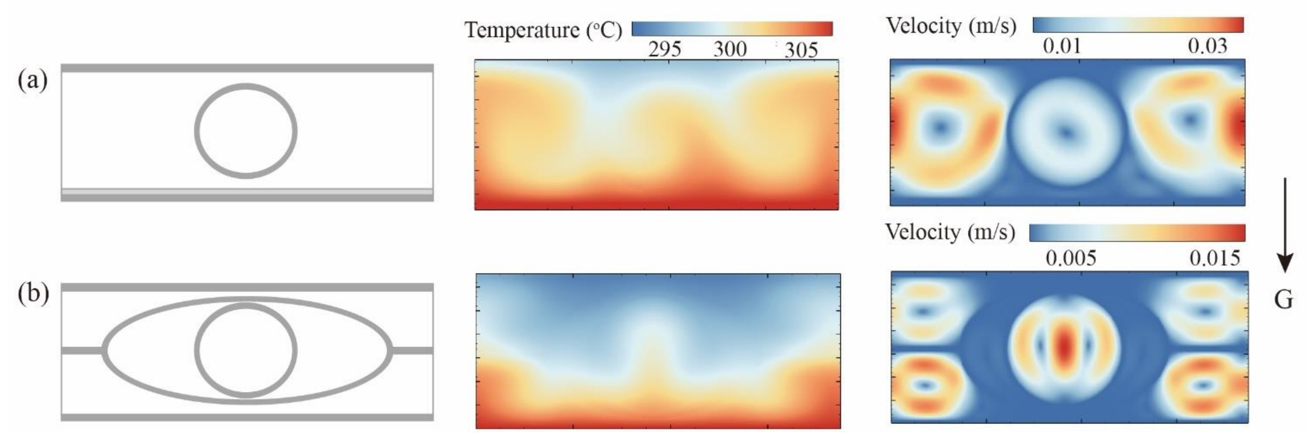

Figure 5-20 Simulated results of the temperature and velocity when the air gap is 25.4 mm, which is set horizontally. (a) Model without connection clasp. (b) Model with connection clasp. The upper surface temperature of the model without connection clasp showed higher temperature then the one with connection clasp. The air velocity within the air gap was higher than the one with connection

clasp.

Then, in order to investigate the influence of the air gap direction on thermal resistance, models, whose gravity direction is along the surface of the fabric system, were constructed. Figure 5-21 shows the simulated results of temperature and velocity when the air gap is 19.1 mm, which is set vertically. Figure 5-21a-b are the models without and with connection clasp, respectively. The results also indicated that the fabric system without the connection clasp had a higher upper surface temperature. The fabric system with the connection clasp had a more uniform upper surface temperature and a much smaller air velocity.

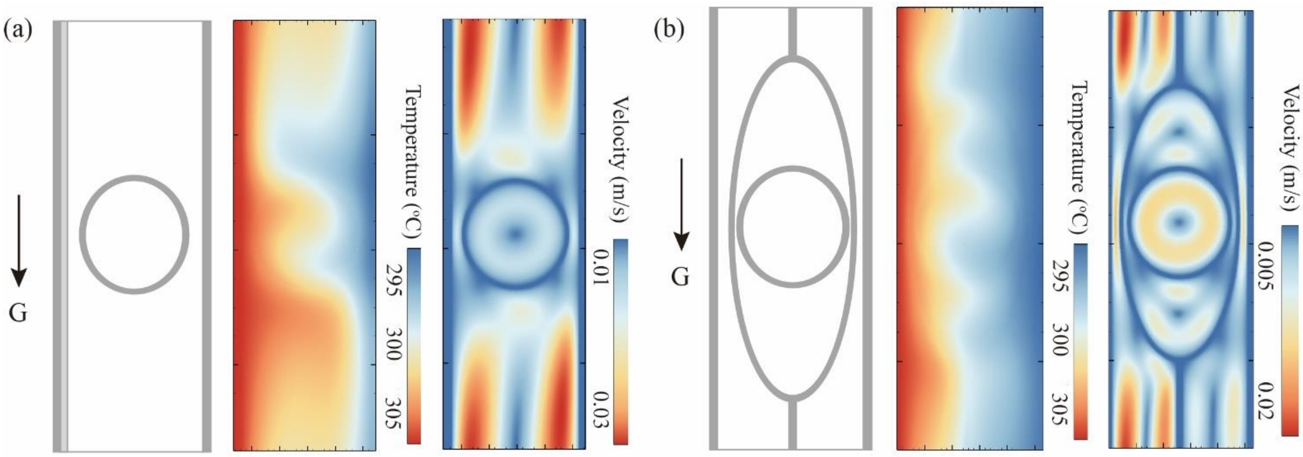

Figure 5-21 Simulated results of the temperature and velocity when the air gap is 19.1 mm, which is set vertically. (a) Model without connection clasp. (b) Model with connection clasp. The upper surface temperature of the model without connection clasp showed higher temperature then the one with connection clasp. The air velocity within the air gap was higher than the one with connection clasp.

Based on the analysis of the air gap and the connection clasp on the thermal properties of the fabric system, it can be concluded that the application of the knitted substrate with the connection clasp can divide the air gap within the fabric system into smaller parts to reduce thermal convection. Thus, heat transfer through the fabric system can be reduced, which can lead to less heat dissipation from the human body. On the other hand, the effect of the connection clasp can work no matter what direction the air gap is. This theoretical analysis in this part can provide reference for the design of the fabric system.

5.6 Results and discussion

5.6.1 Evaluation of the thermal and moisture resistance

The thermal and moisture resistance of the proposed clothing and several commercial garments were tested by the sweating guarded hotplate. Five samples included: soft robotic clothing in deflated state (S-D), soft robotic clothing in inflated state (S-I), Nudown jacket in deflated state (N-D), Nudown jacket in inflated state (N-I) (Figure 5-22a), commercial jacket 1 (C1) (Figure 5-22b), commercial jacket (C2) (Figure 5-22c).

Figure 5-22 Commercial jackets as control samples. Nudown jacket (N) (left). Commercial jacket (C1)

(middle). Commercial jacket (C2) (right).

Figure 5-23 demonstrates the thickness and weight of the samples. Since the soft robotic clothing and the Nudown jacket have adjustable thicknesses, the minimum thickness in the fully deflated state and maximum thickness in the fully inflated state were selected. The value of the S-D is 6.8 mm and the S-I is 21 mm, the difference being 14.2 mm, more than twice that of the S-D. All the thicknesses of the control samples are larger than the deflated soft robotic clothing and smaller than the inflated soft robotic clothing. C1 is the lightest, followed by the Nudown jacket, soft robotic clothing and C2. Soft robotic clothing has a similar weight to C2.

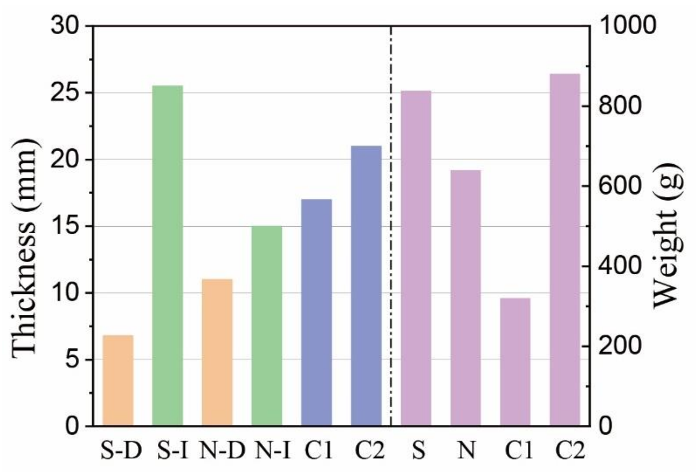

Figure 5-23 Thickness and weight of the proposed soft robotic clothing in deflated and inflated state, the Nudown jacket in deflated and inflated state, commercial jacket 1 and 2.

Figure 5-24a shows the results of thermal resistance. The thermal resistance (Rct) of soft robotic clothing can range from 0.2 to 0.499 $m^2 \cdot K/W$, which is larger than the difference between N-D and N-I. Compared to C1 and C2, soft robotic clothing has smaller thermal resistance under deflated state and larger under inflated state. Figure 5-24b shows the moisture resistance (Ret) of the samples. The moisture resistance of soft robotic clothing ranges from 39.726 to 72.693 m^2·Pa/W, which is smaller than other samples. Especially, the moisture resistance of Nudown jacket is close to 1000 m^2·Pa/W, indicating it is completely impermeable. The results showed that the thermal resistance of soft robotic fabrics increased by 76% (S1) while the moisture resistance only increased by 11.2% (S1) when fully inflated, indicating the adjustability of the soft robotic fabric without sacrificing of moisture transfer between fabric and clothing. After precise design, the value of thermal resistance between the lowest and highest thermal resistance can be achieved. The Rct of commercial warming clothing (C1 & C2) was higher than the lowest Rct of soft robotic fabric but lower than the highest Rct. However, the Rct of C1 and C2 were fixed, unable to adapt to temperature variations. What's more, the higher Ret of both commercial clothing than soft robotic clothing also proved the excellent moisture transmission performance of soft robotic clothing. The lowest Rct of Nudown jacket was 0.1544 m^2·K/W, and the highest Rct was 0.3407 m^2·K/W, an increase of 121%. However, it would make the wearer feel uncomfortable as the moisture resistance approaches 1000 m^2·Pa/W, reflecting poor moisture and vapor transmission properties. Therefore, the soft robotic fabric designed could achieve controllable thermal resistance to adapt to temperature changes with relatively little effect on moisture resistance, which may be a potential candidate for adaptive personal thermal management.

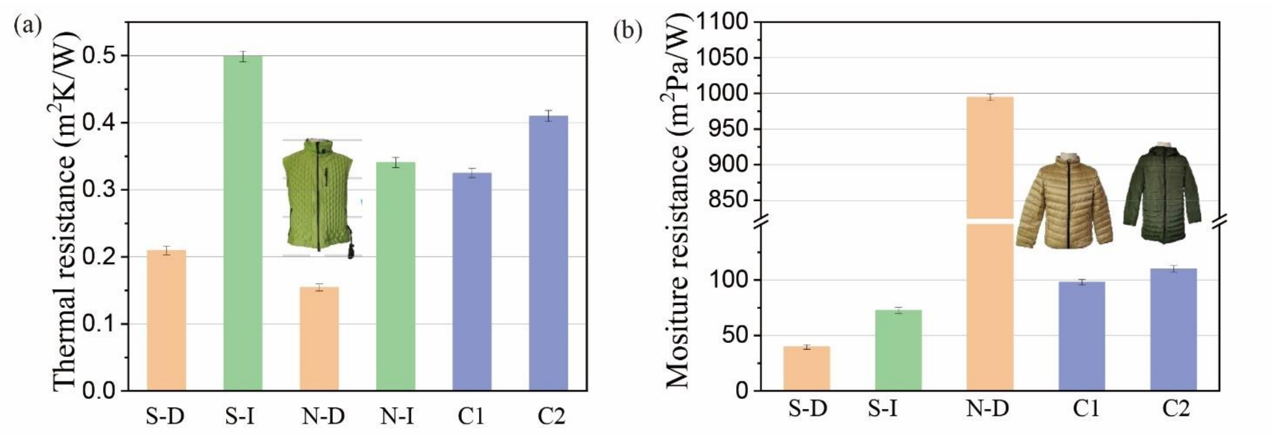

Figure 5-24 Thermal and moisture resistance of the proposed soft robotic clothing in deflated and inflated state, the Nudown jacket in deflated and inflated state, commercial jacket 1 and 2. (a) Thermal resistance. (b) Moisture resistance.

As mentioned above, the proposed soft robotic clothing has an adjustable thickness, which also means that the thermal resistance can be adjusted. Figure 5-25a shows variations in thickness of the proposed clothing. Five levels were set according to the inflation time. The initial stage, I-1, represents a zero-inflation period. Each subsequent stage has an inflation time difference of the same magnitude, implying that the inflation time associated with I-3 is twice that of I-1, which continues in this fashion until the final stage, I-5, which is fully loaded and has inflation time that is four times the duration of I-1. The thickness of the proposed clothing was increased with the increase in inflation time. Figure 5-25b shows thermal and moisture resistance at different stages, which also increased with thickness, as well as inflation time.

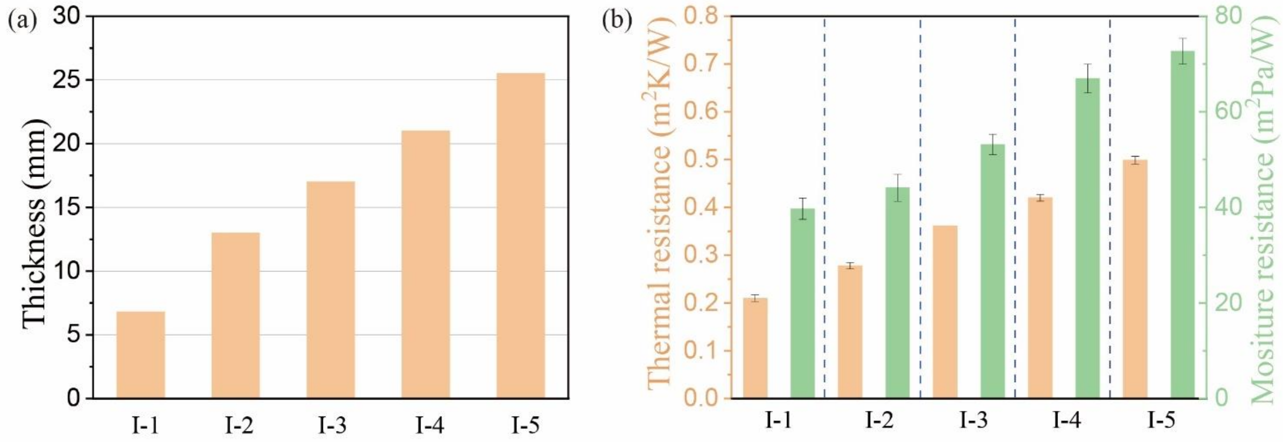

Figure 5-25 Thickness, thermal and moisture resistance of the soft robotic clothing under different inflation time. I-1 is the fully deflated state and I-5 is the fully inflated state. (a) Thickness under different inflation time. (b) Thermal and moisture resistance under different inflation time.

5.6.2 Evaluation of the thermal properties by the heating manikin

The heating manikin, which mimics the heat dissipation of human skin, is used to measure thermal resistance or skin temperature under different thermal conditions. The climate chamber showed in Figure 5-26 allows temperature variation from 5 ºC to 30 ºC. To demonstrate the thermally adaptive performance, the testing modes are adopted: the environmental chamber temperature is fixed, while the skin temperature is monitored and varied with the inflation and deflation of the soft robotic clothing at a constant heating power input for the manikin. Differences in body temperature can be used to characterize thermal adaption capacity.

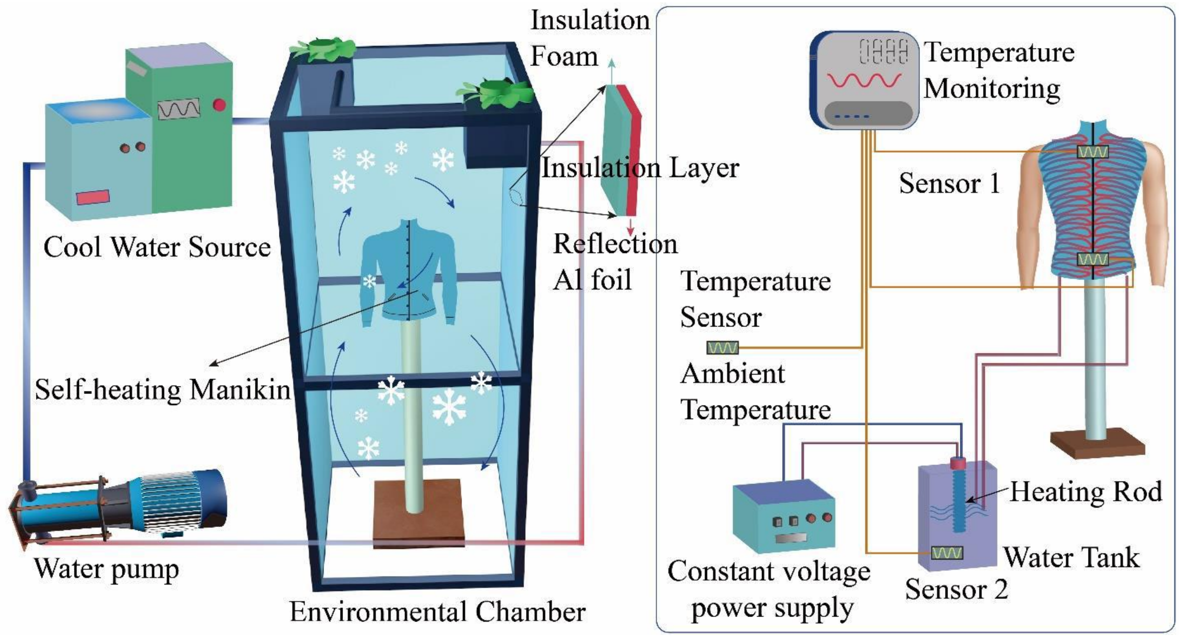

Figure 5-26 Experimental climate chamber. The manikin test and the human trials are conducted in this environmental chamber, which can adjust temperature between 5 ºC to 30 ºC.

Figure 5-27a shows the human manikin purchased from Jingdong. The thermal manikin is covered by a liquid circulation system with the skin temperature varying by a controllable input of heat power. The garment with liquid circulation system is used to mimic human skin. Figure 5-27b shows the experimental setup for the heating manikin test. The heating manikin has a water tank with hot water inside for circulation, whose temperature is controlled by the heating power. The water is heated by a heating element connected to the power supply. The heating element should be completely immersed in water to ensure its life and higher heating efficiency. A control system with pump and control panel was connected to the soft robotic skeleton to achieve thickness variations. The temperature monitoring device would work with the computer to record temperature variations during testing. A digital screen was set up outside to monitor the temperature inside.

Figure 5-27 Experimental setup for heating manikin test. (a) Manikin with a liquid circulation garment. The tubes inside the garment are channels for liquid. (b) Illustration of the test system. The manikin heating system controlled by a power supply. Control system of the clothing for adjustment of thermal resistance. Temperature measurement to record surface temperature variations of manikin. The real-time temperature to reflect the environmental temperature.

Figure 5-28a-b shows the deflated and inflated state of the soft robotic clothing. The variations in thickness are obvious. Figure 5-28c shows the locations of temperature sensors on body skin. The heating power is 74 W and the heat flux is 85 W/m^2, approaching the body metabolic efficiency. During the experiment, the heating flux is constant. Thus, the skin temperature in different states can be used to reflect the thermal insulation of the proposed clothing. In Figure 5-29a, when the environmental temperature reduced from 11.62 ºC to 6.7 ºC, the clothing would transfer from fully deflated state to fully inflated state, the temperature of the three sensors on skin surface increased 0.58 ºC, 0.85 ºC and 1.14 ºC, separately. While if the environmental temperature reduced from 8.05 ºC to 3 ºC, showing in Figure 5-29b, the temperature of the three sensors on skin surface increased 0.25 ºC, 0.11 ºC and 0.18 ºC separately with the clothing transferring from fully deflated state to fully inflated state. The results indicates when the even when the environmental temperature reduces 5 ºC, variations of the temperature on the skin surface are quite small, which can be seemed as unchangeable. This means that if the environmental temperature around the wearers reduces 5 ºC, the wearers only need to pump the clothing into fully inflated state without adding additional clothing to keep warm.

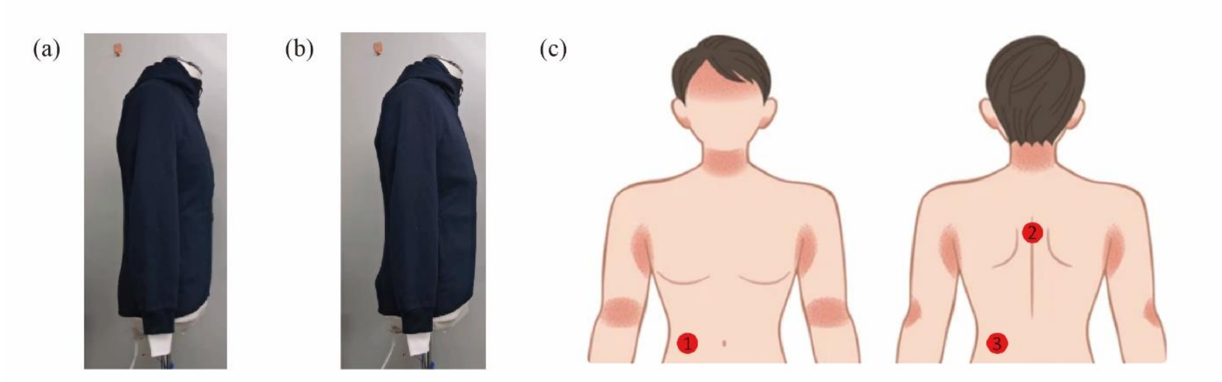

Figure 5-28 Human manikin test. (a) Soft robotic clothing in deflated state. (b) Soft robotic clothing in inflated state. (c) Location of the sensors on body (Heating power = 74 W, Heat flux ≈ 85 W/m^2).

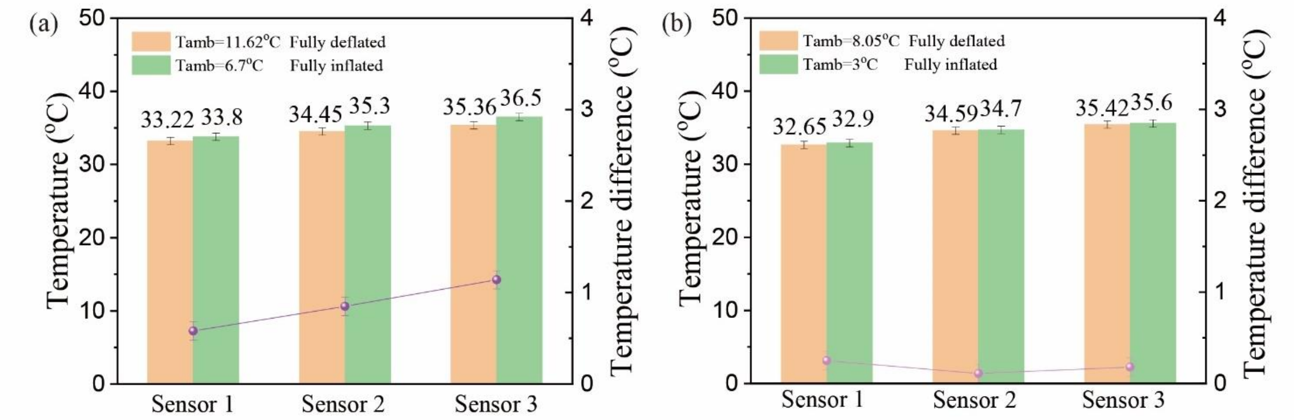

Figure 5-29 Experimental results from human manikin. (a) Skin temperature when the ambient temperature varies between 11.62 ºC and 6.7 ºC. (b) Skin temperature when the ambient temperature varies between 8.05 ºC to 3 ºC.

5.6.3 Subjective evaluation of the thermal comfort by human trials

However, human skin temperature is not only influenced by the environment, but also by their metabolism. Human trials were also conducted. Soft robotic clothing for the men's and women's versions has been prepared. Figure 5-30a showed the woman with soft robotic clothing. A side view was provided to show thickness variations. The left side shows the fully deflated state of the clothing, and the right side shows the fully inflated state. Figure 5-30b showed the man with soft robotic clothing. The left side displays the front view in a fully inflated state of the clothing, and the right side shows back view.

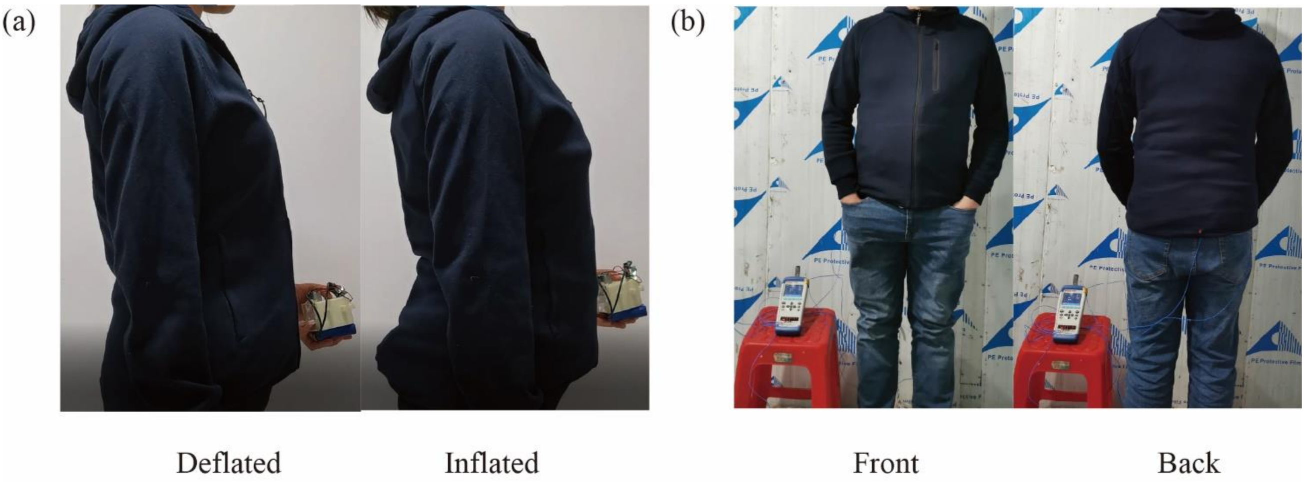

Figure 5-30 Wearers with soft robotic clothing. (a) Side view of the soft robotic clothing in fully deflated (left) and fully inflated state (right). (b) Front (left) and back view (right) of the soft robotic clothing.

Figure 5-31a-b illustrates the experimental results. For man (Figure 5-31a), when the temperature reduced 4.4 ℃, from 10.9 ℃ to 6.5 ℃, the temperature of the sensors on human body reduced 0 ℃ (T_1), increased 1.8 ℃ (T_2) and dropped 0.1 ℃ (T_3) separately. While for woman (Figure 5-31b), when the temperature reduced 5 °C, from 11.5 °C to 6.5 °C, the temperature of the sensors on human body reduced 0.8 °C (T_1), increased 1.5 °C (T_2) and increased 0.4 °C (T_3) separately. For one subject, the temperature of different sensors varying. The possible reason is that not all body parts have the same surface temperature, which may be affected by the location of the blood vessel. While for different subjects, the metabolic rate varies between people, leading to different temperature changes.

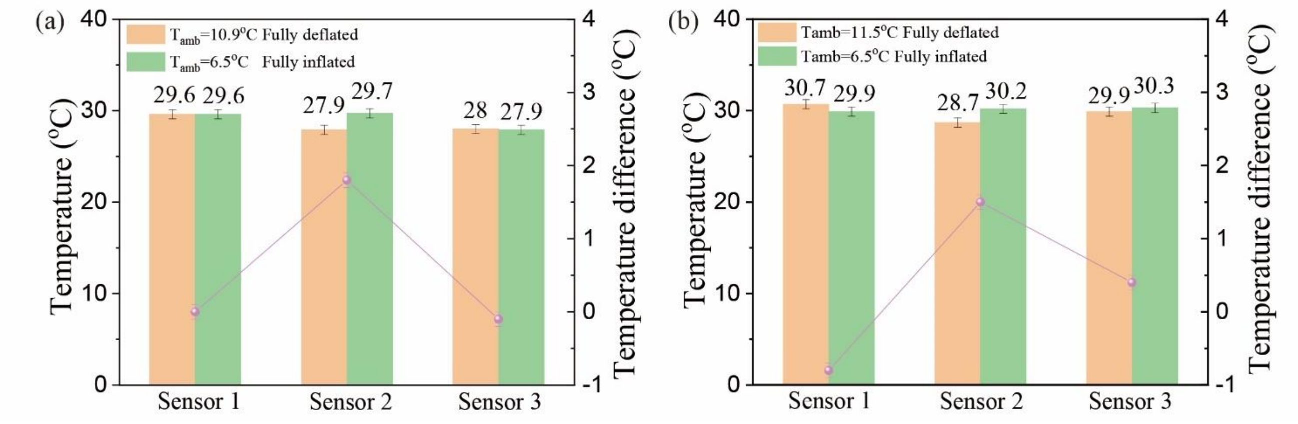

Figure 5-31 Experimental results from human trials. (a) Skin temperature variations of man when the temperature reduced 4.4 °C, from 10.9 °C to 6.5 °C. (b) Skin temperature variations of woman when the temperature reduced 5 °C, from 11.5 °C to 6.5 °C.

In order to investigate the uniformity of the thermal insulation properties, thermal images were also collected, as shown in Figure 5-32. Figure 5-32a shows a front and back view of the clothing in a fully deflated state, and Figure 5-32b displays a front and back view of the clothing in a fully inflated state, which shows a higher surface temperature, indicating that the fully inflated state has better thermal insulation.

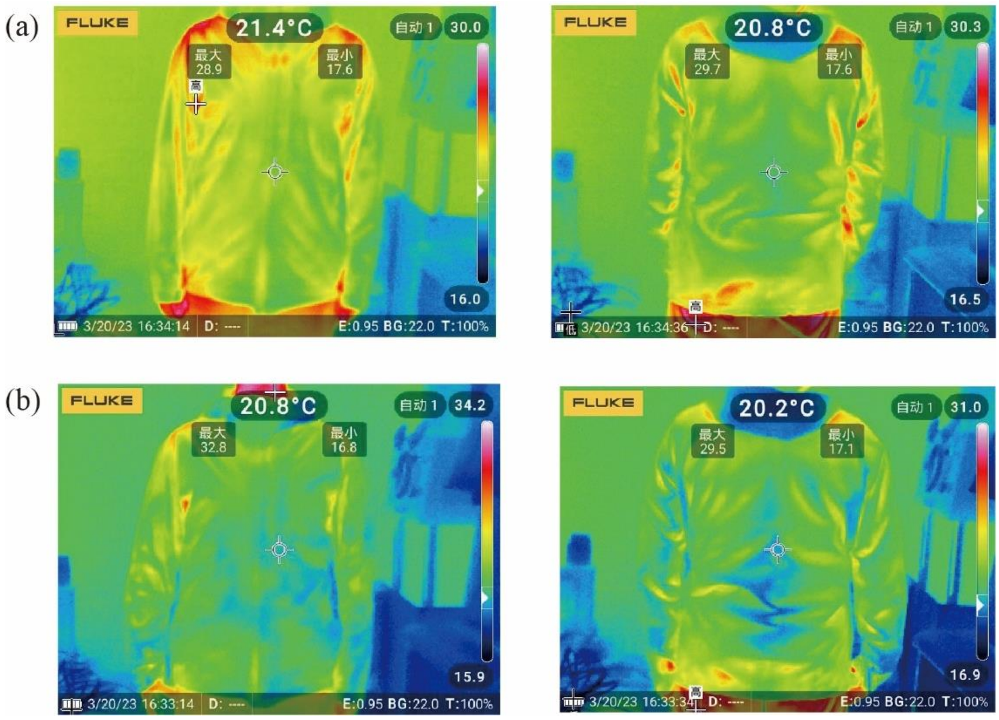

Figure 5-32 Thermal images when clothing under different states. (a) Thermal images of clothing in fully deflated state with front view (left) and back view (right). (b) Thermal images of clothing in fully inflated state with front view (left) and back view (right).

5.7 Summary

Soft pneumatic actuator-driven textiles for controllable body warming have been proposed and fabricated, which can adapt to environmental temperature changes by controlling the air gap between fabrics to achieve tunable thermal resistance with good moisture permeability. Preliminary results have shown that the design strategies are feasible. When the ambient temperature decreases 5 °C, the proposed clothing can transfer form fully deflated state to fully inflated state to maintain the body temperature. Thus, the wearer does not need to add clothing. Future work would focus on 1) optimizing design pattern to expand the working temperature range for wider use; 2) improving moisture permeability to avoid accumulation of sweat; 3) promoting flexibility without limiting body movements; 4) designing and test all clothing in real climate.

Chapter 6 Pneumatic actuator-driven breathable 3D knitted fabric for thermal insulation and radiative cooling

6.1 Introduction

Nowadays, warming in cold conditions and cooling in hot conditions are vital for human beings. In recent years, managing personal thermal comfort has been a hot topic. Thermal conduction and convection regulation are widely used. Another approach is to control the radiative heat transfer of the human body with its surroundings. However, most current methods control only one type of thermal transport mechanism, lacking adaptability to the rapidly changing environment. Fabric and clothing with static thermal performance is suitable for people staying or working in a stable scenario. It is known that the accident occurred during the 100-kilometer mountain marathon held in Gansu Province. The sudden extreme weather occurred in the high-altitude race section from 20 kilometers to 31 kilometers, causing the participants' temperature to drop sharply and then causing 21 deaths. It was a summer day when solar light protection was needed, but a serious loss of heat from the bodies occurred. This event indicates that marathon runners, especially those engaged in complex weather conditions, should not only be concerned with sunburn issues, but should also be aware of the importance of warming up before activities. Under normal conditions, this could be avoided if people could add or remove clothing to adjust the thermostat. Nevertheless, extra clothing may not be available, especially in outdoor conditions [10]. Extreme hot or cold weather conditions are often accompanied by rapid temperature fluctuations, which can lead to serious health problems [128]. Therefore, exploring an effective strategy to design fabric and clothing in dual mode to protect people from a complex and diverse environment is essential.

Motivated by this demand, much research has been conducted to design materials with tunable thermal properties. Materials with more than one layer often exhibit different thermal properties, which have dual modes. Desirable thermal performance can be achieved based on the high selectivity spectral characteristics of each side by flipping the materials [10, 128-131] or automatically controlling the covering relationship of the layers [132]. Besides these dual-mode textiles, the same structure has dynamic thermal properties. Inspired by the dynamic color-changing skin of coleiid cephalopods (squids, octopuses, and cuttlefish), researchers have designed materials with dynamic thermoregulatory, which can adjust their thermal emissivity [94-96, 133]. However, these designs still have some limitations, including a narrow modulation range, unstable structure, and poor breathability. On the other hand, the aforenoted structures focused on the management of thermal radiative performance, not concerning the other modes of heat transfer. Some of them may be used for building thermal management, which is not suitable for personal thermal management.

In hot days and low latitudes, intense solar radiation can increase the ambient temperature in a very short period of time. Therefore, reflecting solar light to achieve efficient radiative cooling is important for people to stay in such conditions. While in cold days and high latitudes, body warming is extremely important. Isolating thermal conduction can be an effective approach. If these two aspects can be combined, fabric and clothing with dual mode to achieve radiative cooling under intense solar light and less heat loss in low temperature conditions can be created.

6.2 Design strategy and working mechanism

In this part, a dual-mode 3D knitted fabric is proposed for body cooling and warming, via a simple and effective methods. As shown in Figure 6-1, when the solar light is absent and the ambient temperature is low, the warming mode is required. The entire fabric system assumes a folded configuration, which has a 3D structure with a larger thickness. The cavity between the fabric can trap still air inside to enhance the thermal resistance of the entire fabric system, thereby minimizing the rate of heat loss from human skin to the ambient environment. This folded structure is the relaxed state of the knitted fabric, which is caused by the unbalanced force acting on the direction of the inner loop of the fabric. When the external solar intensity increases, sensors on the outer layer of the fabric can detect changes in solar radiation intensity, leading to the activation of soft robotics attached to the inner layer of the fabric. When soft robotics are activated, air is pumped in and inflated, shifting from a coiled state to a linear state, driving the coated part to extend and cover the skin part. For cooling mode, the stretched radiative cooling portion covers the skin, reducing internal energy absorption from solar radiation and input infrared radiation from ambient air and conditions. On the other hand, the stretched fabric has a much smaller thickness than the relaxed fabric, which can enhance the transfer of heat and moisture from the skin to the outside, effectively achieving the desired cooling effect.

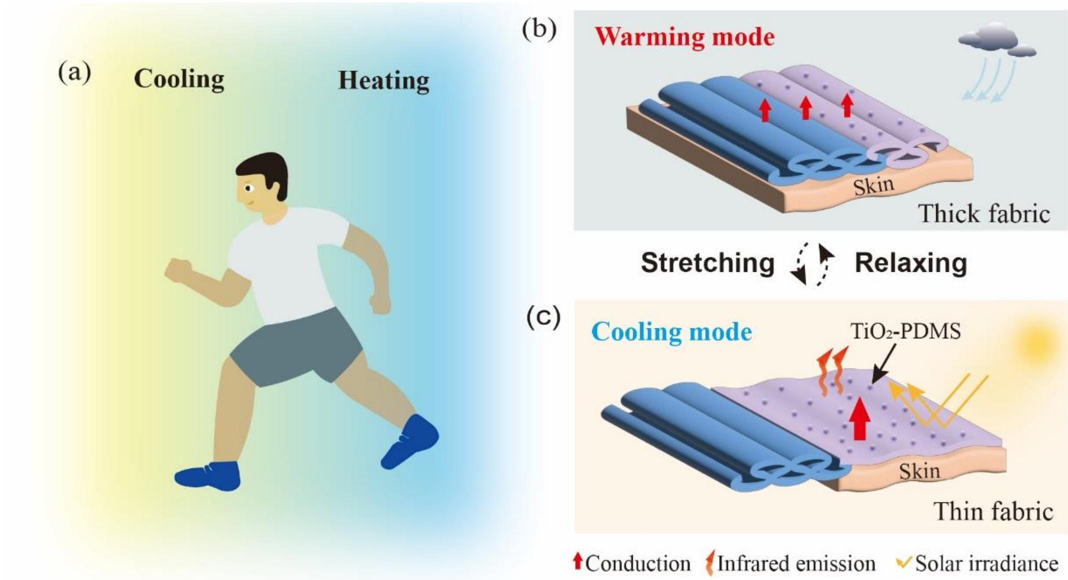

Figure 6-1 Schematic diagram of the dual-mode 3D knitted fabric. (a) The dual mode of the proposed fabric. (b) For the warming mode, the fabric is relaxed with larger thickness to reduce heat loss from human body. (c) For the cooling mode, the coated part of the fabric is stretched to reflect the solar light. Simultaneously, the stretched part has smaller thickness, which can enhance heat transfer to the ambient environment.

The dual mode fabric is designed based on the switchable transformation between the 3D and 2D structure of the knitted fabric in response to changes in solar intensity. When it is cold, the fabric shrinks and stays relaxed state. If the solar intensity is enhanced, the coated part is stretched gradually until completely cover the human skin, which is exposed as much as possible to achieve cooling effect. The deformation of soft robotics is designed based on the inflation process. A peristaltic pump is required to provide sufficient energy.

6.3 Materials and fabrication

6.3.1 Materials

The yarn used in this study for knitting fabrics is cotton, whose specification is 21s/2. The diameter of the single TiO_2 nanoparticles (Sigma) contained these types, 200 nm, 500 nm and 1 μm. PDMS, including part-A and part-B, were purchased from Sigma. Soft actuators were made from the TPU fabric mentioned in previous chapters.

6.3.2 Fabrication of the knitted fabric

The first preparation step is to fabricate 3D knitted fabric. The 3D structure can be knitted on a weft knitting machine with two needle beds. In order to knit the proposed 3D knitted fabric, the needles work on the two needle beds alternatively, knitting the front and back loops individually. The knitting notation is shown in Figure 6-2. The needles knit K courses on the front needle bed firstly to create knit loops. Then, it starts working on the back needle bed to knit N courses, creating a purl loop. A unit may be fabricated, which comprises a K course-knit loop and an N course-purl loop. The fabric can be obtained by repeating this process. Because the loop structure of the knitted fabric tries to be even, the force direction of the knit and purl loop structures is different, resulting in the phenomenon of curling and shrinking the fabric automatically, forming a folded 3D structure. Since the front and back sides of the two parts are directly opposite each other, their respective bending directions are distinct. A schematic cross-section of the fabric is also shown in Figure 6-2. The grape part represents the loops knitted on the front needle bed, and the orange part is knitted on the back needle bed. The height of the folded structure is controllable, which is determined by the number of knit and purl loops in one unit. The more loops, the higher the height of the fabric. However, if there are too many loops, the force generated by different loop directions can be weakened, resulting in unstable structure. Meanwhile, when the number of loops exceeds a certain limit value, the force may disappear, and the fabric will not be folded. On the other hand, if the courses knitted on different needle beds are the same, which also means that the value of K and N is equal, the folded 3D fabric is symmetrical. If K is not equal to N, the structure is asymmetric.

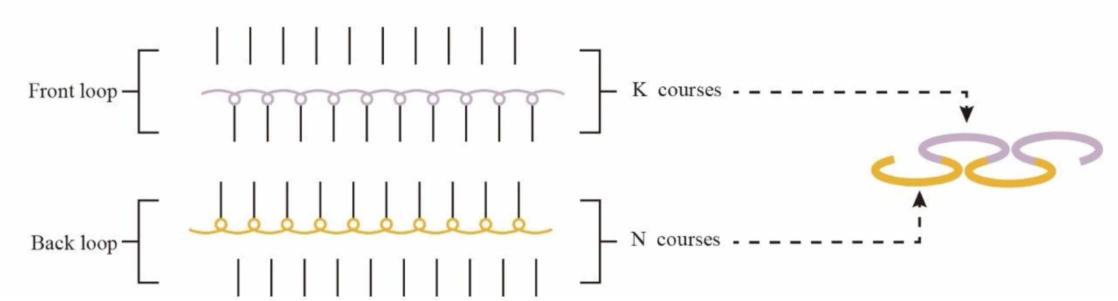

Figure 6-2 Knitting notation of the knitted fabric. The needles knit on the front and rear needle bar alternately to form front and back loops.

Actually, when the fabric is folded, there are cavities inside the fabric, which can store still air to enhance the thermal resistance of the fabric. In order to find the optimal height of the 3D knitted fabric. Three types of samples were designed.

6.3.3 Coating process of the fabric

The second step is to coat the fabric. Before coating, the fabric was washed to obtain a stable state as the cotton fabric is prone to shrinkage due to its structure and composition. Washing with cold water and low heat air drying can stabilize the shape in a further process. And the fabric was also cleaned by ultrasonic to reduce residual impurities. Nanoparticles of TiO_2, including diameters of 200 nm, 500 nm and 1 μm, and polydimethylsiloxane (PDMS) precursors. Firstly, nanoparticles of TiO_2 were dispersed into 20 mL of THF by ultrasonic treatment at 120 W for 30 min and magnetically stirred for another 30 min at room temperature. Then, 4 g PDMS A was added and magnetically stirred to obtain a homogenous suspension. After that, PDMS B was dissolved in 20 mL THF and magnetically stirred for 30 min. At last, the solution obtained in step 3 was added to the solution obtained in step 2 and magnetically stirred for 12 h. The coating solution was completed.

The fabrication process is shown in Figure 6-3a. The cleaned fabric was partially immersed in the coating solution, which was coated multiple times to produce a variety of samples with varying levels of nanoparticle content. After the coating process, all samples were placed on a plate at room temperature in a fume hood, waiting for the THF to evaporate. Then, the samples were transferred to an oven for a curing process, which involved exposing them to temperatures of 80 °C for a duration of 4 h. The purpose of this curing process was to stabilize the coating and prevent the samples from breaking apart under normal wear and tear. Figure 6-3b shows the final fabric, which is partially coated.

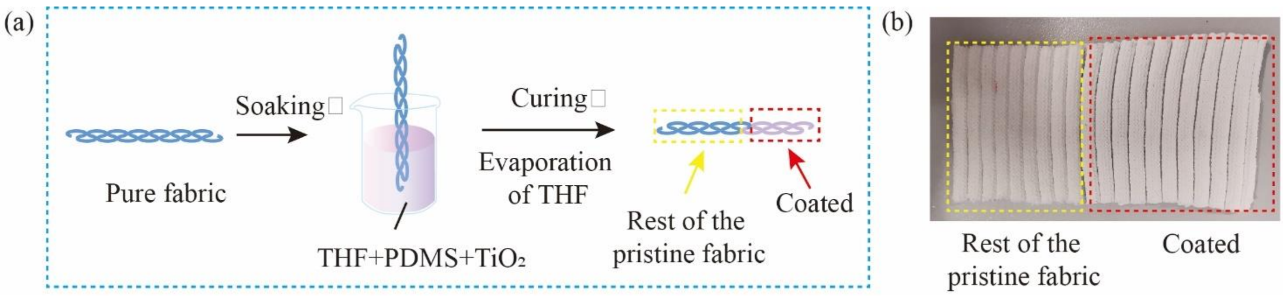

Figure 6-3 Coating process of the fabric and the images of the final fabric. (a) Schematic diagram of the coating process. (b) Image of fabric after coating.

6.3.4 Fabrication of the soft robotics

The third step is to prepare soft robotics as actuators. The method of fabrication of the soft robotic element was the same as the actuators mentioned in Chapter 4. The soft robotic element is a smaller rectangular bag with a silicone tube connected to it. As can be seen in Figure 6-4a, the soft robotic bag is a rectangular bag with a sealed area to prevent air leakage and an unsealed part that functions as an air chamber for deformation. In its free state, the actuator appears as a deflated sheet with a rectangular shape (state 1). Once the fabric is attached to the surface of the fabric, the shape conforms to the shape of the fabric, depicting it as a wave-like deflated sheet (state 2). When the air is pumped in, the deflated actuator tries to assume its original shape, a rectangular air bag, which can lead to a change in the actuator's length. The actuator can be fully inflated by filling it with enough air. The actuator appears to be an inflated airbag (state 3). Therefore, if the actuators are attached to the fabric, the deformation of them can expand the 3D structure and lead to elongation of the fabric. The total width of the actuator is 10mm with 5mm width of the air chamber. The length of the actuator is determined by the final application of the fabric.

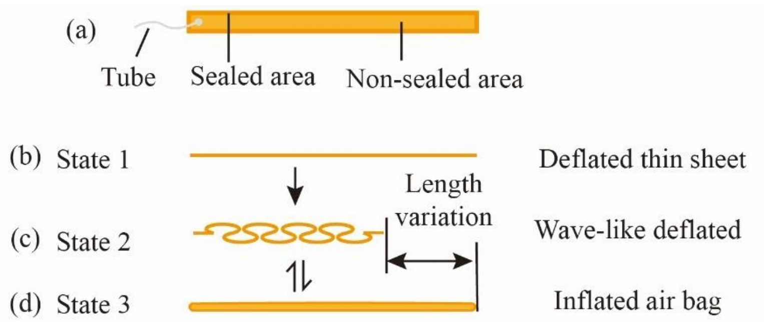

Figure 6-4 Deformation mechanism of the soft robotics. (a) Demonstration of the structure of the single actuator. (b) Side view of the actuator, which is a deflated thin sheet. (c) Side view of the actuator,

which is wave-like deflated thin sheet. (d) Schematic of the inflated actuator.

6.3.5 Integration of the fabric and the soft robotics

After fabrication, the actuators were stitched on the inner layer of the fabric but only partially coated by a sewing machine. At first, the coated part of the fabric is carefully stretched to its maximum length and securely secured to a suitable frame, aiming to ensure that the fabric is stable without flipping in the following process. Next, the soft robotic elements are positioned parallel to the upper layer of the fabric layer with a predetermined distance. The distance between soft robotic elements should be calculated to avoid influence on moisture resistance due to dense distribution or insufficient force to stretch the folded structure. Finally, soft robotic elements are stitched together with the fabric using appropriate sewing techniques and materials. After sewing, the frame can be removed, and the fabric can recover to the folded state. Since soft robotics are made of TPU fabric, it is quite soft and flexible. Thus, when the elements are stitched to the fabric, they can deform as the fabric deforms. The stitches only exist on the edges of the element, not damaging the airbag. Several elements may be required to ensure uniform deformation of the fabric. Figure 6-5 shows the integration of soft robotics and fabric. When the fabric maintains a relaxed state without external force, soft robotics attaches to the bottom layer of the coated part of the fabric and remains curved. If external force is applied, actuators are inflated and try to extend during the inflation process. The extension of the actuators is accompanied by the extension of the folded fabric. Figure 6-5b shows a side and front view of the fabric system, which shows that soft robotics can fit well with curved fabric. Figure 6-6c shows the deformation process of the fabric. When the actuator is inflated, the folded structure can be stretched appropriately.

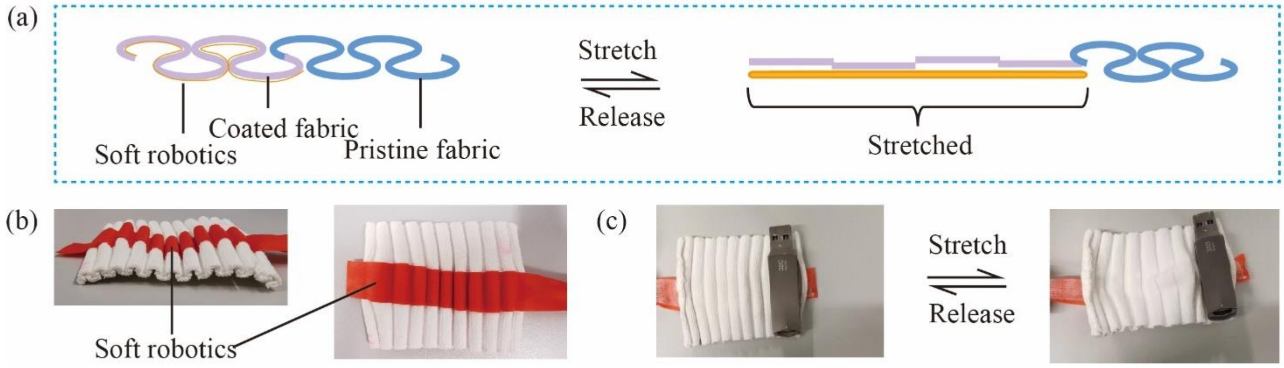

Figure 6-5 Integration of the soft robotics and the fabric. (a) Deformation principle of the fabric. (b) Side and front view of the fabric integrating with soft robotic element. (c) Images to display the deformation process of the fabric.

6.3.6 Design of the control system

Soft robotic units can deform and actuate to achieve reversible deformation of the 3D knitted fabric by changing the amount of air or air pressure of the soft robotic actuators through inflation and deflation. The control device consists of a UV sensor, a peristaltic pump, a tiny single board microcontroller, and a small rechargeable battery. The control device applies electrical energy to drive the peristaltic pump, regulating the amount of air in the soft robotic actuators by inflation and deflation. In response to the UV signal detected by the sensor in the control device, the peristaltic pump operates for inflation or deflation, automatically regulating the structure and thickness of the clothing system. The entire system can be powered by a small rechargeable battery. A high-quality rechargeable battery is selected, which has a service life of more than 2 years. The battery can also be replaceable.

Figure 6-6 is the flowchart of the control system. When the system starts, it initializes firstly. Then the UV sensor works to collect the real-time UV value and send to the center. If the UV value conforms to the preset function, no power is provided, and the pump maintains the stop state. If the temperature is higher than the preset value, forward voltage is provided, and the pump can work to inflate the actuator. Otherwise, the backward voltage is provided, and the pump can work to deflate the actuator.

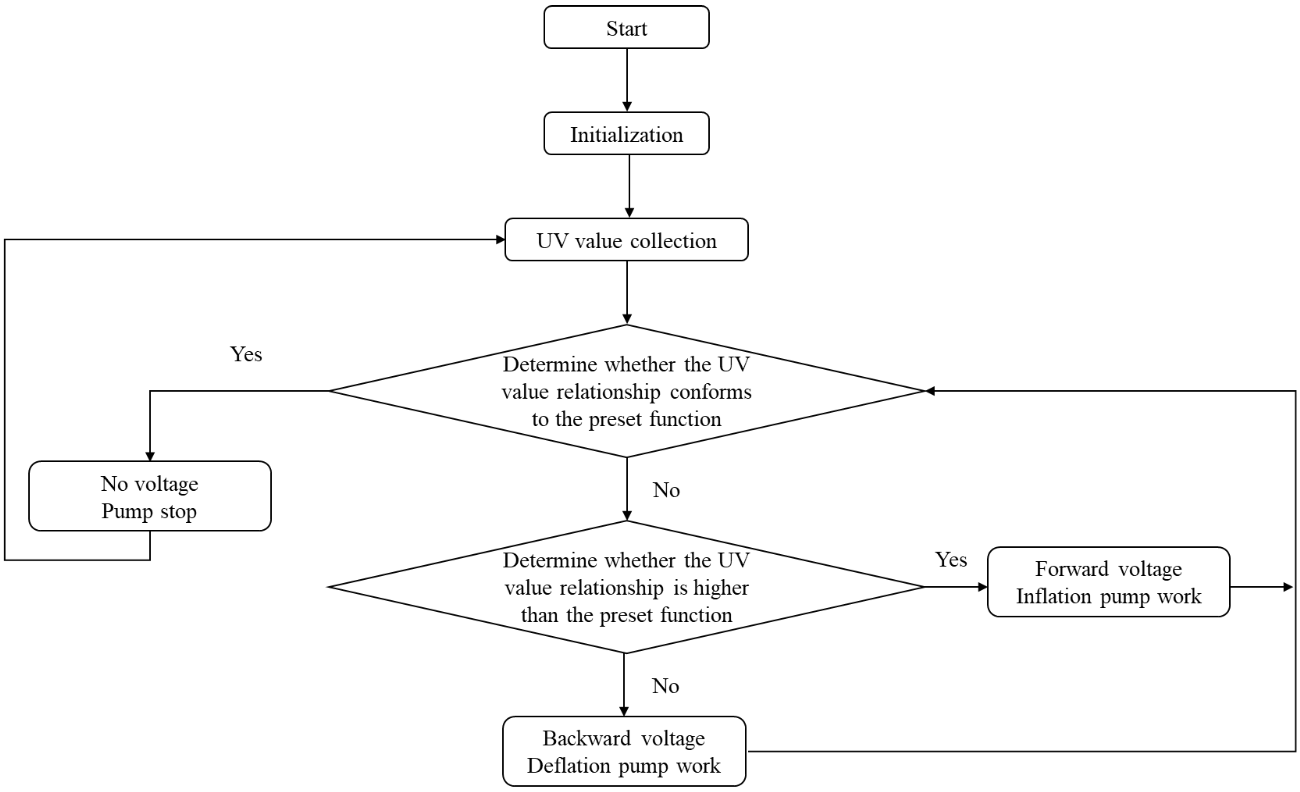

Figure 6-6 Flowchart of the control system.

Figure 6-7a shows a flowchart of the control device. The power supply can provide power to the system to ensure the normal operation of the device. A commercial peristaltic pump is applied to achieve inflation and deflation of actuators. The UV sensor can detect changes in the temperature of the external environment and provide feedback to the control part. Figure 6-7b shows the entire system of the control device. Figure 6-7c-d demonstrates a schematic and image of the overall specification, which contains the locations of the main units.

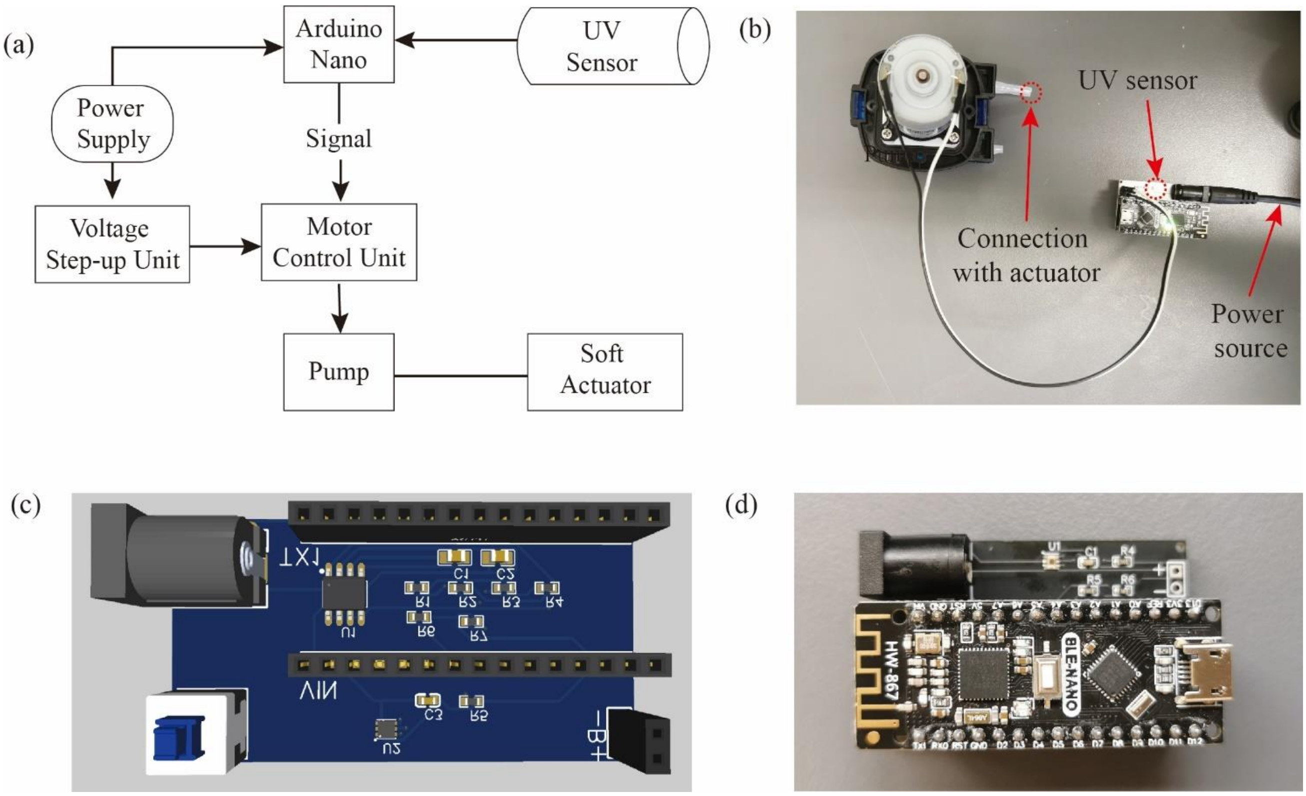

Figure 6-7 Design of the control device. (a) Flowchart of the control device. (b) Control device. (c) Schematic and image of the overall specification. (d) Image of the overall specification

The system control code is attached to the Appendix. To explain the mechanism of the system, part of the code is shown in Figure 6-8. The system has two statuses. If the solar density is higher than the preset value, the system maintains state 1 and the pump works to inflate the actuator to activate, and the fabric is stretched to reflect solar light. Else. The system works to deflate actuators, and the fabric recovers to the relaxed state to keep warm. The code is attached in Appendix-C.

```
void printResult(String text, OPT3002 result) {
  if (result.error == NO_ERROR) {
    Serial.print(text);
    Serial.print(": ");
    Serial.print(result.lux);
    Serial.println(" nW/cm2");
    if (result.lux > 20000 && status == 0) {
        digitalWrite(5, HIGH);    // Set D5 to HIGH
        digitalWrite(6, LOW);   // Set D5 to HIGH
        status = 1;
        delay(5000);              // Keep it HIGH for 5 seconds
        digitalWrite(5, LOW);   // Set D5 to HIGH
        digitalWrite(6, LOW);   // Set D5 to HIGH
        // Since we want to prevent rapid toggling, avoid setting D5 LOW immediately after
    }
    // Check if the lux is lesser or equal to 20000 and the current state of D5 is HIGH
    else if (result.lux <= 20000 && status == 1) {
        digitalWrite(5, LOW);   // Set D5 to HIGH
        digitalWrite(6, HIGH);    // Set D5 to HIGH

        status = 0;
        delay(5000);              // Keep it LOW for 5 seconds
        // Since we want to prevent rapid toggling, avoid setting D5 HIGH immediately after
        digitalWrite(5, LOW);   // Set D5 to HIGH
        digitalWrite(6, LOW);   // Set D5 to HIGH
    }
```

Figure 6-8 Image of the code for the control system.

6.4 Characterization of the 3D knitted fabric

6.4.1 Length and height of the 3D knitted fabric

In this test, three samples were designed. A schematic diagram of the loop structure of a single fabric unit of the three samples is shown in Figure 6-9. For these samples, the values of K and N mentioned above are equal, i.e. 5, 7 and 10 respectively. The yellow part represents the front loop, while the purple part represents the back loop. The images of the fabrics are shown in Figure 6-10. The images in Figure 6-10a make it clear that there is a difference in height between samples, resulting from variations in courses in one unit. As can be seen from Figure 6-10b, the surface of these fabrics is also different. There are wide variations between samples due to the diversity of courses. Specifically, fabrics with more courses tend to exhibit larger widths on the surface and higher vertical height. To provide a more complete understanding of the fabric structure, the folded fabric is stretched, shown in Figure 6-10c, which can more clearly demonstrate the construction of the loop.

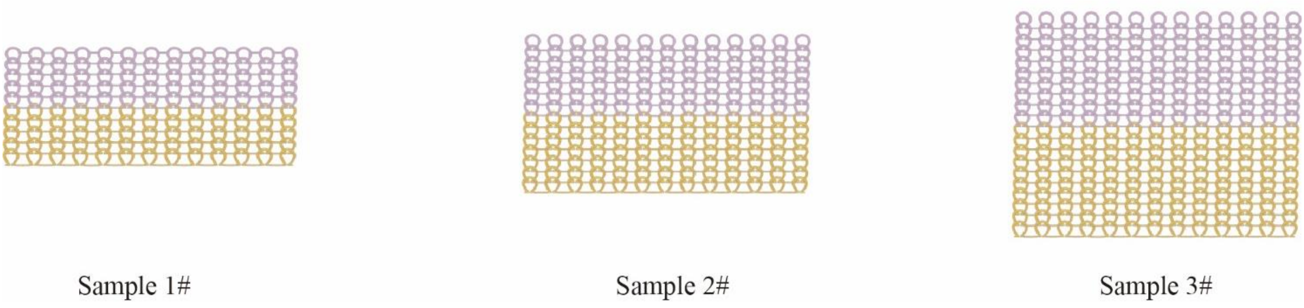

Figure 6-9 Schematic diagram of a single unit in fabric of the three samples. For sample 1#, the total loops in one unit are ten, including five front loops and five back loops. For sample 2#, the total loops in one unit are fourteen, including seven front loops and seven back loops. For sample 3#, the total loops in one unit are twenty, including ten front loops and ten back loops.

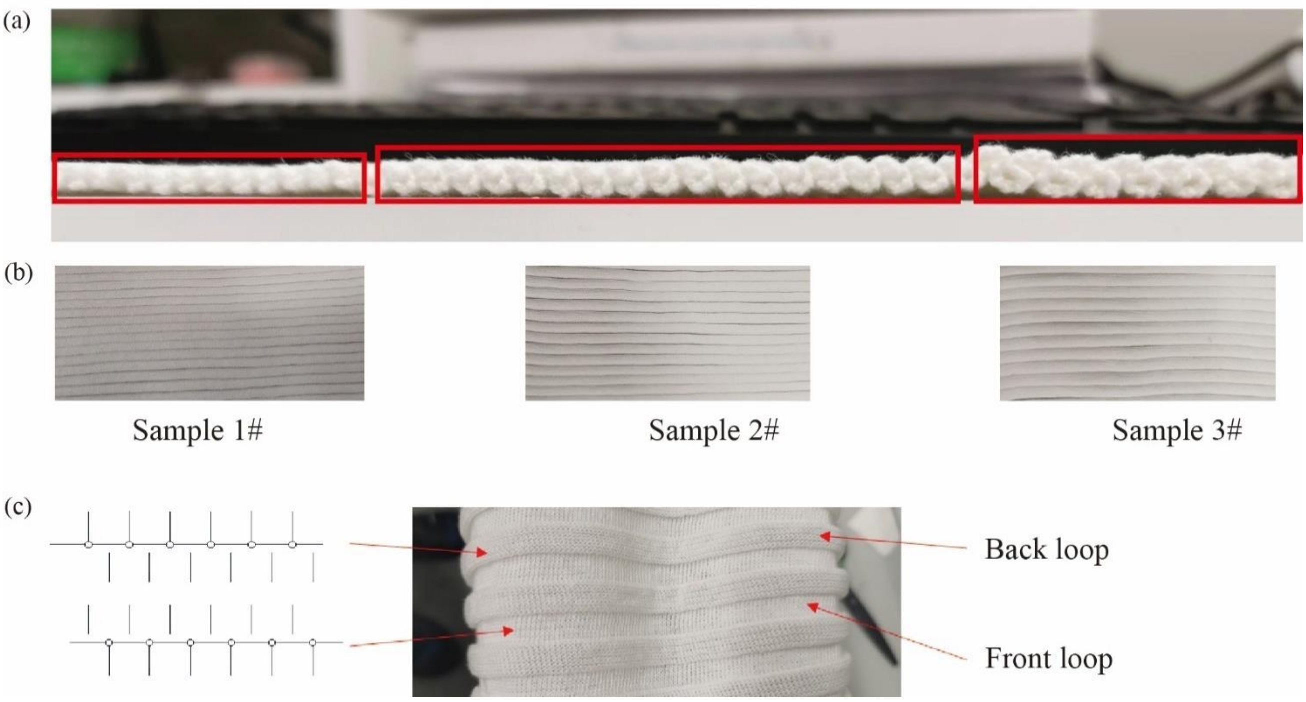

Figure 6-10 3D knitted fabric. (a) Cross section of the three samples. From left to right, they are sample

1#, 2# and 3#, respectively. (b) Surface images of the three samples. (c) Knitting notation (left). The stretched fabric shows the arrangement of the loops in the structure.

As mentioned above, the working principle of the fabric is based on the variation in length, led by the transformation of the fabric between 3D and 2D structures. Therefore, it is crucial to calculate the stretch extension for different fabric samples. Figure 6-11a shows images of the upper surface of the fabric in a relaxed and stretched state. It can be clearly seen that the knit and purl structure is evident when the fabric is fully stretched. And the knit part is slightly lower than the purl part, which is determined by the yarn direction in the loops. Figure 6-11b shows a side view of the fabric. When the strain increases from 0% to 100%, the height of the fabric is also reduced. According to the deformation of the fabric, the elongation of the samples, when the fabric is fully stretched, was calculated, as shown in Table 6-1. The elongation of the three samples is 100%, 140%, and 200% respectively. The elongation of the fabric is vital as the final length of the coated part is determined by it. The stretched coated part should have the same length as the relaxed fabric, ensuring that the skin area covered by the 3D knitted fabric can be fully covered by the coated part. For example, the elongation of sample 1# is 100%. If the original length of the fabric in a relaxed state is 100 mm, the length of the coating part should not be less than 50 mm, which can be extended to 100 mm exactly.

$$Elongation\ (\%) = \frac{the\ stretcehd\ length - the\ orignal\ length}{the\ orignal\ length} \tag{5-1}$$

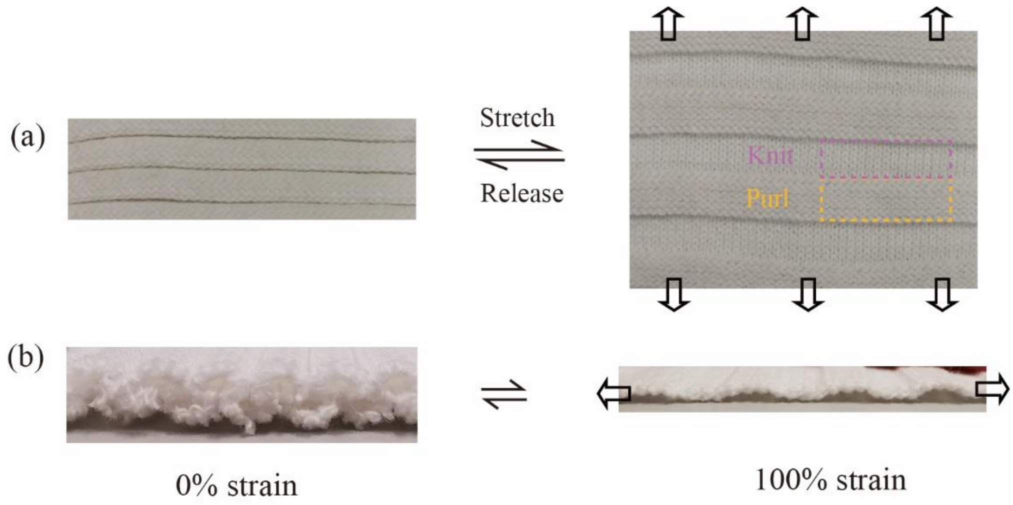

Figure 6-11 Deformation of the fabric. (a) Front view of the fabric in 0% strain and 100% strain. (b) Side view of the fabric in 0% strain and 100% strain.

It is evident that the stretching of the folded fabric is accompanied by a decrease in thickness along the height direction and an increase in length along the surface. The minimum length and maximum thickness occur when the fabric is folded, while the maximum length and minimum thickness are achieved when the fabric is stretched. Notably, the stretched state means that the folded structure was fully unfolded without yarn stretching. The minimum and maximum height and length of the fabrics were summarized in Figure 6-12a and 6-12b, respectively.

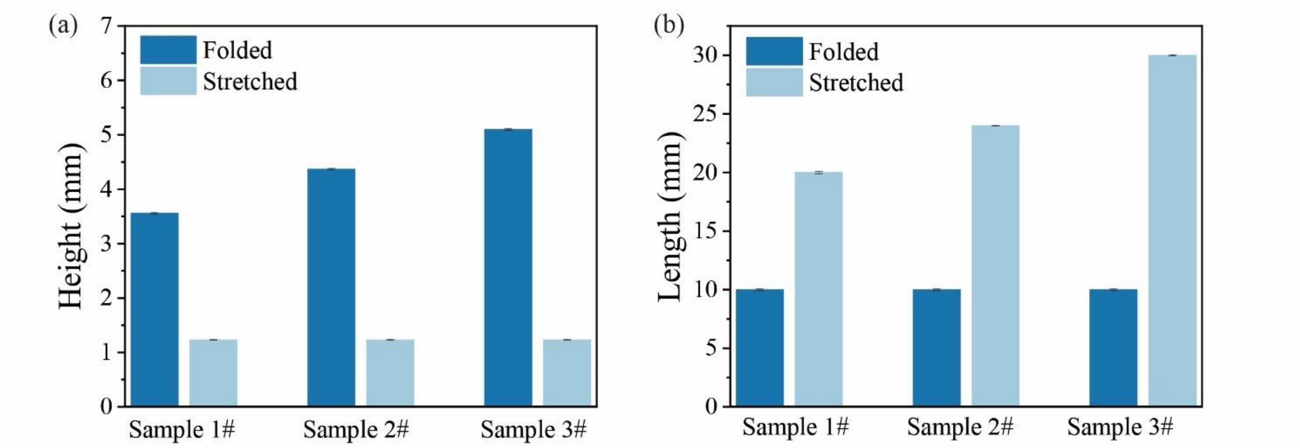

Figure 6-12 Length and thickness of fabrics under different states. (a) Height of fabrics under folded

and stretched state. (b) Length of fabrics under folded and stretched state.

As indicated above, fabric elongation increases with the number of courses in one unit. However, the longer the fabric, the better the performance. Since the fabric has an inherent weight, it is inevitable that when excessive courses are included within a unit, a downward force is generated, and then the fabric is stretched, which is not desirable. To test the length change of fabrics due to their own weight, experiments were designed, shown in Figure 6-13a. Three samples of the same length were selected. Firstly, the fabrics are placed on a horizontal plate and any arbitrary length is selected and marked as L_0, which serves as a reference point for subsequent measurements. Then, the top edges of the fabric are fixed, and the fabric hangs freely with no external forces acting on it. The selected length would increase due to weight, which is measured as L_1. The self-weight elongation can be calculated by the formula below.

$$Self - weight\ elongation\ (\%) = \frac{L_1 - L_0}{L_0} \tag{6-2}$$

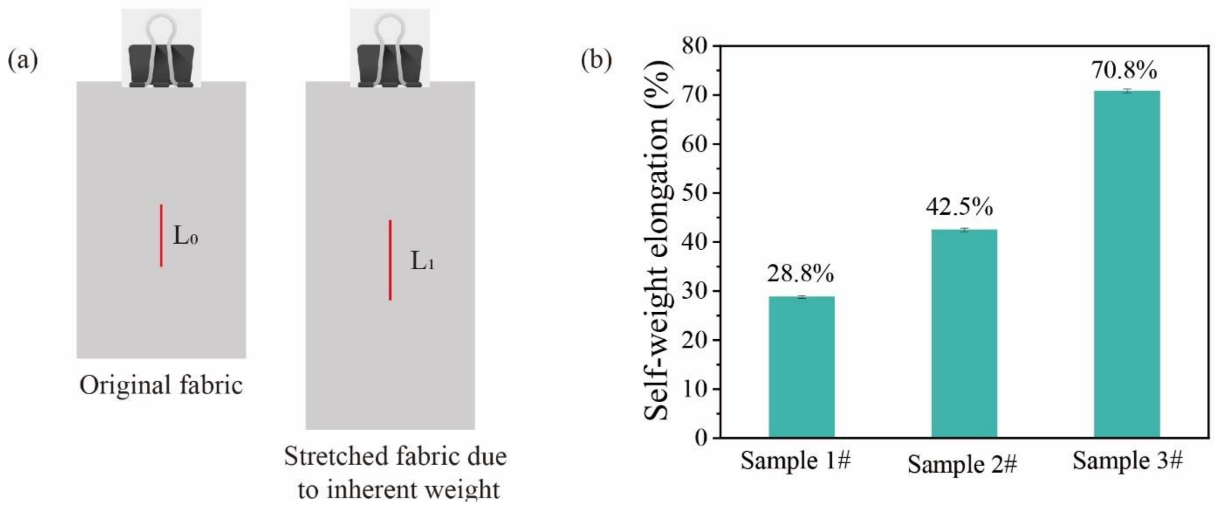

Figure 6-13 Results of the self-weight elongation. (a) Setup of the test. A clip is used to fix the top end of the fabric. The length variations of these three samples are illustrated, where L_0 is the initial length

without force and L_1 is the length under their own weight. (b) Self-weight elongation of different fabrics.

The self-weight elongation of the fabrics is shown in Figure 6-13b. When the sample length is the same, sample 3# has the largest self-weight elongation under its own weight, followed by sample 2# and sample 1#. The possible reason is that more courses in one unit can lead to loosening force between loops, which is easy to stretch due to their own weight. Therefore, the self-weight elongation of fabrics should be considered as the loose structure of the fabric may not only affect the thermal properties but also the aesthetics of clothing.

6.5 characterization of the parameters during coating process

6.5.1 SEM images of coated fabric

In order to test the optimal weight ratio of nanoparticles, solutions with different content of nanoparticles were fabricated. To avoid aggregation of particles, the method of multiple coating times to increase nanoparticle content was adopted. As shown in Figure 6-14, there are no particles attached to the pure fiber. Since the TiO_2 weight ratio is 4.5% to 10%, coating 1 time, the content of particles attached to the fiber surface increases significantly. However, when the weight ratio reaches 10%, there is aggregation of particles. To prove that multiple coatings can increase the number of particles, fiber with a weight ratio of 4.5% and 1 coating was also shown here. It is obvious that the particles on the surface of the fiber coated twice are significantly more than those coated only once. Furthermore, particles on the surface of the fiber coated twice with a weight ratio of 2.5% were more than those coated only once with a weight ratio of 4.5%. Thus, the particle weight ratio of 4.5%, coating 2 times, was adopted in this study.

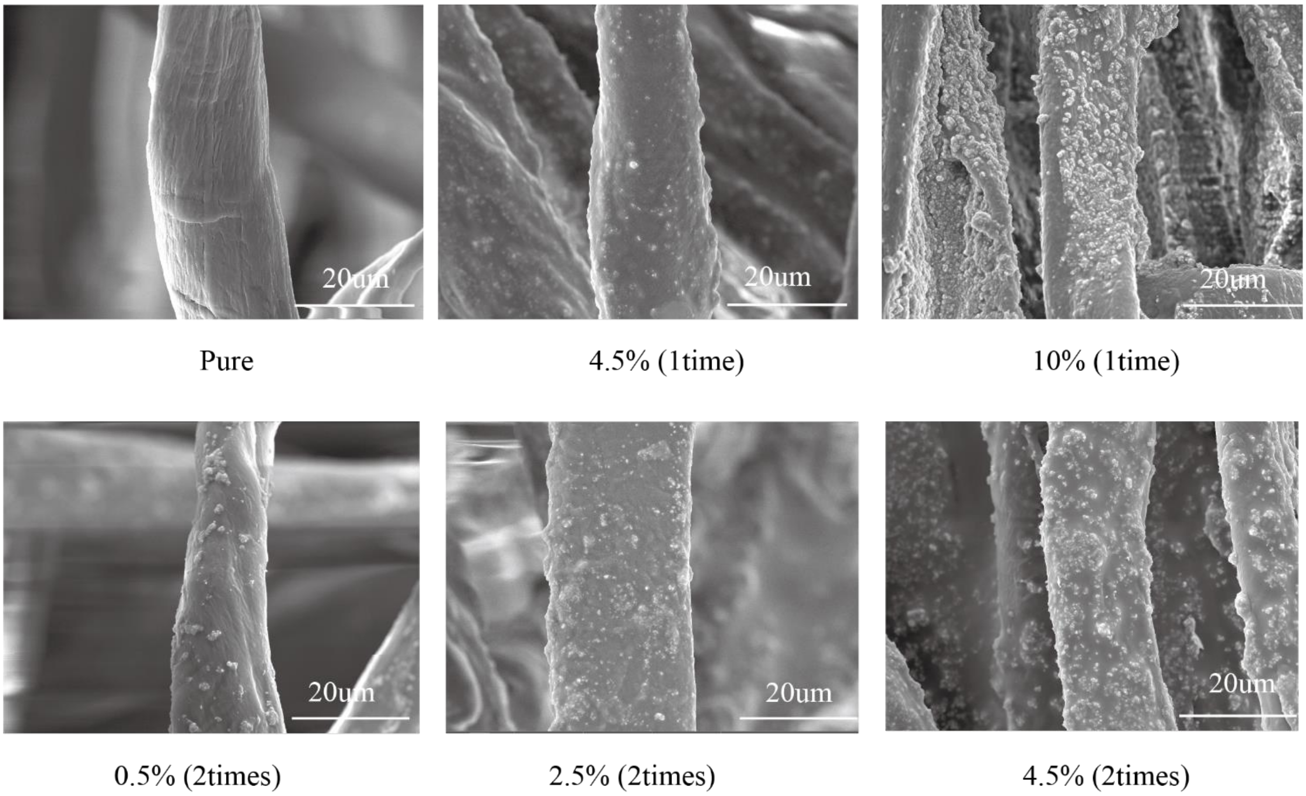

Figure 6-14 SEM images of coated fabric with different particle weight ratio and coating times.

6.5.2 Influence of the diameter of particles and coating times on solar reflectance

1) FDTD simulation of TiO_2/PDMS coating on reflectance

A finite difference time domain (FDTD) simulation is applied to study the effects of particle size on optical properties. Lumerical FDTD Solutions software was used to perform FDTD simulation. To facilitate analysis and reduce simulation time, a two-dimensional model was established. The study area was restricted to the 0.25-2.5 μm range (known as the solar range), with a particular focus on the effect of scattering on the NIR reflectivity of the coating. The TiO_2 particles used in this study had a radius range of 0.1-1.1 μm. The PDMS was selected as the matrix. A schematic of the simulation geometry is shown in Figure 6-15a. The calculated scattering efficiencies are shown in Figure 6-15b.

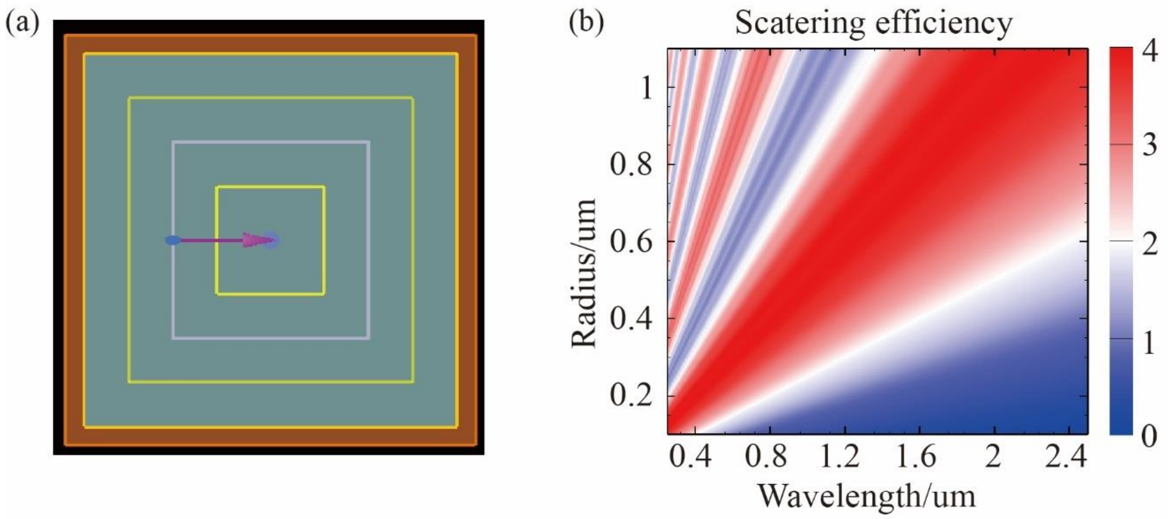

Figure 6-15 FDTD simulation. (a) Schematic of the simulation geometries. (b) FDTD simulation result of scattering efficiency (0.25–2.5 μm).

2) Experiments to investigate of the TiO_2/PDMS coating times on reflectance

Based on the above analysis, the weight ratio of 4.5% coated 2 and 3 times with different diameters would be discussed. The solar reflectance of the samples was first analyzed. Table 6-1 showed the maximum solar reflectance of the samples. The results indicated that even coating times can increase the number of particles on the surface of fabrics, the enhancement of solar reflectance is quite small, increasing only 2%. While for particles of different diameters, the difference between solar reflectance is limited. Therefore, in the following studies, the coating with a weight ratio of 4.5%, coated 2 times and a diameter of 500 nm was investigated.

Table 6-1 Solar reflectance of the samples.

Sample	2 coating times	3 coating times
500 nm, 4.5%	89.5%	89.0%
200 mm, 4.5%	87.0%	88.0%
1 μm, 4.5%	87.0%	88.0%

6.6 Results and discussion

6.6.1 Evaluation of the thermal and moisture resistance

Since the thickness and length of the fabric can change during the deformation process, thermal and moisture resistance should be measured to characterize the thermal properties under different modes. Three designed samples were tested, the results of which are shown in Figure 6-16. Sample 3# has the largest thermal resistance due to the largest thickness among samples, and next is sample 2#, and the smallest is sample 1#. Greater thickness and thermal resistance also mean greater moisture resistance. The moisture resistance of sample 3# is higher than that of sample 2# and 1#. The thermal and moisture resistance of all stretched samples is similar, indicating that stretched fabrics have a 2D structure whose thickness is the thickness of single loops. According to the results collected above, sample 2# is selected to be used for fabric fabrication for both cooling and warming. Sample 2# has comparable thermal and moisture resistance and a much more stable 3D structure, which is vital for such clothing.

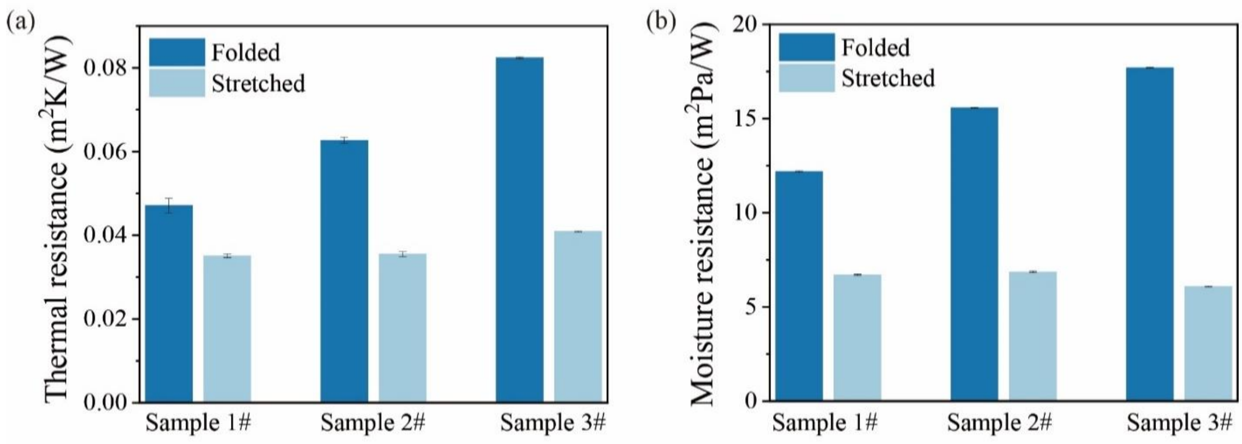

Figure 6-16 Thermal and moisture resistance of fabrics under folded and stretched state. (a) Thermal resistance of fabrics. (b) Moisture resistance of fabrics.

6.6.2 Morphology and optical properties of the warming state

The 3D fabric in a relaxed state is used to achieve body warming due to the large amount of still air stored by its cavity. The warming mode of the proposed fabric is based on the entire fabric system, both the coated part and pristine part of the fabric. The working principle is shown in Figure 6-17a. The folded structure can create cavities between fabric and then store air to block heat dissipation. Thus, the fabric in this relaxed state has a lower thermal conductivity. Figure 6-17b shows the thermal resistance and thickness.

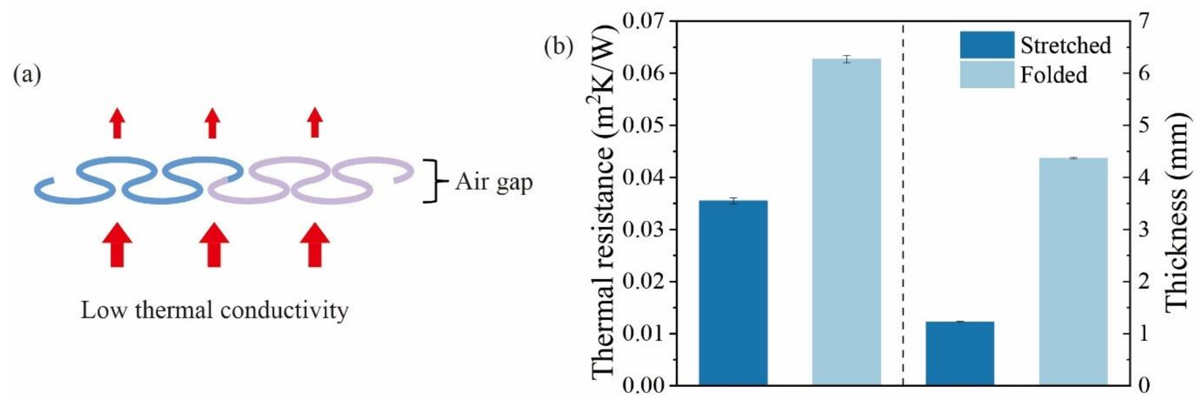

Figure 6-17 Mechanism of the proposed fabric in warming mode. (a) Principle of the warming mode.

(b) Thermal resistance and the thickness of the proposed fabric.

In order to verify whether the thermal insulation performance of the fabric can be affected by the coating, the coated and pure parts were placed on a hot plate simultaneously. Figure 6-18a shows the fabric on the hot plate. The left side is the pure part, and the right side is the coated part. The thermal images shown in Figure 6-18b shows no difference, indicating that the coatings did not affect the thermal conductivity of the fabric. Figure 6-18c demonstrates the thermal conductivity of the folded and coated fabric. It has been observed that the stretched fabric exhibits a higher thermal conductivity than the folded fabric, which is primarily attributed to the significant reduction in fabric thickness that occurs due to stretching. Conversely, the coated fabric, in both states, exhibits lower thermal conductivity than the pristine fabric. This phenomenon is likely due to the presence of coatings, which can effectively reduce the pore size of the fabric, thereby reducing heat loss and subsequently enhancing its thermal resistance. Consequently, this evidence suggests that the presence of coatings does not significantly affect the thermal insulation properties of the fabric.

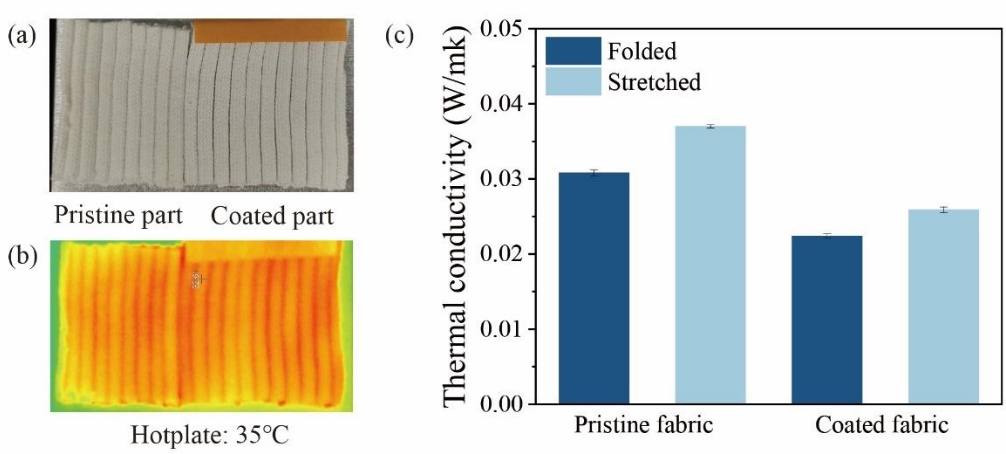

Figure 6-18 Influence of the coatings on thermal insulation performance. (a) Image of the fabric in

warming mode with pristine part (left) and coated part (right). (b) Thermal image of the fabric illustrated in (a) when the hot plate is 35 °C. (c) Thermal conductivity of the folded and stretched fabric.

In order to compare the thermal insulation performance of the fabric in relaxed and stretched state, the relaxed and stretched fabric were place on a hotplate, showing in Figure 6-19a. Then, the thermal images of the fabrics were collected, illustrated in Figure 6-19b-d, when the temperature of the hotplate was 25 °C, 35 °C and 40 °C, respectively. The surface temperature of the relaxed fabric with higher thermal resistance was lower than that of the relaxed fabric. Furthermore, there is a temperature difference between different parts of the relaxed fabric, which is caused by the difference in height between the loops.

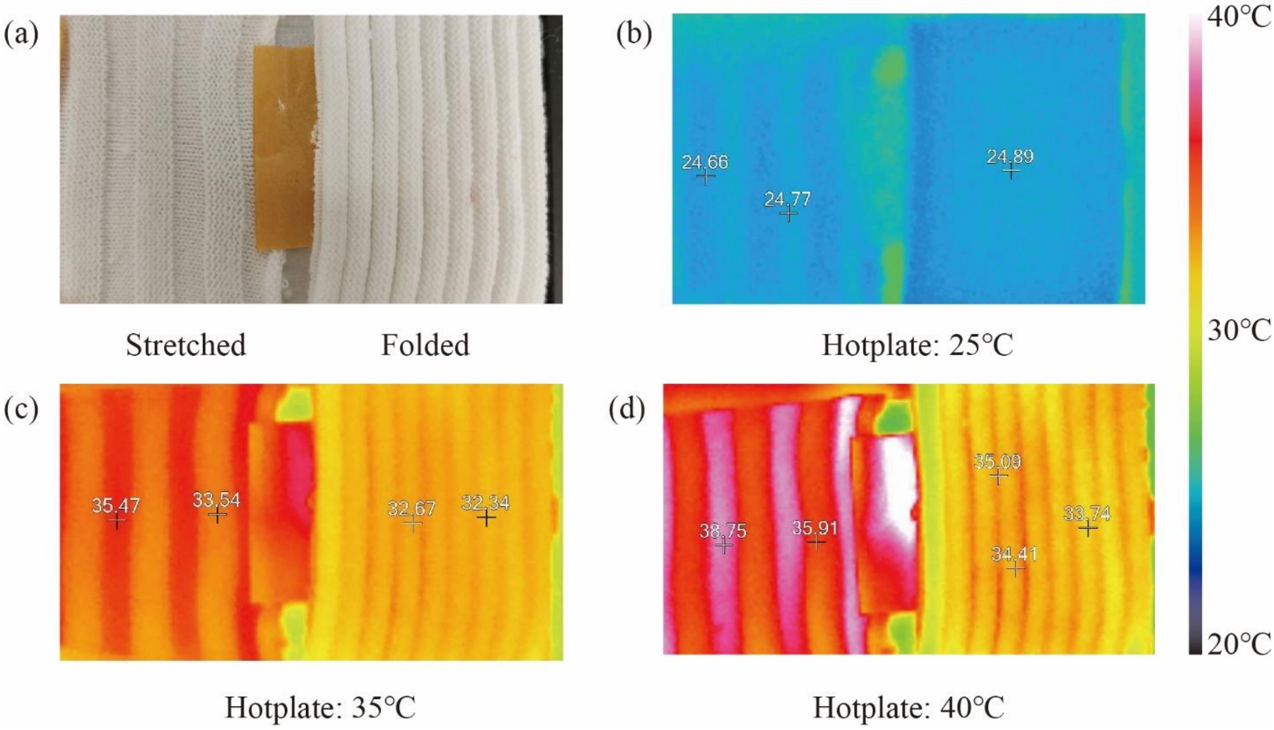

Figure 6-19 Thermal images of the fabric when stretched and relaxed under hotplate. (a) Image of the pristine fabric with stretched part (left) and relaxed part (right). (b-d) Thermal image of the fabric

illustrated in (a) when the hot plate is 25 °C, 35 °C and 40 °C, respectively.

6.6.3 Morphology and optical properties of the cooling state

Figure 6-19a illustrates principle of the cooling state. When the solar density increases, the coated part would be stretched, expanding to cover the skin. The coatings on the surface can efficiently reflect solar light and the thin structure also reduces thermal resistance, enhancing heat transfer from the skin surface to the ambient environment. Figure 6-20c displays the coated part in the relaxed state, and the stretched state was shown in Figure 6-20d. The SEM image of a single fiber with coatings was illustrated in Figure 6-20b. Surface morphology of samples was observed using the Field Emission Scanning Electron Microscope (SEM) (Tescan MIRA).

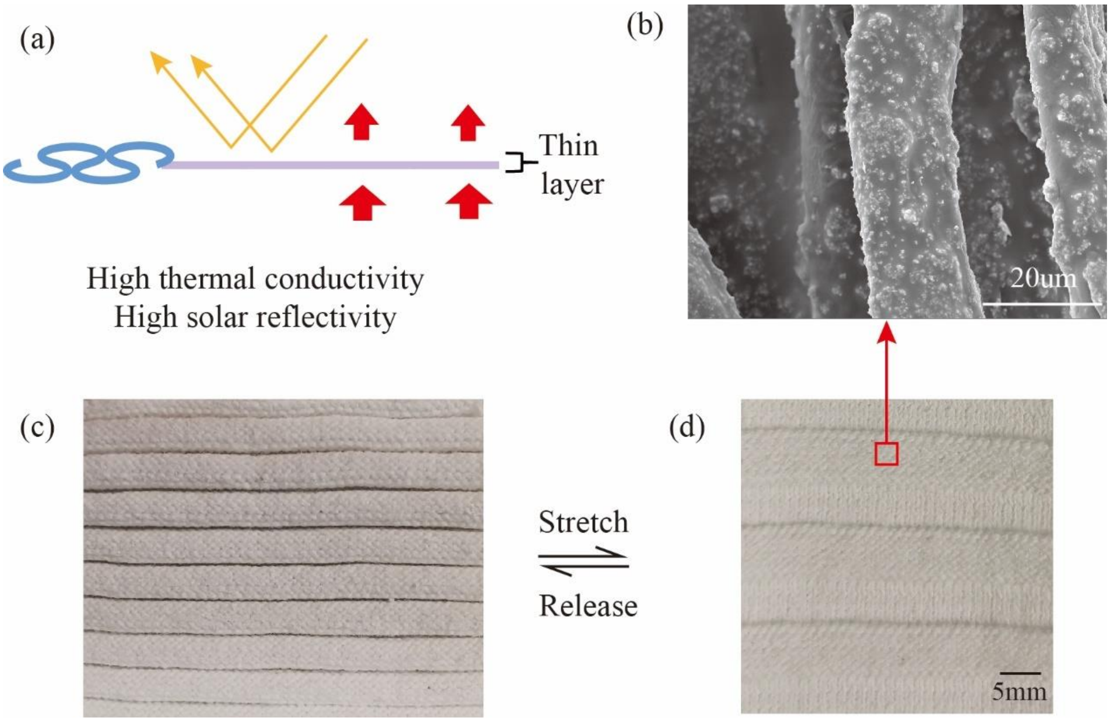

Figure 6-20 Working principle and morphology of the cooling state. (a) Principle of the proposed fabric for cooling. (b) SEM image of the single coated fabric. (c) Coated part of the proposed fabric under relaxed state. (d) Coated part of the proposed fabric under fully stretched state.

The reflectivity and emissivity of the coated part in the stretched state were measured and compared with pristine fabric shown in Figure 6-21. The results indicates that the reflectivity of the coated part is 89.5%, improved by about 11%, compared to the pristine fabric (78%). The emissivity increased approximately 8%. The diffuse reflectivity (0.25–2.5 μm) was analyzed by an ultraviolet–visible-near-infrared (UV–Vis-NIR) spectrophotometer (PerkinElmer) with an integrating sphere. The mid-infrared spectral emissivity (2.5–16 μm) at room temperature was measured by an FTIR spectrometer (PerkinElmer Spectrum 100) equipped with a gold-coated integrating sphere, *via* infrared measurement method.

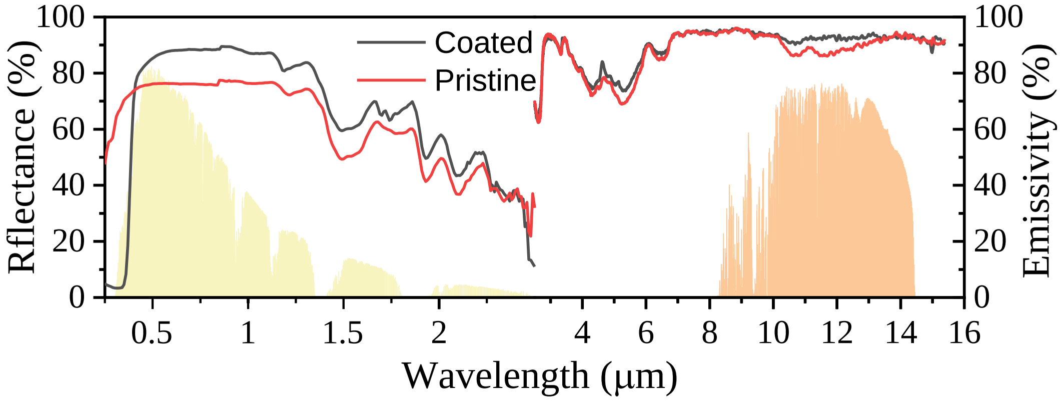

Figure 6-21 Solar reflection and infrared emission of coated fabric

6.6.4 Indoor and outdoor thermal measurement

In order to test temperature variations after using the proposed fabric, tests including indoor and outdoor direct thermal management, as well as in-body thermal measurement were conducted. The fabric was placed under a sunlamp. The measured solar density was 1000 W/m^2. Figure 6-22a is a configuration for fastening the fabric. The stretched fabric was mounted on the surface of a foam box with a thermocouple on the bottom of the fabric to collect the temperature. Temperature variations were illustrated in Figure 6-22b. The temperature of the thermocouple under the coated fabric reduced 5 °C approximately.

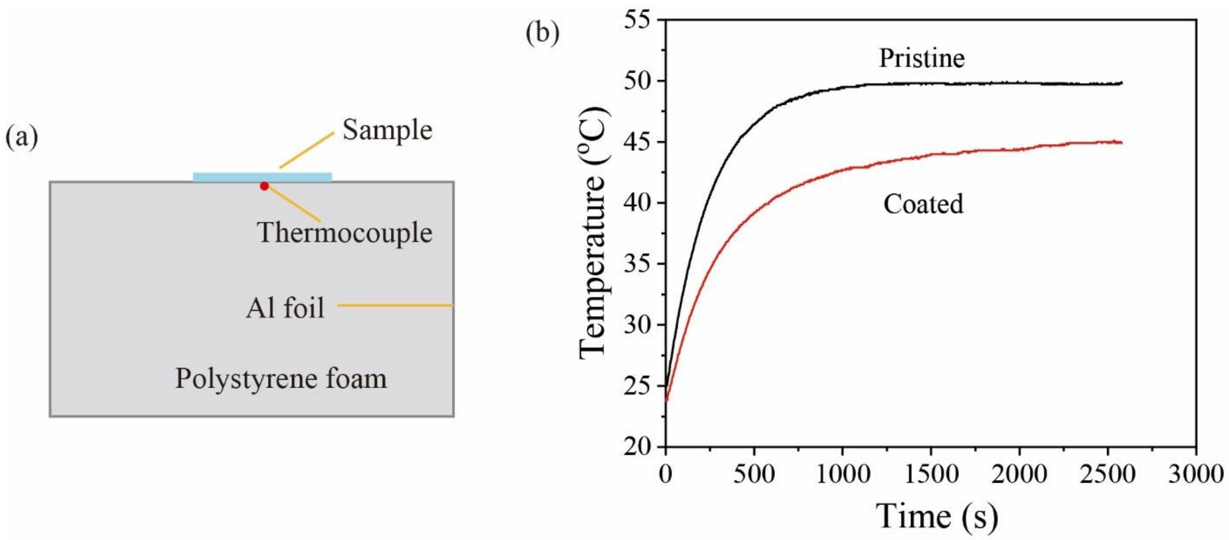

Figure 6-22 Thermal measurement of the proposed fabric under indoor sunlamp. (a) Structure of the setup to fix the fabric. (b) Temperature variations of the coated and pristine fabric.

The setup of the outdoor direct thermal management was shown in Figure 6-23a and the structure of the box to fix the fabric was shown in Figure 6-23b. The results shown in Figure 6-23c indicates that the coatings on the fabric could reduce the temperature about 5 °C when compared with the pristine fabric, indicating that the coatings on the surface can achieve cooling effect efficiently.

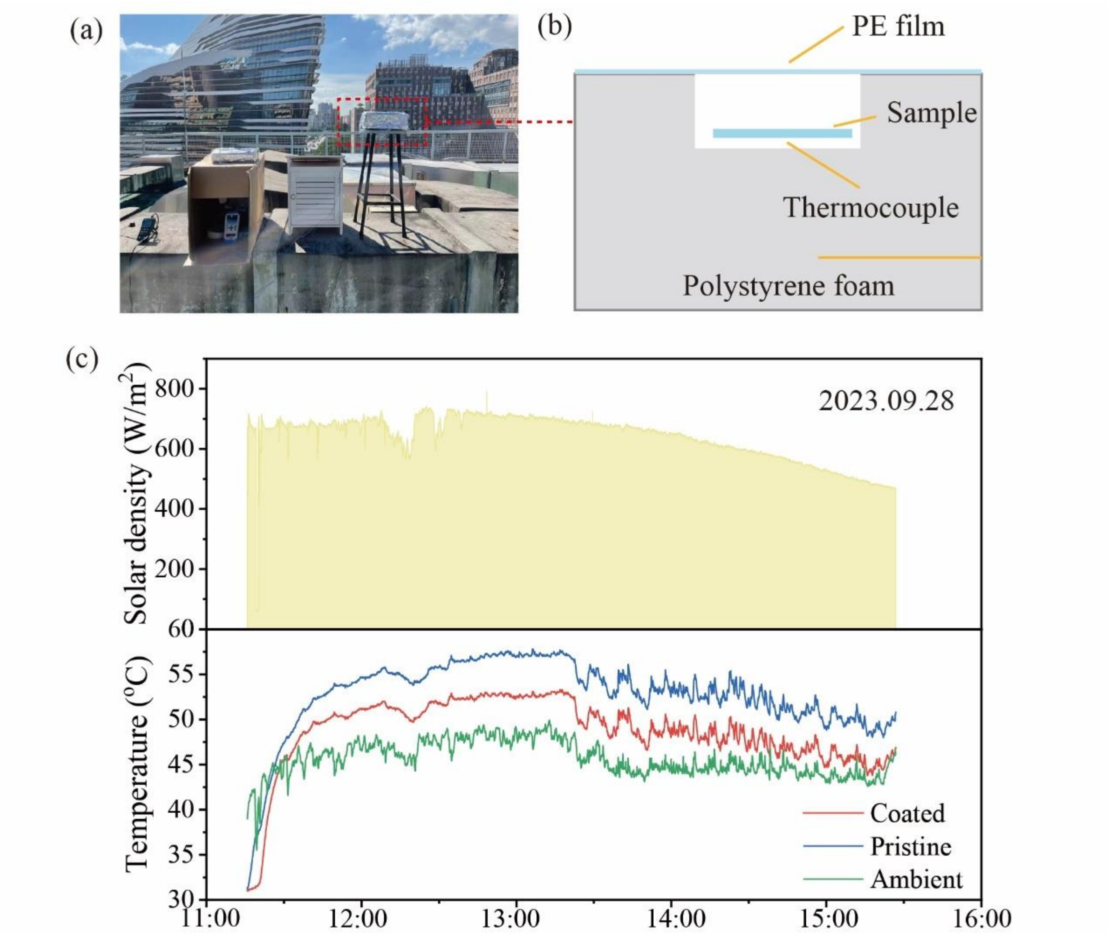

Figure 6-23 Thermal measurement of the proposed fabric under the outdoor sunlight. (a) Setup for the test. (b) Structure of the setup to fix the fabric. (c) Solar density and the temperature variations of the coated and pristine fabric.

The on-body thermal measurements were also performed. Sleeves were first fabricated and worn by a tester. The coated fabric was on the right arm and the pristine was on the left arm. Figure 6-24a and 6-24c were a schematic of the arm covered by the stretched fabric and the arm without fabric. Figure 6-24b is a thermal image of the arm covered by the fabric, while Figure 6-24d shows the thermal image when the fabric is removed. It illustrated that the arm portion covered by the coated fabric had a lower temperature, which could also be demonstrated by the temperature value shown in Figure 6-

24e. The maximum temperature can reach nearly 1 °C.

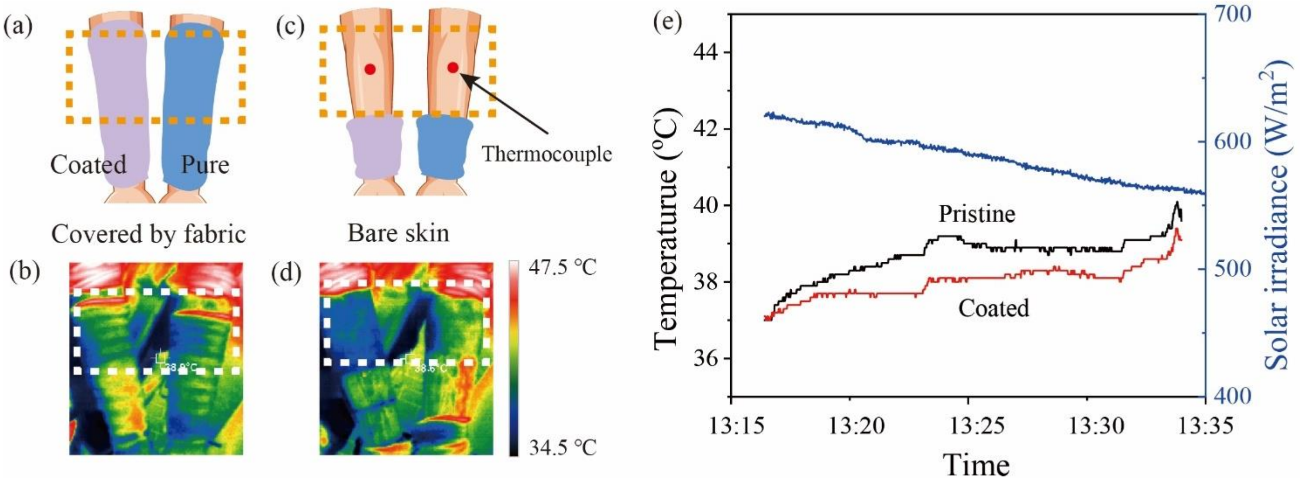

Figure 6-24 Thermal measurement of the proposed fabric by human. (a) Arm covered by coated (left) and pristine fabric (right). (b) Thermal images of the arm when they are covered by fabrics. (c) Arm when the fabrics are removed. (d) Thermal images of the arm when the fabrics are removed. (e) Temperature variations of skin side under solar light.

6.6.5 Evaluation of the durability and wearability

The durability of the proposed fabric was assessed by washing test and repeated stretching experiments. As shown in Figure 6-25a, there was no change in the weight of the pristine fabric, while the weight experienced only a relatively minor shift after 5 washing cycles. This suggests that the particle loss was limited, which means that the potential loss of performance may be negligible. In Figure 6-25b, the increase in fabric length after 1000 cycles of repeated stretching was illustrated. The fabric length at the time of collection after stretching (0 h) and after 24 hours under natural conditions was summarized. For the pristine fabric, the increase in length under both 0 h and 24 h conditions were marginal. The length of the coated fabric may increase substantially after stretching, especially for the fabric coated once, reaching almost 20%. However, after 24 hours, the increase ratio decreased to less than 5%, and subsequently 0%, after 48 hours, the fabrics were able to recover to their original shape, with a stretching recovery rate of 0%. These results highlight the exceptional reversible properties of the coated fabric.

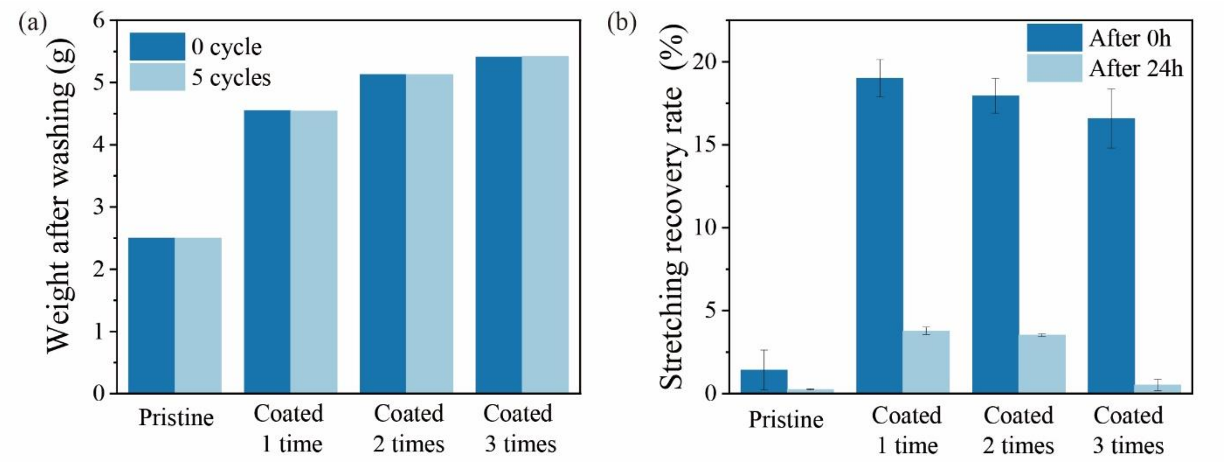

Figure 6-25 Durability of the proposed fabric. (a) Weight of fabrics before and after washing 5 cycles. (b) Stretching recovery rate of fabric after 1000 repeated stretching tests. The length under 0 h represents the value collected at the end of the stretching test, whereas the length under 24 h signifies that the length was collected after 24 h under natural conditions.

The fabric's wearability was also assessed by air permeability, water vapor transmission and tensile tests. Figure 6-26a showed the air permeability of the fabric, including pristine fabric in a relaxed state, pristine fabric in a stretched state, and coated fabric in a stretched state. At 100 Pa, the pristine fabric in the stretched state exhibited the highest air transport volume, followed by the pristine fabric in the relaxed state. The air permeability of the fabric in the stretched state increased by 23% when compared to the fabric in the relaxed state. The results also showed that due to the loose structure of the knitted fabric, the air permeability of the coated fabric under stretched state decreased by 32%, compared with the pristine one under stretched state. The coating on the fabric can affect air permeability, while the coated fabric in a stretched state still allows air transmission. Then tensile tests were also carried out, shown in Figure 6-26b, whose results showed that the application of a coating not only ensured the preservation of fibers and fabrics, but also provided an additional enhancement to the overall strength of the fabric. Mechanical properties were measured using Universal Testing (Instron-4411, INSTRON CORPORATION Co., LTD). The rectangular sample fabric with a size of 7.5 cm × 5 cm was stretched at a constant rate of 300 mm·min^{-1}.

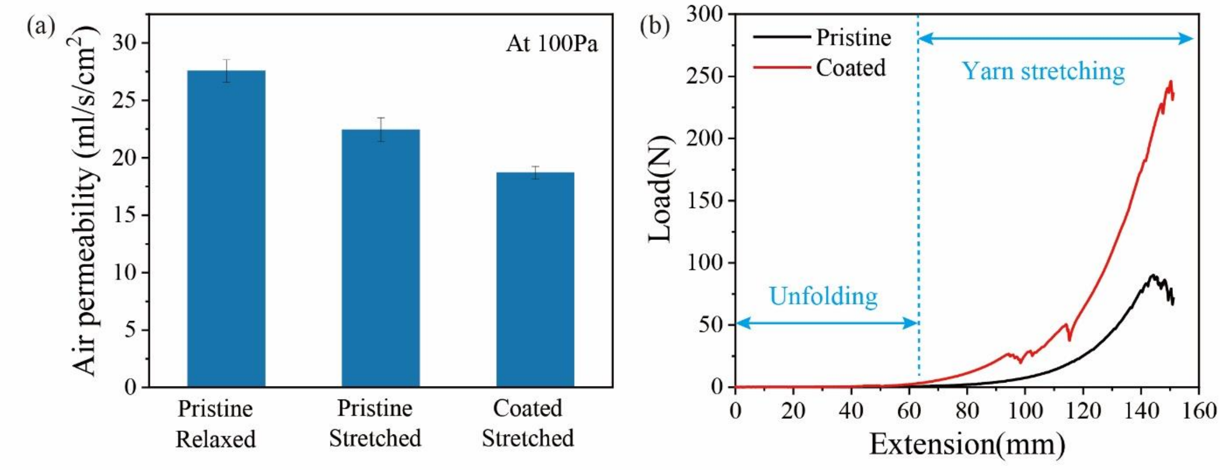

Figure 2-26 Air permeability and tensile strength of the proposed fabric. (a) Air permeability of the pristine fabric and the coated fabric (4.5%, 2 times). (b) Load and extension under tensile test.

Figure 6-27a shows the setup for the water vapor transmission test. A bottle with and without open ends was set as control. And pristine and coated fabric that were stretched to compare the influence of coatings on water vapor transmission. The water loss ratio was illustrated in Figure 6-27b. The bottle with close ends shows almost 0% water loss. And the bottle with an open end has the greatest amount of water loss. In the first 8 hours, the water loss of the pristine fabric seemed to be the same as that of the coated fabric. The possible reason is that the fabric is made of cotton and the cotton fabric has good water absorption. From 24 h, the difference in water loss between pristine and coated fabric is obvious. The bottle covered with pristine fabric demonstrates a large volume of water loss.

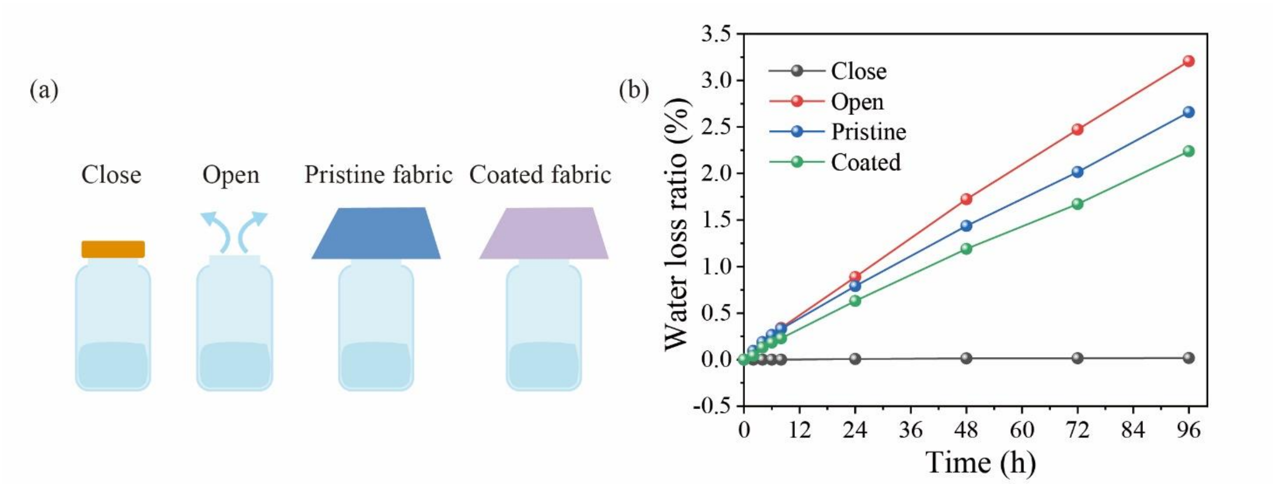

Figure 6-27 Results of water vapor transmission test. (a) Setup of the test. (b) Water loss ratio.

Furthermore, the load required to stretch the folded fabric was also quantified. As the proposed fabric operates by folding and unfolding its 3D structure, the magnitude of the load required to unfold the fabric is a crucial aspect. This is demonstrated in Figure 2-28a where a tension meter was used to increase the fabric length to a certain value (2.5 cm). Subsequently, the load value was recorded and compared (see Figure 6-28b). It is apparent that the uncoated fabric requires the least load, and this gradually increases with the application of coating. However, for practical purposes, a lower load is more convenient.

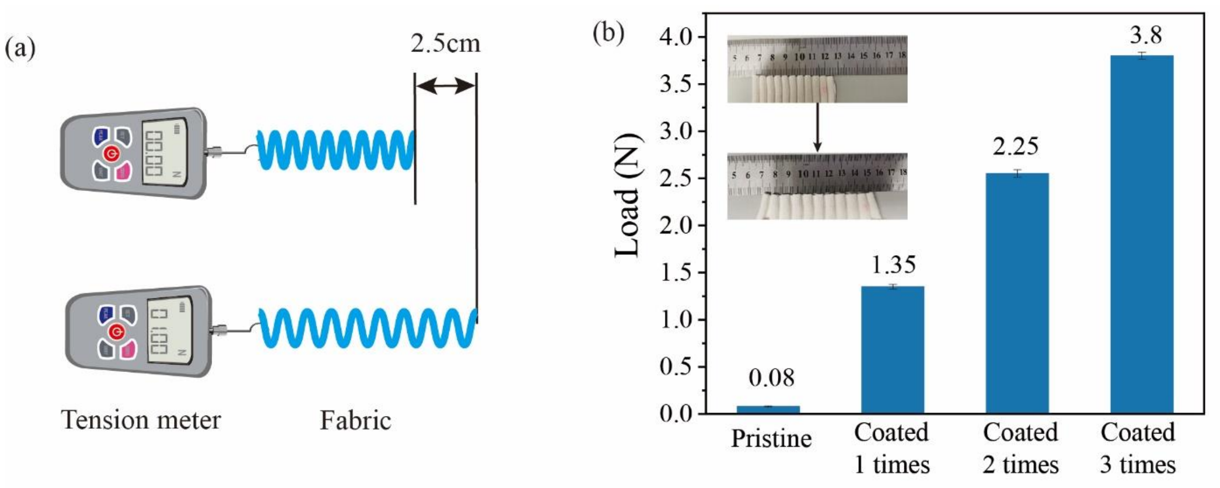

Figure 6-28 Load required to stretch fabric. (a) Testing setup. (b) Load required to increase the length of the fabric to a certain value (2.5 cm).

6.7 Summary

In this chapter, a 3D knitted fabric was proposed for body warming and cooling. The fabric was partially coated with TiO_2 and PDMS. The coated part is used for radiative cooling, while the whole part, including both the coated part and pristine part, is used for thermal insulation. The fabric in a relaxed state with a 3D structure can store still air inside due to the cavity generated by the folding process. Thermal conductivity can be reduced to block heat loss from body parts. If the solar density is enhanced, the coated part can be stretched and completely cover the skin. TiO_2 coatings on the fabric surface can reflect solar light, and PDMS is IR-transparent, allowing infrared light to be emitted from the body to the outside. Simultaneously, compared with the relaxed fabric, stretched fabric has a relatively small thickness, which means higher thermal conductivity, greatly accelerating heat dissipation from the human body. The folding and unfolding of the 3D fabric requires only a small strain, indicating the easy process of changing. Overall, the proposed dual mode fabric provides a feasible method to achieve highly efficient dual mode warming and radiative cooling, which can be applied in conditions with eruptive changes.

Chapter 7 Conclusions and future perspectives

7.1 Conclusions

The aim of the thesis is to integrate soft robotic elements with fabrics to design and develop soft robotic fabric and clothing to achieve personal thermal management. Traditional fabric and clothing have only a fixed thermal performance, which may not adapt to dynamic environmental temperature changes. Failure to maintain human thermal comfort can lead to serious health problems and even death. Therefore, the purpose of this thesis is to address this gap by proposing soft robotic fabric and clothing. The objectives listed have been achieved and the completed work is summarized as follows.

1) The modes of heat transfer between the human body and the ambient environment have been analyzed to provide a theoretical basis for clothing design.
2) The current fabric and clothing to achieve dynamic thermal management has been reviewed. Numerous literature studies have been devoted to proposing fabric and clothing for personal thermal management, referring to various heat transfer models. In addition, an increasing number of commercial products have emerged in succession in routine life. All this indicates that the development of smart fabric and clothing for personal thermal management has become a development trend.
3) In Chapter 4, a soft passive robotic fabric with tunable thermal insulation performance was designed for people who may work in extremely hot conditions, especially firemen. Low

boiling point fluid has been used as heat sensitive materials, which can achieve large volume variations during the phase change process between liquid and vapor. Soft robotic elements with low boiling point behave like thermal switches. When the wearers remain in normal conditions where the temperature is below the boiling point of the fluid, the fluid maintains a liquid state. While the temperature increases, the fluid continuously absorbs heat from the external thermal environment and begins to evaporate, generating a large amount of vapor to activate the elements. The designed soft robotic fabric has lower weight, faster response speed and excellent thermal insulation properties.

4) In Chapter 5, another active soft pneumatic robotic clothing with tunable thermal resistance has been developed. Active control systems have been introduced to integrate with clothing to manage soft robot deformation quickly and safely. The proposed fabric can manage the fabric's thermal resistance while reducing its impact on moisture resistance, always maintaining good breathability and moisture permeability to keep wear comfortable. The results shows that the working range of the clothing can achieve 5 ℃.

5) In Chapter 6, a knitted fabric with a 3D structure is proposed that can transfer between 3D and 2D states, managing thermal performance. Under warming mode, the fabric is relaxed with a larger thickness. The cavity inside the fabric and traps still air and then achieves large thermal resistance. In the meantime, part of the fabric is coated. When the solar density increases, the coated part can be stretched to cover the skin, leading to deformation

of soft robotics. This dual mode textile can be applied to outdoor sportswear as there may be extreme environmental changes when people engage in outdoor activities.

7.2 Limitations of this thesis

Although many effects have been done, there are also some limitations in this thesis, which are as follows:

1) For the soft robotic clothing proposed in Chapter 5, the manikin tests and the human trials only carried out under temperature from 5 ℃ to 11 ℃. More skin points and temperature ranges need to be investigated in the future.
2) The appearance of the prototypes can be improved.
3) More opinions for human trials can be collected to evaluate the wearability.

7.3 Future perspectives

In the current thesis, the adoption of the theoretical design process model, coupled with the well-established prototypes, has led to the formulation of the following recommendations:

1) The opinions of the wearers should be collected and analyzed to improve the designs.
2) More kinds of materials can be applied to fabricate the soft robotics to improve both the functionality and the aesthetics.
3) More prototypes should be fabricated to conduct more human trials, obtaining more results for future development.

4) The AI technology can be introduced to improve the intelligence of the soft robotic clothing.

References

1. Li, L., et al., *Multifunctional Wearable Thermoelectrics for Personal Thermal Management.* Advanced Functional Materials, 2022. **32**(22): p. 2200548.
2. Tan, C.L., et al., *Regulation of body temperature by the nervous system.* Neuron, 2018. **98**(1): p. 31-48.
3. Sessler, et al., *Temperature monitoring and perioperative thermoregulation.* The Journal of the American Society of Anesthesiologists, 2008. **109**(2): p. 318-338.
4. Zhang, X., et al., *Personal thermal management by thermally conductive composites: A review.* Composites Communications, 2021. **23**: p. 100595.
5. Wan, X. , et al., *A transient thermal model of the human body–clothing–environment system.* Journal of Thermal Biology, 2008. **33**(2): p. 87-97.
6. Awais, M., *Thermophysiological simulation of human body-clothing-environment system*. 2020: TUDpress Verlag der Wissenschaften GmbH.
7. Habibi, P., et al., *A review on advanced functional photonic fabric for enhanced thermoregulating performance.* Environmental Nanotechnology, Monitoring & Management, 2021. **16**: p. 100504.
8. Li, X., et al., *Metalized polyamide heterostructure as a moisture-responsive actuator for multimodal adaptive personal heat management.* Science Advances, 2021. **7**(51): p. eabj7906.
9. Yang, L., et al., *Thermal comfort and building energy consumption implications–a review.* Applied energy, 2014. **115**: p. 164-173.
10. Hsu, P.-C., et al., *A dual-mode textile for human body radiative heating and cooling.* Science advances, 2017. **3**(11): p. e1700895.
11. Chu, S., et al., *Opportunities and challenges for a sustainable energy future.* nature, 2012. **488**(7411): p. 294-303.
12. Zhong, H., et al., *Hierarchically hollow microfibers as a scalable and effective thermal insulating cooler for buildings.* ACS nano, 2021. **15**(6): p. 10076-10083.
13. Chen, M., et al., *Passive daytime radiative cooling: Fundamentals, material designs, and applications.* EcoMat, 2022. **4**(1): p. e12153.
14. Peng, Y., et al., *Advanced textiles for personal thermal management and energy.* Joule, 2020. **4**(4): p. 724-742.
15. Wang, Y., et al., *Reversible water transportation diode: temperature-adaptive smart janus textile for moisture/thermal management.* Advanced Functional Materials, 2020. **30**(6): p. 1907851.
16. Peng, L., et al., *Review of clothing for thermal management with advanced materials.* Cellulose, 2019. **26**: p. 6415-6448.
17. Whitesides, G.M., *Soft Robotics.* Angewandte Chemie International Edition, 2018. **57**(16): p. 4258-4273.
18. Sanchez, V., et al., *Textile technology for soft robotic and autonomous garments.* Advanced

functional materials, 2021. **31**(6): p. 2008278.

19. Wang, W., et al., *Harnessing the hygroscopic and biofluorescent behaviors of genetically tractable microbial cells to design biohybrid wearables.* Science Advances, 2017. **3**(5): p. e1601984.
20. Walsh, C., *Human-in-the-loop development of soft wearable robots.* Nature Reviews Materials, 2018. **3**(6): p. 78-80.
21. Yin, R., et al., *Wireless Multistimulus-Responsive Fabric-Based Actuators for Soft Robotic, Human–Machine Interactive, and Wearable Applications.* Advanced Materials Technologies, 2020. **5**(8): p. 2000341.
22. Ma, Z., et al., *Personal thermal management techniques for thermal comfort and building energy saving.* Materials Today Physics, 2021. **20**: p. 100465.
23. Raman, A.P., et al., *Passive radiative cooling below ambient air temperature under direct sunlight.* Nature, 2014. **515**(7528): p. 540-544.
24. Shi, N.N., et al., *Keeping cool: Enhanced optical reflection and radiative heat dissipation in Saharan silver ants.* Science, 2015. **349**(6245): p. 298-301.
25. Ilic, O., et al., *Tailoring high-temperature radiation and the resurrection of the incandescent source.* Nature nanotechnology, 2016. **11**(4): p. 320-324.
26. Xu, P., et al., *Experimental investigation on performance of fabrics for indirect evaporative cooling applications.* Building and Environment, 2016. **110**: p. 104-114.
27. Zhou, H., et al., *One-Way Water-Transport Cotton Fabrics with Enhanced Cooling Effect.* Advanced Materials Interfaces, 2016. **3**(17): p. 1600283.
28. Lao, L., et al., *"Skin-like" fabric for personal moisture management.* Science advances, 2020. **6**(14): p. eaaz0013.
29. Jang, W., et al., *Thickness-dependent thermal conductivity of encased graphene and ultrathin graphite.* Nano letters, 2010. **10**(10): p. 3909-3913.
30. Xin, G., et al., *Highly thermally conductive and mechanically strong graphene fibers.* Science, 2015. **349**(6252): p. 1083-1087.
31. Pop, E., et al., *Thermal conductance of an individual single-wall carbon nanotube above room temperature.* Nano letters, 2006. **6**(1): p. 96-100.
32. Kim, P., et al., *Thermal transport measurements of individual multiwalled nanotubes.* Physical review letters, 2001. **87**(21): p. 215502.
33. Abbas, A., et al., *Improving thermal conductivity of cotton fabrics using composite coatings containing graphene, multiwall carbon nanotube or boron nitride fine particles.* Fibers and Polymers, 2013. **14**: p. 1641-1649.
34. Tang, Z., et al., *Highly machine-washable e-textiles with high strain sensitivity and high thermal conduction.* Journal of Materials Chemistry C, 2020. **8**(8): p. 2741-2748.
35. Ishigami, M., et al., *Properties of boron nitride nanotubes*. in *AIP conference proceedings*. 2003. American Institute of Physics.

36. Gao, T., et al., *Three-dimensional printed thermal regulation textiles.* ACS nano, 2017. **11**(11): p. 11513-11520.
37. Candadai, A.A.,et al., Marconnet, *Thermal conductivity of ultrahigh molecular weight polyethylene: From fibers to fabrics.* ACS Applied Polymer Materials, 2019. **2**(2): p. 437-447.
38. Stapulionienė, R., et al., *Investigation of thermal conductivity of natural fibres processed by different mechanical methods.* International Journal of Precision Engineering and Manufacturing, 2016. **17**: p. 1371-1381.
39. Gao, J., et al., *Structures and properties of the goose down as a material for thermal insulation.* Textile Research Journal, 2007. **77**(8): p. 617-626.
40. Slavinec, M., et al., Klemenčič, *The impact of moisture on thermal conductivity of fabrics.* Anali Pazu, 2016. **6**(1-2): p. 8-12.
41. Cai, G., et al., *Experimental investigation on the thermal protective performance of nonwoven fabrics made of high-performance fibers.* Journal of Thermal Analysis and Calorimetry, 2015. **121**: p. 627-632.
42. Finefrock, S.W., et al., *Measurement of thermal conductivity of pbte nanocrystal coated glass fibers by the 3ω method.* Nano Letters, 2013. **13**(11): p. 5006-5012.
43. Le, N.L., et al., *Evolution of regular geometrical shapes in fiber lumens.* Scientific Reports, 2017. **7**(1): p. 9171.
44. Cui, Y., et al., *A thermally insulating textile inspired by polar bear hair.* Advanced Materials, 2018. **30**(14): p. 1706807.
45. Mikučioniene, D., et al., *Investigation on mechanical and thermal properties of knits from peat fibers and their combination with other natural fibers.* Textile research journal, 2018. **88**(14): p. 1660-1670.
46. Balandin, A.A., *Thermal properties of graphene and nanostructured carbon materials.* Nature materials, 2011. **10**(8): p. 569-581.
47. Yang, H., et al., *Continuous, strong, porous silk firoin-based aerogel fibers toward textile thermal insulation.* Polymers, 2019. **11**(11): p. 1899.
48. Abbas, A., et al., *Improving heat-retaining property of cotton fabrics through surface coatings.* The Journal of The Textile Institute, 2017. **108**(10): p. 1808-1814.
49. Schwurack, R., et al., *Performance enhancement of a thermoelectric system with improved natural convection cooling by utilizing the chimney effect.* Energy Conversion and Management, 2021. **237**: p. 114118.
50. Deer, W. *The importance of layering for the hunter in cool to cold climate environments by tony stoyanovski (tusx clothing)*. 2020; Available from: https://www.wilddeer.net.au/2020/02/05/the-importance-of-layering-for-the-hunter-in-cool-to-cold-climate-environments-by-tony-stoyanovski/.
51. Farooq, A.S., et al., *Fundamentals, materials and strategies for personal thermal management by next-generation textiles.* Composites Part A: Applied Science and Manufacturing, 2021. **142**:

p. 106249.
52. Tong, J.K., et al., *Infrared-transparent visible-opaque fabrics for wearable personal thermal management.* Acs Photonics, 2015. **2**(6): p. 769-778.
53. Ke, Y., et al., *On the use of a novel nanoporous polyethylene (nanoPE) passive cooling material for personal thermal comfort management under uniform indoor environments.* Building and Environment, 2018. **145**: p. 85-95.
54. Shi, M., et al., *Ti3C2Tx MXene-decorated nanoporous polyethylene textile for passive and active personal precision heating.* ACS nano, 2021. **15**(7): p. 11396-11405.
55. Hsu, P.-C., et al., *Radiative human body cooling by nanoporous polyethylene textile.* Science, 2016. **353**(6303): p. 1019-1023.
56. Cai, L.L., et al., *Warming up human body by nanoporous metallized polyethylene textile.* Nature Communications, 2017. **8**.
57. Hsu, P.-C., et al., *A dual-mode textile for human body radiative heating and cooling.* Science Advances, 2017. **3**(11): p. e1700895.
58. Peng, Y.C., et al., *Nanoporous polyethylene microfibres for large-scale radiative cooling fabric.* Nature Sustainability, 2018. **1**(2): p. 105-112.
59. Cai, L.L., et al., *Temperature Regulation in Colored Infrared-Transparent Polyethylene Textiles.* Joule, 2019. **3**(6): p. 1478-1486.
60. Song, Y.-N., et al., *Wearable polyethylene/polyamide composite fabric for passive human body cooling.* ACS applied materials & interfaces, 2018. **10**(48): p. 41637-41644.
61. Song, Y.-N., et al., *Novel passive cooling composite textile for both outdoor and indoor personal thermal management.* Composites Part A: Applied Science and Manufacturing, 2020. **130**: p. 105738.
62. Zeng, S.N., et al., *Hierarchical-morphology metafabric for scalable passive daytime radiative cooling.* Science, 2021. **373**(6555): p. 692-+.
63. Sun, Y.L., et al., *Preparation of Passive Daytime Cooling Fabric with the Synergistic Effect of Radiative Cooling and Evaporative Cooling.* Advanced Materials Technologies, 2022. **7**(3): p. 2100803.
64. Supuren, G., et al., *Moisture management and thermal absorptivity properties of double-face knitted fabrics.* Textile Research Journal, 2011. **81**(13): p. 1320-1330.
65. Nazir, A., et al., *Effect of Design and Method of Creating Wicking Channels on Moisture Management and Air Permeability of Cotton Fabrics.* Journal of Natural Fibers, 2015. **12**(3): p. 232-242.
66. Wang, X.F., et al., *Biomimetic Fibrous Murray Membranes with Ultrafast Water Transport and Evaporation for Smart Moisture-Wicking Fabrics.* Acs Nano, 2019. **13**(2): p. 1060-1070.
67. Dai, B., et al., *Bioinspired Janus textile with conical micropores for human body moisture and thermal management.* Advanced Materials, 2019. **31**(41): p. 1904113.
68. Airoudj, A., et al., Roucoules, *Textile with Durable Janus Wetting Properties Produced by*

Plasma Polymerization. Journal of Physical Chemistry C, 2016. **120**(51): p. 29162-29172.
69. Ou, J.F., et al., *Textile with Janus wetting properties via copper deposition and subsequent chemical vapor deposition of 1-dodecanethiol.* Materials Letters, 2019. **251**: p. 5-7.
70. He, X., et al., *Biospired Janus silk E-textiles with wet–thermal comfort for highly efficient biofluid monitoring.* Nano Letters, 2021. **21**(20): p. 8880-8887.
71. Li, X., et al., *Superabsorbent fabric based on weft-back weave structure for efficient evaporative cooling.* Advanced Materials Interfaces, 2021. **8**(1): p. 2001329.
72. Peng, Y., et al., *Integrated cooling (i-Cool) textile of heat conduction and sweat transportation for personal perspiration management.* Nature communications, 2021. **12**(1): p. 6122.
73. Yu, C., et al., *Electronically programmable, reversible shape change in two-and three-dimensional hydrogel structures.* Advanced Materials, 2013. **25**(11): p. 1541-1546.
74. Su, Y., et al., *Intelligent bidirectional thermal regulation of phase change material incorporated in thermal protective clothing.* Applied Thermal Engineering, 2020. **174**: p. 115340.
75. Meng, Q., et al., *Phase change fibers and assemblies*, in *Handbook of smart textiles*. 2015, Springer Science+ Business Media Singapore. p. 225-251.
76. Iqbal, K., et al., *Phase change materials, their synthesis and application in textiles-a review.* Journal of the Textile Institute, 2019. **110**(4): p. 625-638.
77. He, J., et al., *On the improvement of thermal protection for temperature-responsive protective clothing incorporated with shape memory alloy.* Materials, 2018. **11**(10): p. 1932.
78. Wang, Y., et al., *Thermochromic Silks for Temperature Management and Dynamic Textile Displays.* Nano-Micro Letters, 2021. **13**(1): p. 1-17.
79. Zhong, Y., et al., *Reversible humidity sensitive clothing for personal thermoregulation.* Scientific reports, 2017. **7**(1): p. 1-8.
80. Kim, G., et al., *Human-Skin-Inspired Adaptive Smart Textiles Capable of Amplified Latent Heat Transfer for Thermal Comfort.* Advanced Intelligent Systems, 2020. **2**(12): p. 2000163.
81. Zhang, X.A., et al., *Dynamic gating of infrared radiation in a textile.* Science, 2019. **363**(6427): p. 619-623.
82. Zhao, M., et al., *A study on local cooling of garments with ventilation fans and openings placed at different torso sites.* International Journal of Industrial Ergonomics, 2013. **43**(3): p. 232-237.
83. Zhao, M., et al., *A ventilation cooling shirt worn during office work in a hot climate: cool or not?* International Journal of Occupational Safety and Ergonomics, 2015. **21**(4): p. 457-463.
84. Guo, T., et al., *Design and testing of a liquid cooled garment for hot environments.* Journal of thermal biology, 2015. **49**: p. 47-54.
85. Hong, S., et al., *Wearable thermoelectrics for personalized thermoregulation.* Science advances, 2019. **5**(5): p. eaaw0536.
86. Thalman, C., et al., *A review of soft wearable robots that provide active assistance: Trends, common actuation methods, fabrication, and applications.* Wearable Technologies, 2020. **1**: p.

e3.
87. Buckner, T.L., et al., *Roboticizing fabric by integrating functional fibers.* Proceedings of the National Academy of Sciences, 2020. **117**(41): p. 25360-25369.
88. Foo, E., et al. *Soft robotic compression garment to assist novice meditators*. in *Extended Abstracts of the 2020 CHI Conference on Human Factors in Computing Systems*. 2020.
89. Rus, D., et al., *Design, fabrication and control of soft robots.* Nature, 2015. **521**(7553): p. 467-475.
90. Cui, Y., et al., *Soft robotic fabric design, fabrication, and thermoregulation evaluation.* Textile Research Journal, 2021. **91**(15-16): p. 1763-1785.
91. Cui, Y., et al., *Soft-logic: Design and thermal-comfort evaluation of smart thermoregulatory fabric with pneumatic actuators.* The Journal of The Textile Institute, 2021. **112**(12): p. 1913-1924.
92. Gupta, N., et al., *Review of passive heating/cooling systems of buildings.* Energy Science & Engineering, 2016. **4**(5): p. 305-333.
93. Pan, C.-S., et al., *Thermal comfort and energy saving of a personalized PFCU air-conditioning system.* Energy and buildings, 2005. **37**(5): p. 443-449.
94. Leung, E.M., et al., *A dynamic thermoregulatory material inspired by squid skin.* Nature communications, 2019. **10**(1): p. 1947.
95. Song, S., et al., *A dynamic mechanical stimulated and thermal-healed infrared modulator based on elastomer matrix with metal layer inspired by squid skin.* Materials Today Chemistry, 2022. **24**: p. 100911.
96. Xu, C., et al., and A.A. Gorodetsky, *Adaptive infrared-reflecting systems inspired by cephalopods.* Science, 2018. **359**(6383): p. 1495-1500.
97. Smith, D.S., et al., *Thermal conductivity of porous materials.* Journal of Materials Research, 2013. **28**(17): p. 2260-2272.
98. Gu, X., et al., *Phonon transport and thermal conductivity in two-dimensional materials.* Annual review of heat transfer, 2016. **19**.
99. Shenoy, A., et al., *Convective flow and heat transfer from wavy surfaces: viscous fluids, porous media, and nanofluids*. 2016: CRC press.
100. Voelker, C., et al., *Heat and moisture transfer through clothing.* 2009.
101. Lu, X., et al., *Cooling potential and applications prospects of passive radiative cooling in buildings: The current state-of-the-art.* Renewable and Sustainable Energy Reviews, 2016. **65**: p. 1079-1097.
102. Kang, Z., et al., *Numerical modeling of body heat dissipation through static and dynamic clothing air gaps.* International Journal of Heat and Mass Transfer, 2020. **157**: p. 119833.
103. Wu, J., et al., *Novel Passive Radiation Cooling Materials with High Emissivity Discovered by FDTD Method.* Energies, 2023. **16**(4): p. 1832.
104. Bijarniya, J.P., et al., *Performance simulation of polymer-based nanoparticle and void

dispersed photonic structures for radiative cooling. Scientific Reports, 2021. **11**(1): p. 893.
105. Administration, U.S.F., *U.S. fire statistics.* 2020; Available from: www.usfa.fema.gov/data/statistics/#tab-2.
106. Udayraj, et al., *Heat and mass transfer through thermal protective clothing – A review.* International Journal of Thermal Sciences, 2016. **106**: p. 32-56.
107. Onofrei, E., et al., *Study of heat transfer through multilayer protective clothing at low-level thermal radiation.* Journal of Industrial Textiles, 2015. **45**(2): p. 222-238.
108. Song, G., et al., *Thermal protective performance of protective clothing used for low radiant heat protection.* Textile Research Journal, 2011. **81**(3): p. 311-323.
109. Huang, D., et al., *Thermal protective performance of silica aerogel felt bedded firefighters' protective clothing under fire conditions.* Mater Sci, 2017. **23**: p. 335-341.
110. Zhang, H., et al., *An exploration of enhancing thermal protective clothing performance by incorporating aerogel and phase change materials.* Fire and Materials, 2017. **41**(8): p. 953-963.
111. Shaid, A., et al., *Thermophysiological comfort analysis of aerogel nanoparticle incorporated fabric for fire fighter's protective clothing.* Chemical and materials engineering, 2014. **2**(2): p. 37-43.
112. Jin, L., K., et al., *Effect of aerogel on thermal protective performance of firefighter clothing.* Journal of Fiber Bioengineering and Informatics, 2013. **6**(3): p. 315-324.
113. Zhao, M. *The usage of phase change materials in fire fighter protective clothing: its effect on thermal protection*. in *IOP Conference Series: Materials Science and Engineering*. 2017. **274**(1): p. 012136. IOP Publishing.
114. Lu, Y., et al., *A novel personal cooling system (PCS) incorporated with phase change materials (PCMs) and ventilation fans: an investigation on its cooling efficiency.* Journal of thermal biology, 2015. **52**: p. 137-146.
115. Song, G., *Clothing air gap layers and thermal protective performance in single layer garment.* Journal of industrial textiles, 2007. **36**(3): p. 193-205.
116. Garrad, M., et al. *Driving soft robots with low-boiling point fluids*. in *2019 2nd IEEE International Conference on Soft Robotics (RoboSoft)*. 2019. p. 74-79. IEEE.
117. Mirvakili, S.M., et al., *Solar-Driven Soft Robots.* Advanced Science, 2021. **8**(8): p. 2004235.
118. Narumi, K., et al., *Liquid pouch motors: printable planar actuators driven by liquid-to-gas phase change for shape-changing interfaces.* IEEE Robotics and Automation Letters, 2020. **5**(3): p. 3915-3922.
119. Niiyama, R., et al., *Pouch motors: Printable/inflatable soft actuators for robotics*. in *2014 IEEE International Conference on Robotics and Automation (ICRA)*. 2014. p. 6332-6337. IEEE.
120. Niiyama, R., et al., *Pouch motors: Printable soft actuators integrated with computational design.* Soft Robotics, 2015. **2**(2): p. 59-70.

121. Deng, M., et al., *Effect of air gaps characteristics on thermal protective performance of firefighters' clothing: A review.* International Journal of Clothing Science and Technology, 2018. **30**(2): p. 246-267.
122. Lu, Y., et al., *The effect of air gaps in moist protective clothing on protection from heat and flame.* Journal of fire sciences, 2013. **31**(2): p. 99-111.
123. Udayraj, et al., *Numerical modeling of heat transfer and fluid motion in air gap between clothing and human body: Effect of air gap orientation and body movement.* International Journal of Heat and Mass Transfer, 2017. **108**: p. 271-291.
124. Rossi, R.M., et al., *Phase change materials for the improvement of heat protection.* Advanced Engineering Materials, 2005. **7**(5): p. 368-373.
125. Mandal, S., et al., *Characterizing thermal protective fabrics of firefighters' clothing in hot surface contact.* Journal of Industrial Textiles, 2016. **47**(5): p. 622-639.
126. Li, J., et al., *The relationship between air gap sizes and clothing heat transfer performance.* The Journal of the Textile Institute, 2013. **104**(12): p. 1327-1336.
127. Cengel, Y.A., *Heat and mass transfer*. 2000.
128. Xiang, B., et al., *An easy-to-prepare flexible dual-mode fiber membrane for daytime outdoor thermal management.* Advanced Fiber Materials, 2022. **4**(5): p. 1058-1068.
129. Luo, H., et al., *Outdoor personal thermal management with simultaneous electricity generation.* Nano letters, 2021. **21**(9): p. 3879-3886.
130. Shi, M., et al., *Dual-Mode Porous Polymeric Films with Coral-like Hierarchical Structure for All-Day Radiative Cooling and Heating.* ACS nano, 2023. **17**(3): p. 2029-2038.
131. Yin, H., et al., *Switchable Kirigami Structures as Window Envelopes for Energy-Efficient Buildings.* Research, 2023. **6**: p. 0103.
132. Zhang, Q., et al., *Temperature-dependent dual-mode thermal management device with net zero energy for year-round energy saving.* Nature communications, 2022. **13**(1): p. 4874.
133. Zeng, S., et al., *Dynamic thermal radiation modulators via mechanically tunable surface emissivity.* Materials Today, 2021. **45**: p. 44-53.

Appendices

Appendix A – Design of the peristaltic pump

As shown in Table A-1 and Figure A-1, the specifications of several commercial peristaltic pump are demonstrated. The flow and the weight are the main factors when selecting pumps. However, the lighter pump has smaller flow, while the pumps with higher flow are heavy. Therefore, a peristaltic pump was designed in this study. The design goals of the peristaltic pump for soft robotic clothing mainly consists of two parts: 1) the flow should be higher than 600 mL/min; 2) the whole weight of the designed peristaltic pump should be less than the commercial pumps with similar flow.

Table A-1 Performance comparison of three commercial peristaltic pumps.

Product number	Power (W)	Voltage (V)	Current (A)	Flow (mL/min)	Weight (g)	Roller number
CKP-DC-S08	5	12	0.25	50	110	3
KHM-SW3N40	10	12	0.8	500	261	3
KPHM600-SW3B17L	12	12	0.8	600	382	3
All three commercial peristaltic pumps are actuated by DC brushed motors						

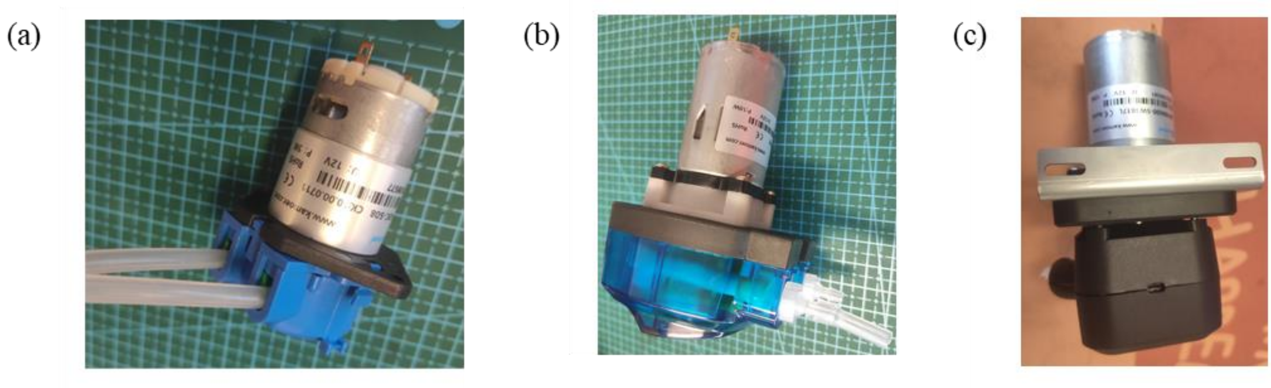

Figure A-1 Images of the three commercial peristaltic pumps. (a) CKP-DC-S08. (b) KHM-SW3N40. (c) KPHM600-SW3B17L.

The main parameters of the peristaltic pump designed for the inflatable clothing are listed in Table A-2. The tube inner diameter and pitch circle diameter of pumps are calculated based on the model set up to calculate the flow. The flow of the designed pump can research 650 mL/min, and the weight is only 109 g. Figure A-2 shows the three views of the pump. And Figure A-3 is the image of the designed pump.

Table A-2 Main designed parameters of designed peristaltic pump.

Parameters	Smaller pump
Pitch circle diameter (mm)	52
Tube inner diameter (mm)	5
Tube outer diameter (mm)	6
Tube thickness (mm)	1

The relative squeeze of the tube y'	15%
Reduction ratio	36:1
Motor rotation speed (rpm)	6800
Whole weight predicted (g)	109
Predicted flow (mL/min)	~ 650

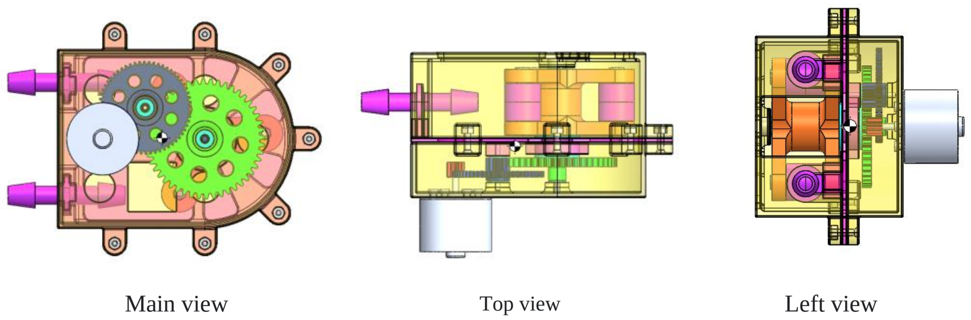

Figure A-2 Three views of two developed peristaltic pump. Main view (left). Top view (middle). Left view (right).

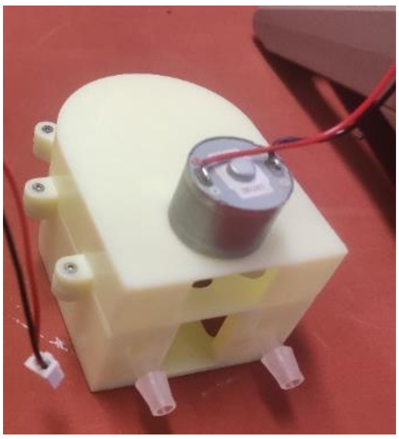

Figure A-3 Image of the designed pump with 3D printed box.

Appendix B – Code for the control system for adjustable thickness

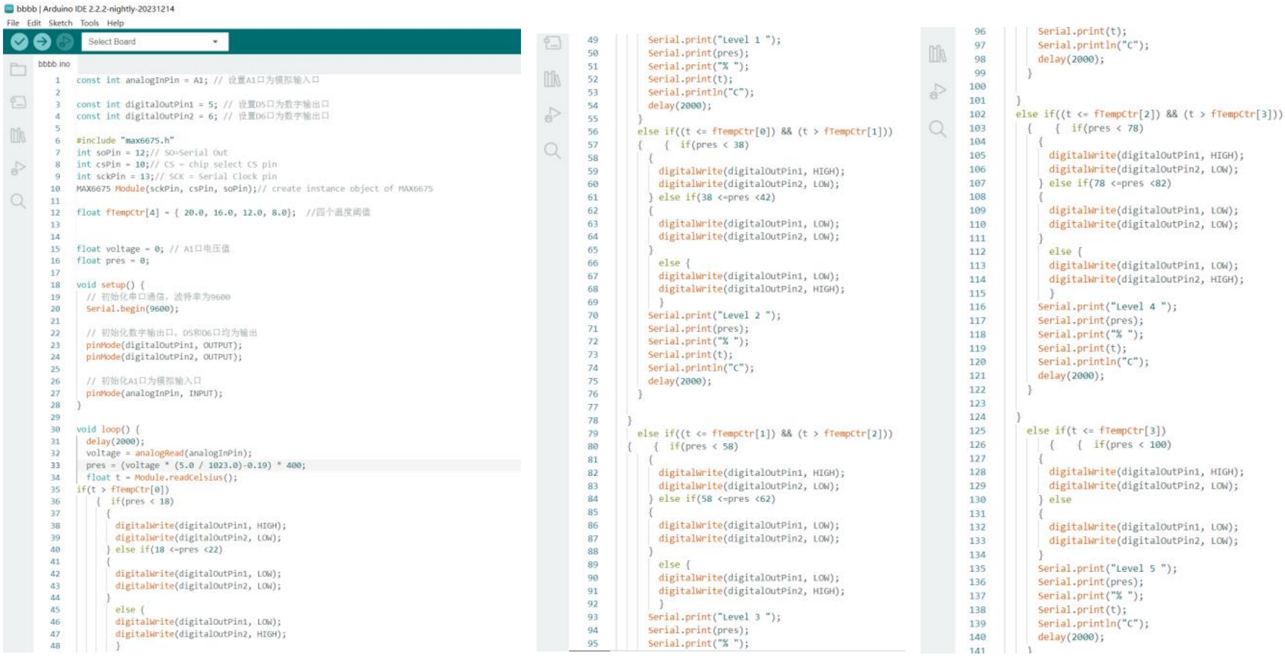

Figure A-4 Code of the control system for the adjustable thickness.

Appendix C – Code for the control system for radiative cooling

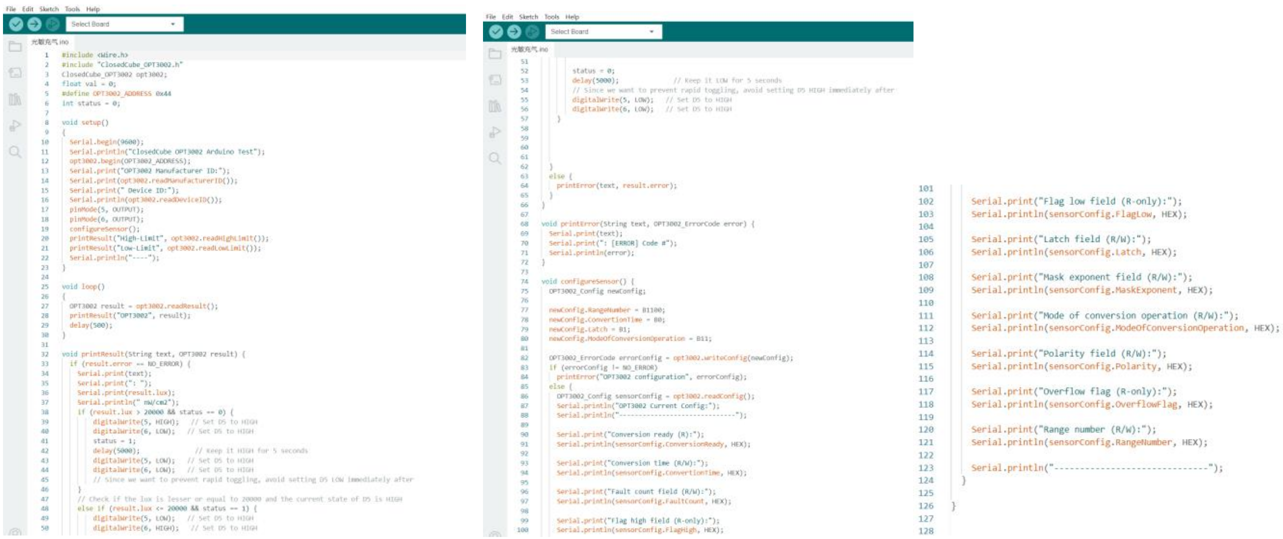

Figure A-5 Code for the control system for radiative cooling.